STUDIES ON THE MOLTEN SALT ELECTRO-DEOXIDATION OF NIOBIUM, TITANIUM, SILICON AND URANIUM OXIDES

By

DUNABOYINA SRI MAHA VISHNU

Enrolment No: CHEM02200804011

Indira Gandhi Centre for Atomic Research
Kalpakkam 603102, Tamilnadu, India

A thesis submitted to the

Board of Studies in Chemical Sciences

In partial fulfillment of requirements

For the Degree of

DOCTOR OF PHILOSOPHY

of

HOMI BHABHA NATIONAL INSTITUTE

December, 2013

Homi Bhabha National Institute
Recommendations of the Viva Voce Board

As members of the Viva Voce Board, we certify that we have read the dissertation prepared by **Dunaboyina Sri Maha Vishnu** entitled "**Studies on the molten salt electro-deoxidation of niobium, titanium, silicon and uranium oxides**" and recommend that it may be accepted as fulfilling the dissertation requirement for the Degree of Doctor of Philosophy.

Chairman - **Dr. T.G. Srinivasan** **Date:** 23.7.14

Guide / Convener - **Dr. K. Nagarajan** k. Naj **Date:** 23/7/14

External Examiner - **Prof. T. Subbaiah** **Date:** 23/7/2014

Member 1 - **Dr. T. Gnanasekaran** **Date:** 23/7/2014

Member 2 - **Dr. C. Mallika** CMallika **Date:** 23.07.14

Technology Advisor - **Dr. K.S. Mohandas** **Date:** 23.07.2014

Final approval and acceptance of this dissertation is contingent upon the candidate's submission of the final copies of the dissertation to HBNI.

I hereby certify that I have read this dissertation prepared under my direction and recommend that it may be accepted as fulfilling the dissertation requirement.

k. Naj

Date: 23/7/14
Place: Kalpakka.

Dr. K. Nagarajan
(Guide / Convener)

STATEMENT BY AUTHOR

This dissertation has been submitted in partial fulfillment of requirements for an advanced degree at Homi Bhabha National Institute (HBNI) and is deposited in the Library to be made available to borrowers under rules of the HBNI.

Brief quotations from this dissertation are allowable without special permission, provided that accurate acknowledgement of source is made. Requests for permission for extended quotation from or reproduction of this manuscript in whole or in part may be granted by the Competent Authority of HBNI when in his or her judgement the proposed use of the material is in the interests of scholarship. In all other instances, however, permission must be obtained from the author.

Dsmahavishnu
23/07/14
Dunaboyina Sri Maha Vishnu

DECLARATION

I, hereby declare that the investigation presented in the thesis entitled "**Studies on the molten salt electro-deoxidation of niobium, titanium, silicon and uranium oxides**" submitted to **Homi Bhabha National Institute (HBNI)**, Mumbai, India for the award of **Doctor of Philosophy** in **Chemical Sciences** is the record of work has been carried out by me under the guidance of **Dr. K. Nagarajan**. The work is original and has not been submitted earlier as a whole or in part for a degree/diploma at this or any other Institution/University.

23/07/14

Dunaboyina Sri Maha Vishnu

LIST OF PUBLICATIONS

International Journal Publications

1. **D. Sri Maha Vishnu**, N. Sanil, N. Murugesan, L. Shakila, C. Ramesh, K.S. Mohandas, K. Nagarajan, 'Determination of the extent of reduction of dense UO_2 cathodes from direct electrochemical reduction studies in molten chloride medium', Journal of nuclear materials, 427 (2012) 200-208.
2. **D. Sri Maha Vishnu**, N. Sanil, L. Shakila, G. Panneerselvam, R. Sudha, K.S. Mohandas, K. Nagarajan, 'A study of the reaction pathways during electrochemical reduction of dense Nb_2O_5 pellets in molten $CaCl_2$ medium', Electrochimica Acta, 100 (2013) 51-62.
3. **D. Sri Maha Vishnu**, N. Sanil, G. Panneerselvam, R. Sudha, K.S. Mohandas, K. Nagarajan, 'Mechanism of direct electrochemical reduction of solid UO_2 to uranium metal in $CaCl_2$-48mol%NaCl melt', Journal of the Electrochemical Society, 160 (9) (2013) D394-D402.
4. **D. Sri Maha Vishnu**, N. Sanil, G. Panneerselvam, S.K. Mahato, K.V. Soja, K.S. Mohandas, K. Nagarajan, 'Factors influencing the direct electrochemical reduction of UO_2 pellets to uranium metal in $CaCl_2$-48mol%NaCl melt', Journal of the Electrochemical Society, 160 (11) (2013) D583-D592.
5. N. Murugesan, **D. Sri Maha Vishnu**, N. Sanil, C. Ramesh, K. Nagarajan, V. Ganesan, 'A novel technique for estimation of metallic uranium using proton exchange membrane based hydrogen sensor', Transactions of Indian Institute of Metals (In press, DOI: 10.1007/s12666-014-0391-x).

International / National conferences:

1. **D. Sri Maha Vishnu**, N. Sanil, N. Murugesan, L. Shakila, C. Ramesh, K.S. Mohandas, K. Nagarajan, Estimation of uranium in UO_2 partially reduced by electro-deoxidation, Book of Abstracts, Fourth International Symposium on Nuclear Analytical Chemistry (NAC-IV), Bhabha Atomic Research Centre, Mumbai, India, November 15-19, 2010, p. 184.
2. **D. Sri Maha Vishnu**, N. Sanil, L. Shakila, K.S. Mohandas, K. Nagarajan, Galvanostatic Electrodeoxidation of niobium pentoxide in molten calcium chloride medium, Proceedings of 3rd International Symposium on Materials Chemistry (ISMC), Bhabha Atomic Research Centre, Trombay, Mumbai, December 7-11, 2010, p. 135.
3. **D. Sri Maha Vishnu**, N. Sanil, L. Shakila, G. Pannerselvam, Swapan Kumar Mehato, K.S. Mohandas, K. Nagarajan, Studies on the direct electrochemical reduction of Nb_2O_5 in MCl (M=Na and K), $CaCl_2$-75 mol % KCl and $CaCl_2$ melts, Book of Abstracts, International Conference on Vistas in Chemistry (ICVC), IGCAR, Kalpakkam, India, October 11-13, 2011, p. 235-237.
4. **D. Sri Maha Vishnu,** N. Sanil, G. Pannerselvam, K.S. Mohandas, K. Nagarajan, Preliminary results on the role of calcium during electro-reduction of solid oxides in molten calcium chloride medium, Proceedings of DAE-BRNS Biennial Symposium on Emerging trends in separation Science and Technology (SESTEC), Mumbai, India, February 27 – March 01, 2012, p. 166.
5. **D. Sri Maha Vishnu**, N. Sanil, L. Shakila, K.S. Mohandas, K. Nagarajan, Studies on electro-deoxidation of metal oxides in molten calcium chloride medium, Chemistry Research Scholars' Meet (CRSM), IGCAR, Kalpakkam, India, July 14-15, 2011.
6. **D. Sri Maha Vishnu**, N. Sanil, G. Panneerselvam, K.S. Mohandas, K. Nagarajan, An innovative study of the electrochemical reduction of solid SiO_2 in LiCl and $CaCl_2$ melts,

Proceedings of DAE-BRNS 4th Interdisciplinary Symposium on Materials Chemistry **(**ISMC), BARC, Trombay, Mumbai, India, December 11-15, 2012, p. 172.

7. **D. Sri Maha Vishnu**, N. Sanil, G. Panneerselvam, K.S. Mohandas, K. Nagarajan, Feasibility studies on the direct electrochemical reduction of solid UO_2 in $CaCl_2$-NaCl eutectic melt, Proceedings of Conference on Molten Salts in Nuclear Technology (CMSNT), BARC, Mumbai, India, January 9-11, 2013, p. 233-235.
8. **D. Sri Maha Vishnu,** N. Sanil, K.S. Mohandas, K. Nagarajan, A preliminary study of the electrochemical behaviour of some molten salts as electrolyte medium for direct electrochemical reduction of solid metal oxides to metals, ibid, p. 230-232.
9. N. Sanil, L. Shakila, **D. Sri Maha Vishnu**, K.S. Mohandas, K. Nagarajan, Studies on the Electro-deoxidation of CeO_2 in the FFC Cambridge process, Abstracts of the Second International Conference on Advances in Nuclear Materials (ANM), Mumbai, India, February 9-11, 2011, p. 151.
10. K.S. Mohandas, N. Sanil, L. Shakila, **D. Sri Maha Vishnu**, K. Nagarajan, Studies on the electrochemical deoxidation of UO_2 in molten calcium chloride, Proceedings of the FRAY International symposium on Metals and Materials Processing in a clean environment, November-2011, Cancun, Mexico, Vol. 3: Molten Salts & Ionic Liquids 2011, p. 239-252.
11. K.S. Mohandas, L. Shakila, N. Sanil, **D. Sri Maha Vishnu**, K. Nagarajan, Galvanostatic studies on the electro-deoxidation of solid titanium dioxide in molten calcium chloride, Proceedings of the FRAY International symposium on Metals and Materials Processing in a clean environment, November-2011, Cancun, Mexico, Vol. 3: Molten Salts & Ionic Liquids 2011, p. 253-268.

Awards:

1. Best poster presentation award:

D. Sri Maha Vishnu, N. Sanil, L. Shakila, K.S. Mohandas, K. Nagarajan, Galvanostatic Electrodeoxidation of niobium pentoxide in molten calcium chloride medium, presented at 3rd International Symposium on Materials Chemistry (ISMC), held at BARC, Mumbai, during december 7-11, 2010.

Dsrimahavishnu
23/07/14
Dunaboyina Sri Maha Vishnu

"What I learnt and where I stand today is because of the inspiration, moral support and blessings from my beloved parents and teachers. I believe that the sincere efforts I made, both physically and mentally, towards this thesis would one day be useful for the society at large and help illuminate the lives of common man."

This thesis is

Dedicated to my parents and teachers

Dsrimahavishnu
23/07/14
Dunaboyina Sri Maha Vishnu

ACKNOWLEDGEMENTS

I would like to express my deepest gratitude to my research supervisor **Dr. K. Nagarajan** for giving me an opportunity to work in an exciting area and giving me his valuable guidance and constant support throughout the course of the work and my stay at IGCAR.

Words are not sufficient to express my gratitude to my technology advisor, **Dr. K.S. Mohandas**, for sharing his knowledge, scientific understanding and experience with me. The freedom and support I enjoyed with him helped me to execute several novel ideas in my work and to carve out this thesis to its present shape.

I would boldly say that the technical quality of the thesis was improved by ideas sprang from several casual discussions that I had with **Mr. N. Sanil** on different aspects of my work. I thank him for his support and critical reading of the manuscripts. The questions posed by him made me to think out of box and to understand things in a better way.

I am pleased to express my deep sense of gratitude to **Dr. S. Anthonysamy** for creating a positive attitude in me towards molten salts. Glossy finished boron carbide pellets showed to me on 31/10/2009 during his classroom teaching of course 'Nuclear Fuel Cycle-I', generated enthusiasm in me to work in the area of molten salts.

I would like to express my sincere thanks to my doctoral committee chairman **Dr. T.G. Srinivasan** and members **Dr. T. Gnanasekaran** and **Dr. C. Mallika** for their timely assessment and suggestions. I am pleased to express my thanks to **Dr. M. Saibaba**, AD, RMG, for providing a good ambience for the research scholars at the JRF Enclave. The excellent facilities at the enclave and his moral support and encouragement helped me to live a comfortable life at Kalpakkam and to fully concentrate on my research work. My thanks are also due to all my teachers who taught me various subjects at BARC training school at IGCAR, which helped me, develop a better understanding and clarity in my work.

I wish to record my sincere thanks to **Dr. G. Panneerselvam** for XRD analysis of the samples, **Dr. V. Chandramouli, Mrs. K.V. Soja and Mrs. Annie** for the oxygen analysis and **Mr. Swapan Kumar Mahato, Dr. R. Sudha, Mr. C.N. Venkateswaran** and **Dr. C. Padma Prabhu** for SEM and EDX analysis of the samples. The cooperation rendered by **Mrs. Annapoorani, Mrs. Uma Maheshwari, Mr. Sekhar and Mr. R. Krishnaprabhu** in the analysis of the samples by ICPOES, ICPAAS and ICPMS is highly acknowledged.

I profoundly thank my collaborators, **Mr. C. Ramesh and Mr. N. Murugesan,** MCD, CG for giving me an opportunity to work in the area of hydrogen sensor, **Dr. U. Kamachi Mudali, Mr. Jagadeesh Sure and Mr. Ravi Shankar,** CSTG, MMG for their cooperation in the work related to electro-deoxidation induced corrosion of high density graphite, though the work could not be projected fully in the thesis due to size restrictions.

I take immense pleasure in thanking **Dr. B. Prabhakara Reddy, Mr. Suddhasattwa Ghosh, Mrs. Vandarkuzhali, Mr. P. Venkatesh** and **Dr. Manish Chandra** for their valuable support. Also I would like to thank **Shri. K.A.S. Kutty, Shri. V. Suresh Kumar and his team** of Chemical Facilities Division for their help and constant support in the design and fabrication of molten salt electrolytic cells and glove boxes for the molten salt laboratory work. I sincerely acknowledge the help and support rendered by my laboratory colleagues **Mr. V. Arun Kumar, Mrs. L. Shakila and Mrs. R. Mohini.** I also thank **Ms. S. Suganthi, Mr. K. Perumal, Mr. Nedumaran, Mr. A.S. Ganapathi, Mr. S. Mariappan, Mrs. Anjali, Mrs. Lali and Mr. Rajeev Kumar** for their good company and cooperation in my work. I express my special thanks to **Mr. V. Arun Kumar** and **Mr. S. Mariyappan** for their kind support during my work in the lab at late hours, over nights and holidays.

I extend my thanks to my seniors **Ch. Jagadeeswara Rao, M. Jayakumar, Biju, Tarun, Trinadh, Rahul, Hari babu, Ashit, Sulatha and Rajini** for their valuable suggestions and moral support. I would like to express thanks to my friends **Mr. Jammu Ravi, Laxmoji, Jagadeesh, Srinivas, Ilaiyaraja**, **Mariyappa, Sharath, Naveen, Bupathi, Herojith, Pradeep, Sudanshu, Mrs. Maneesha, Debasmitha, Pravati** and **Priyada** for making my stay at Kalpakkam most memorable one in my life. I also thank my juniors **Mr. Srihari, Sashwat, Arun Chandran, Benedict Rakesh, Mahendra, Hari Prasad, Venkatesh, Samba, Avinash, Venkata Ramana, Yadagiri, Gopi, Ms. Priyadarshini, Kamali, Meera and Rashmi** for their cooperation.

I am indebted to my father **Shri. D. Bhyrava Murthy**, mother **Smt. D. Mangayamma** and brother **Mr. D. Edukondalu** who would have felt the inconvenience of my long stay away from them at IGCAR and my absence even for important functions. I thank them for their relentless support, love, affection and encouragement for completion of this task.

Dmahavishnu
23/07/14
Dunaboyina Sri Maha Vishnu

CONTENTS

Title Page No.

SYNOPSIS

Metals have played a crucial role in improving the standard and style of living of human beings from the time of the Stone Age to the present scenario of the technologically advanced modern world. Metals and their alloys have not only been serving in several ways to mankind on the earth but also in every effort that is being made by man to explore a new world in the outer space as seen from the recent advancements in the field of space science and technology. Production of metals has been a major activity all the time in the area of chemical metallurgy. Minerals contain metals in various forms such as oxides, sulphides etc. and production of metals from these compounds by chemical and electrochemical methods has been in use over centuries. The oxides of the alkali or alkaline earth metals such as lithium, calcium, magnesium etc. are more stable and their relative stability over the oxides of most of the transition and rare earth metals forms the basis for metallothermic reduction of transition and rare earth oxides to produce metals [1]. Often the compound of metal is converted to the halide form and then reduced to the metal by reacting it with alkali or alkaline earth metals at elevated temperatures. Carbothermic reduction by elemental carbon, one of the cheapest reductants available, at higher temperatures either directly or under vacuum has also been used as a method for the production of a number of metals such as iron, niobium, tantalum etc. [1]. Electrochemistry played a significant role in the production of alkali and alkaline earth metals by electrolysis of their fused salts. In addition to these metals, few other metals such as aluminium, are produced by the electro-reduction of the metal from an electrolyte in which the compound of the metal is dissolved as ions. However, most of the oxides of the metals are ceramic in nature and their dissolution in the electrolyte is negligible and therefore, the production of these metals from their oxides by electrolysis becomes difficult. Also the multivalent nature of the metals (e.g., titanium), though they are converted to a form which is low melting or becomes soluble in an electrolyte, would pose problem by the redox-cycling of the metal ions leading to a suppressed rate of deposition of the metal at the cathode [2]. In addition, electro-deposited metals, which are solids at the operational temperature, would lead to the formation of dendrites causing the shorting of the electrodes eventually creating problems in the successful operation of the electrolytic cells. All these aspects have hindered the development of the conventional electrolytic production method for many metals. Except Hall-Heroults' process where in aluminium is produced by the electrolysis of Al_2O_3 dissolved in molten cryolite (Na_3AlF_6) medium, attempts made towards the production of other metals by electrolysis of their oxides dissolved in a suitable electrolyte medium could not become successful.

Electricity is a boon not only for the electro-metallurgical industries, but also for the day-to-day activities of human life. The growing electricity demand of the world needs to be addressed for which one of the potential options is nuclear energy [3]. Nuclear reactors are a means of production of electricity from the energy derived from controlled nuclear fission of fissile nuclides (e.g., U^{235}) in the nuclear fuels. Though currently operating power reactors exploit the fission reactions caused by neutrons of low energy (thermal neutrons), fast reactors based on fission reactions caused by high energy neutrons (few MeV) are of interest. Fast neutrons can enhance the percentage utilisation of the uranium compared to a thermal reactor. Of the fast reactors, sodium cooled metallic fuelled fast breeder reactors coupled with integrated pyroprocessing technology for spent fuel reprocessing, are considered to be inherently safe, resistant to proliferation and proposed to be the best form of reactor technology in Generation IV concept for production of electricity [4]. Metallic fuels have advantages such as high specific energy of the fuel, breeding gain, lower doubling time etc. and U-Pu-Zr alloys are potential fuels for such reactors. Therefore production of uranium, plutonium and zirconium metals from their oxides is of interest to nuclear industry. Due to the inherent limitations and difficulties in the existing technologies for metals production, new methods offering advantages such as low temperature of operation, less number of process steps, higher energy efficiency, environment friendliness etc. are of interest to both nuclear as well as conventional metallurgical industries for the production of metals.

Production of metals directly from the metal oxides in molten salts is a recent development in the field of electro-pyrometallurgy that offers the above mentioned advantages. The process is called FFC Cambridge process [5]. In this direct oxide electrochemical reduction (DOER) process, the metal oxide is reduced to the metal by electrolysis in a suitable molten salt electrolyte medium such as $CaCl_2$ at temperatures in the range1073 – 1223 K. The solid metal oxide is configured as the cathode and graphite as the anode and the electrolysis is generally carried out by the application of a potential of 3.0-3.1 V, which is well above the theoretical decomposition potential of most of the metal oxides but below that of the electrolyte melt (E_d of $CaCl_2$ is 3.211 V at 1173 K). In experimental studies, the cathode is generally shaped in the form of a pellet and the anode taken in the form of a rod. Electrochemical reduction of oxides of titanium [5], niobium [6], tantalum [7], zirconium [8], chromium [9], iron [10], tungsten [11], aluminium [12], silicon [13], uranium [14] etc. have been reported. The method also has been demonstrated for the production of alloys by reducing preforms made from a mixture of different metal oxides [15]. Nuclear industry is interested in the process for various reasons. Today most of the spent oxide nuclear fuel is reprocessed by the PUREX process. Alternatively the fuel can be reprocessed in the pyrochemical reprocessing route, if the fuel is made available in the metal form. Electro-deoxidation process can be effectively used for this oxide to metal conversion and can thus serve as an intermediate step in the pyrochemical reprocessing of spent oxide nuclear fuels. The metal fuel thus produced can be used in a fast reactor. Secondly, the process allows significant reduction in the volume of the spent oxide fuels, so that the storage space and the cost associated with such facilities for spent-oxide fuel management can be minimised as studied in the Advanced fuel Conditioning Programme (ACP) by Republic of South Korea. Lastly, actinide metals such as U, Pu etc. can be directly produced from their oxides by using the method. In nuclear industry, the process is slightly modified by taking LiCl-Li_2O melt as electrolyte instead of $CaCl_2$, to lower the temperature of operation of the process and platinum, instead of graphite, as the anode to avoid the probable contamination of the melt and the metal produced, by carbon [16]. Since the DOER process is a recent one, many fundamental issues of the process still remain unexplored.

The present study is aimed at the basic understanding of the electrodeoxidation process, getting an insight into its fundamental aspects and to address various uncertainties/discrepancies seen in the literature by systematically investigating the electrochemical reduction of few oxides, having different physical, chemical and electrical properties in different molten salt environments. Accordingly, Nb_2O_5, TiO_2, SiO_2 and UO_2 were chosen as the candidate oxides and $CaCl_2$, NaCl, KCl, LiCl and eutectics of $CaCl_2$-KCl, $CaCl_2$-NaCl, LiCl-KCl-$CaCl_2$ as the electrolyte media for the study. During these studies many partially reduced samples, which contain a mixture of the oxide and its reduced metal, were produced and it was required to analyse the metal content in such samples. Hence an interesting method, namely 'Metal Estimation by Hydrogen Sensor (MEHS)', has been developed as part of the study towards this purpose. The objectives of the present study are as follows.

- Understanding fundamental issues of the electro-deoxidation process taking Nb_2O_5 as the candidate oxide. Studies on the mechanism and the factors influencing the rate of electro-reduction of Nb_2O_5 in different molten salts.
- Investigations on some important, but hitherto not investigated issues in the electro-reduction of TiO_2 and SiO_2 systems.

- Application of the understanding gained from the above systems to the electrochemical reduction of UO_2 pellets to understand the mechanism of reduction and the influence of various parameters on the rate of reduction.
- Development and application of MEHS method for the determination of extent of reduction of partially reduced UO_2 samples, which are essentially U-UO_2 mixtures, obtained from incomplete reduction of UO_2.

The thesis is segmented into 7 chapters and the overview of each chapter is briefly presented below.

Chapter 1

The first chapter gives an introduction to the electro-deoxidation process and discusses, the details of its discovery and initial developments. The chapter also includes a literature survey on the fundamental issues of the process so far reported, the advantages over the existing methods for production of metals and related aspects. Since the method is being studied for electrochemical reduction of various oxides of transition metals and actinides by various researchers all over the world, the current developments of the process in both nuclear as well as other domains are briefly discussed in this chapter. Studies reported in the literature regarding the application of the method for the electrochemical reduction of various oxides of p-block elements (e.g., SiO_2), transition metals (e.g. TiO_2, Nb_2O_5) and f-block elements (e.g., UO_2) are included. Thermodynamic aspects and a discussion on the phase relations by referring to the phase diagrams of oxides systems whose electro-deoxidation chemistry, investigated later, are also briefly discussed. Some of the discrepancies and unexplored aspects in the area of electro-deoxidation process in literature are pointed out and the objectives of the present study which are based on the above discussions are listed. The chapter also gives the structure of the thesis and chapters to follow.

Chapter 2

The experimental methods adopted in the study including the electrolysis are discussed in this chapter. Description of various equipments used and the procedure followed during different stages of the work such as preparation of salt, cathode, anode and reference electrode, design and assembly of the cell, operation of glove boxes, furnaces, potentiostat, power supplies, data acquisition systems etc. are discussed. This chapter also describes the theory involved in the electrolysis. Two modes of electrolysis, viz. the constant current and constant voltage electrolysis have been employed in the studies. Cyclic voltammety was used as an electroanalytical technique for the characterisation of the melt and also to obtain some reduction features of the oxides. The techniques and methods employed during the analysis of the products and melt from the electrolytic experiments are also briefly described. X-ray diffraction technique was used for determination of various phases present in the electrolysed samples. Scanning electron microscopy (SEM) and energy dispersive X-ray spectroscopy (EDX) were employed to study the microstructural characteristics and the elemental analysis, respectively, of the washed and vacuum dried samples obtained from the electrochemical reduction studies. Inert gas fusion technique was used in the determination of the residual oxygen content of the samples. Melt from the electrochemical experiments was dissolved in distilled water and methods have been developed for determination of both water soluble and water insoluble basicity using acidometry and back titration methods, respectively. The salient features of the different techniques used in the work are briefly discussed.

Chapter 3

This chapter deals with the fundamental issues of the electro-deoxidation process by taking Nb_2O_5 as the candidate oxide. A thorough experimental investigation of the pathways of the complex mechanism of electrochemical reduction of Nb_2O_5 to Nb metal in molten $CaCl_2$ was carried out. The results of the cyclic voltammetric and polarisation studies with

Nb_2O_5 electrodes in the melt, which showed that the oxide is electrochemically reactive to Ca^{2+} ions of the melt, are given. The electrochemical reduction experiments were carried out in constant voltage mode at 3.1 V for different durations of time. Partially reduced samples obtained in these studies were analysed and the chemistry of the melt in each case was deduced from the analysis of the pellet as well as that of the melt. The partially reduced samples were carefully analysed by various characterisation techniques such as XRD, SEM-EDX and oxygen analysis. Electrochemical data in combination with the results from XRD, SEM-EDX and the melt analysis etc. were made use of in determining the pathways of reduction. The reduction was found to proceed via the formation and decomposition of the ternary intermediates of the type $Ca_xNb_yO_z$ and suboxides of the form NbO_x. The factors influencing the rate of electrochemical reduction of Nb_2O_5 such as duration of electrolysis, temperature, applied voltage, open porosity of pellets, mode of electrolysis, configuration of the cathode, composition of electrolyte etc. were studied and the results are presented in this chapter. The results of the cyclic voltammetric studies carried out using NaCl, KCl and KCl-25mol.% $CaCl_2$, as electrolytes for the electrochemical reduction of Nb_2O_5 to study the effect of change in the melt on the electro-reduction are also included. A brief note on the electro-deoxidation induced corrosion behaviour of graphite anode in these experiments is also included in the discussion.

Chapter 4

Chapter 4 deals with the electrochemical reduction studies carried out on TiO_2 and SiO_2. The mechanism and rate of electro-deoxidation of the solid oxides during electrochemical reduction depends on the physical, chemical and electrical properties of the chosen oxide. To study this aspect, direct electro-reduction experiments were carried out on TiO_2 and SiO_2 pellets with two different cathode configurations - one in which the pellet was fully dipped in the electrolyte along with the current collector so that conductor-oxide-melt phases coexist and the other in which tip alone was dipped in the electrolyte with the current collector not coming into contact with the melt so that only the oxide-melt phases alone coexist. These experiments were carried out with two different electrolytes, namely, $CaCl_2$ (at 1173 K) and LiCl (923 K). In the latter configuration, the region of the TiO_2 dipped into the melt got reduced indicating that the TiO_2 pellet acted as a conductor by itself whereas the region near the current collector alone got reduced in the case of SiO_2 pellet indicating that the SiO_2 was not an electronic conductor under the experimental conditions. The results of the experiments with TiO_2 and SiO_2 give ample proof for the proposed three phase interline (conductor-oxide-melt) mechanism for the propagation of electro-reduction in a solid oxide matrix. The melt required for reduction at the region of the current collector was provided by the capillary action of the melt. Though similar results were obtained with SiO_2 pellet, TiO_2 pellet became unstable in LiCl melt. Electro-reduction studies were also carried out with TiO_2 powder (1.5 g), sintered at 1423 K and 1673 K, as cathode in molten $CaCl_2$ by constant voltage and constant current modes of electrolysis at 1173 K. The effect of increase in the mass of TiO_2 powder on the electro-deoxidation behaviour was also systematically studied by increasing the mass of TiO_2 to about 10 g. In all the cases, the reduction was found to be better with the powder sintered at 1423 K than that sintered at 1673 K. The results are discussed in this chapter.

Chapter 5

In Chapter 5, the electrochemical reduction studies carried out on UO_2 were discussed. Electro-reduction of powder compacted and sintered UO_2 pellets in molten $CaCl_2$ at 1173 K resulted in the formation of an impermeable uranium metal layer on the surface of the pellet, which prevented the bulk reduction of the pellets. Hence a low-melting $CaCl_2$-48mol.% NaCl salt mixture (m.p. 775 K) was selected and the fundamental mechanism and factors influencing the reduction were studied in the melt. Analysis of the partially reduced samples from experiments carried out in this melt at 923 K showed that the electrochemical reduction of UO_2 to U metal occurred directly without the formation of ternary intermediate compounds or any suboxides of uranium. The rate of electrochemical reduction increased with duration of electrolysis, applied voltage and open porosity of the pellets. The rate, as it appeared, increased with increase in temperature from 923 K to 1023 K and further increase in temperature to 1173 K resulted in a decrease in the rate of electrochemical reduction. The decrease in the rate of reduction at higher temperatures was attributed to the sintering of the uranium metal to form a nonporous layer on the surface of the pellets. Feasibility studies on the application of LiCl-KCl-$CaCl_2$ (50.5: 44.2: 5.3 mol. %) for the electrochemical reduction of UO_2 at a lower temperatures (673 K) were carried out and the reduction of UO_2 was found feasible in the melt. The results of the study are discussed in chapter 5 of the thesis.

Chapter 6

Electro-reduction experiments often results in partially reduced samples and determination of the extent of metallisation (reduction) of the metal oxide electrodes is very important. Chapter 6 presents the results of efforts dedicated to the development of a method towards this purpose. Usami et al. [17] have reported a quantitative method based on the measurement of total hydrogen evolved during reaction of the metal in the metal-metal oxide mixture of such samples. In that study, a gas burette was employed for the measurement of hydrogen. In the present development, the hydrogen measurement part was thoroughly modified with the use of a fuel cell type, polymer electrolyte based, hydrogen sensor. The in-house developed sensor enables online measurement of the hydrogen liberated during the acid dissolution of the metal in the sample. The method was developed taking zinc as the metal and HBr as the acid medium for its dissolution. After successful calibration of the experimental system with zinc+HBr reaction, the uranium metal present in synthetic mixtures of U and UO_2 was estimated. Subsequently the method was employed for the determination of extent of reduction of partially reduced samples containing U-UO_2 mixtures from the DOER studies carried out in different molten salts. From the amount of the liberated hydrogen, the amount of uranium metal in the sample and hence the extent of reduction of UO_2 was determined. The results of the amount of the metal estimated by the MEHS method were compared with those estimated by using Inductively Coupled Plasma Atomic Emission Spectroscopy (ICPAES).

Chapter 7

This chapter summarises the results of the electro-reduction studies carried out with different oxides and discussed in detail in the previous chapters. Based on the results, some conclusions have been drawn on the fundamental and applied aspects of the solid state electro-reduction process of different classes of metal oxides. These conclusions have been further extended to a brief discussion on some very interesting and technically challenging but hitherto unexplored areas of the technologically important electro-reduction process.

The study showed that the electro-reduction behaviour of Nb_2O_5 and TiO_2 electrodes is quite similar in that the mechanism of reduction followed via the formation and decomposition of ternary intermediates and suboxides. The reduction of both the oxides occurred at all points where the oxide electrode was in physical contact with the melt in sharp contrast to that of a SiO_2 electrode where the reduction occurred only at the oxide-conductor-melt three phase interlines. The difference between the initiation and propagation of electro-reduction in electrically conducting oxides like Nb_2O_5 and TiO_2 and electrically insulating oxides like SiO_2 has been clearly brought out in this study.

Though the electrochemical reduction behaviour of UO_2 was found to be similar to that of Nb_2O_5 and TiO_2, the mechanism of electro-reduction was found very different. It has been proved in this study that, unlike Nb_2O_5 and TiO_2, the reduction of UO_2 to U does not involve formation of intermediate compounds and hence is a one step reduction process. It is proved in this study that electro-generation of calcium (in $CaCl_2$ melt) or lithium (in LiCl melt) and its chemical reaction with UO_2 is not necessary for effecting reduction as has been reported. However, for achieving higher reduction rate it may be required to operate cells under the metal deposition conditions. The study showed that $CaCl_2$-48 mol.% NaCl melt could be a better electrolyte medium for electro-reduction of UO_2 than $CaCl_2$ and LiCl-Li_2O melts.

The MEHS method developed as part of this work has proved to be a very handy and useful technique for the determination of extent of reduction of partially reduced U-UO_2 samples. The method, with necessary modifications, can be extended to determine the metal content in partially reduced samples of other oxides as well.

These results apart, there are many important observations pertaining to the electro-deoxidation, which will be presented in this chapter. The electrochemical reduction studies on technically challenging oxides such as ZrO_2, CeO_2 and B_2O_3 may give a better insight into some of the fundamental issues of the electro-deoxidation process and can be attempted in suitable molten salts. Also the use of an inert anode in place of graphite makes the process environment friendly as oxygen is evolved instead of CO_2 and/or CO gases during the process. Development of inert anodes for DOER process is an area of considerable interest and open for investigations.

References

[1] C.K. Gupta, Chemical metallurgy: principles and practices, Wiley-VCH Verlag GmbH & Co. KGaA, Weinheim, 2003, p.359-399.

[2] D.J. Fray, G.Z. Chen, *Mater. Sci. Technol.,* 20 (3) (2004) 295.

[3] J.F. Ahearne, *Energy Economics,* 33 (2011) 572.

[4] T. Abram, S. Ion, *Energy Policy,* 36 (2008) 4323.

[5] G.Z. Chen, D.J. Fray, T.W. Farthing, *Nature,* 407 (2000) 361.

[6] X.Y. Yan, D.J. Fray, *J. Electrochem. Soc.*, 152 (10) (2005) E308.

[7] S.M. Jeong, J.Y. Jung, C.S. Seo, S.W. Park, *J. Alloys Compd.*, 440 (2007) 210.

[8] K.S. Mohandas, D.J. Fray, *Metall. Mater. Trans. B,* 40B (2009) 685.

[9] G.Z. Chen, E. Gordo, D.J. Fray, *Metall. Mater. Trans. B,* 35B (2004) 223.

[10] G. Li, D. Wang, Z. Chen, *J. Mater. Sci. Technol.*, 25 (6) (2009) 767.

[11] M. Erdogan, I.Karakaya, *Metall. Mater. Trans. B,* 41B (2010) 798.

[12] X. Y. Yan, D. J. Fray, *J. Appl. Electrochem.*, 39 (2009) 1349.

[13] K. Yasuda, T. Nohira, R. Hagiwara, Y.H. Ogata, *Electrochim. Acta* 53 (2007) 106.

[14] K. Gourishankar, Redey, M.Williamson, *Light metals*, TMS (2002) 1075.

[15] X.Y. Yan, D.J. Fray, *J. Alloys Compd.*, 486 (2009) 154.

[16] K. Nagarajan, B.P. Reddy, S. Ghosh, G. Ravishankar, K.S. Mohandas, U.K. Mudali, K.V.G. Kutty, K.V. Kasiviswanathan, C.A. Babu, P.K. Sundaram, P.R.V. Rao, B. Raj, *Energy Procedia,* 7 (2011) 431.

[17] T. Usami, M. Kurata, T. Inoue, H.E. Sims, S.A. Beetham, J.A. Jenkins, *J. Nucl. Mater.*, 300 (2002) 15.

List of figures

List of tables

Glossary

AMD	Atomic Minerals Directorate
BARC	Bhabha Atomic Research Centre
BWRs	Boiled Water Reactors
CC	Constant Current
CE	Counter Electrode
CEPM	Counter Electrode Potential Monitoring
Con-V	Constant Voltage
CV	Cyclic Voltammetry
DAS	Data Acquisition System
DOER	Direct Oxide Electrochemical Reduction
EC	Electrolytic conditions
EDXA	Energy Dispersive X-ray Analysis
FFC	Fray-Farthing-Chen
FPs	Fission Products
HD	High Density
HDG	High Density Graphite
ICPMS	Inductively Coupled Plasma Mass Spectrometry
ICPOES	Inductively Coupled Plasma Optical Emission Spectroscopy
IP	Indicator Pellet
IPT	Indicator Pellet Technique
KAERI	Korea Atomic Energy Research Institute
MFBRs	Metallic fuelled Fast Breeder Reactors
MOX	Mixed Oxide Fuels
NC	Non-electrolytic conditions

NFC	Nuclear Fuel Complex
OCP	Open Circuit Potential
OP	Open Porosity
PHWRs	Pressurised Heavy Water Reactors
PUREX	Plutonium Uranium Reduction Extraction
PyG	Pyrolytic Graphite
RO	Residual Oxygen
SEM	Scanning Electron Microscope
SNMFs	Spent Nuclear Metallic Fuels
SNOFs	Spent Nuclear Oxide Fuels
SS	Stainless Steel
TD	Theoretical Density
TIB	Total Insolubilised Basicity
TRUs	Transuranium elements
TSB	Total Solubilised Basicity
UGP	Uniformly Ground Product
UPD	Under Potential Deposition
XRD	X-Ray Diffraction
3PI	Three Phase Interline

CHAPTER 1

Introduction

Metals, either in their pure form or as alloys, are of paramount importance in modern technology. During the early ages, copper (bronze-age) and iron (iron-age) played crucial roles successively in shaping human civilization. The discovery of iron followed by stainless steels eventually replaced the earlier widely used bronze and it is difficult to envision the modern world without the use of steels. The role of metals in improving the standard and style of human life is enormous. For instance, wherever strength has to be combined with light weight, aluminium or titanium is a must. Without these metals we can’t imagine the existence of aviation industry and a large aeroplane leaving the ground for flight. Use of metals in the making of ships, railways and automobiles changed the life of human beings forever. Defence, space, nuclear and conventional industries also have been the major users of various metals and their alloys. The manufacture of the solar cells, automobiles, TV sets, batteries, computers, laptops, cell phones and other technologically important appliances depend on metals or the alloys. In short, metals are essential and integral part of the society that we live in.

The production of metals from their compounds is a subject of considerable interest and importance in the field of chemical metallurgy. Metals, except gold and silver, are available in the form of compounds in the minerals in the earth crust. All other metals are produced from the minerals by using either chemical or electrochemical methods. Chemical methods are based on the relative stability of the compound of the reductant over that of the metal compound [1]. Many metals such as Nb, Ti, Zr, Ta etc. which are of great importance in modern technology are being produced from their compounds industrially by reduction with electropositive metals like Ca, Mg and Li as reductants (metallothermic reduction) or carbon as the reductant (carbothermic reduction) [1]. Electrochemical methods are used for the production of metals from the aqueous solution (e.g., Ni, Zn, Cu) or the molten salts (e.g., Na, K, Mg, Li) of the compounds. Reactive metals like Na, K, Mg and Li can only be produced by molten salt electrolysis, as the metal deposition potential is more negative than that for hydrogen evolution. Most of the transition and rare earth metals are available in nature as their oxides. Gaining these metals by conventional electrolysis becomes difficult due to poor solubility of their oxides in molten salts. Except Hall-Heroult process for production of aluminium, where Al_2O_3 dissolved in molten cryolite (Na_3AlF_6) is electrolysed, no other process could be commercialised for the production of metals from their oxides by molten salt electrolysis. Even if, by additional process steps, the metal oxides are converted to other chemical forms which dissolve in molten salts, their chemical nature in the molten salt medium may not allow the extraction of metals by electrolysis. A case in point is the electrowinning of titanium metal from titanium chloride melt. Titanium exists in the +2, +3 and +4 oxidation states in the melt, which causes the so called ‘redox cycling’ of the metal ions during electrolysis which causes the efficiency of the process to be poor [2]. Direct electrochemical conversion of the metal oxides to metals could potentially reduce the number of steps and difficulties associated with the multi-valency of some metals and hence the cost of the metal production.

1.1. The Fray-Farthing-Chen (FFC) Cambridge process

Recently a process for the direct electrochemical reduction of the metal oxides to metals in molten salts, called Fray-Farthing-Chen (FFC) Cambridge process, has been reported [3,4]. In the conventional electrolytic processes, the metal compound either in its liquid form or as dissolved in a suitable electrolyte medium is electrolysed to gain the metal. Under the influence of the applied potential, the cations and anions move in the opposite directions to discharge at the cathode and anode, respectively resulting in the production of metal at the cathode and non-metallic component at the anode. Unlike this method, the FFC process reported by Prof. Derek Fray’s group at the Materials and Metallurgy department of the University of Cambridge, UK is a new concept wherein the metal compound is directly electro-reduced in its solid state [3,4]. A schematic diagram of the process with metal oxide (MO_2) is shown in Fig. 1.1.

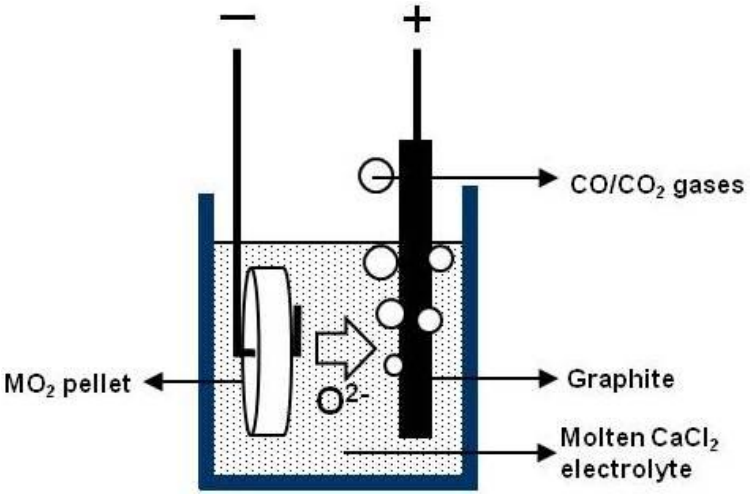

Fig. 1.1. Schematic diagram of the electrochemical reduction of oxide by FFC Cambridge process.

In this relatively simple process, hereafter termed direct oxide electrochemical reduction (DOER) process, the electrodeoxidation is carried out in an electrolytic cell in which the solid metal oxide is configured as the cathode, graphite as the anode and molten $CaCl_2$ as the electrolyte medium. Electro-reduction is carried out by the application of a voltage which is above the theoretical decomposition potential of the metal oxide but below that of the electrolyte melt. Generally, the process is carried out at a constant potential of 3.0 - 3.1 V in molten $CaCl_2$ medium at 1073 - 1173 K. The decomposition potentials of the calcium chloride melt in this temperature range are in the range of 3.27 V - 3.21 V. The applied potential causes oxygen from the metal oxide to be ionised and released as O^{2-} ions into the melt, which gets discharged at the graphite anode as CO/CO_2 gases, leaving behind the metal at the cathode. The solid metal oxide is generally taken in the form of a pellet which is prepared by pressure compaction of the powder followed by sintering in air at high temperature (1273 - 1573 K). The sintering temperature is selected depending on the nature of the oxide. The high temperature sintering helps the pellet to get sufficient mechanical strength so that it does not crumble in the molten salt even as it undergoes many chemical and physical changes during its conversion to metal in the cell. A typical electrodeoxidation cell can be represented as

$$\textbf{Cell: } C(s)/CaCl_2, CaO(l)/MO_2\ (s) \qquad (1.1)$$

The half-cell reactions with MO_2 as the cathode are as follows:

At cathode: $MO_2 + 4e^- \rightarrow M + 2O^{2-}$ (1.2)

At anode: $2O^{2-} + C \rightarrow CO_2 + 4e^-$ and / or (1.3)

$2O^{2-} + 2C \rightarrow 2CO + 4e^-$ (1.4)

Net cell reaction: $MO_2 + xC \rightarrow M + xCO_{2/x}$ (x = 1 for CO_2 and 2 for CO) (1.5)

Reaction (1.2) represents the deoxidation reaction at the cathode, which may consist of one or more individual reactions. The electro-deoxidation, under a constant applied voltage, can be monitored using the electro-deoxidation curve as given in Fig. 1.2. The current, due to oxygen ions, decreases with time and stabilizes at the minimum background levels for a reasonable period of time which is considered as the end of the reduction process.

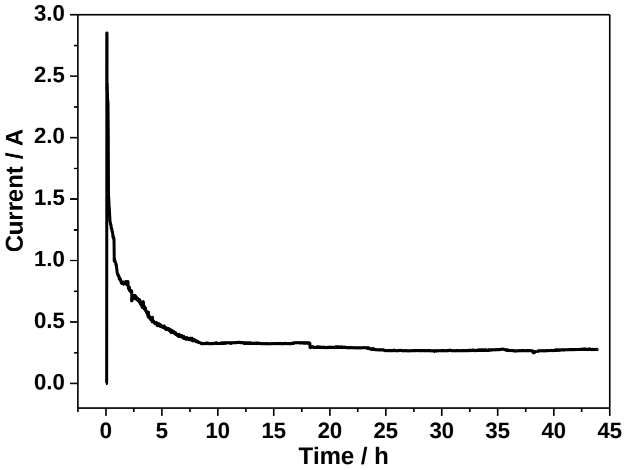

Fig. 1.2. Typical current behaviour of an FFC cell under constant applied voltage.

The process is relatively simple when compared to the conventional, high temperature chemical and electrochemical metal production processes and the conversion takes place in a single step. The solid oxide is not dissolved in the molten salt electrolyte and remains as a solid block throughout the process of conversion of the oxide to the metal. Most of the oxides which are employed as cathodes in the process are semiconductors (e.g., TiO_2) or insulators (e.g., SiO_2) [4-9]. Since the process is different from the well established conventional electrochemical processes, it demands innovative designs of the cells, electrodes and methods of analysis. The process is influenced by various parameters like the stability of the oxide, chemical nature of the electrolyte melt in which the process is carried out, applied voltage, mode of electrolysis, duration of electrolysis, porosity of the oxide preform, temperature, current density, concentration of O^{2-} ions in the melt and the nature and configuration of the oxide electrode in the cell. Calcium chloride is generally selected as the electrolyte due to its (i) good solubility for oxide ions (~ 20 mol.% at 1173 K) (ii) easy availability (iii) low cost (iv) good solubility in water etc. The process has attracted the attention of researchers world over and several studies from various laboratories across the world have been reported on the electro-reduction of the oxides of transition metals like titanium [2-4,10-40], niobium [41-50], tantalum [51-53], zirconium [11,15,54-56], chromium [39,57-59], iron [60], tungsten [61], some of the p-block elements like silicon [62-75], aluminium [76,77] and f-block elements such as uranium [78-90]. The process can also be employed for the preparation of alloys. In this case, a mixture of respective oxides is used as the cathode preform. Many studies have been reported in this regard [91-106]. When large difference exists between the melting points of the alloying metals, it is difficult to get a homogeneous alloy by melting together the constituent metals. Alloy preparation by the DOER process does not suffer from this limitation, as the alloys are not formed by melting of metals here. In fact, it is proved that metals and alloys with near-net shape can be produced by the DOER process [91]. Peng et al. [92] reported the electrolytic synthesis of consolidated Zr and Zr-2.5 Nb tubes from sintered tubular oxide preforms used as cathode in the FFC cell. Hu et al. [91] produced Ti-6Al-4V in various shapes from a mixture of the corresponding oxides slip-cast to the required shapes and it is proposed that the presence of V_2O_3 assisted the reduction of TiO_2 without the in situ formation of perovskites. A number of alloys such as $TbFe_2$ [93], $CeNi_5$ [94], Nb-10Si and Nb-18Si [95], Ni_2MnGa [96], Co-30wt.%Cr [97], Nb_3Sn [98], $TbNi_5$ [99], TiNi [100,101], Ti-10wt.%W [102,103], Ti-15wt.%Mo [104], Nb_3Al [105], $CeNi_4Cu$ [106] etc. also have been produced by the DOER process.

Apart from metal oxides, metal sulphides such as MoS_2 [107] and Cu_2S [108] have also been reduced by the DOER process. It is suggested that it can be a promising method of reduction of, not only oxides, but also sulphides to metals. Though majority of the DOER studies have been carried out in molten $CaCl_2$, some studies have also been reported in other salt melts such as LiCl-Li_2O [83,89,90], binary and ternary melts of $CaCl_2$ with other salts like NaCl [41,98], KCl [109], $BaCl_2$ [58]. Gibilaro et al. [14,86] used fluoride melt, viz. LiF-CaF_2-2wt.% Li_2O as the electrolyte and demonstrated the electrochemical reduction of titanium and uranium oxides to the respective metals.

The process of direct oxide electrochemical reduction was discovered through experiments on TiO_2 in the year 1997 [3,4]. Since then titanium oxide has been chosen as a candidate material for the study of the electro-reduction process. Several studies have been reported on the electro-reduction of TiO_2 [2,11-40,110-113]. Since the method is a promising alternative to the conventional Kroll process [114], many metal industries showed overwhelming interest in the development of the DOER process for titanium production. Metalysis, a company based in UK today holds the exclusive right to exploit the patented FFC process for all metals including Ti and the company reportedly operates a pilot plant to demonstrate the process [115]. An Australian company, BHP Billiton claims to have taken steps to operate a 100 kg batch cell for the production of Ti sponge [110]. A Norway based company namely ‘Norsk Titanium’, in collaboration with ‘Norsk Hydro’, carried out basic and scaling up experiments towards developing the process to larger scales and could achieve reduction of sizeable quantities of TiO_2 to Ti within electrolysis durations of less than 24 h

[116]. In India, Defence Metallurgical Research Laboratory (DMRL), Hyderabad has been developing the process for Ti metal and cells with an input TiO_2 quantity of 3-5 kg are being operated now [110]. Apart from the reduction of the aforementioned metal oxides, the process is also being studied for reduction of actinide oxides in nuclear industry.

The nuclear context

Nuclear energy is one of the potential options to address the energy crisis and fulfill the growing demands of electricity, which has become an inevitable basic requirement for day-to-day activities of human life [117,118]. Countries such as USA, Russia, France, Japan, UK and Republic of Korea have been operating nuclear reactors for the production of electricity. To cope up with the existing and anticipated demands of electrical energy by its growing population and industries, India has been developing nuclear energy with different kinds of nuclear reactors. The schematic of the three stage Indian nuclear power programme [119,120] is shown below.

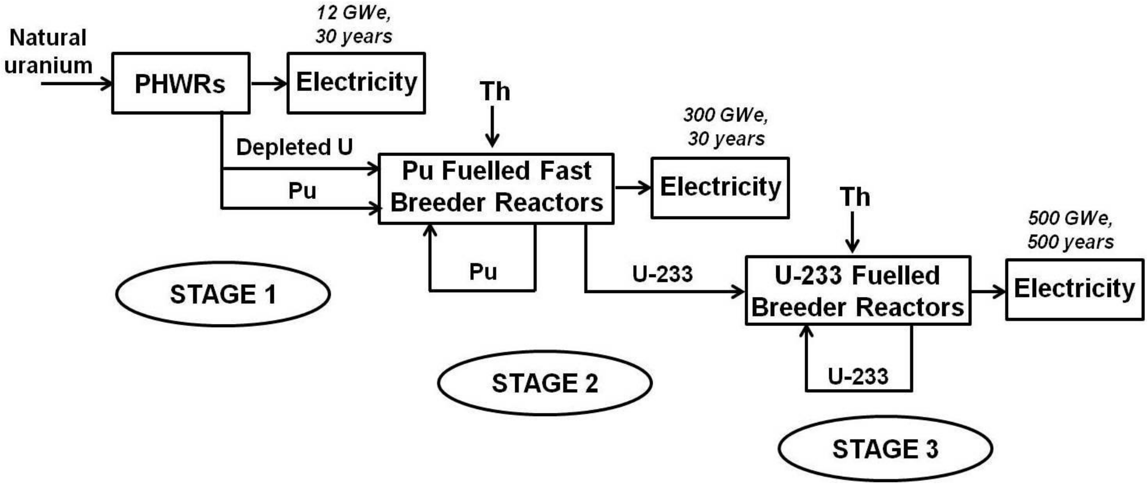

Fig. 1.3. A schematic representation of the three stage Indian nuclear power programme [120].

Uranium compounds such as oxides and carbides or solid solutions with the corresponding plutonium compounds are used as nuclear fuels. Actinide metals and their alloys can also be used as fuels in nuclear reactors. The metal fuels, (e.g., U-19Pu-10Zr), have been projected to have several advantages over the use of oxide ceramic fuels, for use in

Fast Breeder Reactors (FBRs). The metal-fuelled reactors enable extraction of higher amount of power from unit length of the fuel (linear power) and possess other advantageous features like highest breeding potential, nuclear proliferation resistance by virtue of the possibility of pyrochemical reprocessing of the spent fuels, co-location of all related facilities etc. [84,121]. Obviously, the direct oxide electrochemical reduction process is of interest in nuclear technology in the context of production of actinide metals like U and Pu and transition metals like Zr towards preparation of metal fuels. The chemical reduction processes by which these metals are produced today are very cumbersome and alternate electrochemical processes like DOER is of great importance.

Another important area where DOER finds application in nuclear technology is in the pyrochemical reprocessing of spent oxide fuels (spent fuel is the fuel which is recovered from a nuclear reactor after it undergoes permissible level of fission). As mentioned previously, most of the nuclear reactors use the oxide fuel and the spent fuel from these reactors need to be reprocessed to recover the actinides U and Pu. The reprocessing is currently carried out by the Plutonium Uranium Extraction (PUREX) process wherein the fuel is dissolved in concentrated HNO_3 and the metals are subsequently extracted by Tributyl phosphate (TBP) as the extractant. Alternatively, spent oxide fuel can be reprocessed by first converting it into an alloy by electro-reduction process and subject it to a pyrochemical process based on molten salt electrorefining process.

Pyrochemical reprocessing of spent nuclear fuels

Pyrochemical reprocessing is based on molten salt electrorefining ideally suited for reprocessing of spent metal fuels. In this process the spent fuel is electro-refined in a molten bath of LiCl-KCl at 773 K [122]. The spent fuel is used as the anode and steel or a pool of cadmium metal as the cathodes. During electro-refining, the different constituent elements of the spent fuel are separated to different parts of the cell as depicted in Fig. 1.4. The U and Pu metals that are recovered can be used for fabrication of fuels for metal-fuelled FBRs.

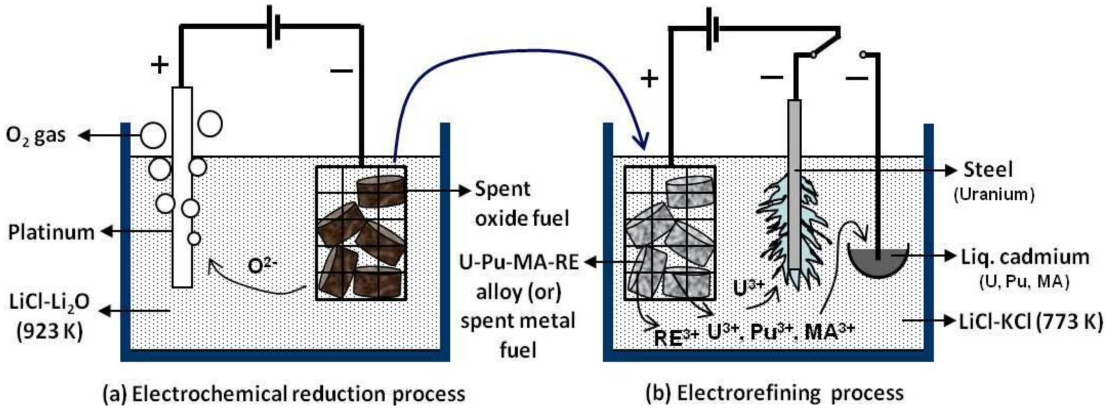

Fig. 1.4. Schematic of the electrochemical reduction and electrorefining processes (RE - rare earths, MA - minor actinides).

The spent oxide fuel cannot be reprocessed by the molten salt refining process as the solubility of the oxides is very poor in the molten salt. But the fuel can be processed by the pyrochemical method, provided the oxide fuel is reduced to metal form. Direct Oxide Electrochemical Reduction finds application in this regard to convert spent oxide fuel to a metallic alloy of (U-Pu-MA-RE) [80,84,123-125]. The alloy can then be processed by the molten salt electrorefining process to extract the actinide metals as explained above (Fig. 1.4). The DOER process, therefore, would serve as a link between the oxide fuel based nuclear reactors and metal fuel based reactors. A schematic of the oxide and metal fuel cycles and the link between the two by the electro-reduction process (DOER) is given in Fig. 1.5. A large volume of data have been generated on the electro-reduction of the actinide oxides [78-90,126-132], mixed oxides (MOX) [133,134], inactive (unirradiated) mixtures of oxides simulating the spent oxide fuel composition called ‘SIMFUEL’ [124,135,136] and active (irradiated) spent oxide fuels [80,123,137,138] by nuclear research institutes of Republic of Korea, Japan and USA. UO_2 is the major constituent of a spent oxide fuel (more than 95%) and hence most of the studies have been reported on the electro-reduction of UO_2 [78,79,82-90].

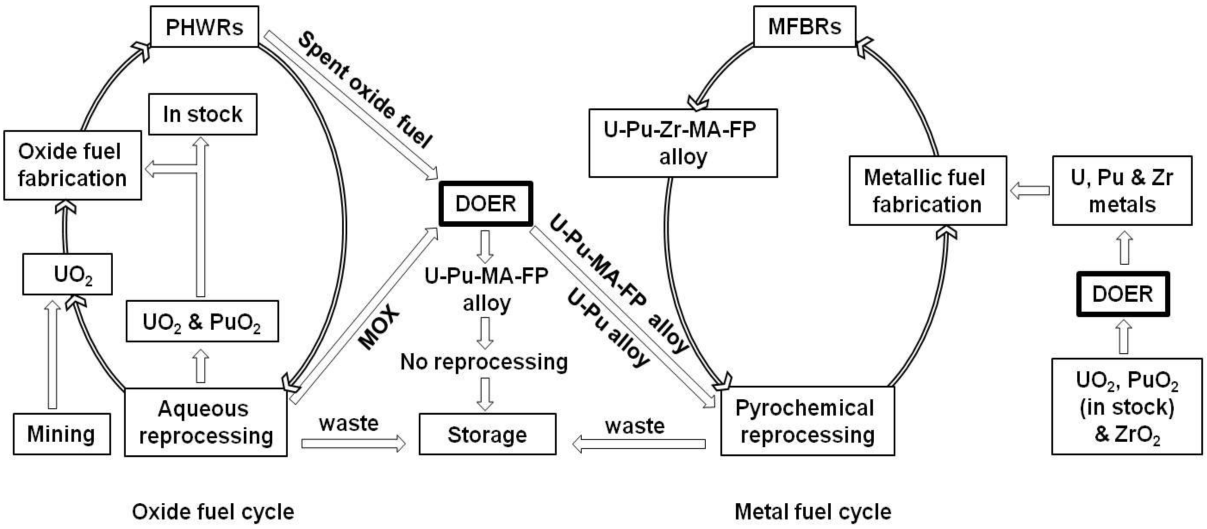

Fig. 1.5. Schematic showing nuclear oxide and metal fuel cycles linked by the DOER process (PHWRs – pressurized heavy water reactors, MFBRs – metal fuelled fast breeder reactors, MOX – mixed oxides, MA – minor actinides, FP – fission products).

While $CaCl_2$ or a molten salt mixture of $CaCl_2$ with other chlorides (e.g., $CaCl_2$-48mol.% NaCl) have been used as electrolyte in the FFC Cambridge process with graphite as anode at ~1173 K, LiCl-Li_2O melt at 923 K with Pt as the anode is used in the electro-reduction work with actinide oxides and spent fuels. This was necessitated due to the difficulty in operating molten salt cells at high-temperatures with highly radioactive fuel materials, corrosion of the cell and other structural materials at high temperatures of operation, contamination of the actinide metal with carbon and associated difficulties in the operation of oxide containing melts with graphite anodes etc. The schematic of a typical cell for electro-reduction of UO_2 is given in Fig. 1.6.

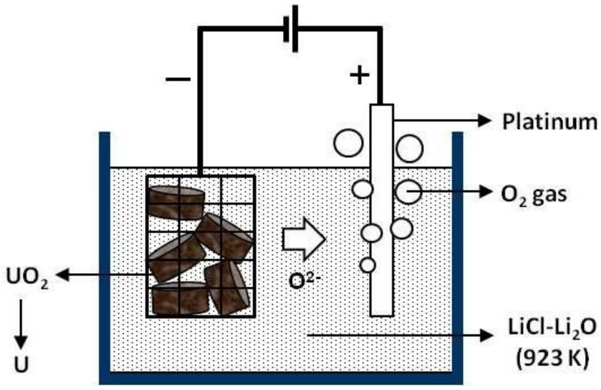

Fig. 1.6. Schematic of the electrochemical reduction cell with UO_2 as the cathode.

The cell and cell reactions, in general, are represented as

$$\textbf{Cell: Pt/LiCl, Li}_2\textbf{O(l)/MO}_x\textbf{ (s)} \qquad (1.6)$$

Half cell reactions:

$$\text{Cathode:} \quad MO_x + 2x\,e^- \rightarrow M + xO^{2-} \qquad (1.7)$$

$$\text{Anode:} \quad xO^{2-} \rightarrow x/2\,O_2\,(g) + 2x\,e^- \qquad (1.8)$$

$$\text{Net cell reaction:} \quad MO_x \rightarrow M + x/2\,O_2\,(g) \qquad (1.9)$$

Korea Atomic Energy Research Institute (KAERI) has made significant strides in the development of the DOER technology for the nuclear application. In 2006, KAERI demonstrated reduction of 20 kg of U_3O_8 powder [81] as part of its Advanced Spent Fuel Conditioning Process (ACP) [136], 10 kg of SIMFUEL in 2010 [129] and 17 kg of UO_2 pellets [83] in the recent past. The PyRoprocessing Integrated inactive DEmonstration (PRIDE) facility, commissioned recently, to demonstrate the entire spectrum of the oxide pyroprocessing technology in the engineering scale (10 ton/year) by KAERI will be yet another major development in the electro-reduction technology.

1.2. The process of transformation of the oxide electrode to metal in the DOER process

Under the influence of the applied potential, electrons are pumped into the oxide cathode of a DOER cell. Initially it was considered that the oxygen present in the metal-oxygen bonds in the electrode are broken by the influence of the applied potential and the oxygen thus released abstracts electrons available on the electrode to convert itself as O^{2-} ions and the ions are transported to the anode where it is discharged as per equations (1.2) to (1.4). However, more detailed studies on the mechanism of electro-reduction with different metal oxides proved that the cation of the electrolyte melt (Ca^{2+} in the case of $CaCl_2$) reacts electrochemically with the oxide electrode so that different ternary compounds and sub-oxides (for example, different $Ca_xTi_yO_z$ and Ti-O compounds in the case of DOER of TiO_2 in $CaCl_2$ melt) are formed during the course of electro-reduction of the electrode [12,16,18].

The electro-reduction, in such cases, essentially proceeds via the formation and decomposition of the intermediate compounds. The various chemical phases thus formed inside the electrode have different crystal structures and therefore the electrode undergoes many physical changes too during the reduction process. A typical electro-reduction curve of TiO_2 electrode in $CaCl_2$ melt showing the different compounds formed at various stages of electrolysis and the microstructure of some of the phases are given in Fig. 1.7 [12].

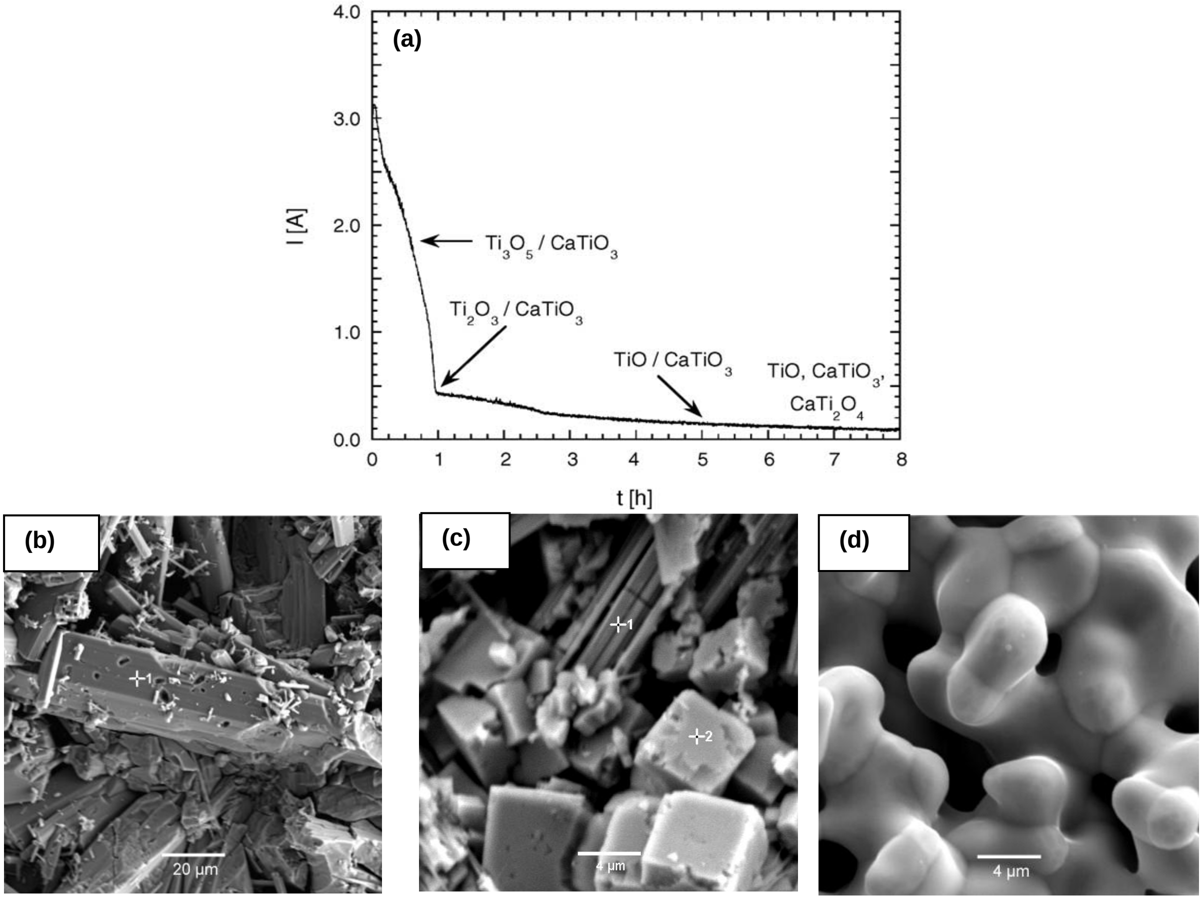

Fig. 1.7. (a) A typical I-t curve of the electro-reduction of TiO_2 in $CaCl_2$ melt reported by Schwandt and Fray [12]. Different chemical compositions of the electrode during its transformation to Ti metal are indicated on the curve. (b), (c) and (d) show the microstructures of the electrode at different stages of electrolysis [12].

Partial reduction often leads to the formation of various visibly distinguishable regions across the cathode pellets, which contain different phases. Fig. 1.8 (a) and (b) show the SEM images of the cross sections of partially reduced samples of TiO_2 [11] and ZrO_2 [54] pellets reported by Mohandas and Fray. Such features were observed in case of other oxides too [79].

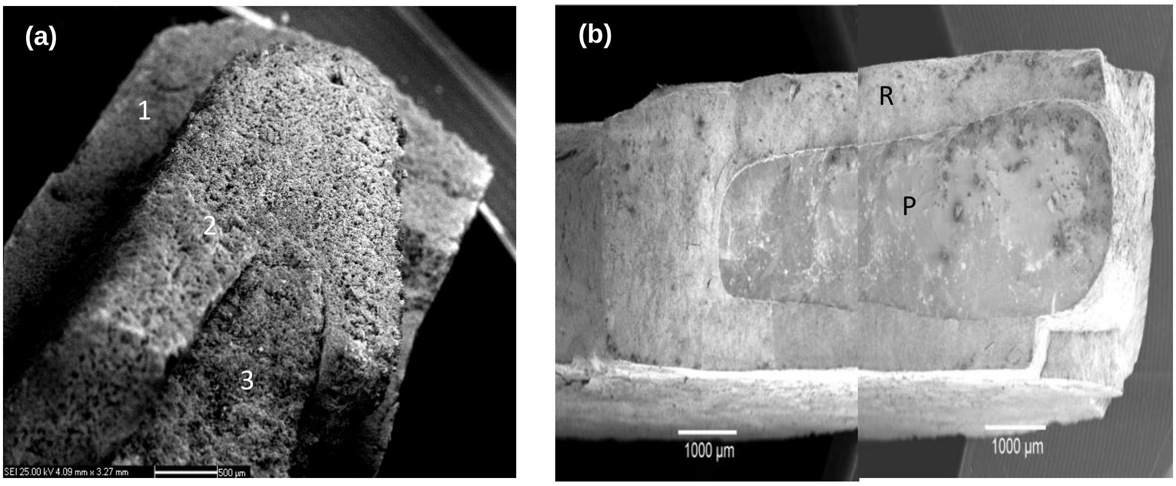

Fig. 1.8. The cross section of (a) partially reduced TiO_2 pellet showing various regions indicated by '1, 2 and 3' having different compositions and (b) a ZrO_2 pellet with reduced outer (R) and unreduced bulk (P) parts [11].

The electro-reduction of the oxide can take place only at those points where the three components, viz. the oxide, the electron and melt co-exist. So, for efficient reduction, it is necessary that the solid oxide preform is made sufficiently porous for the melt to be in contact with maximum area of the electrode and is also electronically conducting. Oxides like TiO_2 and Nb_2O_5 are sufficiently conducting at the high working temperature of the process, but it is not the case with oxides like SiO_2 and Al_2O_3. The different electrical conductivity characteristics of oxides, therefore, demand different electrode designs for achieving efficient reduction.

Chen et al. [57] proposed a three phase interline (3PI) mechanism for electro-reduction of solid oxides. In this mechanism, the reduction begins at the conductor-oxide-melt three phase interlines (3PIs) as shown in Fig. 1.9. The reduction of the oxide electrode in contact with the electrolyte melt starts at those points where it is in contact with the cathode current collector (electron supplier) and slowly extends to the other parts of the solid preform. It is observed that the surface of a pellet reduces preferentially compared to the bulk as the release of the electro-generated O^{2-} ions to the melt is easier at those areas of the pellet. The electro-reduction is a slow process due to the slowness of the diffusion of oxygen in the solid oxide grains and also due to the difficulty for transport of the electro-generated O^{2-} ions through small capillaries at the bulk parts of the solid electrode. However, a proper design of the cathode can make the process substantially faster.

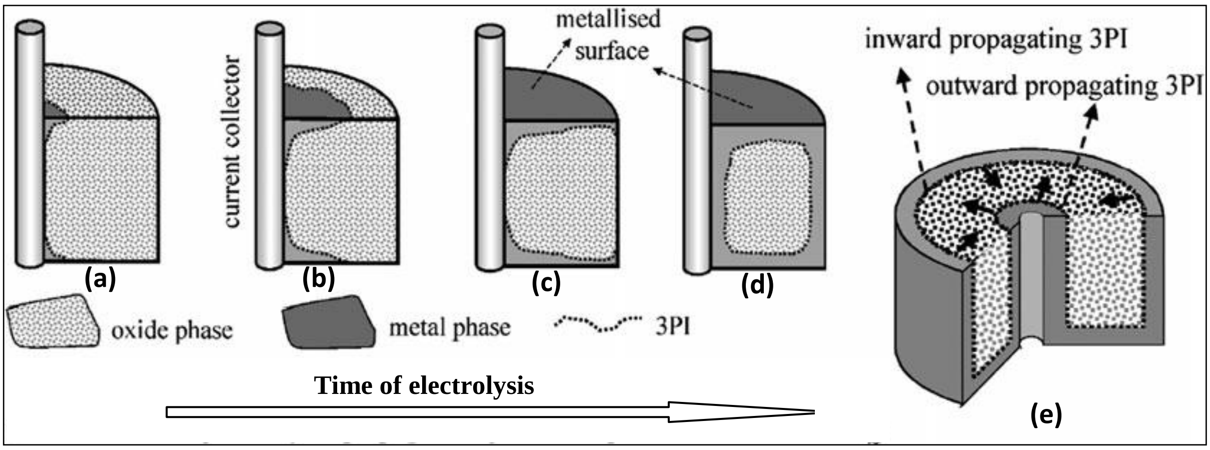

Fig. 1.9. Schematic representation of the three phase interline (3PI) mechanism of propagation of reduction in cylindrical metal oxide pellets [57].

As mentioned previously, it has been proved that several metals/alloys can be produced from their respective oxides by the DOER process. A large number of publications on various aspects of the process with different metal oxides are now available in the literature [6-8,139]. Nb, Ti and U are strategically and technologically important metals and many studies have been reported on the DOER of these metals. However, a critical assessment of the information available showed that the available data can be augmented by further research so as to develop a more comprehensive understanding of the reduction process of these metals. Hence the oxides of these three metals have been selected for study in this thesis work. As stated before, electrical characteristics of the oxide electrodes have a strong influence on their electro-reduction behaviour. SiO_2 possesses electrical properties which are radically different from that of the other three oxides and hence this oxide has also been selected for study with an aim to develop a better understanding of the influence of electrical properties of the oxide on the electro-reduction. A more focussed discussion on the importance of these metals and the available information on the DOER of these oxides are given below.

1.3. Literature survey

1.3.1. TiO_2

Titanium (atomic number, 22) is the 9th most abundant metal in the earth’s crust and 4th most suitable structural metal after iron, aluminium and copper. It has very high strength (equal to that of stainless steel), but low density (4.54 g/cc) and hence is preferred as structural metal in high-strength and low weight demanding applications like aeroplanes, cars etc. to save fuel. Due to the good strength to weight ratio, it finds use in making hockey sticks, tennis bats etc. The metal can also be used in space applications (extra terrestrial regions), chemical plants (resistance to acid/alkali attack) and ship building (resistance to highly corrosive saline water). It is also resistant to bio-corrosion and hence finds use in making of body implants (dentistry, bones joining etc.) [140]. The metal is also of great importance in strategic sectors like defence, nuclear energy etc. Titanium metal is often used in the form of its alloys (e.g., Ti-6Al-4V) for better strength and good strength/weight ratio [141].

In spite of the potential applications, titanium metal is not widely used due to its limited availability and hence prohibitive cost. Titanium metal is produced by Kroll process [114], in which $TiCl_4$ vapours are chemically reduced to Ti by Mg. It is a batch process with low yield, which makes the metal costs high. If Ti can be produced at reasonable price, it has the potential to replace steel in all its applications. Hence efforts are being made all over the world to produce titanium metal at a reasonable cost. Though several methods have been attempted, none could be made industrially successful yet. Naturally the DOER process attracted worldwide attention for conversion of titanium dioxide to titanium metal.

The direct oxide electrochemical reduction was first reported by observing that the oxygen present in titanium metal could be removed by the cathodic deoxygenation and the subsequent reduction of TiO_2 pellets to Ti metal by Prof. Fray’s group at Cambridge

University [3,4]. Since then several studies have been reported on different aspects of DOER of TiO_2 [2,11-40,110-113]. As discussed previously, Schwandt and Fray [12] showed that the electro-reduction of TiO_2 proceeds via the formation and decomposition of various Ca-Ti-O ternary intermediates and suboxides of titanium. Bhagat et al. [18] also gave more or less similar mechanism by determining in situ the phases formed by white beam synchrotron XRD. Attempts were also made to study the mechanism by cyclic voltammetry of the oxide electrode [39].

The rate of the overall reduction was influenced by kinetics of microstructural phase transformations occurring in the cathode [35]. Bixia et al. [26] observed that the TiO_2 pellets sintered in the temperature range of 1273 - 1373 K for duration of 4 h were found to undergo better reduction. Pritish Kar and Evans [111] and Ojaghi and Assadi [113] reported modelling of the electro-reduction of TiO_2 pellets in molten salts. The electro-reduction of TiO_2 was reported in LiCl based melts too and found to occur via the formation/decomposition of Li-Ti-O compounds and suboxides of Ti [13,25,37,38]. Hur et al. [38] could produce Ti from TiO_2 powder by reaction with Li generated via in situ electrolysis of Li_2O in LiCl-Li_2O melt at 923 K. Gibilaro et al. [14] established the feasibility of the reduction of TiO_2 and TiO to titanium in molten LiF-CaF_2 at 1123 K using gold as the anode. They proposed that the reduction of the bulk of the TiO pellets was relatively difficult compared to the bulk of TiO_2 pellets, though the pellets taken were of the order of ~250 mg. Electrochemical reduction of TiO_2 thin films to titanium was reported in a low melting LiCl-KCl-$CaCl_2$ eutectic (52:12:36 mol.%) at 723 K [142].

Most of the above mentioned studies were carried out with TiO_2 pellets. The use of pellets has the advantages such as ease of handling, easier recovery of the electrolysis product and its cleaning but suffers from the disadvantage of the difficulty in the reduction of the bulk. In this regard, it is ideal to use TiO_2 powder itself as the electrode, like in the case of reduction of U_3O_8 powders carried out by Jeong et al. [81]. Studies on the electro-reduction behavior of TiO_2 powders in $CaCl_2$ medium have not been reported in the literature yet, though recently Kartik Rao et al. [112] patented a process in this regard. Hence a systematic study of the electro-reduction behavior of TiO_2 powder was taken up as the part of this thesis work. Also some novel experiments were carried out with TiO_2 pellets to understand the influence of electrical conductivity of the oxide electrode on its electro-reduction.

1.3.2. Nb_2O_5

Niobium is an important transition metal that finds use mainly as an additive to construction steels [41]. The role of niobium is vital in the context of preparation of alloys having superior corrosion resistance for a wide range of applications such as launch vehicles, space crafts, nuclear power reactors etc. [41,143,144,145]. Niobium also has unique properties such as biocompatibility, shape memory effect etc. [42] and could be exploited for potential applications in medicine and surgery. Niobium is also employed for preparing NbTi alloy and Nb_3Sn intermetallic which show superconductivity [146]. The resistance of niobium against chemical attack by nitric acid (in all concentrations), dil. HCl and dil. H_2SO_4 makes it a metal of choice for making containers in chemical and nuclear industry [144].

Traditionally, niobium is prepared by metallothermic and carbothermic reduction of its oxides, fluorides and chlorides at high temperatures [147-150]. These conventional processes are labour-intensive and cumbersome and hence the cost of the metal is high. New, economically viable and environment friendly technologies are necessary to replace the old production processes. Several studies on the DOER of niobium oxides have been reported in this context.

Electro-deoxidation of Nb_2O_5 pellets in molten $CaCl_2$-NaCl eutectic was studied by Yan and Fray [41,43-45]. They proposed a conceptual mechanism and experimentally demonstrated the influence of various parameters on the electro-deoxidation process of

Nb_2O_5 pellets. Attempts were made by Xu et al. [46] to accelerate the reduction process by increasing the oxygen vacancies in the Nb_2O_5 precursor by the addition of carbon, $CaCO_3$ and CaO. Wang et al. [47] tried to determine the mechanism of electro-reduction of Nb_2O_5 in equimolar $CaCl_2$ and NaCl by employing AC impedance method, in addition to the conventional cyclic voltammetry (CV), chronoamperometry and constant voltage electrolysis techniques. Jeong et al. [48] reported an indirect (electro-generated lithium induced), constant current electro-reduction of Nb_2O_5 powder taken in a porous magnesia crucible in LiCl-Li_2O melt at 923 K using Pt rod as anode. Qiu et al. [49] observed the spontaneous conversion of Nb_2O_5 to $CaNb_2O_6$, when dipped in to $CaCl_2$ melt containing CaO and they could obtain Nb metal by the application of a minimum voltage of 2.4 V for electrolysis. Electro-reduction of Nb_2O_5 pellets in molten $CaCl_2$ under computer-aided control (CAC) of the electrode voltage was reported by Wu et al. [42] and a significant lowering in the energy consumption of the process was claimed by application of the technique. More recently, Song et al. [50] discussed the microstructural phase transformations in the Nb_2O_5 cathode during electro-reduction in $CaCl_2$-NaCl-1wt.% CaO melt. Many researchers have reported the formation of various ternary intermediates of the type $Ca_xNb_yO_z$ along with suboxides of Nb in partially reduced samples collected during cathodic deoxidation of Nb_2O_5 in $CaCl_2$ melt [41,42,44-47,49,50].

The mechanism of Nb_2O_5 reduction reported in most of the above studies is based on transient electrochemical measurements carried out on tiny oxide samples. Removal of oxygen from a solid oxide electrode by cathodic polarisation will be influenced to a great extent by the diffusion of oxygen from it and this in turn will be dictated by the morphology of the solid electrode. In the case of a pellet electrode, the surface of the electrode preferentially gets reduced compared to the interior parts and the extent of reduction decreases from surface towards the bulk. In other words, the surface and inner layers of the electrode can be reduced to different extents, especially in the beginning stages of electrolysis, and it is necessary to get the composition of the different layers in order to understand the manner in which the reduction is propagating through the solid matrix. Alexander et al. [10] have shown that the mechanism of electro-reduction of TiO_2 pellet electrodes can be different, when the pellets are sintered at two different temperatures. Mohandas and Fray [11,54] have shown that the mechanism of electro-reduction of ZrO_2 pellets is related to their physico-chemical characteristics. These results suggest that the mechanism of electro-reduction of a metal oxide arrived at based on results obtained on a tiny oxide sample may not be exactly similar to that of a larger preform like a powder-compacted pellet electrode. In such cases, it would be meaningful to deduce the reduction mechanism based on studies carried out with the large pellet itself as the sample electrode. Schwandt and Fray [12] have reported the mechanism of electro-reduction of TiO_2 based on the chemical composition of TiO_2 pellets subjected to different durations of cathodic polarization in calcium chloride melt. The same method has been adopted for investigating the electro-reduction mechanism of Nb_2O_5 in this study. The powder compacted Nb_2O_5 pellet electrode specimens were electrolysed for different durations of time along a complete electro-deoxidation curve and the physically distinct layers present in the partially electro-deoxidised samples were analysed for their chemical composition. Dense Nb_2O_5 pellets have been used, which made the diffusion of oxygen from the inner part of the pellet slower so that the oxide layers could be made reduced to different extents, stabilised for separation and analysis. During these studies, it was noticed that a striking relationship existed between the chemical composition of the oxide electrode and that of the electrolyte melt at different points of time during electrolysis, which in turn was useful in understanding the pathways of the electro-reduction of the oxide electrode. Hence the chemical composition of the bulk electrolyte and the salt adhering to the cathode pellet were separately determined to understand their influence on the results to the electro-reduction of the Nb_2O_5 pellets. The influence of various parameters on the electrochemical reduction of Nb_2O_5 pellets was also studied and the details of the study are presented.

1.3.3. UO_2

Uranium is a metal of paramount importance in nuclear industry. Its oxides and carbides in combination with similar compounds of other actinide metals like plutonium are used as fuels in nuclear reactors. Uranium metal can also be used as fuel in the form of an alloy with other metals (e.g., U-19Pu-10Zr). Currently the metal is being produced chemically via the reduction of the fluorides of uranium with magnesium at high temperatures. Like Ti and Zr, production of uranium from its oxides is also very cumbersome and labour intensive and hence alternate production processes are of interest.

Research organisations like Korea Atomic Energy Research Institute (KAERI), Korea; Argonne National Laboratory (ANL), USA; Central Research Institute of Electric Power Industry (CRIEPI), Japan have been making significant R&D efforts to convert uranium oxides to U metal by the DOER process [83,78,79]. Lithium chloride melt containing 1-3 wt.% Li_2O has been used as the electrolyte in the DOER process for U production with platinum as the anode at 923 K [78-83,85-87,135]. Calcium chloride melt offers a better reducing environment than lithium chloride melt and the melt (at ~1173 K) was used in most of the electro-reduction studies of other solid oxides [4,8,63,139]. However, the high melting $CaCl_2$ electrolyte (m.p., 1045 K) is not favoured in the DOER of UO_2 as the reduced U metal forms an impermeable metal film on the surface due to sintering of the metal at the high operation temperature of the cell [79]. The metal film covers the surface of the solid electrode and thus prevents the accessibility of the melt to the bulk parts of the preform and hence the reduction of such of those areas of the electrode. In this context, it was thought that using an electrolyte melt containing calcium chloride at an operation temperature much lower than 1173 K, could possibly be a solution to the problems faced. This possibility has been explored in the thesis work. A salt composition of $CaCl_2$-48mol.% NaCl with a melting point of 775 K offered such a possibility and hence was selected as the electrolyte in the present study. Preliminary studies had indicated that the electrolyte melt at 923 K has many desirable features for the electro-reduction of UO_2 including a low rate of corrosion of the graphite anode. In order to develop a thorough understanding on the fundamental aspects of the electro-reduction of UO_2 in general and the reduction behaviour in $CaCl_2$-48mol.% NaCl melt in particular, a systematic study of the electro-reduction of UO_2 pellets was carried out in the melt. The influence of parameters such as temperature, duration of electrolysis, applied voltage, mode of electrolysis and open porosity of the UO_2 pellets on its electrochemical conversion to U metal in the melt has also been studied. In addition, attempts were also made to generate some information on the oxidative corrosion behaviour of the graphite anodes, used in these experiments, under different experimental conditions.

Various workers have proposed different mechanisms for electro-deoxidation of uranium oxides in LiCl-Li_2O melt at 923 K. Park et al. [127] and Jeong et al. [130] proposed that reduction of U_3O_8 takes place through chemical reaction of lithium metal which is electro-generated at the oxide cathode under the polarising conditions. Gourishankar et al. [78] predicted that reduction of UO_2 to uranium in LiCl-1wt.% Li_2O melt should occur via a multi-step electron transfer reaction involving the formation of intermediate phases. However, based on results of the constant current electrolysis and cyclic voltammetric studies, Biju Joseph et al. [85] proposed that the reduction could be taking place by a single step electron transfer and devoid of formation of any intermediates. More recently, Choi et al. [83] emphasized the role of the ratio of cathode/anode surface area in the attainment of high current density for the process and reported a sizeable production of uranium metal from powder compacted and sintered UO_2 pellets. Jin-Mok Hur et al. [132] reported that under potentially deposited lithium could be playing a role in the reduction process. In the present study, though with a different electrolyte melt and anode, efforts have been made to gain a better understanding on the mechanism of electro-reduction of UO_2 pellets by following the chemical changes that occurred in the oxide electrode during the course of the reduction process.

1.3.4. SiO_2

SiO_2 is an interesting oxide, which possesses very different electrical properties when compared to the other three oxides discussed above. The properties which make DOER of SiO_2 so interesting are (i) SiO_2 is an insulator [5] whereas the other oxides are relatively good conductors (ii) Si has a tendency to form Si_xM_y (M = Ca or Li) compounds with Ca or Li [73] in $CaCl_2$ or LiCl melts whereas the metals of other three oxides do not form such compounds and (iii) Si doesn't have any stable intermediate oxidation states; it has only +4 and 0 oxidation states whereas the other metals have multiple oxidation states. Several studies have been reported on the electrochemical reduction of SiO_2 [62,63-75].

The insulating nature of SiO_2, it is expected, makes it behave differently in a DOER cell compared to the other oxides. Nohira et al. [62] reported pinpoint electrochemical reduction of a quartz plate (SiO_2) by employing a 'contacting electrode' cathode configuration in $CaCl_2$ melt and it is shown that the quartz plate got reduced only at those points where the electron-conducting wire was in contact. The reduction extended to the adjoining SiO_2 particles as the freshly formed silicon made electron-conducting bridges to those particles. The electrochemical reduction was reported to occur via the reaction, $SiO_2 + 4e^- \rightarrow Si + 2O^{2-}$ [64] and by strictly following the 3PI mechanism, discussed previously [151]. This aspect was verified by some novel experiments with SiO_2 pellet electrodes and the results are compared with those obtained with conducting oxide (TiO_2) electrodes to demonstrate the influence of electrical conductivity of an electrode on its electrochemical reduction.

1.4. Incomplete electro-reduction of solid oxide preforms and determination of the extent of reduction

Often it has been reported that the reduction of thick solid preforms by DOER is not uniform and complete and that the surface gets reduced better than the bulk. Incomplete reduction of the preforms could be due to several reasons such as (i) passing of less charge than that actually required for full reduction (ii) the high stability of the compounds generated during electro-reduction (iii) kinetic hindrance to the reduction of the bulk of pellet etc. The probable reasons for such a behavior in the context of electrochemical reduction of thick ZrO_2 pellets have been discussed by Mohandas and Fray [54]. Many studies have been reported which presented samples that are incompletely reduced as given in Fig. 1.10 for (a) ZrO_2, (b) UO_2 and (c) SiO_2. The reduced and unreduced regions in the samples are indicated by legends ‘1’ and ‘2’, respectively.

In some cases, despite passing more than the charge required for reduction, the oxide electrode, especially the bulk parts, remained unreduced. For instance, during the electrochemical reduction of uranium dioxide (in the form of pellets or discs) in $CaCl_2$ melt at 1073 K, the pellets were often found to get reduced partially [79]. Since UO_2 is one of the systems undertaken for study, a knowledge on the extent of reduction and its propagation in the pellet was required for a better understanding of the reduction process. For this it was required to estimate the amount of metallic uranium present in the incompletely reduced solid product. Many methods have been reported for estimation of the metal in presence of its oxides in partially reduced UO_2 samples [152,123,126,153,154]. One such method depends on quantitative measurement of hydrogen released from reaction between the metal and an appropriate acid and then estimating the amount of metal reacted with the acid. In this thesis work, the quantitative estimation of uranium metal present in incompletely reduced samples was carried out by using an in-house developed proton exchange membrane based hydrogen sensor (PEMHS) [155-158]. The details of the technique are discussed in chapter 2.

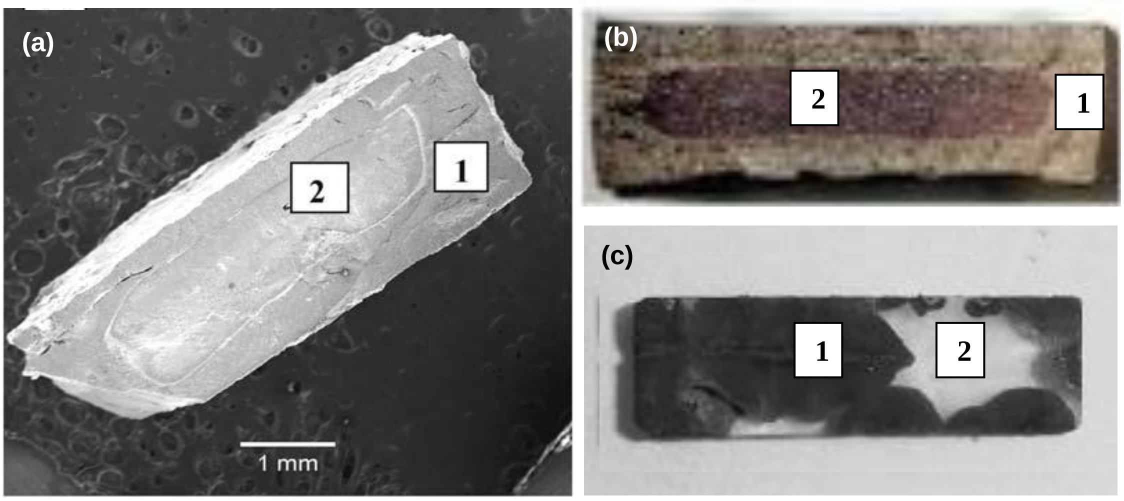

Fig. 1.10. Incompletely reduced samples obtained from DOER (a) SEM image of the cross section of ZrO_2 pellet [54] (b) photograph of the cross section of UO_2 pellet [87] (c) photograph of SiO_2 (quartz plate) [74]. The region indicated by '1' is reduced and that by '2' is unreduced.

1.5. Phase diagrams of Nb-O, Ti-O, Si-O and U-O in the context of electrochemical reduction of Nb_2O_5, TiO_2, SiO_2 and UO_2.

The DOER process is strongly influenced by the electrical conductivity of the solid cathode and the stability of the oxide in addition to many other parameters mentioned previously. Phase diagrams can be used to get first hand information on the metal-oxygen system and hence a direction to study the electro-reduction process of the oxide. The phase diagrams of Si-O [168], U-O [169], Ti-O [170] and Nb-O [171] systems are given in Figs. 1.11 (a-d).

The Gibbs energies of formation of the four oxides, viz. Nb_2O_5, TiO_2, SiO_2 and UO_2 at 1173 K are -1390.15, -732.22, -716.69, -883.66 kJ/mol [159], respectively. The data show that SiO_2 is the least stable among the four oxides and hence its reduction process is expected to be the least difficult one thermodynamically. However, SiO_2 is an insulator even at high temperatures (electrical conductivity of SiO_2 is in the range of 10^{-11} - 10^{-9} $\Omega^{-1}cm^{-1}$ in the temperature range 1073 - 1223 K [5]) and hence the reduction can be expected to be difficult from the angle of electrical conductivity of the electrode. The phase diagram of Si-O (Fig. 1.11a) shows that SiO_2 is the only stable compound in the Si-O binary system and the system does not have any suboxides. This, in other words, means that Si does not have multiple valence in the Si-O system and hence the reduction should take place in one step transfer of four electrons, i.e., +4 to 0. The multiple valence of an oxide could make the solid cathode electrically conducting during electro-reduction and obviously this advantage is not there for SiO_2. These unique properties of SiO_2 should indicate that multiple electron supply points to the electrode are necessary for a faster reduction of the preform, which indeed was proved experimentally by Nohira et al. [62]. In the absence of lower valence than +4 (Fig. 1.11b), a UO_2 electrode can also be expected to behave in a more or less similar way to that of SiO_2. However, the semiconducting nature of UO_2 [160,161] may provide a better electrical conduction to the solid electrode. However, the thermodynamic stability of the oxide is higher compared to SiO_2 and this may demand a higher energy for the reduction of UO_2. In contrast to the aforementioned two oxides, the phase diagrams Ti-O (Fig. 1.11c) and Nb-O (Fig. 1.11d) show the existence of suboxides of Ti and Nb. The enhanced electrical conduction of the matrix by way of the multiple valence and semi-conducting nature of these oxides [162-167], therefore can be expected to significantly favour their electro-reduction. However, the difference in the thermodyanamic stability of the two compounds would make the reduction energetically different. The existence of highly conducting Magnelli phases in sub-stochiometric TiO_2 [Ti_nO_{2n-1} (where $4 < n < 10$)] enables the electrode to be highly conducting in the beginning stages of the electrolysis itself. The influence of the physico-chemical characteristics of the different oxides in their electro-reduction will be discussed at appropriate places in the forthcoming chapters.

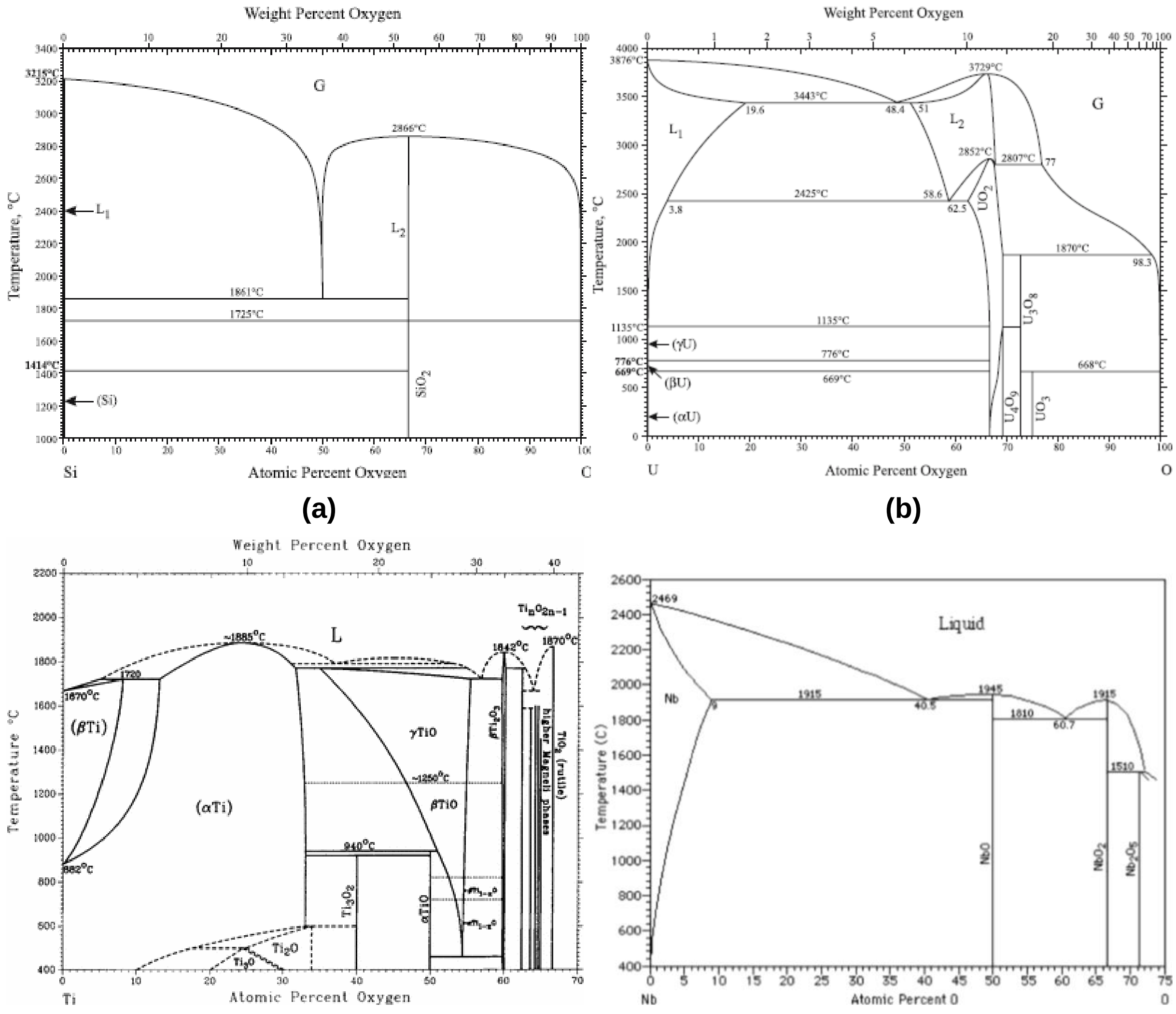

(a) (b)

(c) (d)

Fig. 1.11. Phase diagrams of (a) Si-O (b) U-O (c) Ti-O and (d) Nb-O systems [168-171].

1.6. Objectives of present work

The study is aimed at probing the fundamental aspects of electro-reduction of Nb_2O_5, TiO_2, SiO_2 and UO_2 with techniques and approaches that were hitherto not applied to the metal oxides, and thus to augment the information on DOER of these oxides already available in the literature. The specific issues taken up for detailed study are,

1. A systematic study of the electro-reduction mechanism of Nb_2O_5 to Nb in $CaCl_2$ melt at 1173 K by analysis of the chemical composition of the electrodes and electrolyte melt during different stages of electro-reduction and the influence of various factors on the electro-reduction.

2. Investigations on the fundamental issues of DOER of TiO_2 powder in $CaCl_2$ melt.
3. A demonstration/study of the difference in the DOER of an electrically conducting (TiO_2) and electrically non-conducting (SiO_2) electrode in $CaCl_2$ melt.
4. A study of the mechanism and factors affecting the reduction of UO_2 in low melting $CaCl_2$-48mol.% NaCl melt.
5. Develop a simple method for determination of the extent of reduction of partially electro-reduced UO_2 samples and the progress of reduction through the solid oxide.

1.7. Organisation of the thesis

The thesis presents the results of the investigations carried out with the above objectives. The results of the investigations are presented in detail in the ‘core chapters - 3, 4, 5 and 6’. The core chapters are preceded by two chapters, the ‘Introduction’ and ‘Experimental’ and are succeeded by a chapter on the ‘Summary and conclusions’ of the thesis. The first chapter introduces the background and literature survey pertaining to the work. The second chapter describes the experimental aspects behind the work carried out. Third chapter is dedicated to the study of fundamental aspects of DOER of Nb_2O_5 in $CaCl_2$ melt and under different experimental conditions. A few interesting but hitherto unexplored aspects of the DOER of TiO_2 and SiO_2 are presented in chapter 4 of the thesis. A detailed study of the mechanism of DOER of UO_2 in $CaCl_2$-48mol.% NaCl melt and factors influencing the reduction are discussed in chapter 5. Chapter 6 is dedicated to the discussion on the development of a method, called ‘Metal Estimation by Hydrogen Sensor (MEHS)’, employed for determination of the extent of reduction of partially reduced UO_2 samples containing U-UO_2 mixtures obtained from DOER studies. Chapter 7 summarises the results of the thesis work discussed in the previous chapters. The thesis is concluded with some suggestions for future work.

CHAPTER 2

Experimental techniques, chemicals, facilities and instrumentation

2.1. Introduction

The experimental techniques and methods adopted in the study are discussed in this chapter. Details of various chemicals and equipments used, principles and the procedure followed during different stages of the high temperature electro-reduction work and methods of analysis of the products and electrolyte salt are discussed. In addition, the chapter describes briefly the theory involved in the cyclic voltammetric studies, electrolysis etc. The principles and procedure employed for the development of a hydrogen sensor based uranium estimation method are included towards the end of this chapter.

2.2. Chemicals and materials

Moisture free salts, to be used as electrolyte, were prepared from as received salts such as $CaCl_2.2H_2O$ (Extra Pure, Merck), NaCl (Extra Pure, Lobachemie), KCl (Extra Pure, Lobachemie) and LiCl (Anhydrous, Sigma Aldrich). Different oxide powders, viz. Nb_2O_5 (>99.9 % purity, Alfa Aesar), TiO_2 (>98% purity, Rankem, India), SiO_2 (>99.5% purity, Alfa Aesar) and UO_2 (nuclear grade, obtained from Atomic Minerals Directorate, Hyderabad and Nuclear Fuel Complex, Hyderabad) were used in the preparation of electrodes (pellets) in the DOER work. Polyvinyl alcohol (binder), polyethylene glycol (plasticiser) and isopropyl alcohol (for slurry preparation) were used in the preparation of the pellets. Acid-base titration, to obtain the chemical composition of the electrolyte melt, was carried out with standard chemicals and indicators. In the work on the estimation of uranium metal in a mixture of uranium and uranium oxide by the hydrogen sensor method, zinc wire (>99.9% purity, Metals-Byproducts co., UK), uranium metal (obtained from BARC, Mumbai), UO_2 (obtained from Atomic Minerals Directorate, Hyderabad) and 48% HBr (Lobachemie, India) were used.

Tantalum (cup or wire) or stainless steel (cup or wire) were employed to hold the oxide electrode in the molten salt cell. It also served as the electrical lead to the oxide electrode. Graphite rods (M/s. Nickunj Group, Mumbai) were employed as anodes in the electro-reduction cells. Nickel wire, NiO powder (Sigma Aldrich, 99.8% purity) and one end closed alumina tube (M/s. Naskar ceramic, India) were made use of in the preparation of reference electrodes. Alumina crucibles were used as containers of the molten salt in the cells. An inert atmosphere glove box facility available in the Direct Oxide Reduction Programme (DORP) laboratory, Indira Gandhi Centre for Atomic Research (IGCAR), the details of which are described later, was used for handling air sensitive chemicals and freshly prepared metal and a vacuum oven for drying of the salts.

2.3. High temperature electro-reduction experiments

2.3.1. Preparation of salt

Principle: Salts, such as calcium and lithium chlorides, used in the present study invariably contain water and it was required to remove it completely prior to their use in the electrochemical process. Thermogravimetric analysis (TGA) of $CaCl_2.2H_2O$ showed that the occluded water could be rapidly removed at temperatures above 373 K [33]. A fraction of the salt undergoes hydrolysis to form $Ca(OH)_2$ which gets converted to CaO while heating. Lowering the temperature of drying would help in minimizing the hydrolysis reaction [20]. Though the water of crystallisation is removed at 517 K as observed in the TG analysis [33], the application of vacuum during the drying process, hastens the removal of the adsorbed as well as water of crystallization from the salt even at a low temperature of 473 K.

Procedure: Anhydrous $CaCl_2$ was prepared from commercially available $CaCl_2.2H_2O$ by pre-drying under argon at a flow rate of 15 LPH at 423 K for 24 h, followed by drying at 473 K for 48 h under vacuum (~ 10^{-3} mbar) in an oven as shown in Fig. 2.1. The CaO content of the dried salt was estimated by acid-base titration method and was found to be ~ 0.0057 mol%. Other salts such as NaCl, KCl and LiCl were dried under vacuum at 473 K for 48 h. They contained no oxides as determined by titration method. All the vacuum dried salts were stored inside an argon atmosphere glove box for preventing the absorption of moisture from the atmosphere. Either an individual salt such as $CaCl_2$ or a combination of two or more salts such as KCl-25mol.% $CaCl_2$, $CaCl_2$-48mol.% NaCl or LiCl-KCl-$CaCl_2$ (50.5: 44.2: 5.3 mol.%) were used as electrolytes in different experiments. The eutectic salt mixtures were prepared by weighing and mixing the component salts in appropriate quantities.

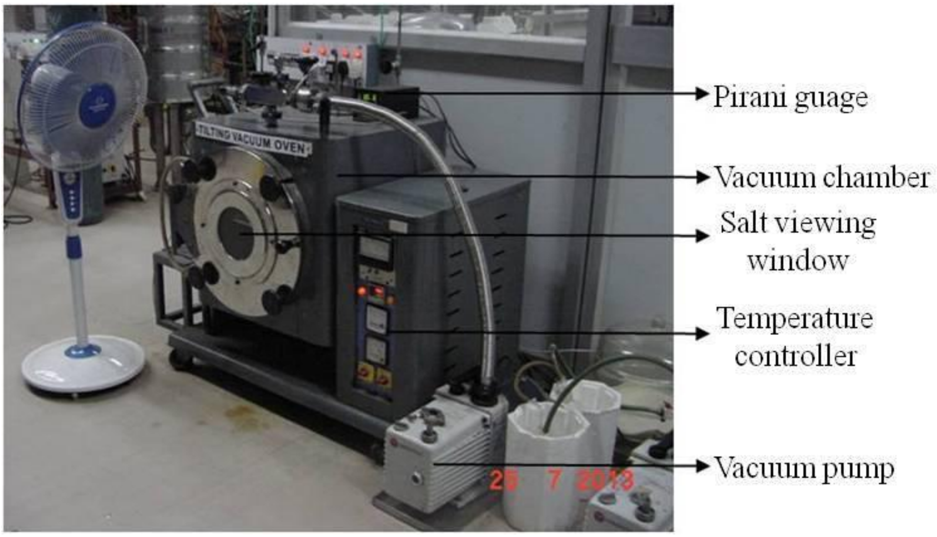

Fig. 2.1. The vacuum oven employed for drying of salts.

2.3.2. Preparation, sintering and porosity measurements of oxide pellets

Principle: Most of the oxides of metals such as Nb, Ti etc. are ceramic in nature. When powders/pellets of such a metal oxide is heated and maintained at temperatures above 2/3 of its melting point, individual particles coalesce to form lager particles. With increase in the temperature and/or time, the open spaces present within the matrix shrink and some of them lose connectivity completely and are called closed pores. The other pores which are open to surface are called open pores. If the high temperature treatment is done for longer duration of time, even the closed pores could vanish and the density of the preform could reach close to its theoretical density. This process of densification due to diffusion is called sintering [172,173]. The open porosity (OP) of the oxide pellets is of interest in the DOER work since it increases the available surface area for electrochemical reaction and hence the rate of electrochemical reduction [11]. It is determined by Archimedes principle and using the following equation:

$$\% \text{ pen porosity} = [(W_{wpa} - W_{dpa}) / (W_{wpa} - W_{wpw})] \times 100 \qquad (2.1)$$

where, W_{wpa} is the weight of the water impregnated pellet in air, W_{dpa} - the weight of dry pellet in air and W_{wpw} - the weight of the water impregnated pellet in water. Total porosity and closed porosity of the pellet can be determined by the following equations

$$\% \text{ total porosity} = [(TD - MD) / (TD)] \times 100 \qquad (2.2)$$

$$\% \text{ closed porosity} = \% \text{ total porosity} - \% \text{ open porosity} \qquad (2.3)$$

where, TD represents theoretical density and MD - the measured density calculated from the geometrical dimensions and mass of the pellet.

Procedure: Nb_2O_5, TiO_2 and SiO_2 powders were used in the preparation of pellets. The average particle size, i.e., d(0.9), of the as received Nb_2O_5, TiO_2 and SiO_2 powders was analysed by a particle size analyzer (Master sizer 2000, M/s. Malvern instruments) and was found to be about 37.1 µm, 16.1 µm and 7.9 µm, respectively. In each case, the oxide powder was mixed with 1 wt.% polyvinyl alcohol (binder) and 0.5 wt.% polyethylene glycol (plasticiser). The mixture was made into slurry in isopropyl alcohol and thoroughly ground using a mortar and pestle and dried at about 373 K. The dried mass was again ground by adding isopropyl alcohol and dried. The procedure was repeated three times to facilitate the homogenisation of the mixture. The powder obtained after evaporation of the alcohol was uni-axially compressed into 12.5 mm (~1.5 g) and 25 mm dia. (~3 g) pellets under a load of 1.5 T using a hand driven hydraulic press as shown in Fig. 2.2a using a die with a 12.5 mm or 25 mm dia. bore and an appropriate plunger (given in inset of Fig. 2.2a). The green pellets thus obtained were then sintered in air at the desired temperature (T_s), generally in the range of 1173 K – 1773 K, for 3 h in a sintering furnace (Carbolite, RHF 1600, UK), shown in Fig. 2.2b. A typical temperature programme, as given below, was used in the heating.

$$\text{RT} \xrightarrow{\text{5 K/min}} \text{873 K} \xrightarrow{\text{1 h}} \text{873 K} \xrightarrow{\text{5 K/min}} T_S \xrightarrow{\text{3 h}} T_S \xrightarrow{\text{5 K/min}} \text{773 K} \xrightarrow[\text{cooling}]{\text{Natural}} \text{RT}$$

where, RT denotes the room temperature. The sintered pellets were weighed accurately using an electronic balance (A & D company limited, Japan) and their dimensions measured. The pellets were impregnated with water under vacuum for about 3 h. A density measurement kit as shown in Fig. 2.2c, obtained from the same company, was employed to measure the weight of the water impregnated pellet in air and water. The pellets after porosity measurement were dried at 423 K for 6 h under vacuum for removal of moisture and were used in the preparation of the cathodes in the electro-deoxidation experiments.

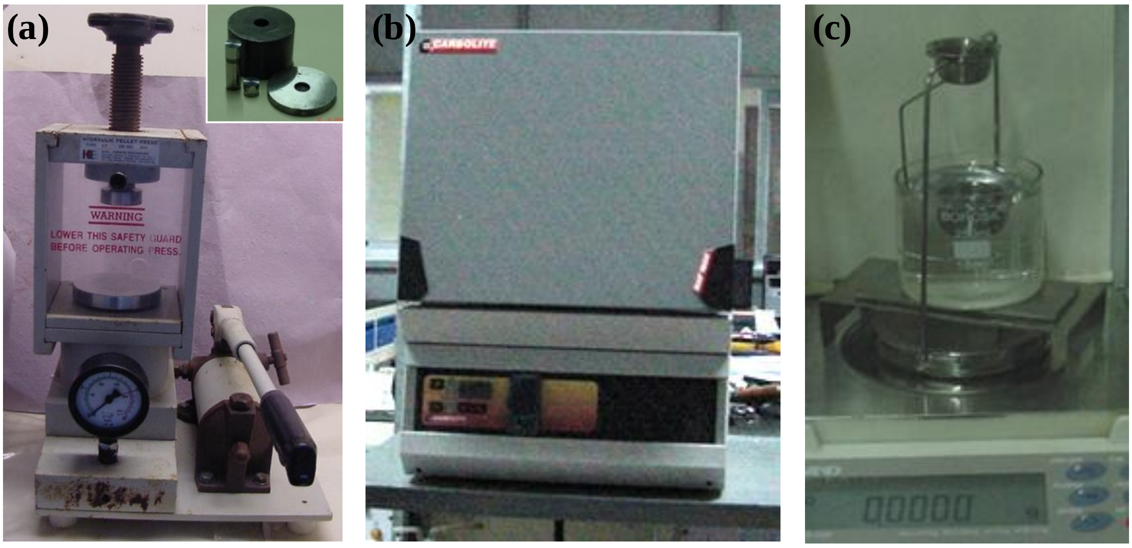

Fig. 2.2. The equipments used in the preparation of pellets and their open porosity measurements, (a) hand driven hydraulic press with inset showing a die and plunger (b) sintering furnace (c) density measurement set up for determination of open porosity.

2.3.3. Preparation of the oxide cathode assembly

The sintered oxides, as pellet, powder, and/or broken pieces, were used as cathodes. Photographs of a typical electrode assembly (Fig. 2.3a) and the bottom portions of various cathode assemblies used in the study are shown in Fig. 2.3.b-j. The oxide samples were either tied with a metallic wire of suitable material (Fig. 2.b-f) or held in a perforated cup (Fig. 2.g-j). In most of the electro-reduction experiments on Nb_2O_5, pellets (~1.5 g each, ~4 mm thick and ~11 mm dia.) were placed in a tantalum cup (20 mm OD, 30 mm long and with 40 holes of ~1.5 mm dia. drilled on its cylindrical surface) as shown in Fig. 2.3g. In such cases, each pellet was wrapped around with a 1 mm dia. tantalum wire to increase electrical contact area of the electrode. In some experiments, the oxide pellet (mass ~3 g, ~20 mm dia., ~2.5 mm thick, open porosity 5-10%) was tied with a tantalum wire to enhance the electrical contact area (Fig. 2.3e). In a few cases, the tantalum wire was tied close to the edge of the pellet to enable experiments to be carried out with the oxide alone in contact with the melt (Fig. 2.3.b). In such cases, a hole of about 1-2 mm is drilled through the pellet at about 4 mm from the edge. TiO_2 (mass 1.5 g or 3 g, 25 mm dia.) and SiO_2 (1.5 g, 25 mm dia.) pellets were also tied with a Ta wire in a similar way. In experiments where TiO_2 powders were used as the cathode, the powders were contained in stainless steel crucibles. Depending on the mass of the powder taken, stainless steel crucibles of two different sizes (18 mm dia. x 22 mm height for 1.5 g of the powder and 22 mm dia. x 40 mm height for 10 g of the powder) either lined inside (Fig. 2.3j) or wound outside (Fig. 2.3i) with SS wire mesh were used.

UO_2 pellets (~1.5 g, 12.5 mm dia., 3-5 mm thick, ~13% open porosity), prepared by powder compaction and sintering at 1823 K under reducing atmosphere for 3 h and placed in a perforated tantalum cup were employed as cathodes in some experiments where $CaCl_2$ was employed as the electrolyte. For rest of the experiments, UO_2 pellets (~15 g each) obtained from Atomic Minerals Directorate (AMD, Hyderabad) and Nuclear Fuel Complex (NFC, Hyderabad) were used. The OP of the pellets was determined using Archimedes' method and found to be ~5% in case of pellets obtained from AMD and ~48% for those from NFC. These were cut into pellets of 14.30 mm dia. x ~2.0 mm thick x 2.5 g mass and one such pellet tied to 1.2 mm SS wire as shown in Fig. 2.3d, was employed as the cathode in each experiment. The electrodes were attached to 1.75 mm dia. SS rods as current collectors which were insulated from the body of the reactor cell by tightly sealing them in alumina tubes as shown in Fig. 2.3a.

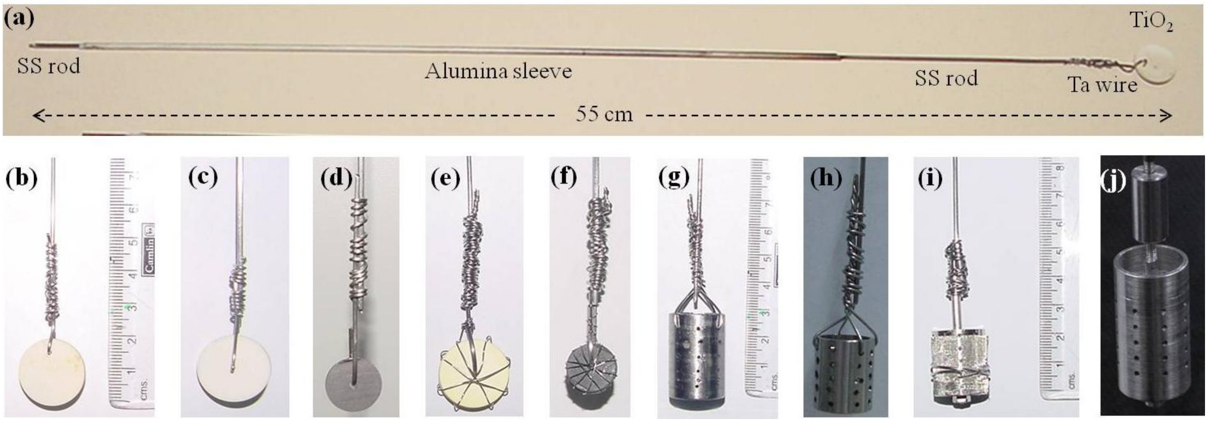

Fig. 2.3. Photographs of different cathode assemblies.

2.3.4. Preparation of anode

Graphite rods supplied by M/s. Nickunj Group, Mumbai, were used as the anodes (10 mm dia., 100 mm long and density, 1.85 g/cc) in most of the experiments. Prior to use in the experiments, the graphite rods were degassed under vacuum at 973 K for 3 h. The rod was polished with an emery sheet and cleaned with acetone to remove the resistive oxide layer on the surface and thus to provide a fresh electrode surface to the melt in each experiment. An internal threading (M3) was made at one of the ends of the graphite rod which was then tightly screwed to a SS rod (3 mm dia.) having an external threading (M3) to hold the rod intact during electrolysis. The graphite rods were weighed prior to use. Fig. 2.4 shows the photograph of a graphite anode assembly. In some experiments, a pyrolytic graphite sheet was used as the anode by tying it to a 3 mm dia. stainless steel rod.

Fig. 2.4. Photograph of a graphite rod anode along with SS current collector.

2.3.5. Reference electrode preparation

Three kinds of reference electrodes were employed and tested for their stability in the melt for extended periods of time, so that it could be used to monitor the electrode potential during the entire course of an electro-reduction reaction. The electrodes were: 1) Graphite pseudo-reference electrode-I (GPRE-I) in which the graphite rod was dipped as such into the melt in the DOER cell, 2) Graphite pseudo-reference electrode-II (GPRE-II) in which the graphite rod was placed in the reference electrolyte contained in a one end closed alumina tube having a pin hole at the bottom for electrical contact between the reference electrolyte and cell electrolyte and 3) a Ni/NiO reference electrode. The first two reference electrodes were employed only in few earlier experiments. Otherwise, Ni/NiO reference electrodes, which exhibited better stability, were used in most of the studies.

A schematic of the Ni/NiO reference electrode is shown in Fig. 2.5. The reference electrode assembly had a 600 mm long Ni wire (1.25 mm dia.) embedded in NiO powder housed in a one-end-closed alumina tube having an orifice (<1mm dia.) at the closed end. A thick pad of quartz wool was placed at the hole in the closed end to prevent entry of the main cell electrolyte into the reference cell compartment. The open end of the alumina tube with the Ni wire projecting out was sealed leak-tight with a sealant.

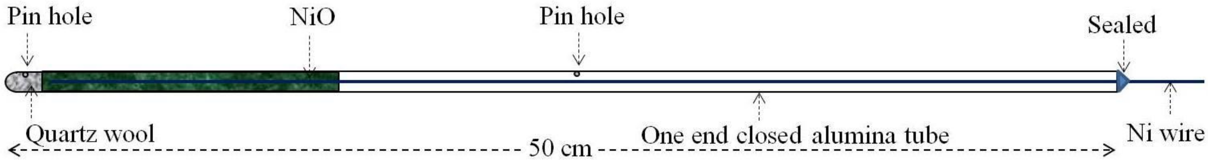

Fig. 2.5. Schematic of a Ni/NiO reference electrode.

2.3.6. Design of the electrolytic reactor

A new electrolytic reactor was designed and fabricated for high temperature molten salt work. Fig. 2.6 shows the drawing and details of the top flange, reactor and the photograph of the reactor. The stainless steel reactor has a long cylindrical body which was welded to a thick flange. The mating flange of the reactor is provided with veco type couplings with teflon feedthroughs which allow the introduction of electrically-insulated electrodes to the reactor vessel in a leak-tight manner. The flange also has been provided with argon gas inlet/outlet so that the experiments can be carried out under the inert gas blanket. The two flanges mate leak-tightly by placing a grafoil gasket in between and tightening with bolts and nuts. Stainless steel fins provided below the vessel flange and a fan blowing air on to the fins help to cool the flange and thus protect the teflon feedthroughs and the O-ring seal (when O-ring is used instead of grafoil gasket) during the high temperature operation of the cell. The use of fins for cooling, in place of the conventional water cooling, could avoid accidents otherwise possible by stoppage of coolant flow by pump/electrical failure or by leakage of water during unattended and long-term operation of the high temperature cells. Also, the absence of water cooling, helps facilitate the reactor vessel to be taken inside the dry argon atmosphere glove box without having concern of moisture contamination of the box. Again, Pyrophylite discs were employed inside the reactor as barriers and thermal insulators to maintain the temperature of the top flange below 353 K. They also acted as guides for the electrodes.

During the operation of the reactor, it was observed that the temperature of the top flange was maintained within the acceptable levels even after removal of both the pyrophylite discs. Taking this into consideration, another similar reactor was designed and fabricated, whose size was slightly smaller than that shown in Fig. 2.6. The grafoil gasket and veco coupling with rigid teflon feedthroughs in the earlier design were replaced by viton O-ring and veco type coupling with viton O-rings, respectively in the new cell. The pyrophylite was replaced by SS disc which acted as a spacer as well as heat shield. SS rods, used as the current collectors, were sealed in 3 mm dia. 300 mm long alumina sleeves to insulate them from the body of the reactor (Fig. 2.3a). The use of O-rings allowed easy tightening of the top flange with the reactor by means of C-clamps instead of bolts and nuts, which made the assembling/disassembling of the cell inside the argon atmosphere box easy. Molten salt experiments were carried out with both the reactors.

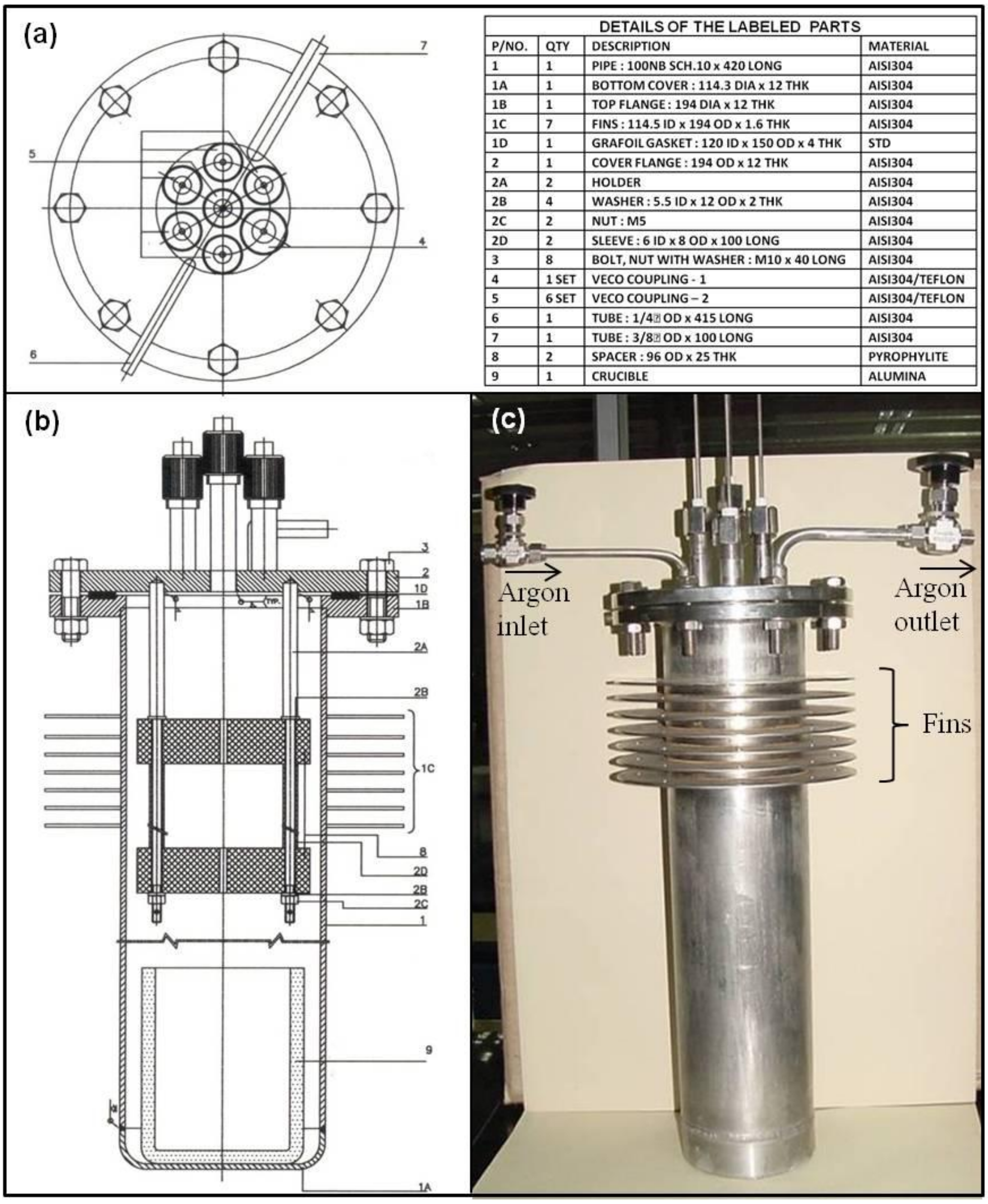

DETAILS OF THE LABELED PARTS

P/NO.	QTY	DESCRIPTION	MATERIAL
1	1	PIPE : 100NB SCH.10 x 420 LONG	AISI304
1A	1	BOTTOM COVER : 114.3 DIA x 12 THK	AISI304
1B	1	TOP FLANGE : 194 DIA x 12 THK	AISI304
1C	7	FINS : 114.5 ID x 194 OD x 1.6 THK	AISI304
1D	1	GRAFOIL GASKET : 120 ID x 150 OD x 4 THK	STD
2	1	COVER FLANGE : 194 OD x 12 THK	AISI304
2A	2	HOLDER	AISI304
2B	4	WASHER : 5.5 ID x 12 OD x 2 THK	AISI304
2C	2	NUT : M5	AISI304
2D	2	SLEEVE : 6 ID x 8 OD x 100 LONG	AISI304
3	8	BOLT, NUT WITH WASHER : M10 x 40 LONG	AISI304
4	1 SET	VECO COUPLING - 1	AISI304/TEFLON
5	6 SET	VECO COUPLING – 2	AISI304/TEFLON
6	1	TUBE : 1/4″ OD x 415 LONG	AISI304
7	1	TUBE : 3/8″ OD x 100 LONG	AISI304
8	2	SPACER : 96 OD x 25 THK	PYROPHYLITE
9	1	CRUCIBLE	ALUMINA

Fig. 2.6. High temperature molten salt reactor: (a) Top view of the reactor top flange (b) Schematic of the reactor and (c) Photograph of the assembled reactor. Details of various parts of the reactor are also given.

2.3.7. The double module argon atmosphere glove box facility

The molten salt work necessitated the use of an inert atmosphere (dry) box, with special features. A photograph of the double module argon atmosphere glove box available in the Direct Oxide Reduction Programme (DORP) laboratory, IGCAR, employed during the study is given in Fig. 2.7. A brief description of the set up is given below. The two glove boxes (I and II) are connected by a connecting/transfer port. The pressure of the positive pressure box was maintained in the range of + 20 to 40 mm water column with respect to atmosphere. Totally three ports were attached to the glove box – (i) a horizontal port for material transfer attached to one of the glove boxes (ii) a horizontal evacuable transfer port to the other glove box (not shown) and (iii) a vertical port for facilitating the transfer of electrolytic reactor in/out of the second glove box.

Fig. 2.7. Photograph of the double module argon atmosphere glove box facility for molten salt work. The numbers indicate various parts: 1 – glove box-I, 2 – glove box-II, 3 – horizontal port, 4 – vertical port and 5 – purification tower.

It was required to use moisture-free salts in the molten salt work. The evacuable transfer port of the second box was provided with electrical heaters for this purpose. Periodically the sample gas from the glove box facility was checked for its oxygen and moisture contents by passing through an oxygen analyser (Nucon 4316P, India) and moisture analyser (Systech, UK), respectively. Two leak tight gas purification towers, packed with molecular sieves and copper based catalyst, were employed for minimizing the moisture and oxygen contents of the glove box assembly. Automated or manual recirculation of the argon gas in the glove box assembly, through the purification towers, was done using a hermetically sealed blower for achieving a purity level of < 10 ppm each of oxygen and moisture inside the facility during handling of the salts/air sensitive samples after electrolysis. Glove box-I was also provided with electronic balances for weighing the air sensitive salts and samples.

A vertical port, as shown in Fig. 2.8 was attached to the bottom of glove box-II for easy transfer of experimental reactor assemblies. The box also was equipped with an automated crane which can handle a maximum weight of 25 kg, which is well above the typical weight of the electrolytic reactor vessel, vertically through the port and move it horizontally within the box to keep it at any point inside the box. The port and crane were installed in the box for the safe transfer of electrolytic reactor vessel into and out of the box. The port would facilitate the transfer of the cell in/out of the box in the vertical configuration. This arrangement helps to avoid spillage of salt within the reactor as well as the breakage or bending of the outward projecting electrode connections during transfer.

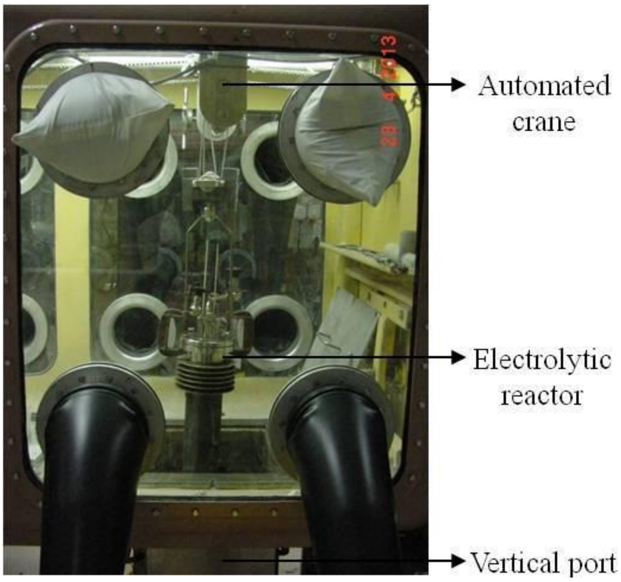

Fig. 2.8. Photograph showing the crane lifting an experimental cell kept in the vertical transfer port of the argon atmosphere glove box assembly.

2.3.8. Setting up of the electro-reduction cell

Assembling of the electro-reduction cell was carried out inside the glove box facility. High Density (HD) alumina crucibles (70 mm OD, 64 mm ID and 110 mm height, supplied by M/s. Naskar ceramic, India) were used as containers for molten salt. About 260 g of the vacuum dried salt ($CaCl_2$ or other salts or salt mixtures) was taken in the alumina crucible and placed in the leak tight reactor vessel, whose design and details are discussed previously. The different electrodes were also installed in the reactor using the veco-coupling/teflon feedthrough arrangement explained previously and the reactor was made leak tight with the help of the O-ring seal. The vessel thus loaded inside the glove box assembly was taken out and heated slowly in a resistance heating furnace, in a step wise manner by using a programmable temperature controller (Shinko, Japan) to the desired temperature. Continuous purging of purified argon at a flow rate of 0.1 - 0.2 litres per minute was maintained through the cell throughout the process. A photograph of the cell inside the furnace is shown in Fig. 2.9.

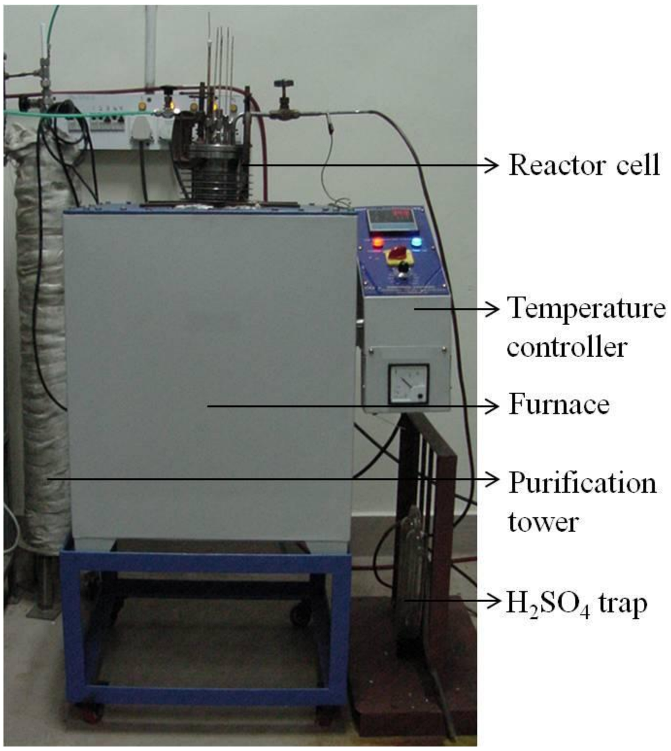

Fig. 2.9. Photograph of the electro-reduction cell assembly.

The gas from the reactor was bubbled through a H_2SO_4 trap to prevent back diffusion of air into the cell. A typical heating programme employed for heating the electrolytic cell to the experimental temperature included heating to 573 K at 100 K/h and dwelling at 573 K for 1 h followed by heating to the required temperature at a heating rate of 5 K/min. The temperature of the melt was measured using a K-type thermocouple placed in a thermowell.

2.3.9. Pre-electrolysis of the melt

Despite careful drying, transfer and storage of the salt within the glove box, it is possible that some moisture might still be present in the salt or might be picked up during transfer operations. This moisture must be removed before the actual electrochemical experiments. Therefore, pre-electrolysis of the melt was carried out by applying 2.8 V between a molybdenum coil and a graphite rod for removing moisture and redox active impurities present in the melt. Pre-electrolysis was continued until the background currents reached very low values and the typical time durations are in the range of 1 h – 24 h.

2.3.10. Cyclic voltammetric (CV) studies on the melt

Principle: CV is the widely used technique for studying the redox behaviour of electroactive species, determination of mechanism of electrochemical reactions etc. [174]. In this technique, the potential of a working electrode (WE) is changed at a particular scan rate, ν (in V/s) with respect to a reference electrode (RE) from an initial value (start potential) to a given value (switching potential) and scanned in the backward direction to reach the starting potential. During the process, the current flowing across the working and the counter electrodes (CE) is measured. The response is represented by a plot of current (Y-axis) versus the WE potential (X-axis) and is called a cyclic voltammogram. Some of the important parameters for the cyclic voltammogram of an electroactive solute species in an electrolyte are the cathodic peak potential (E_p^c), the anodic peak potential (E_p^a), the cathodic peak current (i_p^c), the anodic peak current (i_p^a) and the half peak potential ($E_{p/2}$, the potential where $i_p=i_{p/2}$).

Based on whether the reaction at the WE is controlled by charge transfer or mass transfer or by both, electrochemical processes taking place at the WE are categorized into a reversible process, a quasi-reversible process and an irreversible process.

(i) Reversible process: Here, the reaction is controlled by mass transfer (diffusion) and not by charge transfer. In this case, E_p, $i/\nu^{1/2}$, i_p^a/ i_p^c (=1) and the wave shapes are independent of scan rate (ν). For soluble-soluble reversible couple,

$$|E_p^c - E_p^a| = 2.29\ RT/nF \quad (2.4)$$

where, R is the universal gas constant, T – absolute temperature, F – Faraday constant and n – number of electrons involved in the reaction. If A – area of the electrode, C_o is the bulk concentration of electro-active species in mol/cm^3 and D_o is diffusion coefficient of the species in cm^2/s, the peak current in such a case is given by Randles-Sevcik equation [174]

$$i_p = 0.4463\ nFC_oA\nu^{1/2}D_o^{1/2}(nF/RT)^{1/2} \quad (2.5)$$

For a soluble-insoluble reversible couple,

$$|E_p-E_{p/2}| = 0.77RT/nF \quad (2.6)$$

The current in such a case is given by Berzins-Delahay equation

$$i_p = 0.61\ nFC_oA\nu^{1/2}D_o^{1/2}(nF/RT)^{1/2} \quad (2.7)$$

(ii) Quasi-reversible process: Here the reaction is controlled by both diffusion and charge transfer kinetics. Important characteristics of CV are that the peak potential shifts with change in scan rate and the average of the cathodic and anodic peak potentials remains constant, even though the difference between them increases.

(iii) Irreversible processes: Here, the reaction is mostly controlled by charge transfer. A shift in the peak potential with change in scan rate and a large separation between E_p^c and E_p^a and often the disappearance of the peak in the reverse scan are the characteristics of irreversible process. For such a process Matsuda and Ayabe [174] gave the following equation

$$|E_p-E_{p/2}| = 1.857(RT/\alpha n_\alpha F) \quad (2.8)$$

Where 'n_α' represents no. of electrons involved in the charge transfer reaction and 'α', the charge transfer coefficient with its value in the range $0.1 \leq \alpha \leq 0.9$.

For a soluble-insoluble irreversible or quasi-reversible system, the current is given by Delahay equation [174]

$$i_p^c = 0.496\ nFC_oAD_o^{1/2}(\alpha n_\alpha F\nu/RT)^{1/2} \qquad (2.9)$$

Procedure: A potentiostat (Autolab PGSTAT-30) was used to carry out cyclic voltammetry (CV) of different electrodes in the molten salts. During these studies, a tungsten wire (area, 0.04 cm^2) and a high density (HD) graphite rod (area, 1.10 cm^2) were employed as working electrodes (WEs) for the cathodic and anodic polarizations, respectively in chloride melts. A graphite rod (10 mm dia., 100 mm long and density, 1.85 g/cc) and a Mo coil were employed as counter electrodes during the cathodic polarization of tungsten and anodic polarization of graphite. A Ni/NiO reference electrode, prepared as discussed in section 2.3.5, was used in the CV studies. The potential of Ni/NiO was checked periodically against that for the deposition of M^{n+}, the cation of the melt, on the tungsten WE and found to remain constant within ±1 mV for 3 h during the study. The stability of the reference electrode was good enough for the kind of measurements reported in this study. The same reference was also used for monitoring the half-cell potentials of the electro-reduction cell and found to shift by ~ 20 mV during electrolysis for 44 h, as would be discussed later. The potentials were represented vs. that for M/M^{n+} and the conversion was achieved by making use of the M/M^{n+} potential of the melt measured by the cyclic voltammetry of the tungsten WE. In some cases, CV studies were also carried out with tip of the solid oxide pellet as the WE. In the case of the oxide pellet electrode, it was tied with a 1 mm dia. tantalum wire using a 1.5 mm hole made near its edge (Fig. 2.3b). The pellet was vertically introduced into the cell in such a way that its bottom just touched the electrolyte melt. The metal part of the electrode was kept away from the melt in order to exclude the possibility of electrochemical reactions taking place on it and corrupting the current-potential profile of the oxide working electrode. In some cases, the solid oxide pellet was wrapped around with a tantalum wire (Fig. 2.3e) and the whole assembly was fully dipped into the melt to function as the WE. In such cases the current was generally above 1 A and hence a current booster (Fig. 2.10) in conjunction with the potentiostat was employed. The potential of the counter electrode during CV studies in some experiments was monitored with respect to the reference electrode by using a data acquisition / switch unit (DAS) (Agilent 34970A). The photograph of a typical instrumental assembly for carrying out cyclic voltammetry is shown in Fig.2.10.

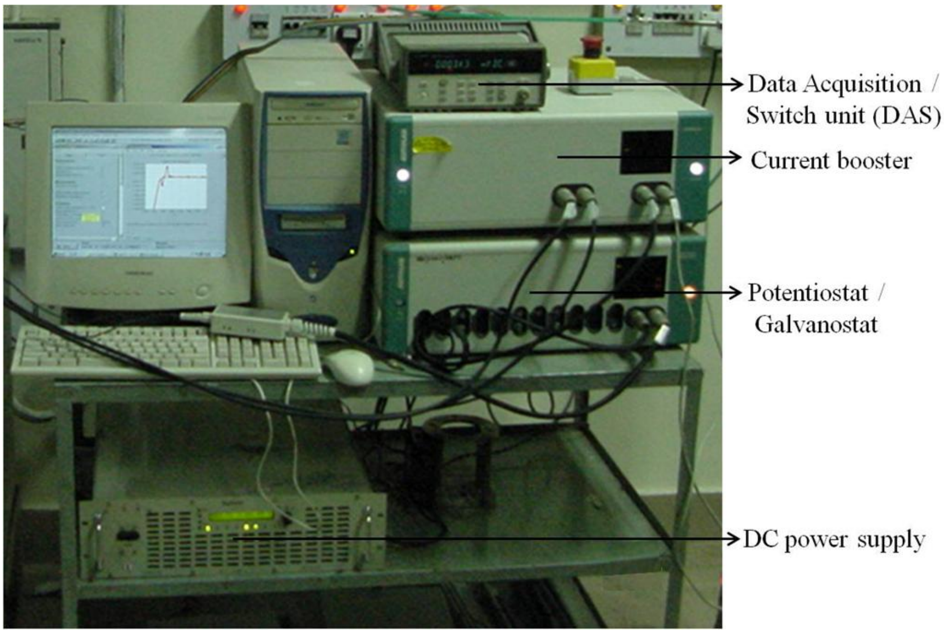

Fig. 2.10. Photograph of the instrumentation for cyclic voltammetry and electrolysis studies.

2.3.11. Polarization studies on the melt

The decomposition potentials of the melts were measured by recording the current response to a step-wise increase of the applied potential from 1.0 V to 4.5 V using a DC power supply (Digitronics A0250-18, India) shown in Fig. 2.10. A tantalum or stainless steel (SS) wire or the oxide pellet wrapped with a tantalum wire was used as the cathode and a graphite rod as the anode in such measurements wherein the oxide pellet was Nb_2O_5 / TiO_2 / UO_2.

2.3.12. Electro-reduction experiments

Principle: As described previously in chapter 1, the electro-deoxidation is carried out by cathodically polarising the solid metal oxide against a graphite counter electrode in an appropriate molten salt medium at a suitable temperature in the constant voltage or constant current mode of electrolysis.

Procedure: Two different DC power supply units (Digitronics A0250-18, India and PGK Electronics, Chennai, India) were used in the constant voltage (Con-V) and constant current (CC) modes of electrolysis. The reduction experiments were mostly carried out in $CaCl_2$ melt at 1173 K and $CaCl_2$-NaCl melt at 923 K. Other salts such as NaCl, KCl, KCl-$CaCl_2$ and LiCl were employed as electrolytes in some specific cases. Some fundamental studies were also carried out in LiCl-KCl-$CaCl_2$ (50.5: 44.2: 5.3 mol.%) melt at 673 K. The electrolysis was carried out at a voltage of 3.1 V in Con-V mode and at a current of 0.2 A or 0.5 A in CC mode. During electrolysis in Con-V mode, generally a high current is observed in the beginning which gradually decreases with time and the experiment is stopped when the current decreased to a minimum background value and remained there for quite some time. The potentials of cathode (vs. Ni/NiO reference), anode (vs. Ni/NiO reference) and cell were monitored throughout the course of the experiment and the data logged using a data acquisition / switch unit (Agilent 34970A). The schematic of the cell assembly and the electrode configurations for potential measurement are given in Fig. 2.11. After electrolysis, the electrodes were lifted to the upper low temperature region of the reactor and cooled under argon flow. The reactor was taken inside the argon atmosphere glove box for further processing of the products. The electrolysed pellets were washed with distilled water until the products were free from the salt and then vacuum dried at room temperature. The thoroughly washed and vacuum dried products were carefully subjected to visual observation. In general, the cross section of partially reduced samples showed different visibly distinct layers. The products thus obtained are analysed by different techniques such as X-ray diffraction (XRD), scanning electron microscopy (SEM), energy dispersive X-ray spectroscopy (EDX) and residual oxygen analysis. In some cases, the salt adhering to the sample was removed and the sample was used as such for X-ray diffraction analysis. The details of the specific procedures that were followed in the experiments with different oxides are described in the relevant chapters.

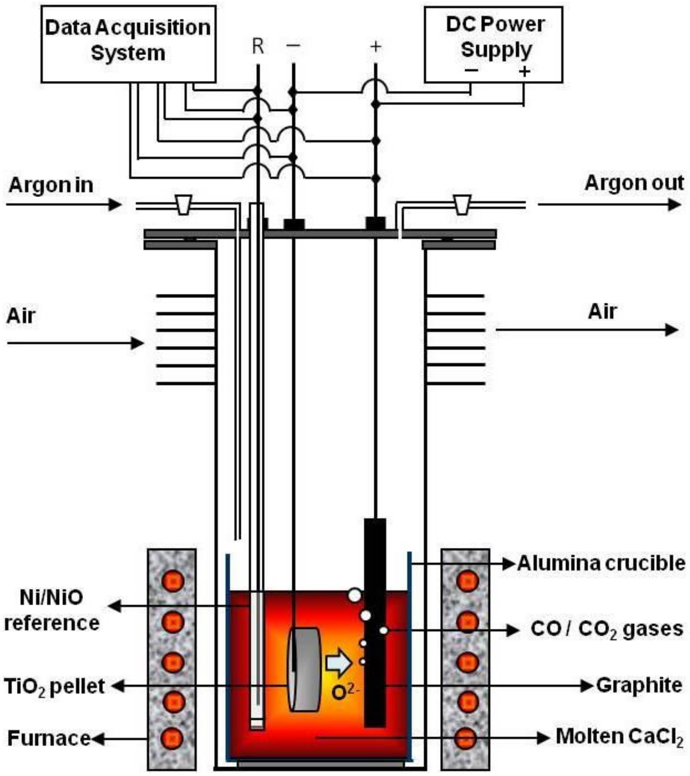

Fig. 2.11. Schematic of the electro-reduction cell assembly with electrical connections.

2.3.13. X-ray diffraction analysis of products

Principle: Structural information of a crystalline material can be gained by recording the X-ray diffractogram of the sample. The diffractograms obtained from interference of the X-rays diffracted by the surface atoms of a sample follows the Bragg's law, $n\lambda = 2d\sin\theta$, where n is the order of reflection, λ – the wave length of X-rays used, d – the interplanar distance of the diffracting planes of the crystal and θ – the angle of scattering. The diffraction pattern of a compound is the finger print for its identification.

Procedure: The phase identification of the starting materials and the products of electrolysis was carried out by the X-ray diffraction technique. If the product contained more than one visually distinguishable and physically separable layer, the layers were carefully separated, ground to powder and analysed by X-ray diffraction. A PANalytical 1011 X-ray diffractometer with CuK_α radiation ($\lambda = 1.542$ A°) was used for recording the XRD patterns. Wherever different layers, present in the samples, could not be separated and individually analysed, a uniformly ground mass of the product (UGP) was subjected to XRD analysis. The following procedure was adopted in some cases where critical phase analysis of unwashed product was required.

In most of the cases of electro-reduction experiments of UO_2, the samples for XRD analysis were prepared inside the argon atmosphere glove box. The salt adhering to the electrolysed pellets was physically removed to the maximum extent possible and the surface was cleaned by rubbing with a sand paper and analysed by XRD. A representative sample of the pellet was uniformly ground to powder form and again analysed by XRD to enable analysis of the chemical phases present in the bulk. The polished surface as well as the uniformly ground mass of the pellets were fully covered with an organic polymer tape to protect them from atmosphere during the XRD analysis.

2.3.14. Microstructural and elemental analysis of products

Principle: Scanning electron microscope (SEM) was employed for analysis of the microstructure of the samples. In this technique, the specimen is scanned with an electron beam from an electron gun operating at voltages of about 30 kV and the beams of electrons reflected or back scattered are collected and displayed on a cathode ray tube, which is photographed. The image shows the microstructural features of the sample. The sample must be an electronic conductor for SEM analysis and if not, a thin gold coating is applied to make it conducting.

Energy dispersive X-ray (EDX) analysis was employed for qualitative and semi-quantitative analysis of the elemental composition of the sample. In this method, the incident beam of electrons has sufficient energy to knock out an electron from the inner shell of an atom. When the vacancy is filled by another electron from the higher energy level, the excess energy is released as an X-ray photon, which is the characteristic of the element. In the EDX spectrum of intensity versus energy, the energy gives information about the element and the intensity helps in its semi-quantitative analysis.

Procedure: The microstructural and the elemental analysis of the fractured surface of the samples / products of electrolysis as well as the starting materials was carried out by employing a scanning electron microscope (Philips model XL 30) and energy-dispersive X-ray spectrometer (EDX), respectively, working at 30 kV. During the EDS analysis, a working distance of 10 mm was maintained and a sampling time of about 50 s or 100 s per spectrum was employed. Secondary electron images of the freshly broken cross sections and the surfaces of all the conducting samples were taken as such, whereas the samples which were not conducting (for example, SiO_2) were coated with gold by using sputter-coating technique at a current of 20 mA for typical time periods of 1 – 3 minutes depending on the nature of samples. If the samples were powders, then they were spread on a carbon tape and sputter coated. In case of the electro-reduction experiments of UO_2 pellets, a portion of the electrolysed samples were washed with 1:1 ethanol-water mixture for sufficient time to remove the occluded salt and dried under vacuum at room temperature for 12 h. The samples were broken inside the glove box to minimise the exposure of the freshly broken surface to atmosphere. Care was taken to minimise the exposure of the samples to air.

2.3.15. Oxygen analysis of products of electro-reduction

Principle: Inert gas fusion technique was employed for the residual oxygen analysis of the samples, whose principle is as follows. The sample, containing oxygen, taken in a high pure graphite crucible is heated to very high temperatures (in the range of 2700 K – 3200 K) in helium atmosphere. The oxygen present in the sample quantitatively reacts with the crucible and the CO formed is oxidised to CO_2 and analysed using thermal conductivity or infrared detector. The residual oxygen content of the sample is in turn determined from the CO_2 generated.

Procedure: Oxygen analysis of the samples was carried out with ELTRA ONH2000 analyser. The instrument is calibrated by taking standards having a known concentration of oxygen. A known mass of the sample in the range 10 – 40 mg is taken in a high pure tin holder and the end is then crimped. The holder is then inserted to the sample insertion port. The rest of the operations are pre-programmed and computer controlled. The sample automatically falls according to the programme into the previously degassed high pure graphite crucible present in the leak tight induction heating chamber. The output is given as the mass % or ppm of oxygen.

2.3.16. Melt analysis

During the course of the electro-reduction, various chemical changes take place on the oxide electrode, which in turn make changes in the composition/chemistry of the melt. In the case of $CaCl_2$ melt with graphite as the anode, the concentration of CaO in the melt changes and compounds like CaC_2 and $CaCO_3$ as well as calcium metal are introduced into the melt with time. It is necessary to dissolve the $CaCl_2$ salt in water to perform any wet chemical analysis with it. However, dissolution of the salt in water would convert the CaO, Ca and CaC_2 present in the salt to $Ca(OH)_2$. Hence the total basicity arising from these soluble species, herein called ‘total solubilised basicity (TSB)’ and expressed in terms of the wt.% of CaO, was estimated by the acid-base titration method. However, since $CaCO_3$ is not soluble in water, a back titration method was used to estimate the basicity of the insoluble residue, called herein as the ‘total insolubilised basicity (TIB)’ and expressed as wt.% of $CaCO_3$ present in the melt.

Both the pellet electrode and the entire mass of the frozen bulk electrolyte were separately collected after terminating the electro-reduction experiments at the end of pre-determined periods of time and treated separately with distilled water and filtered. The filtrate solutions obtained after dissolving the salt mass adhering the cathodes were analysed by acid-base titration for the total amount of base present in the cathode, i.e., the ‘total solubilised basicity of the cathode (TSB-C)’. Similarly the filtrate obtained after dissolution of the electrolyte was estimated, as mentioned above, to obtain the ‘total solubilised basicity of the melt (TSB-M)’. Also the melt solution was analysed by Inductively Coupled Plasma Mass Spectrometry (ICPMS) for the presence of metal ions (such as Fe, Cr, Ni, Al etc.) generated from corrosion and dissolution of the electrode, current collector and container materials. The undissolved residue part of the solution was vacuum dried at 333 K for 12 h, powdered and analysed by XRD for identification of the phases present. The residue was further dissolved in excess 0.25N HCl and the amount of $CaCO_3$ (i.e., TIB) present was estimated based on titration with 0.5N NaOH. Some residue still remained and it was collected separately by the method of centrifugation. The acid-treated melt residue thus obtained was vacuum dried, ground and again analysed by XRD for identification of the phases present in it. Salts such as NaCl, KCl and LiCl employed for electrochemical reduction experiments were also subjected to similar analysis.

2.4. Metal Estimation by Hydrogen Sensor (MEHS) method: Principle and procedure

Electrochemical reduction of UO_2 often resulted in partial or incomplete reduction. To estimate the amount of metallic uranium present in the product and hence to determine the extent of reduction of UO_2, a hydrogen sensor based method called Metal Estimation by

Hydrogen Sensor (MEHS)' has been developed whose principle and procedure for hydrogen estimation are given below.

2.4.1. Principle of the hydrogen sensor

A schematic of the Proton Exchange Membrane Hydrogen Sensor (PEMHS) employed in the study is shown in Fig. 2.12. The sensor is an electrochemical device operating in amperometric mode at room temperature and functions on fuel cell principle. A proton exchange membrane (PEM) (Nafion® 117) is used as electrolyte and screen printed platinum as electrodes on either side of the membrane. The barrier provided on the sensing electrode side limits the hydrogen flux reaching the sensing electrode. The limiting current produced due to diffusion limited oxidation of hydrogen on exposure of sensing electrode to hydrogen and counter electrode to air is linearly proportional to the hydrogen concentration.

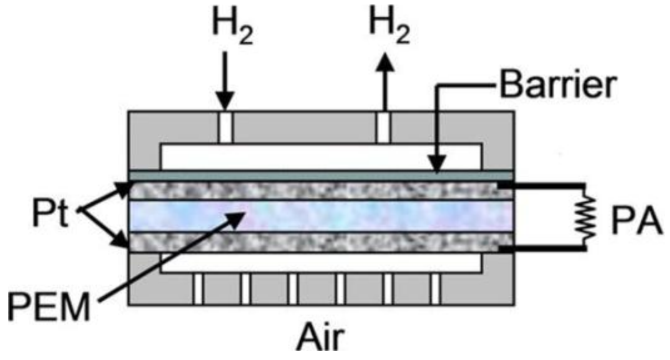

Fig. 2.12. Schematic of the sensor used in MEHS method. PA denotes pre-amplifier.

The electrochemical reactions occurring at the electrodes and overall reaction at the sensor are given below

Sensing electrode: $H_2 \rightarrow 2H^+ + 2e^-$ (2.16)

Counter electrode: $2H^+ + \frac{1}{2}O_2 + 2e^- \rightarrow H_2O$ (2.17)

Overall reaction: $H_2 + \frac{1}{2} O_2 \rightarrow H_2O$ (2.18)

The limiting current of the sensor measured by using a preamplifier (PA) is converted to concentration of hydrogen by the display unit using the slope and intercept values stored during calibration of the sensor. Once calibrated, the sensor can be used to measure any unknown concentration of hydrogen and display the concentration directly.

2.4.2. Principle of metal estimation by hydrogen sensor (MEHS)

The MEHS method was demonstrated using reaction of zinc and uranium metals with hydrobromic acid (HBr). The respective reactions are as follows

$$Zn_{(s)} + 2HBr_{(aq)} \rightarrow ZnBr_{2(aq)} + H_{2(g)}\uparrow \quad (2.19)$$

$$U_{(s)} + 4HBr_{(aq)} \rightarrow UBr_{4(aq)} + 2H_{2(g)}\uparrow \quad (2.20)$$

H_2 released from the reaction is carried by the argon carrier gas to the PEM hydrogen sensor and its concentration is measured online as a function of time as given in equation (2.21). The amount of the metal can be quantitatively measured using the total amount of H_2 evolved.

$$C_{H2} = (E_{H2}/F) \times 10^{6} \quad (2.21)$$

Where, C_{H2} is concentration of hydrogen in argon (in ppm), E_{H2} is hydrogen release rate in standard centimetre cube per minute (sccm) and F is flow rate of argon (sccm),

$$E_{H2} = C_{H2} \times F \times 10^{-6} \quad (2.22)$$

$$E_{H2}\,\mathrm{dt} = F \times 10^{-6}\, C_{H2}\,\mathrm{dt} \quad (2.23)$$

$$N_{H2} = {}_{ti}\int^{tf} E_{H2}\,\mathrm{dt} / V_o = (F \times 10^{-6} / V_o) \times {}_{ti}\int^{tf} C_{H2}\,\mathrm{dt} \quad (2.24)$$

$$W_m = N_{H2} \times 2A/z \quad (2.25)$$

Where, V_o is std. volume; A is gram atomic weight of metal; z is oxidation state of metal ion in acid solution; N_{H2} is number of moles of H_2 and W_m is the mass of the metal dissolved. From the measured concentration of H_2 in argon (C_{H2}), the hydrogen release rate (E_{H2}) as a function of time, number of moles of H_2 (N_{H2}) and the number of moles of metal dissolved (N_m) can be obtained by equations (2.23), (2.24) and (2.25), respectively. To minimise the error, the quantitative estimation of the metal could also be carried out using an equation generated from the calibration plot of number of moles of hydrogen liberated vs. number moles of the metal taken.

2.4.3. Assembly and calibration of MEHS experimental set up

The schematic of the hydrogen measurement set-up is shown in Fig. 2.13 and photograph of the experimental set-up in Fig. 2.14. The metal-acid reaction is carried out in the double-walled glass vessel (reaction chamber) and the hydrogen gas released is carried by flowing stream of argon gas first to a column containing silica gel and then to the sensor. A teflon magnetic stirrer was used to agitate the acid during the reaction. Silica gel removes the moisture present in the gas mixture. The concentration of hydrogen present in the gas mixture is measured by the sensor, the electrical signals are further amplified by the pre-amplifier and the processed data stored in the computer. The display unit gives the concentration as a function of time. Initially hydrogen gas mixtures of known concentrations were passed through the sensor and the calibration curve was generated.

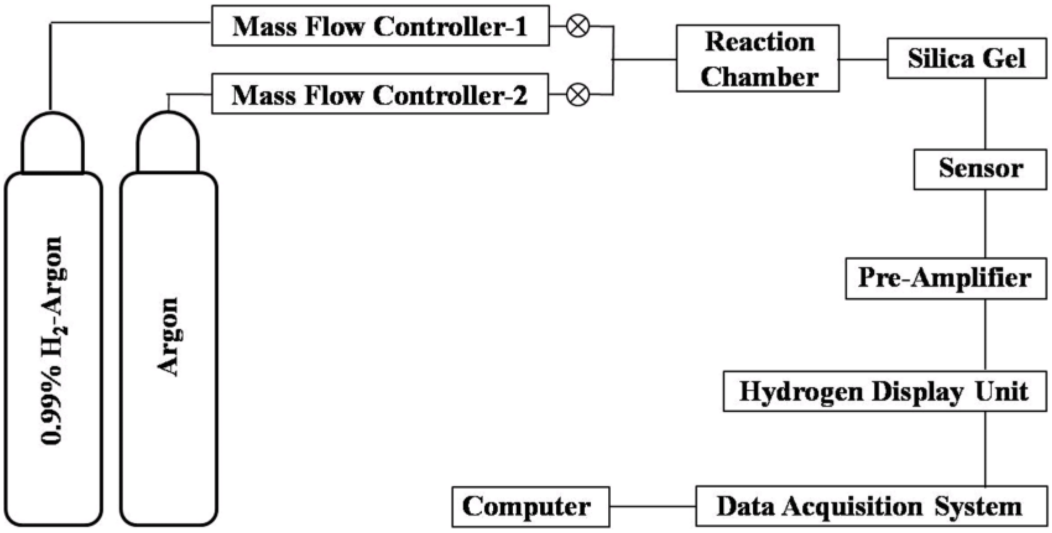

Fig. 2.13. Schematic of the experimental set up.

Prior to metal estimation experiments, the PEM hydrogen sensor was calibrated for hydrogen concentrations up to 5,000 ppm (for Zn+HBr reaction) and up to 3,000 ppm (for U+HBr reaction) in argon. Subsequently, to demonstrate the use of the system for measurement of hydrogen gas from metal-acid reaction, small pieces of Zn metal and small slices of nuclear grade U weighing in the range 25-80 mg were allowed to react with HBr acid in the glass reaction vessel and the concentration of the hydrogen gas measured using PEMHS, as explained above, was estimated with the help of the calibration curve.

The preliminary experiments with very small samples of Zn in HBr solution released very high concentration of H_2 beyond the calibration range of 5,000 ppm. To control the H_2 release rate, Zn samples were coated with an impervious film with only pin-hole area exposed to the HBr solution. The experiments were repeated with U samples. Since dissolution of a metal in acid is also a function of temperature, all the experiments were carried out at 298 K maintained using a thermostat. After the completion of each experiment, approximately 10 mL of acid solution was sampled and analysed for U using inductively coupled plasma optical emission spectroscopy (ICPOES) for comparison of results.

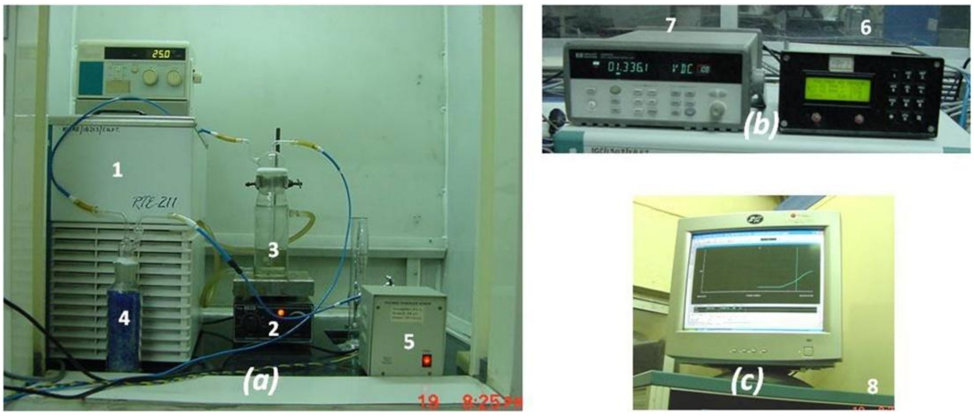

Fig. 2.14. Photographs of experimental set up: a) (1) Thermostat (2) Magnetic stirrer (3) Reaction chamber (double walled) (4) Silica gel column (5) Sensor and Pre-amplifier assembly (b) (6) Hydrogen display unit (HDU) (7) Data acquisition system (DAS) (c) (8) Hydrogen concentration displayed by the computer.

2.4.5. Estimation of uranium in U-UO_2 by MEHS method

UO_2 powder, initially characterized by XRD, was used for preparing standard mixtures of U-UO_2 for calibration of the method. Subsequently, the samples of electrolysed products from the DOER experiments were used for the determination of the extent of reduction. For estimation of U in U-UO_2 samples using the sensor, the sample was carefully introduced into the glass reaction chamber containing 100 mL of 48% HBr. The H_2 liberated from the reaction of the U metal with HBr was measured using the sensor, as discussed previously, from which the amount of metallic U in the sample was determined. After the completion of each dissolution experiment, 10 mL of the sample from the supernatant solution of HBr was collected and analysed for its U content by ICPOES. More detailed discussion on the estimation of U metal present in the electro-deoxidised uranium oxide samples will be given in chapter 6.

CHAPTER 3

Studies on the direct electrochemical reduction of Nb_2O_5 pellets in molten calcium chloride medium

3.1. Introduction

Niobium is an important transition metal that finds use in high end applications in modern science and technology [41,42,143,144,146]. Direct Oxide Electrochemical Reduction (DOER) is a promising alternative to high temperature metallothermic and carbothermic reduction processes for the production of Nb. Studies on the electrochemical reduction of Nb_2O_5 to Nb in molten salts has been reported since 2002 [41-50]. In the present study, powder compacted and sintered Nb_2O_5 pellets were electro-reduced under different experimental conditions, mainly with an aim to probe the mechanism of electro-reduction. Powder compacted and sintered Nb_2O_5 pellets were electro-reduced for different durations of time along a complete electro-reduction curve and the different physically distinct layers of the partially reduced samples were analysed to arrive at the mechanism. Some innovative methods such as counter electrode potential monitoring (CEPM) during cyclic voltammetric (CV) studies, indicator pellet technique (IPT), total solubilised basicity (TSB) and total insolubilised basicity (TIB) of melt, were conceived and applied to obtain a comprehensive understanding of the reduction process. Experiments were also carried out for studying the influence of factors such as temperature of electrolysis, applied voltage, open porosity of the pellets, composition of the electrolyte etc. on the electrochemical reduction of Nb_2O_5 pellets. Some data generated on the behaviour of graphite anodes during electro-reduction process were also used in the overall analysis of the reduction process. The results are discussed in detail in this chapter.

3.2. Experimental

Cyclic voltammetric (CV) studies were carried out with tungsten, the tip of Nb_2O_5 pellet (Fig. 2.3b) (for cathodic polarization) and high density graphite (for anodic polarization) as working electrodes, high density graphite (HDG) and Mo coil as the counter electrodes and Ni/NiO as reference electrode in $CaCl_2$ melt at 1173 K. As cyclic voltammograms were recorded, the potential of the counter electrode (CE) was monitored, in some experiments, using a high-impedance multimeter. Polarisation studies were carried out with a Ta wire or a Nb_2O_5 pellet as the cathode and graphite as the anode. Electro-reduction experiments were carried out under different experimental conditions such as different duration of electrolysis (2, 9, 22, 26, 35, 44 and 56 h), temperature (1173 K and 1073 K), applied voltage (2.5 V and 3.1 V), open porosities of pellets (~10% and ~42%), modes of electrolysis (constant voltage (Con-V) and constant current (CC) modes) etc. to understand the influence of various parameters on the electro-reduction of Nb_2O_5 pellets, weighing ~3 g. In general, most of the experiments were carried out at 3.1 V for 44 h except the experiments related to the study of parameters - duration of electrolysis and applied voltage. The cathode potentials, throughout the course of the reduction experiments, were monitored using a Ni/NiO reference electrode. As the reduction of Nb_2O_5 pellet was in progress, potential of another Nb_2O_5 pellet, herein called indicator pellet (IP), immersed in the melt was monitored to obtain information on the chemical changes taking in the melt. The electro-reduced pellets and the indicator pellets recovered from the cells were subsequently analysed for their chemical composition, microstructure and oxygen content. The electrolyte salts from these experiments were also analysed for their TSB and TIB. TSB of the salt adhering to the cathode was also separately determined.

3.3. Results and discussion

3.3.1. Cyclic voltammetry (CV) and decomposition potential measurements

The cathodic and anodic potential limits of $CaCl_2$ melt, at 1173 K, determined by cyclic voltammety of inert tungsten wire (area 0.04 cm^2, cathodic polarisation) and a high density graphite rod (area 1.10 cm^2, anodic polarisation) working electrodes (WE) are depicted in Figs. 3.1a and 3.1b. A graphite rod and a molybdenum coil were used as the respective counter electrodes (CE) in the above measurements. Obviously the reactions at the cathodic and anodic limits of the melt are $Ca^{2+} + 2e^- \rightarrow Ca$ and $2Cl^- \rightarrow Cl_{2(g)} + 2e^-$, respectively. From the measured potentials of calcium deposition (0.00 V vs. Ca/Ca^{2+}) and chlorine evolution (3.235 V vs. Ca/Ca^{2+}), the decomposition potential of $CaCl_2$ melt is calculated as 3.235 V. This value agrees excellently with the reversible decomposition potential of $CaCl_2$ at 1173 K, deduced from the Gibbs energy of formation of $CaCl_2$ ($\Delta G^o_{f,1173K}$ = 619.6 kJ/mol., $E_{d,1173K}$ = - 3.211 V).

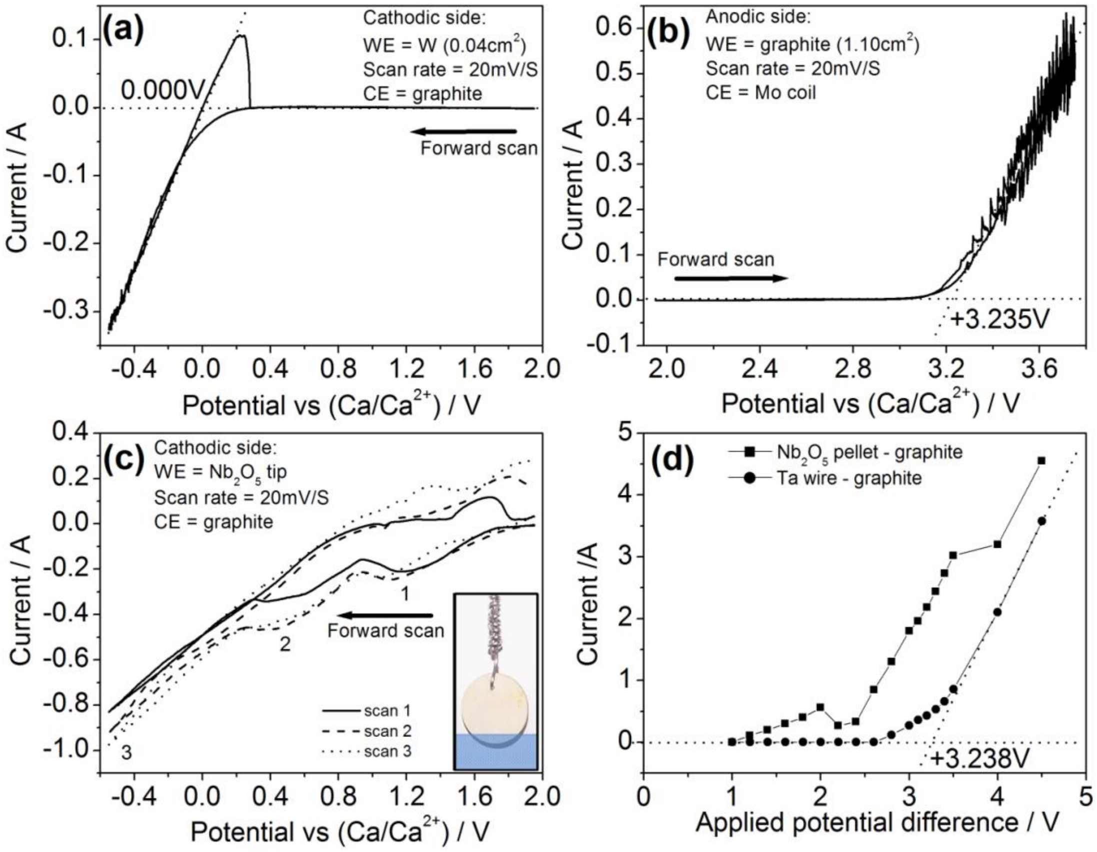

Fig. 3.1. Cyclic voltammograms obtained with different WEs in $CaCl_2$ melt at 1173 K (a) tungsten - cathodic polarisation (b) graphite - anodic polarisation and (c) tip of the Nb_2O_5 pellet - cathodic polarisation. Schematic of the Nb_2O_5 electrode is given in the inset in (c). (d) Polarisation curves obtained during cathodic polarisation of Nb_2O_5 pellet and tantalum wire in $CaCl_2$ melt at 1173 K. A graphite rod was used as the counter electrode.

CV response of the tip of a Nb_2O_5 pellet (20.2 mm dia., 2.3 mm thick, OP ~ 5%) with a graphite rod as the CE is shown in Fig. 3.1c. Unlike in the case of the CV of W electrode (Fig. 3.1a), the cathodic currents can be seen to start at potentials far positive to Ca deposition and this shows that the oxide electrode is electrochemically reactive in the melt at potentials positive to calcium deposition. Two reduction waves (designated as ‘1’ and ‘2’) appearing before calcium deposition in the forward scan clearly show that different reduction reactions are taking place on the electrode. The current response makes it clear that Nb_2O_5 is a good electronic conductor at the experimental temperatures.

The polarisation curves independently obtained with a tantalum wire and Nb_2O_5 pellet as cathodes against a graphite anode in $CaCl_2$ melt are given in Fig. 3.1d. In the case of the inert tantalum electrode, no significant current was noticed until the decomposition potential of the electrolyte (3.238 V). However, the current started to increase from 1.0 V onwards, when Nb_2O_5 pellet was used as cathode in place of the Ta electrode. This again indicated a possible electrochemical reaction of the melt with the metal oxide electrode. After the experiment, the polarised Nb_2O_5 pellet was analysed by XRD, which revealed the presence of $CaNb_2O_6$ and NbO_2 phases. This result as well as the current waves observed during cathodic polarisation of Nb_2O_5 electrode in the CV experiment (Fig. 3.1c), unambiguously confirms that the Nb_2O_5 pellet is cathodically reactive in the $CaCl_2$ melt. Ca^{2+} ions are known to get inserted to cathodically polarised Nb_2O_5 electrodes in $CaCl_2$ based melts to form ternary calcium compounds [42,49,50].

3.3.2. The Counter Electrode Potential Monitoring (CEPM) during CV studies

The potential of the WE is controlled and the CE is left to float during CV studies. Monitoring the potential of CE may provide insight into the reactions taking place at individual electrodes, particularly when metal oxides are employed as WEs. In this context, an innovative technique, called counter electrode potential monitoring (CEPM), was conceived and employed. The concept was experimentally demonstrated in $CaCl_2$ melt. Figs. 3.2a and 3.2b show the responses of the graphite counter electrode when W and tip of Nb_2O_5 pellet (scan ‘1’ shown in Fig. 3.1c) are cathodically polarised in $CaCl_2$ melt. Other current/potential data relevant to the system are also given in the figures. The Ca/Ca^{2+} and Cl_2/Cl^- potentials are indicated by dotted lines parallel to x-axis. The potentials of WEs, W and Nb_2O_5 and the graphite CE are given w.r.t. Ca/Ca^{2+} potential.

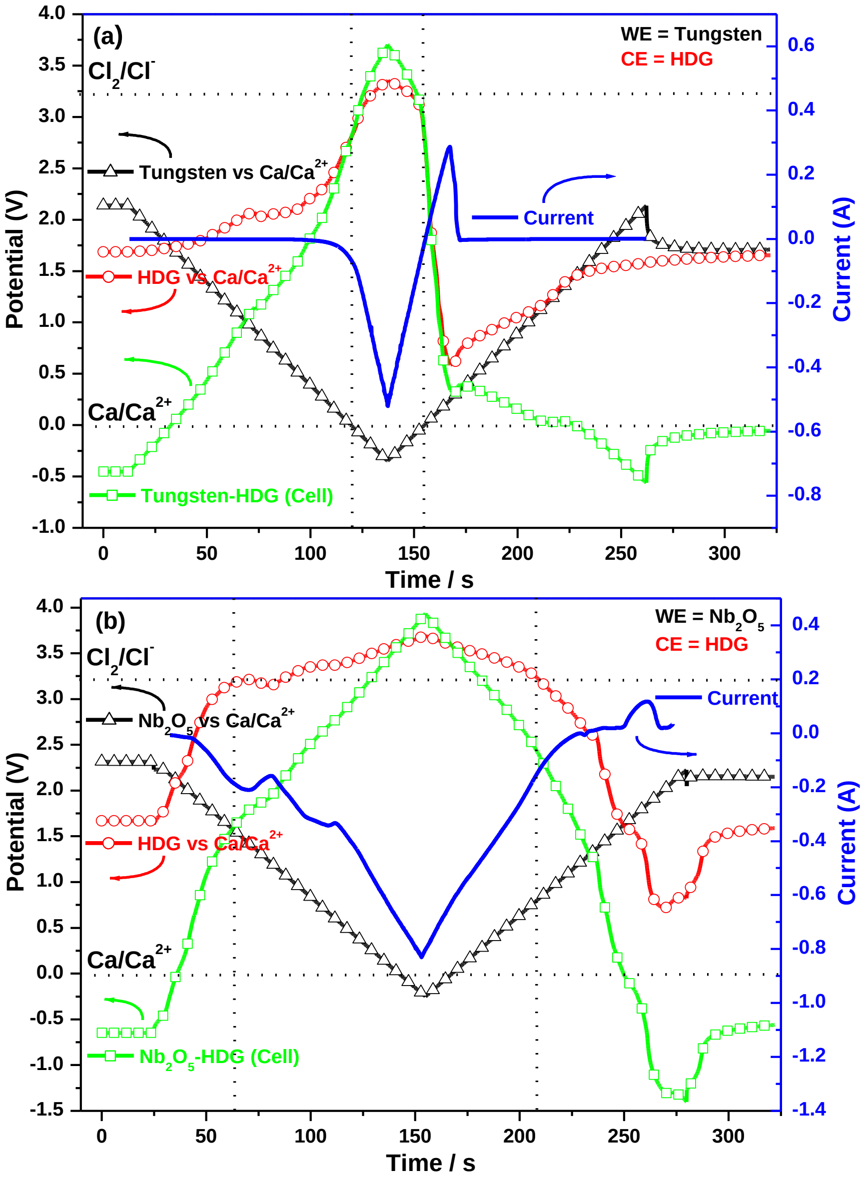

Fig. 3.2. The variation of potentials of (a) Tungsten WE and (b) Nb_2O_5 WE and graphite CE during CV measurements in $CaCl_2$ melt at 1173 K. Corresponding current-time curves and overall cell voltages are also given in the figures. The potentials of WE and CE are given w.r.t. Ca/Ca^{2+}.

In Fig. 3.2a, as the potential was scanned in the cathodic direction, the current started increasing significantly when Ca started depositing on the W working electrode. During this period, the graphite CE was slowly polarised (on its own) in the anodic direction from the open circuit potential (OCP) and the electrode potential increased slowly to attain the final potential of > 3.25 V when the W cathodic potential was more negative to the calcium deposition potential. The response curves make it abundantly clear that the chlorine gas was evolved on the graphite CE, when the W cathode potential was sufficient to deposit Ca metal on it. This in other words means that the $CaCl_2$ electrolyte was decomposed as Ca and Cl_2 at the potential limits of the electrodes, as discussed above. However, a similar exercise carried out with the tip of Nb_2O_5 electrode as the WE against a graphite CE gave rise to current and electrode potential curves with different shapes (Fig. 3.2b) than that given in Fig. 3.2a. It is clear from the potential curves that the graphite (CE) potential was above the chlorine evolution potential, even as the cathode potential remained positive to calcium deposition potential of the Nb_2O_5 WE. Also, unlike in the case of W working electrode, Nb_2O_5 WE allowed current to flow at a wide range of cathode potentials. The CV data in combination with the counter electrode potential data thus clearly show that the Nb_2O_5 cathode is reactive in the pure $CaCl_2$ melt and the corresponding anode reaction is predominantly chlorine evolution on the graphite anode.

The concept can be applied to gain insight into the reactions taking place at individual electrodes during the electrochemical reduction of other metal oxides too particularly in the case of electro-reduction of UO_2 in LiCl-Li_2O melts, wherein Pt is used as the anode. A better insight into the different anodic reactions could be gained by using this technique.

3.3.3. Electro-deoxidation of Nb_2O_5 pellets in $CaCl_2$ melt

In order to obtain a complete electro-reduction pattern of Nb_2O_5 pellet, two dense Nb_2O_5 pellets (~1.5 g each) placed in a tantalum cup were electro-deoxidised at a constant applied voltage of 3.1 V using HDG rod as the anode. The typical behaviour of current, cathode and anode potentials is shown in Fig. 3.3A. The results of XRD and SEM analysis of the pellets before and after electrolysis are given in Fig. 3.3B.

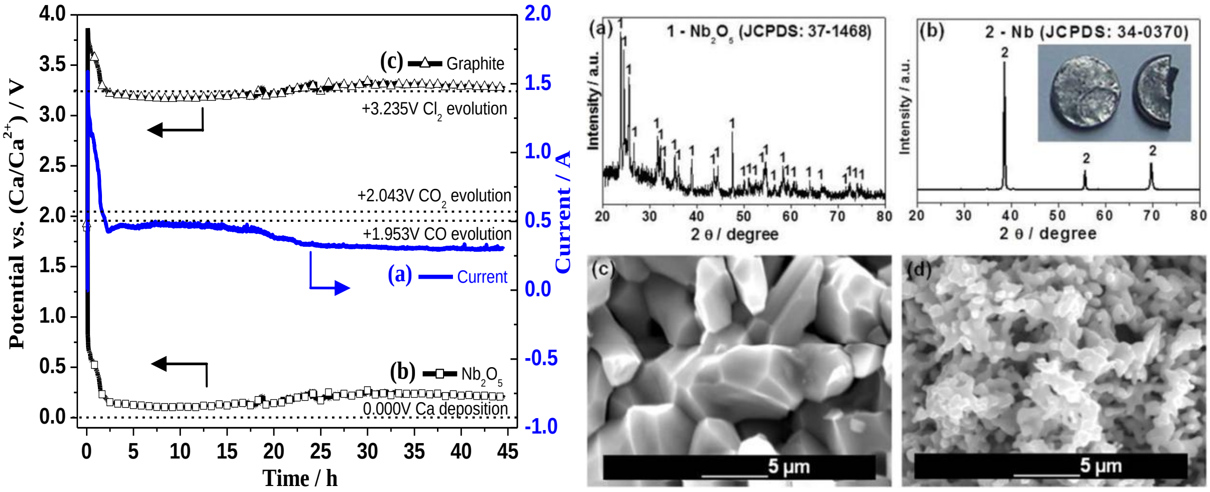

(A) (B)

Fig. 3.3. (A) Half-cell potentials (b, c) and I-t curve (a) of the electro-reduction cell, graphite / $CaCl_2$ / Nb_2O_5 at 1173 K during electrolysis at constant applied potential, 3.1 V for 44 h. (B) XRD spectra of the surface of (a) Nb_2O_5 pellet sintered at 1673 K for 3 h and (b) the pellet after electrolysis. Photograph of the polished pellets was given in inset of (b). SEM images of the fractured surface of the pellet referred to (a) and (b) are shown in (c) and (d), respectively.

In Fig. 3.3A, the cathode potential became more and more cathodic as the electrolysis was continued. The potential became 0.210 V in ~2.5 h and remained more or less stable at the potential for ~15 h and thereafter moved marginally in the anodic direction to 0.250 V. The anodic potential, after showing a high value (~4.0 V vs. Ca/Ca^{2+}) at the start of the experiment decreased to a value below 3.25 V in 2.5 h and thereafter remained more or less stable until the end of experiment which lasted for 44 h. The current followed the cathodic voltage pattern with three distinct regions, i.e., 0-2.5 h, 2.5-22 h and for the rest of the electrolysis period. In addition to the measured potentials of cathode and anode shown in Fig. 3.3A, dashed lines are also drawn to show the potentials of Ca deposition (0.000 V) and Cl_2 evolution (+3.235 V) obtained from the CV measurements. Also the theoretical potentials deduced for CO and CO_2 evolution on a graphite anode in $CaCl_2$ melt containing ~0.005mol.% CaO are given in the figure. The X-ray diffraction patterns of the Nb_2O_5 pellet before and after electrolysis are given in Fig. 3.3B (a) and (b), respectively. Corresponding SEM images of the fractured surface of pellets are given in Fig. 3.3B (c) and (d), respectively. Metallic Nb was the only phase observed in the product after electrolysis.

Distinctly large grains were converted to relatively smaller nodular grains of Nb after electrolysis. The residual oxygen content of the reduced product was determined by inert gas fusion technique and found to be ~ 6,400 ppm.

In order to study the changes that are occurring during the course of electrolysis, different Nb_2O_5 pellets were electrolysed for different periods of time viz. 2, 9, 22, 26 and 35 h. The currents traced more or less the same path and the variation of currents in the experiments N-1 - N-6 is given in Fig. 3.4. The photographs of the products obtained from each experiment are given in the insets of the corresponding current-time profile.

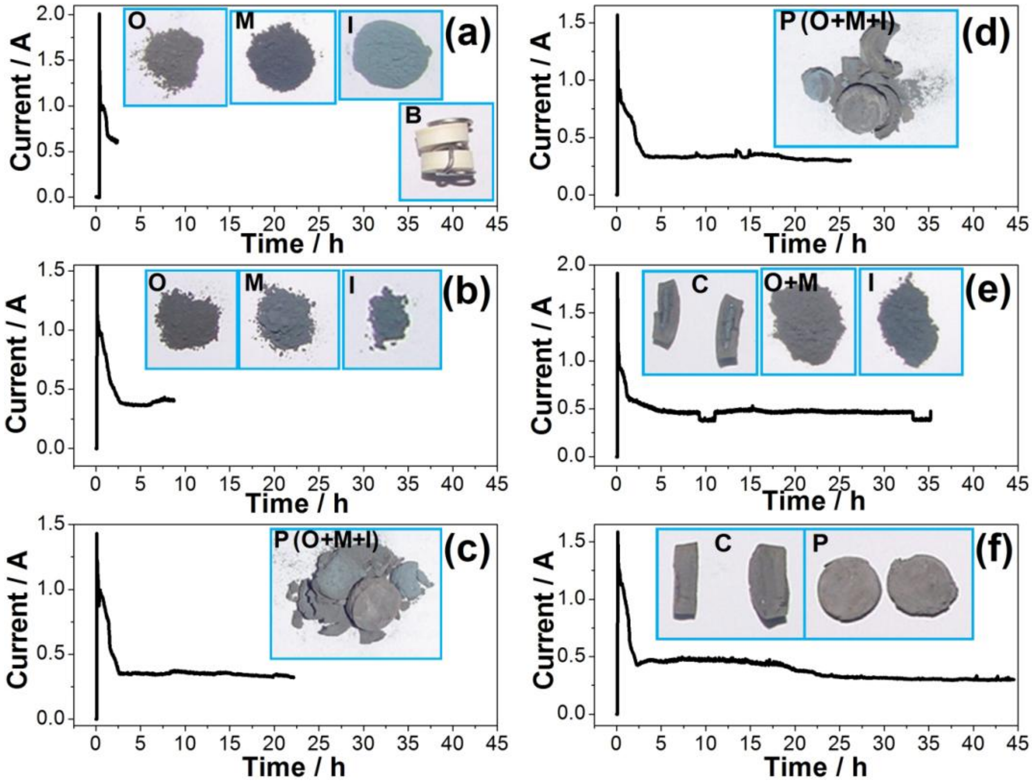

Fig. 3.4. Variation of current during electro-reduction of two Nb_2O_5 pellets (wt. ~1.5 g each, ~11 mm dia., ~ 4 mm thick) at 3.1 V for different periods of time in $CaCl_2$ melt at 1173K. (a) 2 h (b) 9 h (c) 22 h (d) 26 h (e) 35 h and (f) 44 h. Photographs of various regions of the pellets are given in insets, with legends O-Outer region, M - Middle region, I - Inner region, B - Before electrolysis P - Product after electrolysis and C - Cross section. The photograph of the electrode assembly with two Nb_2O_5 pellets is shown as inset in (a).

A description of the various physically distinct regions observed in the products and the phases identified in them are given in Table 3.1. The X-ray diffractograms of representative samples of the visibly distinct and electrochemically significant regions of the electrolysed pellets, separated carefully, are given in Fig. 3.5. The existence of similar phases in partially electrolysed Nb_2O_5 pellets has been reported by Yan et al. [41,45] and Song et al. [50].

Table 3.1. Results of Nb_2O_5 electro-reduction experiments.

Expt. ID	Duration of electrolysis (h)	No. of regions in the product	Details	Phases identified by XRD
N-1	2	3	Thin outer surface layer (grey)	Nb, $Nb_{0.532}Ta_{0.468}H_{0.93}$ (t)
			Middle (dark grey)	Nb, Nb_2O_5, NbO_2 and $CaNb_2O_6$
			Inner (bluish violet)	Nb_2O_5
N-2	9	3	Outer (grey)	Nb, $Nb_{0.532}Ta_{0.468}H_{0.93}$
			Middle (dark grey)	$CaNb_2O_6$, NbO_2 and Nb_2O_5
			Inner (greyish violet)	Nb_2O_5, $CaNb_2O_6$ and NbO_2
N-3	22	3	Outer (grey) + middle (brown)	Nb
			inner most (light blue)	Nb (M), $Ca_3Nb_2O_8$ and $Ca_4Nb_2O_9$
N-4	26	3	Outer (grey) + middle (light grey)	Nb, $Nb_{0.532}Ta_{0.468}H_{0.93}$ (t)
			inner most (light blue)	Nb, $Ca_3Nb_2O_8$, $Ca_4Nb_2O_9$ and $CaNb_2O_6$ (t), $CaNbO_3$ (t) and NbO_2 (t)
N-5	35	3	Outer (grey)	Nb, $Nb_{0.532}Ta_{0.468}H_{0.93}$
			Middle (violet) + inner most (bluish violet)	$CaNb_2O_6$, NbO_2, Nb_2O_5, Nb and $CaNbO_3$(t), NbO (t),$NbO_{0.7}$ (t), Nb_6O (t), Nb_4O_5 (t)
N-6	44	1	Uniform	Nb (NbC at surface)

t=trace

Pellets electrolysed for 2 h (N-1) and 9 h (N-2) were found to have three distinctly different layers. The outer layers in both the cases were found to be Nb metal (JCPDS: 34-0370) with small amounts of $Nb_{0.532}Ta_{0.468}H_{0.93}$ (Table 3.1). The XRD pattern of the sample (Fig. 3.5a) showed all the peaks of Nb metal, but with slight deviation in the peak positions. This could be due to dissolved oxygen in the metal. The thickness of the metal layer was found to increase with the duration of electrolysis. Ta metal wire used as electrical lead to the pellet, it appears, formed an alloy with the Nb metal and was converted to its hydride during the post electrolytic treatment of the cathode in water. The dark greyish middle layer of N-1 and N-2 comprised of calcium niobates and suboxides of Nb. The innermost layer contained the unreduced Nb_2O_5. The N-3 and N-4 samples too showed three different layers with different chemical compositions. The notable feature of these samples was the presence of significant quantities of higher calcium niobates of the form $Ca_xNb_2O_{5+x,}$ where x = 3 and 4, i.e., $Ca_3Nb_2O_8$ and $Ca_4Nb_2O_9$ in the inner most layer, which were absent in N-1 and N-2.

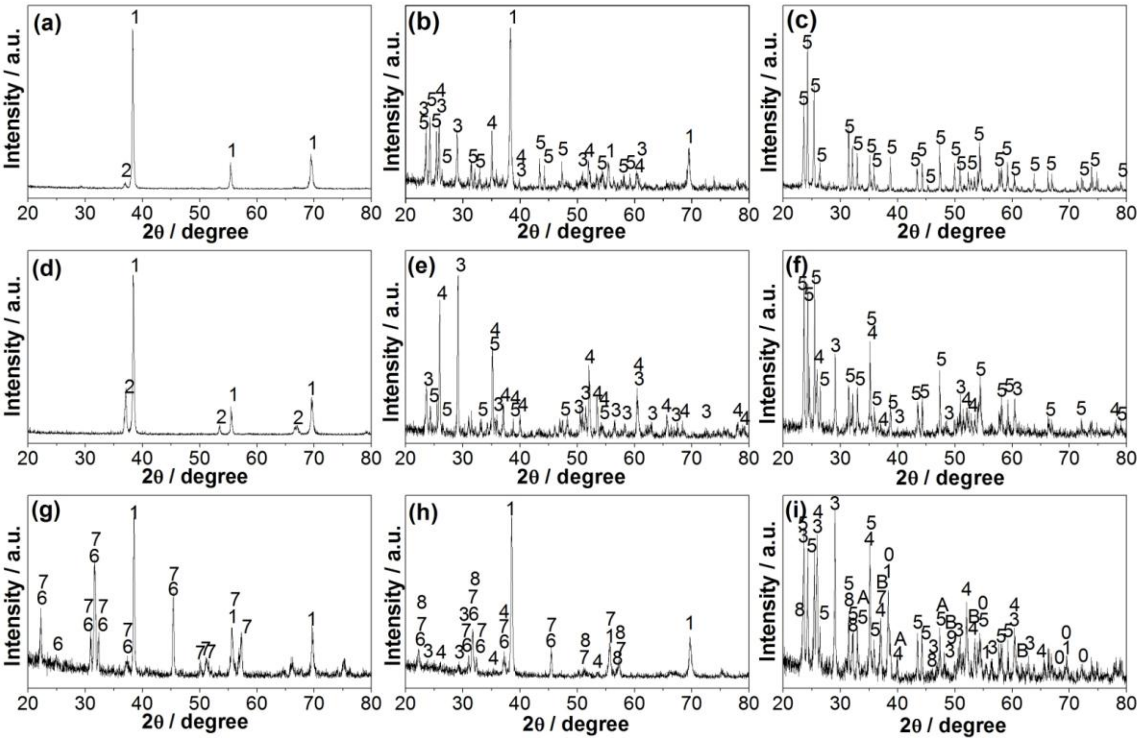

Fig. 3.5. XRD patterns of different physically distinguishable parts of the Nb_2O_5 pellets electrolysed for different durations; after 2 h: (a) surface (b) middle (c) inner; after 9 h: (d) surface (e) middle (f) inner; after 22 h: (g) inner; after 26 h: (h) inner and after 35 h: (i) inner region. 1-Nb, 2-$Nb_{0.532}Ta_{0.468}H_{0.93}$, 3-$CaNb_2O_6$, 4-$NbO_2$, 5-$Nb_2O_5$, 6-$Ca_4Nb_2O_9$, 7-$Ca_3Nb_2O_8$, 8-$CaNbO_3$, 9-$NbO_{0.7}$, 0-$Nb_6O$, A-$Nb_4O_5$ and B-NbO.

Fig. 3.6a shows the typical microstructure of the bulk of the sample from N-3 with appreciable amounts of Ca (27.71 at.%) and O (56.93 at.%) along with Nb (15.37 at.%) as shown by the EDX spectrum given in Fig. 3.6b. The pellets after 35 h of electrolysis (N-5) showed again three layers, but the calcium niobates that were found in N-3 and N-4 samples were absent. Pellets electrolysed for 44 h (N-6) got uniformly and completely converted to Nb metal with a residual oxygen content of ~ 6,400 ppm. The above findings show that the electrochemical reduction proceeds via the formation and decomposition of calcium containing intermediate compounds and the extent of reduction depends on the duration of electrolysis. The extent of reduction is the highest on the surface of the pellet and it decreases along the distance from surface to inner centre of a pellet. These aspects will be discussed in detail in section 3.3.7.

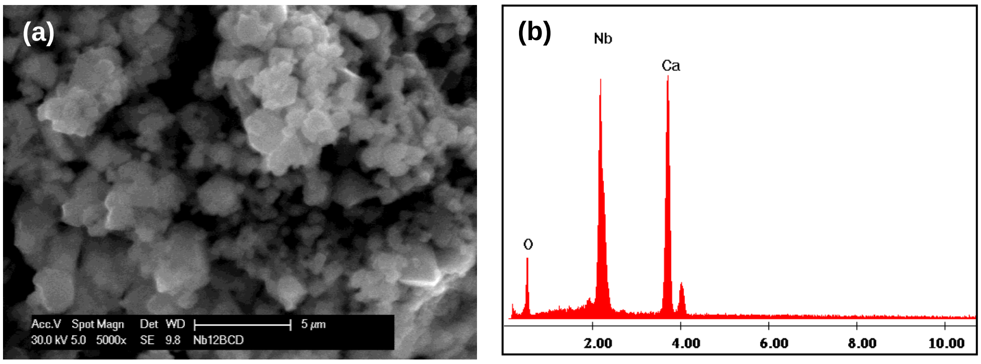

Fig. 3.6. (a) SEM image and (b) EDX spectrum of the bulk of the pellet electrolysed for 22 h.

Change of composition of electrolyte melt during electro-deoxidation and measurements on the total solubilised basicity (TSB) and total insolubilised basicity (TIB)

The concepts of TSB and TIB in understanding the melt chemistry and the procedure followed for their determination have been discussed in chapter 2. The variation of the TSB-C (cathode) and TSB-M (melt) from the above experiments (N-1 - N-6) are shown in Fig. 3.7 (a) and (b), respectively.

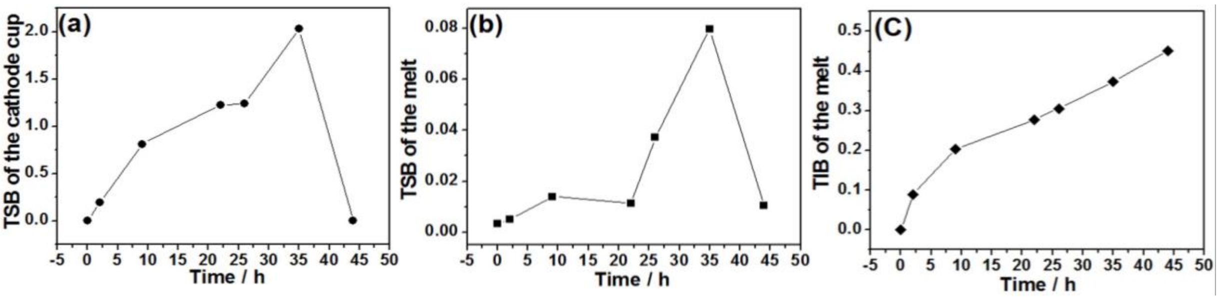

Fig. 3.7. Variation of (a) total solubilised basicity (TSB) of the cathode cup assembly, (b) melt and (c) total insolubilised basicity (TIB) of the melt with time during the electro-reduction of Nb_2O_5 pellets in $CaCl_2$ melt at 1173 K.

The TSB-C increased rapidly during the initial few hours of electrolysis (~10 h) and thereafter the increase was slow until around the mid period of electrolysis. Again it increased steeply for a few hours and in the next ten hours or so towards the end of electrolysis, it decreased significantly to register a low value that was close to the starting value. The TSB-M (Fig. 3.7b) during the above periods, on the other hand, showed a very modest increase until about the middle of the electrolysis and thereafter increased sharply to a very high value before showing a significant decrease towards the end of electrolysis as observed in the case of TSB-C. It can be seen that the variations of TSB-C and TSB-M were more or less similar from the mid period of electrolysis until the end of electrolysis. The basicity of the melt is predominantly due to the presence of CaO and hence the significant variation of the TSB-M and TSB-C implies that the concentration of CaO at the electrode and also in the melt is undergoing significant changes on account of the cathodic polarisation of the oxide electrode. Reactions in which CaO is both generated and consumed can be inferred from the typical TSB behaviour. Removal of oxygen from the electrode is necessary for deoxidation and hence generation of O^{2-} (as CaO) at the electrode and its subsequent dissolution in the melt is to be expected. The CO_2 gas produced at the graphite anode during electro-deoxidation dissolves in the melt and gets converted to $CaCO_3$ by reaction with the CaO present in the melt. Earlier, Pistorius et al. [70] reported similar observations in the case of electrochemical reduction of SiO_2 pellets in $CaCl_2$-CaO melt at 1173 K. The variation of the TIB of the melt at various time periods of electro-deoxidation, shown in Fig. 3.7c, is therefore related to the TSB-C and TSB-M shown in Fig. 3.7a and 3.7b, respectively. These aspects will be discussed in more detail in following sections in the context of the mechanism of electro-reduction of Nb_2O_5.

3.3.4. The change of composition of the melt during electrolysis and the indicator pellet technique (IPT)

The role of elemental calcium in direct electrochemical reduction of metal oxides with respect to Nb_2O_5 was investigated in the present study by a new method called ‘indicator pellet technique’. In this technique, a Nb_2O_5 pellet (~0.5 g, ~1.3 mm thick and ~11 mm dia.)

tied with Ta wire was immersed into $CaCl_2$ melt and its galvanic potential was monitored w.r.t. Ni/NiO reference. This was done under two conditions: (i) Non-electrolytic Conditions (NC), where no electrolysis is performed in the melt and (ii) Electrolytic Conditions (EC), where the electrolysis of another set of Nb_2O_5 pellets is performed in the melt. Fig. 3.8a shows the galvanic potentials recorded for 44 h for two pellets one under NC and the other under EC. In Fig. 3.8a, four plateau or stable potential regions, designated as region-1, 2, 3 and 4, were seen in the latter against only one plateau in the case of the former.

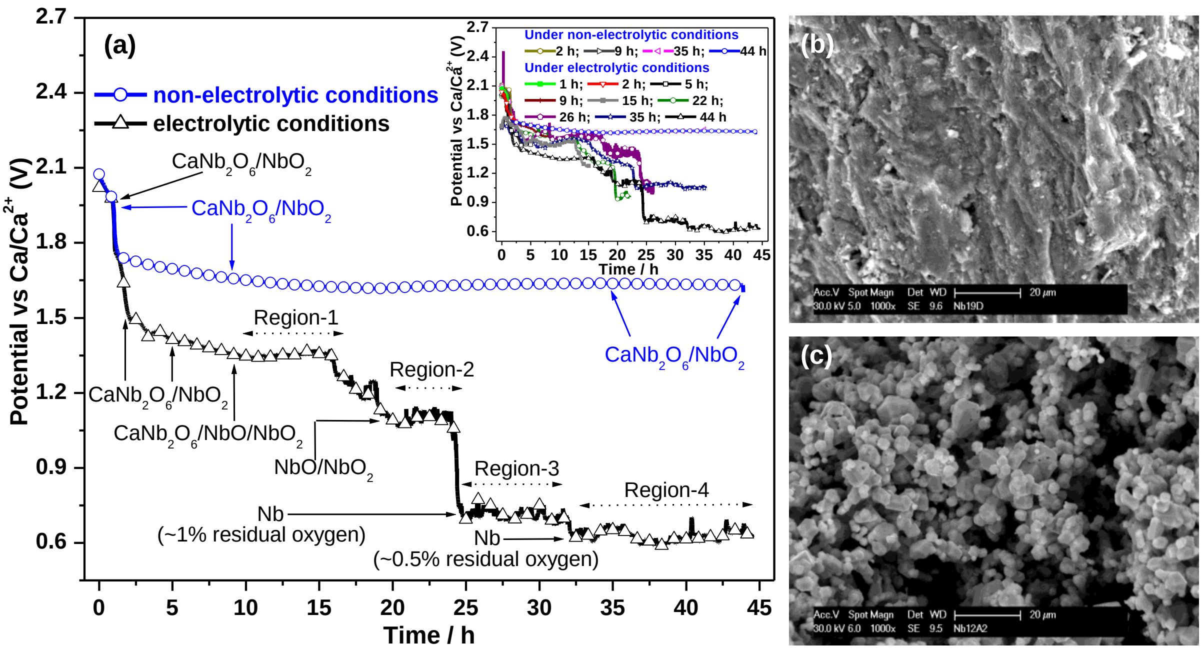

Fig. 3.8. (a) Potentials of the indicator pellets with time employed for 44 h under non-electrolytic and electrolytic conditions. Inset shows the indicator pellets employed for different time periods as indicated. SEM image of cross section of indicator pellet employed for (b) 44 h under non-electrolytic conditions (c) 22 h under electrolytic conditions. XRD confirmed the phase as Nb in the latter case.

The XRD analysis confirmed Nb as the phase present in the former case whereas it was a mixture of $CaNb_2O_6$ and NbO_2 in the latter case. The galvanic potentials of the pellets from the experiments, repeated for different time periods to identify the phases formed at various potential stability regions under both EC and NC are given in inset of Fig. 3.8a. Under NC, the pellets after 2, 9, 35 and 44 h showed only a mixture of $CaNb_2O_6$+NbO_2. Under EC, the galvanic potentials of indicator pellets traced more or less same path, although the time required for acquiring and its duration of stay at a stable region of potential differed. The reasons for this were attributed to the changing chemistry or composition of the melt and the possibility of chemical reaction of Nb_2O_5 with CaO and/or Ca generated in the melt during the course of electrolysis. XRD analysis of the pellets showed that the stability in potentials at regions-1, 2, 3 and 4 corresponded to the formation of $CaNb_2O_6$+NbO+NbO_2, NbO+NbO_2, Nb (with ~1% residual oxygen) and Nb (with ~0.5% residual oxygen), respectively. The presence of $CaNb_2O_6$ in the indicator pellet under NC suggested that the pellet chemically reacted with the CaO present in the melt. The indicator pellet employed under EC for 22 h and above was converted to Nb. The residual oxygen content of the Nb obtained decreased with increase in duration of immersion and after 44 h, the indicator pellet was converted to Nb metal with a residual oxygen content of ~ 4,500 ppm. Figs. 3.8 b and c show the microstructures of indicator pellets employed under NC for 44 h and EC for 22 h, respectively.

Fig. 3.8c shows the porous matrix of the pellet with relatively smaller spherical grains of Nb obtained after 22 h under EC. However under NC, the distinct grains of Nb_2O_5 present initially in the pellet (Fig. 3.3Bc) were converted to dense matrix (Fig. 3.8b) due to the reaction of CaO from the melt with the grains leading to the formation of $CaNb_2O_6$ and remained as such even after 44 h of immersion. Since the applied voltage during EC is beyond the decomposition potential of CaO and Nb metal produced is inert towards Ca^{2+} ions, the decomposition of CaO at Nb metal and Ta cup cathode is expected to produce Ca metal at activities less than unity, which gets dissolved in to the melt. The reduction of the indicator Nb_2O_5 pellet under EC, shown above, must have occurred due to reaction with the elemental Ca generated during the electrolysis, which was not observed for indicator pellet employed under NC. It can be concluded from the results that Ca metal was generated during the electrochemical reduction of Nb_2O_5 at 3.1 V in $CaCl_2$ melt at 1173 K even as the potential was below the decomposition potential of $CaCl_2$ (3.235 V) and the calcium metal chemically reacted with the Nb_2O_5 pellet to reduce it to the metal. This must be applicable to the electro-reduction of most of the oxides reported in $CaCl_2$ melt under similar potential conditions. The indicator pellet tests also indicated the chemical formation of $CaNb_2O_6$ and Nb metal via the formation of the various intermediates.

3.3.5. Behaviour of graphite anode during electrolysis

The loss of weight of the graphite anode during electrolysis is mostly due to the formation of CO/CO_2 gases and erosion under the electrolytic cell conditions. The formation of CO/CO_2 gas can be linked to the deoxidation of cathode. The photograph of anodes before and after electrolysis is shown in Fig. 3.9A and the corresponding weight losses measured after electrolysis are given in Fig. 3.9B.

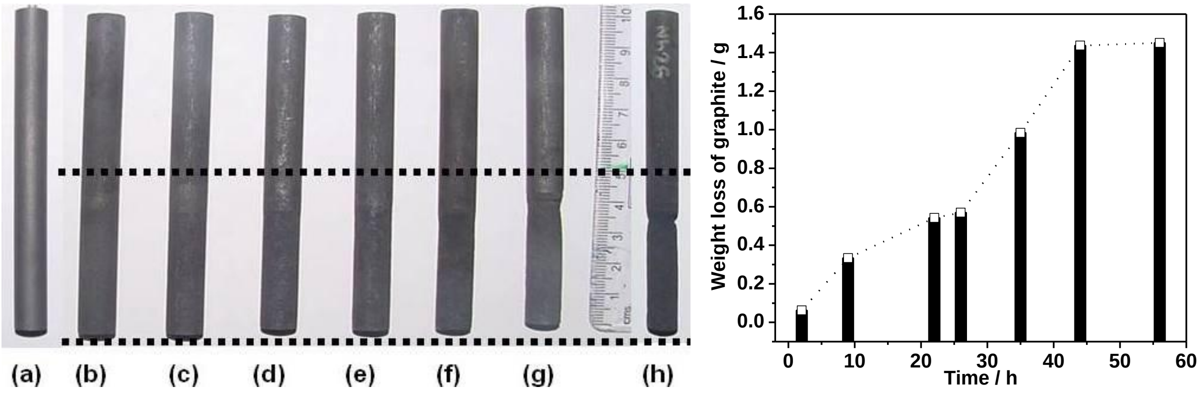

(A) (B)

Fig. 3.9. (A) Photograph of the graphite rods employed as anodes (a) before electrolysis and after electrolysis for (b) 2 h (c) 9 h (d) 22 h (e) 26 h (f) 35 h (g) 44 h and 56 h (B) Weight loss of graphite with time of electrolysis.

The part of the anode that was dipped in the melt (~4 cm) appeared to have corroded more with time and this was reflected in the weight loss measurements in Fig. 3.9B. It was observed, in general, that in experiments carried out for longer durations of time, the side of the graphite facing the cathode (Nb_2O_5 pellets) corroded preferentially and the intensity of the attack was severe at the melt - gas plenum or interface and decreased towards the bottom. SEM images of the regions of graphite dipped in the melt, given in Fig. 3.10, revealed many interesting aspects.

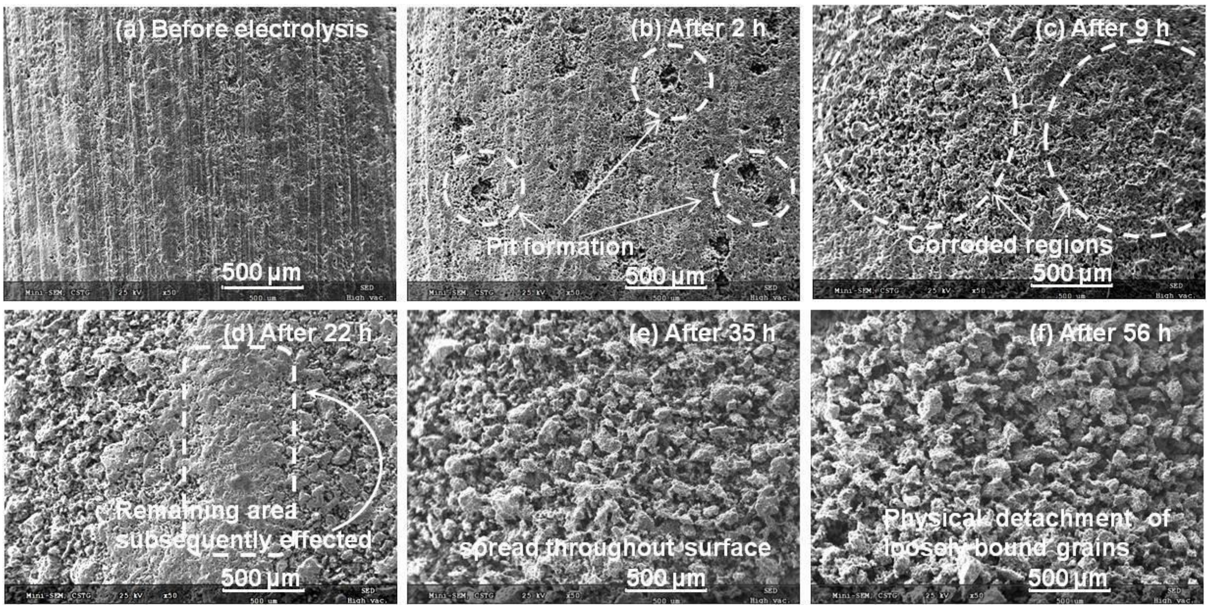

Fig. 3.10. SEM images of the surface of graphite (a) before electrolysis and after electrolysis for (b) 2h (c) 9h (d) 22 h (e) 35 h and (f) 56 h.

The surface of graphite, primed as discussed in chapter 2, before electrolysis contained longitudinal scratches generated due to polishing of the surface. After 2 h, formation of pits of about 150 µm in size was observed (Fig. 3.10b). An immersion test of graphite in molten $CaCl_2$ for 44 h under NC showed that the surface of the graphite remains unaffected, when exposed to the melt at 1173 K. It was reported that chlorine evolution at the surface of graphite at lower current densities (~0.04 A cm^{-2}) causes practically no degradation of its surface [175,176]. Therefore, oxide ions present in the melt / generated at the cathode would have got oxidized by carbon consuming reactions (CO/CO_2 formation) in combination with Cl_2 evolution (based on potential in Fig. 3.3A) at the anode that would have lead to destruction of its surface by forming pits. Further attack in the vicinity of the pits by oxidation of oxide ions would have enlarged the attacked areas (Fig. 3.10c). The damage of such regions expanded to adjacent regions (Fig. 3.10d) and covered the entire surface causing severe etching of the grains in 35 h (Fig. 3.10e). During the rest of the electrolysis, further oxidation along with physical detachment of the loosely bound grains (Fig. 3.10f) caused much weight loss of the graphite. It was interesting to note that the weight loss was not significant after 44 h (Fig. 3.9B). This indicated that once the reduction of Nb_2O_5 to Nb is completed electro-deoxidation induced corrosion of graphite becomes insignificant. Within the limited study, it can be discerned from Fig. 3.9B that the rate of electro-deoxidation induced corrosion of graphite was high between 0 - 9 h and 26 - 44 h of electrolysis. However, based on sluggish rise in weight loss of graphite between 9-26 h of electrolysis, it appears that the corrosion rate of graphite was relatively less which may be an indication of a decreased rate of release of oxide ions from the cathode during this period.

3.3.6. The mechanism of electro-deoxidation of dense Nb_2O_5 pellets

The chemical composition of the different partially electrolysed samples, corresponding TSB-C, TIB and TSB-M data in addition to the vital information gained from CV, polarisation, CEPM, IPT and corrosion and weight loss of graphite anodes at various time periods of electrolysis together were used to arrive at the mechanism of electro-reduction of Nb_2O_5 to Nb. All the probable reactions that could have occurred during the cathodic polarisation process are listed in the analysis given below. All the reactions are written in such a way that the electro-neutrality of the melt is preserved, i.e., the number of electrons consumed in the cathodic reactions is equated to those released at the anode in the corresponding anodic reactions.

As discussed earlier, three stages of electrolysis, viz. initial, intermediate and final stages are identified for the reduction process during 0-2.5 h, 2.5-22 h and 22 h to end of electrolysis. The major reactions / changes that occur during the 3 stages are discussed below:

3.3.6.1. Initial stage of electrolysis

It can be seen from Fig. 3.3A as well as Fig. 3.4 that the current, anodic and cathodic potentials at the start of the experiment are the highest and thereafter decreased rapidly (compared to the latter part of the curves) to lower values in about ~2.5 h. A shoulder on all the three curves in Fig. 3.3A during this period and a more or less stable region on which the curves have landed can be taken as an indication of the end of a distinct phase of the cathodic process. As discussed earlier, the innermost layer of the Nb_2O_5 pellets retrieved after 2 h remained as unreduced Nb_2O_5, the intermediate layer showed the presence of Nb, Nb_2O_5, NbO_2 and $CaNb_2O_6$. The surface layer was converted to Nb metal. This in addition to the results of CV studies as well as the observation that the reactions take place at low cathodic potentials suggests that the electro-reduction was proceeding via formation of low-energy calcium intermediate compounds as

$$2Nb_2O_5 + Ca^{2+} + 2e^- \rightarrow CaNb_2O_6 + 2NbO_2 \qquad (3.1)$$

This initial reaction would have been taking place at all areas of the pellet where the melt was in contact with as the pellet was conducting. Obviously this would have happened to the two layers (outer and middle) during the period of electrolysis. As the electrode was under the impressed potential condition, subsequent reactions, which require higher energy would have been taking place at the surface layer, as indicated by the cathodic potential. These reactions, which finally converted the surface layer to Nb metal, will be discussed in the following section. Presence of unreduced Nb_2O_5 at the innermost part of the pellet indicates that those parts of the dense pellet were not in contact with the electrolyte melt.

Since a very insignificant amount of CaO was present only in the electrolyte, it is reasonable to assume that the Ca^{2+} required for the cathodic reaction (3.1) was essentially derived from the $CaCl_2$ melt. This, in other words, means that the anodic reaction corresponding to the cathodic reaction (3.1) must have been

$$2Cl^- \rightarrow Cl_{2(g)} + 2e^- \qquad (3.2)$$

The facts such as graphite (CE) polarised to potential of Cl_2 evolution during cathodic polarisation of Nb_2O_5 pellets during the combined CV-CEPM studies (Fig. 3.2b) and the anodic potentials during the initial stage of the electrolysis (Fig. 3.3A) remained always higher than that of the reversible chlorine potentials give ample proof for this. However, as the electrolysis of the surface layer was continuing, as indicated by the presence of the Nb metal layer, some amount of O^{2-} ions could have been electro-generated and a part of which could have been released to the melt with passage of time. The marginal increase of TSB of the cathode and the melt (Fig. 3.7a and 3.7b) are in line with the above mechanism. As O^{2-} ions become available in the melt, the anodic reactions involving release of CO and CO_2 would also have been taking place simultaneously, which is also supported by the weight loss and pitting corrosion of graphite anode (Figs. 3.9B and 3.10b) observed during this period.

$$O^{2-} + C \rightarrow CO_{(g)} + 2e^- \qquad (3.3)$$

$$2O^{2-} + C \rightarrow CO_{2(g)} + 4e^- \qquad (3.4)$$

The increase in the TIB of the melt (Fig. 3.7c) during the first two hours of electrolysis too indicates such a possibility.

The high current at the start of electrolysis, which is seen to be decreasing as the electrolysis proceeds, can be attributed to the extent of electro-active area available for the cathodic reaction. The three phase (conductor-oxide-electrolyte) contact area on which the electrochemical reactions occur decreases with time and hence the magnitude of the current too follows the trend. It has been established that during the beginning stages of electro-reduction of TiO_2, high-conducting Magnelli phases (TiO_{2-x}) are formed which significantly assist in the electro-reduction [12]. Similar sub-stoichiometric compounds [Nb_2O_{5-x}] are also reported in the Nb-O system, whose electrical conductivity is reported to increase with the increasing value of ‘x’ [177]. It is possible that such phases formed during the cathodic polarisation enhanced the electrical conductivity of the electrode. Also Ca-Nb-O compounds like $CaNb_2O_6$ are reported to be good electronic conductors [45].

3.3.6.2. Intermediate stage of electrolysis

As the cathodic polarisation is continued, more and more of the electrochemically generated phases decompose increasing the oxide content of the cathode as is evident from

Fig. 3.7a. As the CaO produced at the cathode dissolves in the melt, the CaO content of the melt also should have increased. But as per the data given in Fig. 3.7b, it is not so. On the other hand the TIB of the melt is seen to increase in this period of electrolysis, which shows that a reaction between the dissolved CaO and CO_2 in the melt is taking place to produce $CaCO_3$. As a portion of the CaO is released to the melt, formation of CO_2 becomes the prominent anodic reaction in this phase of electrolysis and hence formation of more and more $CaCO_3$ in the melt (and hence an increase in the TIB of melt) with passage of time is quite possible [70]. The remaining calcium oxide generated at the cathode accumulates there so that its concentration at the cathode becomes more than that of the melt.

The following reactions can be written for the cathodic generation of CaO from the electrolysis of the product of electrolysis that existed in the cathode at the end of 2 h of electrolysis, i.e., $CaNb_2O_6$ and $2NbO_2$.

$$2NbO_2 + Ca^{2+} + 2e^- \rightarrow CaNbO_3 + NbO \quad (3.5)$$

$$CaNbO_3 + 2e^- \rightarrow Ca^{2+} + NbO + 2O^{2-} \quad (3.6)$$

$$NbO + (1-\delta)Ca^{2+} + 2(1-\delta)e^- \rightarrow (1-\delta)Ca^{2+} + Nb[O]_\delta + (1-\delta)O^{2-} \quad (3.7)$$

$$NbO_2 + 2e^- \rightarrow NbO + O^{2-} \quad (3.8)$$

$$NbO_2 + 2(2-\delta)\, e^- \rightarrow Nb[O]_\delta + (2-\delta)\, O^{2-} \quad (3.9)$$

$$NbO + 2(1-\delta)\, e^- \rightarrow Nb[O]_\delta + (1-\delta)\, O^{2-} \quad (3.10)$$

$$CaNb_2O_6 + 2(3-\delta)\, e^- \rightarrow CaNbO_3 + Nb[O]_\delta + (3-\delta)\, O^{2-} \quad (3.11)$$

$$CaNb_2O_6 + 2e^- \rightarrow Ca^{2+} + 2NbO_2 + 2O^{2-} \quad (3.12)$$

Though expected, compounds like $CaNbO_3$ and NbO could not be detected in the sample by XRD analysis. It is likely that these compounds decomposed and transformed to $CaNb_2O_6$ and NbO_2. Of the reactions shown above, reactions (3.7)-(3.11) do not alter the CaO content, reactions (3.6) and (3.12) enhances whereas reaction (3.5) decreases the CaO content of the cathode and hence that of the melt. Part of the CaO released into the melt might have decomposed due to the applied voltage (3.1 V) generating Ca in the melt, which is indicated by the formation of NbO phase in the IP after 9 h (Fig. 3.8a). Yan et al. [45] reported electrochemical reactions similar to those represented by equations (3.1), (3.9) and (3.10).

The removal of the O^{2-} ions (or CaO) from the surface of the pellet by dissolution in the melt is relatively easy. However, this will not be the case for CaO present inside the pellet and hence CaO will accumulate inside the pellet. The accumulated CaO in turn can react with the various oxide phases present in the cathode to form higher ternary intermediates. The presence of higher ternary intermediates, $Ca_3Nb_2O_8$ and $Ca_4Nb_2O_9$ in samples N-3 and N-4 and a decreased rate of corrosion of graphite (Fig. 3.9B) during this period can be considered as the direct proof of this possibility. The following reactions can be written for formation of the above compounds from the chemical phases found in the sample, N-2.

$$Nb_2O_5 + CaO \rightarrow CaNb_2O_6 \qquad (3.13)$$

$$NbO_2 + CaO \rightarrow CaNbO_3 \qquad (3.14)$$

$$1/2Nb_2O_5 + CaO \rightarrow 1/2Ca_2Nb_2O_7 \qquad (3.15)$$

$$1/2CaNb_2O_6 + CaO \rightarrow 1/2Ca_3Nb_2O_8 \qquad (3.16)$$

$$Ca_2Nb_2O_7 + CaO \rightarrow Ca_3Nb_2O_8 \qquad (3.17)$$

$$1/3Nb_2O_5 + CaO \rightarrow 1/3Ca_3Nb_2O_8 \qquad (3.18)$$

$$1/3CaNb_2O_6 + CaO \rightarrow 1/3Ca_4Nb_2O_9 \qquad (3.19)$$

$$1/2Ca_2Nb_2O_7 + CaO \rightarrow 1/2Ca_4Nb_2O_9 \qquad (3.20)$$

$$Ca_3Nb_2O_8 + CaO \rightarrow Ca_4Nb_2O_9 \qquad (3.21)$$

$$1/4Nb_2O_5 + CaO \rightarrow 1/4Ca_4Nb_2O_9 \qquad (3.22)$$

As these reactions take place, the amount of CaO present in the cathode and hence its rate of release to the melt decreases, which in turn is reflected as a ‘decrease’ in the TSB of the melt at 22 h of electrolysis (N-3). The increasing TIB value during this period indicates the conversion of some amount of CaO to $CaCO_3$. Reaction (3.15) is likely to take place, but the phase is not identified in the product of the electrolysis in the present case, although it was reported by Yan et al. [45]. It is possible that the chemical compound underwent reaction (3.17) by the time the sample was collected and hence could not be identified.

The XRD analysis of N-3 and N-4 showed that even the innermost layer of the electrolysed pellet contained Nb metal. It is possible that the following reactions were taking place at the cathode. Niobium present in partially electro-reduced samples could contain significant quantities of dissolved oxygen in it as represented by '$\underline{Nb}$' in the following equations.

$$1/5Ca_4Nb_2O_9 + 2e^- \rightarrow 4/5Ca^{2+} + 9/5O^{2-} + 2/5\underline{Nb} \qquad (3.23)$$

$$1/2Ca_4Nb_2O_9 + 2e^- \rightarrow 2Ca^{2+} + 3O^{2-} + 1/2NbO_2 + 1/2NbO \qquad (3.24)$$

$$1/5Ca_3Nb_2O_8 + 2e^- \rightarrow 3/5Ca^{2+} + 8/5O^{2-} + 2/5\underline{Nb} \qquad (3.25)$$

$$1/5Ca_2Nb_2O_7 + 2e^- \rightarrow 2/5Ca^{2+} + 7/5O^{2-} + 2/5\underline{Nb} \qquad (3.26)$$

$$1/5CaNb_2O_6 + 2e^- \rightarrow 1/5Ca^{2+} + 6/5O^{2-} + 2/5\underline{Nb} \qquad (3.27)$$

$$1/2CaNbO_3 + 2e^- \rightarrow 1/2Ca^{2+} + 3/2O^{2-} + 1/2\underline{Nb} \qquad (3.28)$$

The above electrochemical decomposition reactions, obviously, would have caused a significant accumulation of CaO at the cathode, which is reflected in the steep increase of the TSB of both the cathode and the melt after 22 h of electrolysis (Figs. 3.7a and b). This in turn resulted in the significant reaction of the CaO with dissolved CO_2 to form $CaCO_3$, which is reflected in the increase of TIB of the melt from 22 to 35 h. After 35 h, higher calcium niobates were not observed and only appreciable levels of $CaNb_2O_6$ along with traces of $CaNbO_3$ were seen in the product. The presence of a lower level of $CaNb_2O_6$ after 26 h and a significantly higher level of $CaNb_2O_6$ along with appreciable levels of Nb_2O_5 in sample N-5 further indicated the possibility of phase decomposition of higher calcium niobates [reactions (3.29-3.32)] as reported by Qiu et al. [49] and Song et al. [50].

$1/4Ca_4Nb_2O_9 \rightarrow CaO + 1/4Nb_2O_5$ (3.29)

$1/3Ca_3Nb_2O_8 \rightarrow CaO + 1/3Nb_2O_5$ (3.30)

$1/2Ca_2Nb_2O_7 \rightarrow CaO + 1/2Nb_2O_5$ (3.31)

$CaNb_2O_6 \rightarrow CaO + Nb_2O_5$ (3.32)

Simultaneously, following electrochemical reactions would have occurred at the cathode to produce many suboxides and Nb metal that were detected by the XRD analysis of N-5.

$1/4Ca_4Nb_2O_9 + 2e^- \rightarrow Ca^{2+} + 2O^{2-} + 1/4NbO + 1/4\underline{Nb}$ (3.33)

$1/2Ca_3Nb_2O_8 + 2e^- \rightarrow 3/2Ca^{2+} + 5/2O^{2-} + 1/2NbO_2 + 1/2NbO$ (3.34)

$1/4Ca_3Nb_2O_8 + 2e^- \rightarrow 3/4Ca^{2+} + 7/4O^{2-} + 1/4NbO + 1/4\underline{Nb}$ (3.35)

$1/2Ca_2Nb_2O_7 + 2e^- \rightarrow Ca^{2+} + 2O^{2-} + 1/2NbO_2 + 1/2NbO$ (3.36)

$1/4Ca_2Nb_2O_7 + 2e^- \rightarrow 1/2Ca^{2+} + 3/2O^{2-} + 1/4NbO + 1/4\underline{Nb}$ (3.37)

$1/2CaNb_2O_6 + 2e^- \rightarrow 1/2Ca^{2+} + 3/2O^{2-} + 1/2NbO_2 + 1/2NbO$ (3.38)

$1/4CaNb_2O_6 + 2e^- \rightarrow 1/4Ca^{2+} + 5/4O^{2-} + 1/4NbO + 1/4\underline{Nb}$ (3.39)

$2/5CaNb_2O_6 + 2e^- \rightarrow 2/5Ca^{2+} + 7/5O^{2-} + 1/5Nb_4O_5$ (3.40)

$CaNbO_3 + 2e^- \rightarrow Ca^{2+} + 2O^{2-} + NbO$ (3.41)

While reactions (3.23)-(3.41) occur at the cathode, a fraction of the released oxide ions only undergoes anodic reaction to generate the number of electrons consumed at the cathode. The tremendous accumulation of CaO from the cathode bulk this way is reflected in the steep increase of the TSB of the cathode and the melt (Fig. 3.7a and b). The TIB of the melt too increased significantly during this stage (Fig. 3.7c). The Nb_2O_5 formed by phase decomposition of higher niobates (represented by (3.29)-(3.32)) at the bulk, undergoes the electrochemical insertion reactions to form $CaNb_2O_6$ and suboxides as per reaction (3.1). This process continues until the whole mass is converted to suboxides by taking electrons from the external source. In other words, this reaction is driven by the applied potential. The produced suboxides may directly release oxygen ions into the melt or again get converted to a mixture of lower calcium niobates (which again release Ca^{2+} and O^{2-} into the melt) and low-valent oxides. The deoxidation of the outer layers of the pellet makes its surface highly porous and this in turn paves way for contact of calcium chloride melt to the bulk areas of the pellet. As the electrolysis is continued, the reaction front moves inwardly. Obviously all these conditions favour dissolution of the O^{2-} ions, present in the bulk, in the $CaCl_2$ melt.

A marked difference can be noticed from ~ 20 h of electrolysis in both the current and potential curves given in Fig. 3.3A. The current is seen to show a significant decrease around this time. The more or less stable cathodic potential started shifting in the anodic direction and the anodic potential towards higher values. The changes in the current and potential patterns should, obviously, be related to the cell reaction. The decrease of current can be related to the decrease in the active electrode area. From Fig. 3.7 a, b and c it is clear that significant CaO is produced at the cathode at around 20 h as a result of reactions (3.23-3.41) described above. It is reasonable, therefore, to assume that the available reaction sites for calcium impregnation reaction were decreasing and this was reflected in the decrease of current. The release of CaO to the melt and formation of $CaCO_3$ in the melt as shown by the TSB and TIB curves, indicate the possibility of new cathodic reactions including redox cycling of CO_3^{2-} ions, which all would have contributed to the change in the cathodic potential. The cell is under constant voltage mode (3.1 V) and hence it is required that the impressed voltage (minus the IR and polarisation losses) be distributed between the cathode and anode. As the current decreased after 22 h, the IR drop of the cathode decreased which in turn is shown by the decrease of the cathode potential. Correspondingly the anode potential showed an increase as is evident from Fig. 3.3A.

3.3.6.3. Final stage of electrolysis

The applied potential is well above the decomposition potential of CaO, which helps in the decomposition of CaO. The decomposition reaction can take place on the metal part of the cathode as well as on the freshly electro-formed Nb cathode. The resulting calcium metal dissolves in the melt. This Ca reacts with the oxygen remaining at the cathode as well as that of the IP (Fig. 3.8a). The reduction of Nb_2O_5 IP to Nb is an ample proof of the generation of Ca at activities well below unity during the process. A set of possible chemical reactions at the cathode at the later stage of electrolysis can be as follows:

$$Ca^{2+} + 2e^- \rightarrow Ca \text{ (at the surface of Nb)} \quad (3.42)$$

$$CaNb_2O_6 + Ca \rightarrow 2CaO + 2NbO_2 \text{ (at the bulk)} \quad (3.43)$$

$$Nb_2O_5 + Ca \rightarrow CaO + 2NbO_2 \text{ (at the bulk)} \quad (3.44)$$

$$NbO_2 + Ca \rightarrow CaO + NbO \text{ (at the bulk)} \quad (3.45)$$

$$NbO + (1-\delta)\, Ca \rightarrow (1-\delta)\, CaO + Nb\, [O]_\delta \text{ (at the bulk)} \quad (3.46)$$

$$Nb[O]_\delta + (\delta-\mu)Ca \rightarrow (\delta-\mu)CaO + Nb[O]_{(\delta-\mu)} \text{ (surface \& bulk, where } \delta>\mu) \quad (3.47)$$

These processes are repeated until all the oxides decompose and the electrode is changed to Nb metal with dissolved oxygen present in it ($\underline{Nb}$). Similar results were reported in the case of the electrochemical reduction of TiO_2 in $CaCl_2$ melt by Schwandt et al. [12]. As the cathodic polarisation is continued, the de-oxygenation of the $\underline{Nb}$ cathode takes place and eventually the whole of the electrode is converted to Nb metal. The current should continuously decrease, though very marginal, until the end of the experiment indicating the removal of oxygen. However, the electrolysis curve given in Fig. 3.3A shows that the current remains more or less stable after attaining a minimum value. This can be due to secondary cell reactions [70]. Also the calcium metal being generated in the cell [reaction (3.42)] towards the end of the electro-deoxidation reaction can dissolve in the melt and contribute to the electronic conductivity of the melt to give rise to the background current.

The decomposition of CaO due to electrolysis and the reaction of CaO with dissolved CO_2 to form $CaCO_3$, could decrease the concentration of the dissolved CaO. Out of these two reactions, the conversion of CaO to $CaCO_3$ only resulted in a decrease of the TSB of the melt.

As concentration of CaO in the melt decreases this way, more and more of the CaO trapped at the cathode area diffuses out to the melt so that the TSB of the cathode is decreased. Needless to mention, the TIB of the melt is increased under these conditions. $CaCO_3$ present in the melt can undergo decomposition at the elevated temperature of operation. Also the redox cycling of CO_3^{2-} and formation of TaC (X-ray diffractogram given in Fig. 3.11) as per the reaction

$$Ta + CO_3^{2-} + 4e^- \rightarrow TaC + 3O^{2-} \qquad (3.48)$$

decrease the concentration of $CaCO_3$ in the melt. A similar reaction of CO_3^{2-} with electro-generated Nb metal to form NbC is possible (Table 3.1). Due to these reactions, the rate of increase of the TIB of the melt, though expected to increase drastically towards the end of electrolysis, was not as high as can be seen from Fig. 3.7c.

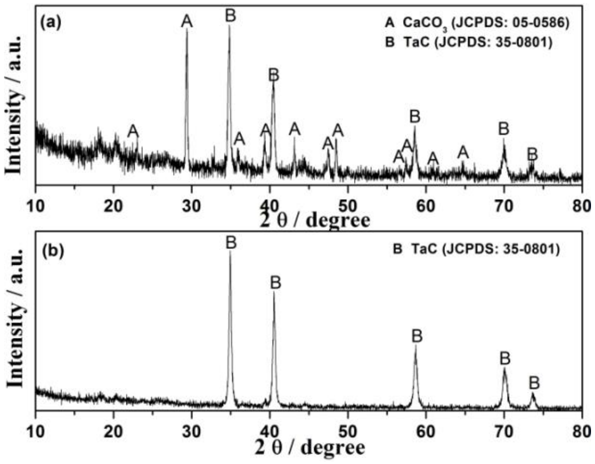

Fig. 3.11. X-ray diffractograms of melt residue (a) before treatment with 0.25 N HCl and (b) after treatment with 0.25 N HCl.

3.3.7. The physical model of electro-reduction of a high dense Nb_2O_5 pellet

It was seen that the cross section of dense Nb_2O_5 pellets electrolysed for different durations of time had physically distinct layers having different chemical compositions. The surface layer was seen to be reduced to Nb in all the samples and the extent of metallisation decreased as the distance from the surface towards the inner centre of the pellet was increased. From the analysis made above, it can be concluded that an oxide particle is converted to the respective metal particle via. three reaction steps either independently one after the other or simultaneously. The three steps are; step ‘A’- initial formation of calcium insertion compounds and suboxides, step ‘B’- decomposition and deoxidation of the calcium compounds and step ‘C’-de-oxygenation by electro-deoxidation followed by chemical reaction with the electro-generated calcium metal. Based on the observations, an empirical model of the reduction process occurring in a dense, thick and electrically conducting oxide pellet has been proposed here.

The physical progress of the electro-reduction reactions taking place in a dense oxide pellet is depicted in Fig. 3.12. The pure oxide phase, the calcium insertion reaction phase, the intermediate compounds phase and the metal phase are shown by different shades in Fig. 3.12a-g. Similarly, the extent of occurrence of the three different steps A, B and C during the electrochemical reduction is represented by the relative thicknesses of the respective arrows. When a Nb_2O_5 pellet is lowered into the melt (Fig. 3.12a) and the potential applied, the reaction taking place primarily is the electrochemical insertion of Ca^{2+} from the melt into the cathode to give rise to Ca-Nb-O intermediate compounds and suboxides. This is shown in step ‘A’ (Fig. 3.12b), by a thick-lined arrow. During this step, steps ‘B’ and ‘C’, (represented by thin, dashed and dotted lines) have not commenced. With time, the calcium insertion reactions and hence the thick-lined arrow moves towards the inner parts of the pellet. As the calcium insertion reactions progress to the bulk, the step B commences at the surface of the pellet and this is indicated by an increase in the thickness of the dashed arrow (Fig. 3.12c and d). Due to step ‘B’, the open porosity of the pellet was increasing, as indicated by the broken lines on the surface of the pellet. It is assumed that the oxide pellets used in this model is sufficiently conducting and hence the steps ‘A’ and ‘B’, in principle, can take place on any part of the pellet subject to coexistence of the three essential components necessary for electro-reduction, viz. the oxide, the electron and the electrolyte [151]. The predominance of a particular step depends on the location of the particles from the surface. When the metal oxide layer is very thin, the different reactions mentioned above can take place on it sequentially so that all the particles in the layer can be reduced to metal rather quickly. Hence the surface layer gets reduced fast. However, for a particle in the inner layer, contact with the electrolyte melt is difficult. Even when electrolyte contact is established, the oxide ions released from the particles cannot escape the electrode, as easily as that of a particle on the surface of the solid. This condition favours the formation of higher calcium niobates in the bulk of the pellet. Such kinetic limitations to electrochemical reactions and removal of oxygen causes different layers in the solid to undergo different levels of changes so that an incompletely reduced pellet shows different layers having different chemical compositions across the thickness of the pellet. As the cathodic polarisation is continued, the formation of elemental calcium commences on the surface of the pellet as well as on the metallic current leads and this in turn reacts with the cathode to effect further removal of oxygen as CaO (step 'C'). This is indicated by an increased thickness of the dotted arrow. The increase in the thickness of the arrow from Fig. 3.12e to Fig. 3.12h shows the increasing role of calcium in the reduction process towards the end of electrolysis. Eventually, the pellet gets converted to Nb metal. The distance between the arrow heads in the above model indicates the time span between the steps 'A', 'B' and 'C'.

The predominance of a particular step among the three steps A, B and C depends on parameters such as the electrical conductivity of the metal oxide and the intermediate phases formed during the reduction process, electrochemical reactivity of the oxide electrode towards the cation of the melt, physical parameters of the metal oxide preform such as density, thickness, particle size, and stability of the intermediate products, cathode configuration, pre-treatment and particle size of the oxide precursor powder, porosity, sintering conditions of the solid electrode, electrolysis voltage etc. The effect of these aspects on the electro-deoxidation of ZrO_2 were discussed in detail by Mohandas and Fray [11,54].

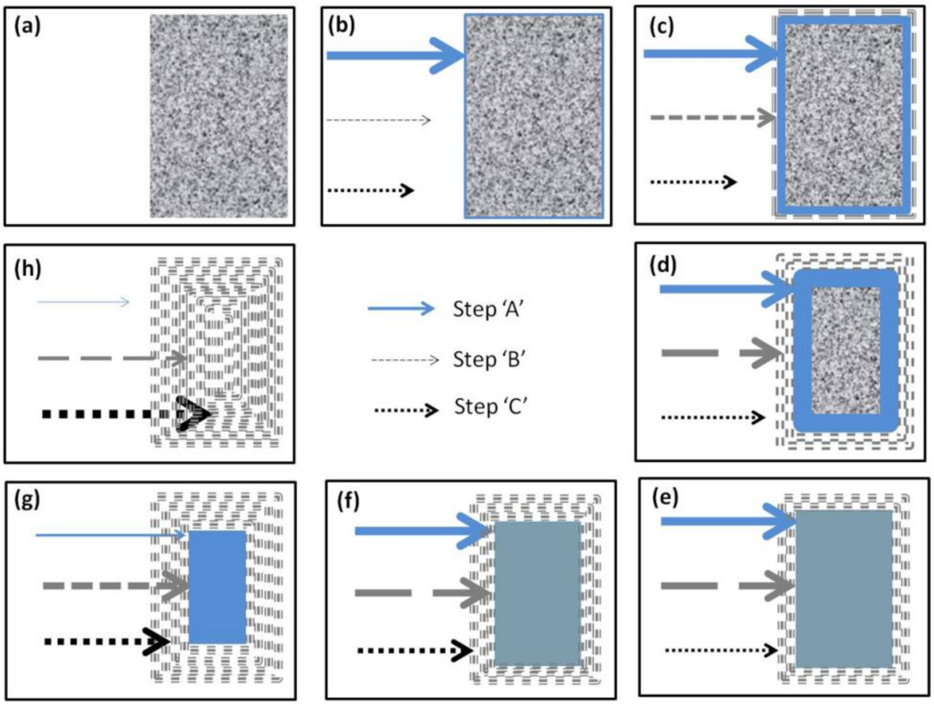

Fig. 3.12. Schematic of the progress of electrochemical reduction in dense Nb_2O_5 pellets. Gradual changes occurring towards complete conversion of the dense oxide pellet to metal are depicted in (a) to (h). Steps 'A', 'B' and 'C' represent calcium insertion followed by simultaneous oxygen rearrangement, deoxidation via intermediate-suboxide formation and electro-generated-calcium-induced reduction, respectively. The thicknesses of different arrows in the figure represent the predominance with which each step manifests in the sample under cathodic polarisation. All the three steps are necessary for conversion of an oxide particle/layer to the metal and those can take place sequentially or simultaneously depending on the physical conditions of the oxide preform and electrolysis conditions.

An understanding on various factors which may influence the electro-reduction process is of interest to scale up the process to higher quantities.

3.3.8. Factors influencing the electrochemical reduction of Nb_2O_5 pellets

A series of electro-reduction experiments have been carried out to investigate the influence of various parameters on the DOER of Nb_2O_5 pellets in molten salts. Since the Nb_2O_5 pellets electrolysed for 44 h were completely reduced to Nb, most of the experiments were carried out for 44 h and the results were compared with those of N-6. The key results of the study are given below.

3.3.8.1. Time of electrolysis

Results of experiments carried out for different durations were discussed previously. In addition, one more experiment was carried out for 56 h to check for the effect of prolonged time of electrolysis on the product. The pellets electrolysed for 44 h (N-6) and above (56 h) were uniformly converted to Nb metal, although the residual oxygen of Nb in the latter case was found to be less (~ 5,000 ppm) than that of the former (~ 6,400 ppm). In all other cases, the pellets were partially reduced and showed the presence of various Ca-Nb-O compounds, suboxides and Nb in the products. The depth to which metallisation occurred increased with time. The charges passed for 44 h and 56 h of electrolysis were found to be 17.71 Ah and 24.19 Ah and the corresponding current efficiencies were estimated to be 16.8% and 12.6%, respectively. Therefore, from the results it is evident that once the reduction is complete, further increase in time of electrolysis decreases the current efficiency of the electro-reduction process.

3.3.8.2. Temperature of electrolysis

The results of the electro-reduction experiments carried out at 1173 K and 1073 K showed that the currents observed at 1173 K were found to be higher than those observed at 1073 K and the corresponding charges passed were found to be 17.7 Ah and 11.5 Ah. The pellets electrolysed at 1173 K were fully reduced whereas in the latter case only the surface was reduced to Nb metal and bulk remained partially reduced and showed the presence of $CaNb_2O_6$ and NbO_2 with trace levels of Nb_2O_5, NbO and Nb. The results showed that the rate of reduction decreased, when temperature was decreased from 1173 K to 1073 K.

3.3.8.3. Applied voltage

The results of two reduction experiments carried out at 3.1 V and 2.5 V were compared. Though complete reduction occurred in both the cases, the product appeared spongy in the latter case. The microstructural and EDX analysis of cross section of the pellet in the latter case (Fig. 3.13) showed the formation of Nb grains of three different morphologies. The grain size of Nb obtained at lower voltage was larger (Fig. 3.13) than that at the higher voltage (Fig. 3.3Bd) though the residual oxygen contents in both the cases were similar (~6,400 ppm). The analysis of the currents and the charges passed for initial 26 h of electrolysis in both the cases indicated that the rate of reduction was relatively high when the applied voltage was 3.1 V compared to that at a lower voltage (2.5 V).

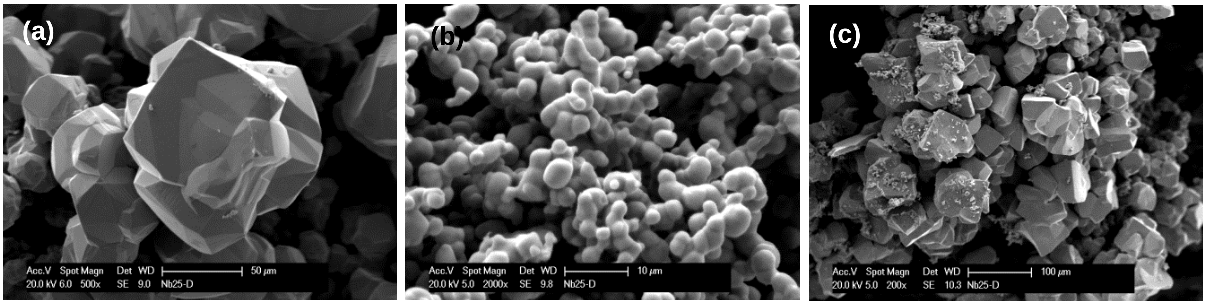

Fig. 3.13. SEM images of the cross section of the pellet reduced at 2.5 V showing three different microstructures (a, b and c) of Nb.

3.3.8.4. Porosity of pellets

Nb_2O_5 pellets of OP ~10% (N-6) and ~42% electrolysed for 44 h were completely converted to Nb. The charges passed in each of these cases were found to be 17.7 Ah and 18.7 Ah, respectively. The currents observed with porous pellets during the initial 5 h were relatively higher compared to that with the dense pellet. Another experiment was carried out with porous (OP ~42%) Nb_2O_5 pellets for 22 h. The pellets employed were completely converted to Nb metal though the high density pellets (OP ~10%) electrolysed under similar experimental conditions for 22 h (N-3) showed only partial reduction. Therefore, the results indicate that the reduction is enhanced by increasing the open porosity of the pellets.

3.3.8.5. Nature of the anode

Two different graphite materials – high density graphite (HDG, density 1.84 g/cc) and pyrolytic graphite (PyG, density 2.22 g/cc) have been investigated as anodes in the electro-reduction of Nb_2O_5 pellets for 20 and 44 h. Total charges passed in both the cases, after similar duration of electrolysis, were found to be similar. However, the weight losses of HDG after 22 and 44 h were found to be higher (0.8069 g and 0.9419 g) compared to that of PyG (0.2492 g and 0.6467 g). Contamination of the product (carbide formation) and melt contamination by carbon particles was high when HDG was used as the anode. The melt was relatively clean when HDG was replaced with PyG.

3.3.8.6. Mode of electrolysis

Two modes, i.e., constant voltage (Con-V) and constant current (CC) modes, have been employed for the electro-reduction of Nb_2O_5 pellets. The V-t curves during CC mode of electrolysis and photographs of the products from the two modes of electrolysis are given in Figs. 3.14A and B, respectively. In the Con-V mode (at 3.1 V), the pellet was stable during electrolysis and complete reduction to Nb was achieved with the pellet remaining intact. However, in CC mode of electrolysis at 0.5 A and 0.2 A (Fig. 3.14A), the pellet was found to delaminate during the electrolysis leading to its detachment from the current collector although small amount of mass remaining adhered to the current collector was found to be Nb metal. Even though, the magnitude of the applied current in CC mode was different in the two experiments, the voltage of the cathode remained at ~ 1 V vs. Ca/Ca^{2+} for significant duration leading to various phase changes in the pellet. Probably this would have lead to its destabilization. Also, it was reported that the CaO generated in the vicinity of cathode enhances the dissolution of niobium oxides in $CaCl_2$ melt [45] and this could have further destabilized the pellet. However in Con-V mode at 3.1 V, a higher cathodic voltage is felt on the pellet, for instance as in Fig. 3.3A, which probably would have lead to the instantaneous metallization at the surface and this would have helped to maintain mechanical integrity of the pellet during the electro-reduction process. The pellets from Con-V mode showed metallic sheen after polishing (Figs. 3.14B b and c) which was not the case with the products retrieved from the melt from CC mode of electrolysis. The retrieved products were found to be Nb in the latter cases too. However the residual oxygen content of the samples retrieved from the melt (Fig. 3.14B d and e) were high (~ 3.5%) compared to that retrieved from the tantalum wire current collector (~ 6,000 ppm) (Fig. 3.14Bf). The cell voltages in CC mode remained at ~ 3 V for significant durations. The mass retrieved from the melt would have undergone reduction by another mechanism as discussed in section 3.3.4.

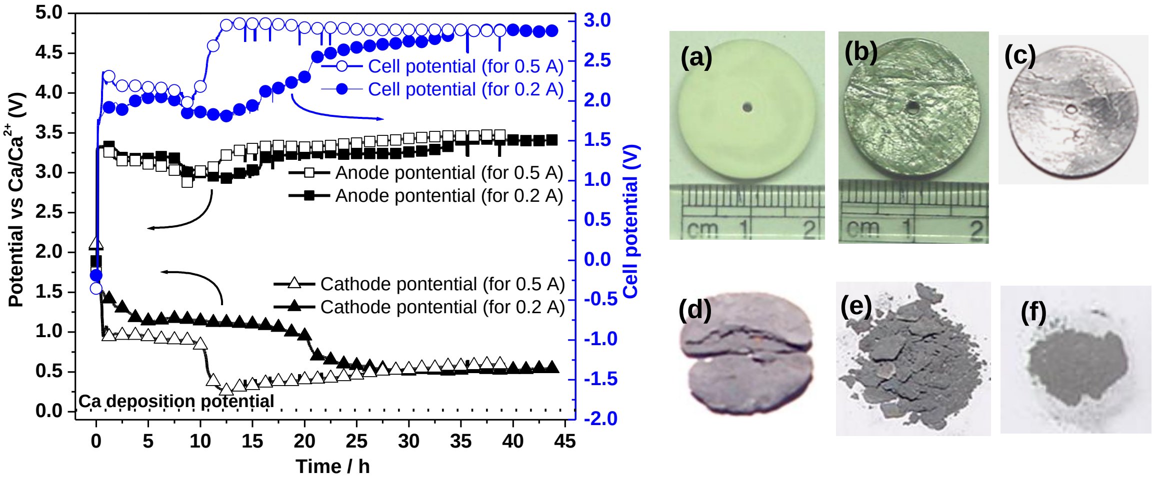

(A) (B)

Fig. 3.14. (A) V-t curves during the constant current electro-reduction of dense Nb_2O_5 pellets at 0.5 A and 0.2 A in $CaCl_2$ melt at 1173 K (B) Photographs: Before electrolysis (a) Nb_2O_5 pellet; After electrolysis in constant voltage (3.1 V) mode for (b) 20 h and (c) 44 h; In constant current mode the pellets became unstable and dislodged from the current collector. The products from experiments carried out at 0.5 A for 40 h and 0.2 A for 44 h, retrieved from the melt, are shown in (d) and (e), respectively. The mass retrieved from the tantalum current collector in the latter case is shown in (f).

3.3.8.7. Cathode configuration

To study the effect of cathode configuration, Nb_2O_5 pellets of three different configurations were electrolysed at 3.1 V: (a) The pellets were taken in a perforated Ta cup as in N-6 (b) Pellets were tied with a Ta wire followed by electrolysis in fully immersed position and (c) Pellets were tied with a Ta wire followed by electrolysis in tip (~4 mm) immersed position without the current collector in touch with the melt. Electrolysis with the first configuration has been discussed in section 3.3.3. The currents observed during electrolysis in tip immersed condition were relatively lower than that in fully immersed conditions which can be attributed to the less electro-active area available for reaction in the tip immersed pellet. Though the pellet was completely reduced in the latter case, in the former case the pellet, partitioned in to three regions, showed various phases. The tip region was fully reduced with traces of carbide phase formation whereas the intermediate region showed increased levels of carbide. The top region contained $CaNb_2O_6$ along with suboxides of Nb. It was observed that although the carbide formation cannot be avoided, its formation can be minimized by fully immersing the pellet to a sufficient depth. It was observed that when a perforated cup was employed to contain the pellets, it acted as a hindrance for the dissolution of the CaO generated at the pellets during the process. The dissolution of CaO is more facilitated when the pellet was tied with Ta wire and electrolysed in fully immersed condition. Therefore, this configuration helps for better reduction which is also supported by less residual oxygen (~ 4,400 ppm) of Nb and the higher current efficiency (19.15%) compared to those with the other two configurations.

3.3.8.8. Container effect

The effect of the container material of the electrolyte on the electro-reduction of Nb_2O_5 was studied by taking crucibles made up of SS and alumina. Relatively higher currents were observed when SS was used as the container when compared to that of alumina and the total charges passed were found to be 26.44 Ah and 17.71 Ah, respectively. Though the pellets were completely converted to Nb in both the cases, the current efficiency for the reduction of Nb_2O_5 to Nb in case of SS container was less (11.36%) than that of alumina container (16.77%). Also the residual oxygen content of Nb in the former case (2.9%) was found to be higher when compared to that in the latter (~ 6,400 ppm). The container which acts as a getter for Ca, for instance alumina, may decrease the calcium content of the melt and hence the electronic conduction and may increase the efficiency of the process. Therefore, the use of alumina crucible as the container over SS crucibles is advantageous to avoid higher background currents, enhance the efficiency of the reduction process and for obtaining Nb of lower residual oxygen content. The results of higher current efficiency of the process with refractory ceramic crucible from the present study are in line with those observed by Schwandt et al. [22] for the electro-reduction of TiO_2.

3.3.8.9. Melt composition

Electro-reduction experiments of Nb_2O_5 were carried out in various melts such as NaCl, KCl, KCl-25mol.% $CaCl_2$ and the results are compared with those from $CaCl_2$ melt.

i) NaCl melt

The I-t curves for the electro-reduction of Nb_2O_5 pellets in NaCl melt using graphite as the anode for 9, 22 and 44 h at 1173 K along with photographs of the products in insets are given in Fig. 3.15A and the microstructures of the products are shown in Fig. 3.15B. After 9 and 22 h electrolysis, the pellets contained two regions – the outer spongy grey coloured reduced region (Nb) and the inner mass containing bluish violet - granite like particles as shown in insets (a) and (b) of Fig. 3.15A, respectively. The pellet was uniformly reduced to Nb after 44 h and the current efficiency was found to be 16.26% which was almost the same as that observed in case of $CaCl_2$ melt (16.77%). The microstructures of the inner regions shown in Figs. 3.15A a and b are shown in Figs. 3.15B a and c, respectively whereas that of the metal layers of the pellets given in Figs. 3.15A b and c are given in Figs. 3.15B b and d, respectively. EDX analysis showed that they are composed of Na, Nb and O. During electrolysis, insertion of Na^+ ions into the smaller grains of Nb_2O_5 (micrograph given in Fig. 3.3B c) would have increased the size of the grains (as shown in Fig. 3.15B a and c). X-ray analysis of the granite like bulk mass showed a distinct phase, whose XRD pattern doesn’t match with the known Na-Nb-O compounds and for the sake of discussion the compound was represented as $Na_xNb_yO_z$. After 44 h of electrolysis, the product was found to be spongy (residual oxygen, 1.4%) and significantly porous as shown in Fig. 3.15B d. The bulk of the pellet contained $Na_xNb_yO_z$ as the major phase along with trace levels of Nb and $NaNbO_3$

after 9 h and significant levels of Nb after 22 h after electrolysis. Therefore, the electro-reduction of Nb_2O_5 in NaCl melt followed the path Nb_2O_5→Na-Nb-O compounds →Nb.

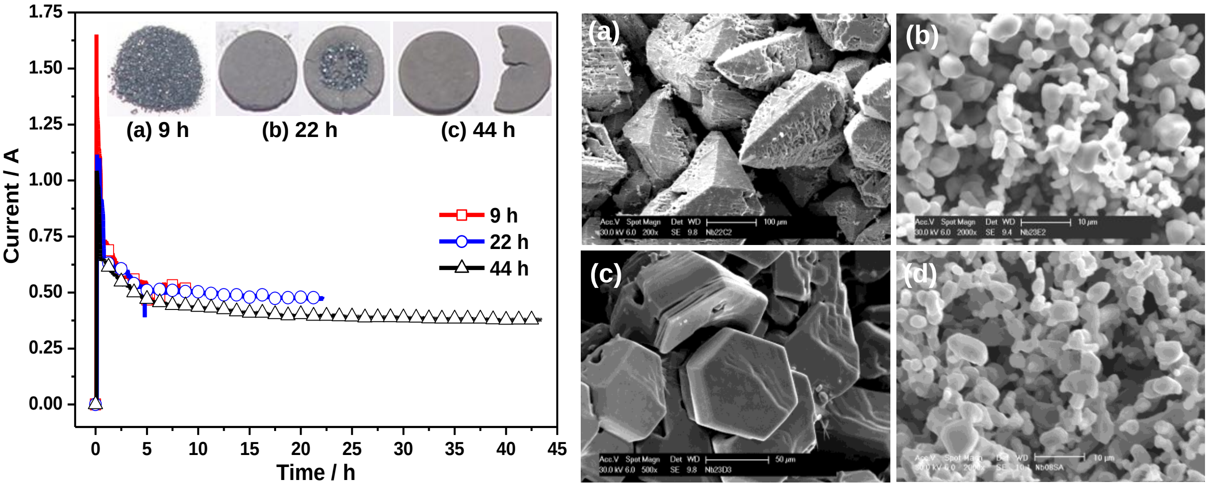

(A) (B)

Fig. 3.15. (A) I-t curves for the electro-reduction of Nb_2O_5 pellets at 3.1 V using graphite as the anode in NaCl melt at 1173 K. Inset shows the photographs of the products after electrolysis for 9, 22 and 44 h. (B) SEM images of the cross section of products after (a) 9 h (b) surface after 22 h (c) bulk after 22 h and (d) bulk after 44 h.

ii) KCl and KCl-25mol.% $CaCl_2$ melts

Similar experiments, as discussed above, were carried out in KCl and KCl-25mol.% $CaCl_2$ melts at 1173 K. Nb_2O_5 pellets were reduced to Nb metal in both the melts though the magnitudes of reduction currents were relatively lower compared to those in $CaCl_2$ and NaCl melts. The residual oxygen content of Nb obtained after 40 h (Q=12.18 Ah) of electrolysis in KCl melt was found to be 2.4% whereas that in the product from the experiment carried out for 42 h (Q=13.41 Ah) in KCl-25mol.% $CaCl_2$ was 3.7%. Also the pellets were found crumbled after electrolysis and this suggested that the intermediates formed during electrolysis decreased the mechanical integrity of the pellet.

iii) $CaCl_2$ melt

The electro-reduction of Nb_2O_5 pellets in $CaCl_2$ melt was previously discussed in sections 3.3.3 and 3.3.8.1.

Reduction of Nb_2O_5 to Nb occurred in NaCl and KCl despite its poor solubility for Na_2O and K_2O, in contrary to previous reports which predicted that the electrochemical reduction of solid oxides would be difficult in such melts [178]. However, it was noticed that the residual oxygen contents of the produced Nb was relatively less in case of $CaCl_2$ when compared to other melts employed in the study. Unlike calcium, the chemical reduction of Nb_2O_5 by Na or K is thermodynamically not feasible at 1173 K. Therefore, the electro-reduction of Nb_2O_5 to Nb in NaCl or KCl suggests that the metallothermic reduction is not mandatory for electro-reduction to occur though it aids in attaining lower residual oxygen content in the reduced metal.

3.4. Conclusions

Innovative procedures such as Indicator Pellet Technique, Counter Electrode Potential Measurement and melt characterisation by TSB and TIB have been employed for the first time to gain insight in to the DOER of Nb_2O_5 pellets. The CV, polarisation and CEPM studies indicate that the Nb_2O_5 is electrochemically reactive with Ca^{2+} ions of the melt, which was confirmed by the analysis of the partially electro-reduced samples. Nb_2O_5 pellets could be completely converted to Nb metal by the cathodic polarisation at potentials positive to the reversible Ca/Ca^{2+} potential of the $CaCl_2$ melt. The formation and decomposition of Ca-Nb-O compounds and suboxides of Nb was observed with time during the electro-reduction of Nb_2O_5 in the melt. The results of the calcium induced reduction of Nb_2O_5 indicator pellet to Nb via the formation of NbO_2 and NbO gives ample proof for the generation of Ca metal (at activities below unity) in the melt during the electro-reduction process and this could have also partly contributed to the reduction of the oxide. Successful reduction of dense Nb_2O_5 pellets to Nb in NaCl and KCl melts under similar experimental conditions, however, proved that the metallothermic reduction of the oxide is not mandatory for the electro-reduction to occur. The correlation of the chemical changes that are taking place in $CaCl_2$ melt given by

TSB and TIB to that occurring inside the cathodically polarised oxide pellet, brought out in this study, is unique and has helped in understanding the process better. Based on the results of the study a probable mechanism for the electrochemical reduction of dense Nb_2O_5 pellets in $CaCl_2$ melt has been proposed. The mechanism involves 3 steps – (i) insertion of Ca^{2+} ions into Nb_2O_5 matrix (ii) reduction of the oxide via the formation and decomposition of ternary intermediates and suboxides of Nb and (iii) calcium induced reduction of the oxide, the three steps either occurring simultaneously or subsequently. Based on the results, a model for the reduction of dense Nb_2O_5 pellets was also proposed. Various factors influencing the electro-reduction of Nb_2O_5 have been investigated. The reduction was found to be enhanced by increase in temperature from 1073 to 1173 K, applied voltage from 2.5 to 3.1 V, open porosity of the pellet from ~10 to ~42 % and time of electrolysis. Once the metallisation is completed, the efficiency of the reduction was found to decrease with increase in the duration of electrolysis and the efficiency was found to increase when alumina was used as the container material in place of stainless steel.

CHAPTER 4

Some interesting investigations of the electrochemical reduction of TiO_2 and SiO_2 in molten $CaCl_2$ and LiCl electrolytes

4.1. Introduction

Though electrochemical reduction of TiO_2 pellets by the FFC Cambridge process has been studied extensively [2-4,10-40] and reported by different groups, not much information is available on the reduction behaviour of TiO_2 powders. Therefore, electro-reduction experiments were carried out with sintered TiO_2 powders in $CaCl_2$ melt in both constant voltage (Con-V) and constant current (CC) modes of electrolysis. The effect of sintering temperature and increase of the mass of the TiO_2 powder on its electro-reduction behaviour were investigated.

TiO_2 and SiO_2 are two different classes of oxides with regard to their chemical and electrical characteristics. The thermodynamic stability and electrical characteristics of an oxide electrode is known to have strong influence on its electro-reduction. In order to gain understanding on these fundamental issues of electro-reduction, some novel experiments were carried out with TiO_2 and SiO_2 pellet electrodes in both high melting $CaCl_2$ and low-melting LiCl melts. The results of the investigations are presented in this chapter.

4.2. Experimental

$CaCl_2$ melt (at 1173 K) was employed as the electrolyte in most of the experiments. In some experiments LiCl melt was employed at 923 K. TiO_2 (anatase) powder sintered at 1423 K and 1673 K for 3 h was employed in the study. XRD of the sintered powder showed that the anatase was converted to rutile during sintering. Microstructurally the sintered powders showed significant changes when compared to the anatase present initially as shown in Fig. 4.1. The original anatase contained TiO_2 grains of extremely small size (~ 150 nm, Fig. 4.1a) as compared to 1-4 µm (1423 K) and 6-12 µm (1673 K) in rutile powders obtained after sintering at the respective temperatures (Figs. 4.1b and c). The individual particles grouped as colonies of 10-20 µm were seen to get agglomerated by fusing of neighboring colonies to form ‘spherical’ entities having an average size of 57 µm (1423 K) and 68 µm (1673 K) after sintering at the respective temperatures.

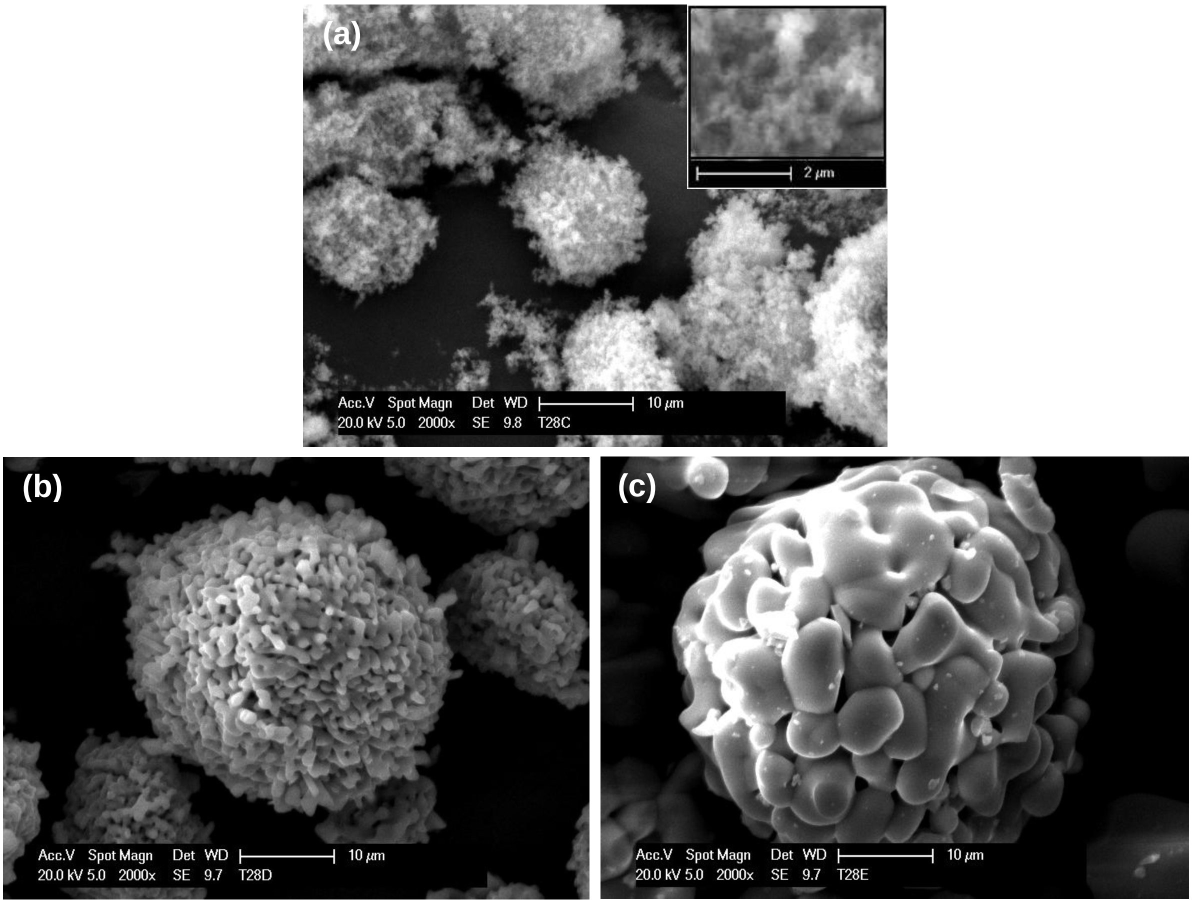

Fig. 4.1. SEM images of (a) as received TiO_2 powder (anatase) and TiO_2 powder after sintering for 3 h at (b) 1423 K and (c) 1673 K. Inset in (a) shows smaller grain size of anatase.

The cathode assembly consisted of perforated SS cups with a lining of SS mesh (pore size ~ 40 µm) in which the TiO_2 powders (~1.5 g or ~10 g) were taken. Tap density of the powder was maintained in the range of 1.5 – 2.0 g/cc. CV and polarization experiments were carried out with TiO_2 pellets. TiO_2 and SiO_2 pellets sintered at 1573 K were employed as electrodes for comparison of their electro-reduction behaviour. In all the cases sintering was done for 3 h. Electrolysis experiments were carried out with the pellets either fully immersed in the melt (i.e., along with the current collector wire) or the tip alone in contact with the melt (the current collector wire not in contact with melt) as shown in Fig. 4.2a and 4.2b, respectively. The recovery of the products of electrolysis and their subsequent analysis were carried out by XRD, SEM-EDX and oxygen analyser, as described previously in chapter 2.

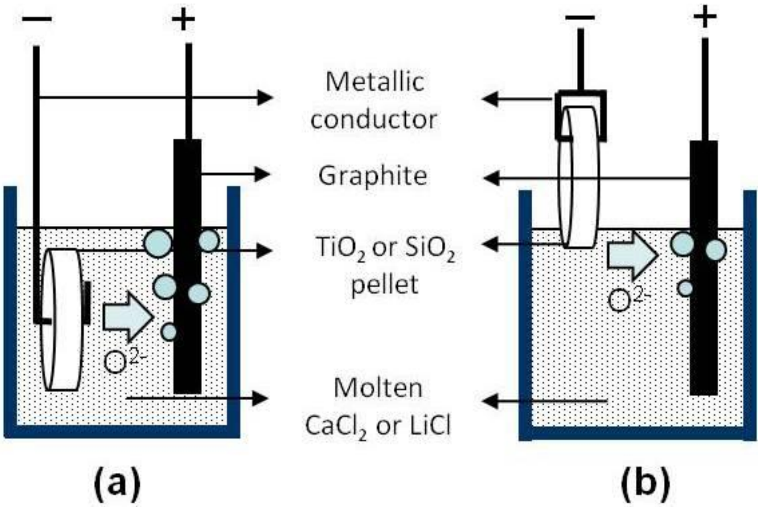

Fig. 4.2. Schematic of the electro-reduction with the oxide pellet electrode in (a) fully immersed and (b) tip alone immersed conditions.

4.3. Results and discussion

4.3.1. CV and polarisation experiments of TiO_2 pellets in $CaCl_2$ melt

The cyclic voltammograms obtained with an inert tungsten wire and the tip of a TiO_2 pellet as the working electrodes in separate CV experiments with a graphite rod as the counter electrode in $CaCl_2$ melt are shown in Fig. 4.3a. The voltammograms on the tip of the TiO_2 electrode corresponding to 1st, 5th and 11th potential cycles are only given in the figure. The calcium deposition on the W electrode was found to occur at 0.00 V (vs. Ca/Ca^{2+}) and indicated as 'blank' in the figure. The TiO_2 electrode did not show any electrochemical features in the initial few potential cycles in the potential window +0.2 V to +2.2 V vs. Ca/Ca^{2+} and the slope of the CV looked similar to that of a resistor (curve '1'). But after few repeated cycles in the potential window, the CV started showing a reduction current wave at 0.7 V positive to the reversible calcium deposition potential of the melt (curve '5'). In the successive cycles, the reduction peak was observed to shift to more cathodic potentials and in the 11 cycle the peak appeared at +0.5 V vs. Ca/Ca^{2+} (curve '11'). This electrode behaviour indicated that it was electrochemically active in the melt. A polarisation experiment was subsequently carried out with tantalum and TiO_2 as the cathodes against graphite counter electrode in the $CaCl_2$ melt and the results are shown in Fig. 4.3 b. The polarisation curves showed that the TiO_2-graphite cell is able to pass current at ~1.5 V when compared to the reversible decomposition potential of $CaCl_2$, i.e., 3.24 V as measured with the tantalum-graphite cell. Due to the large surface area of the TiO_2 electrode and slow reactivity of the electrode under the CV conditions, it was difficult to obtain the precise potential at which the TiO_2 electrode was reducing in the melt. Also shifting of the reduction current wave with the potential cycling makes it difficult to ascertain the exact potential for reduction of the oxide. However, the CV and polarisation experimental results do confirm that the TiO_2 electrode is reactive in the melt and the electrochemical reactions take place at potentials positive to the reversible calcium deposition potential of the melt.

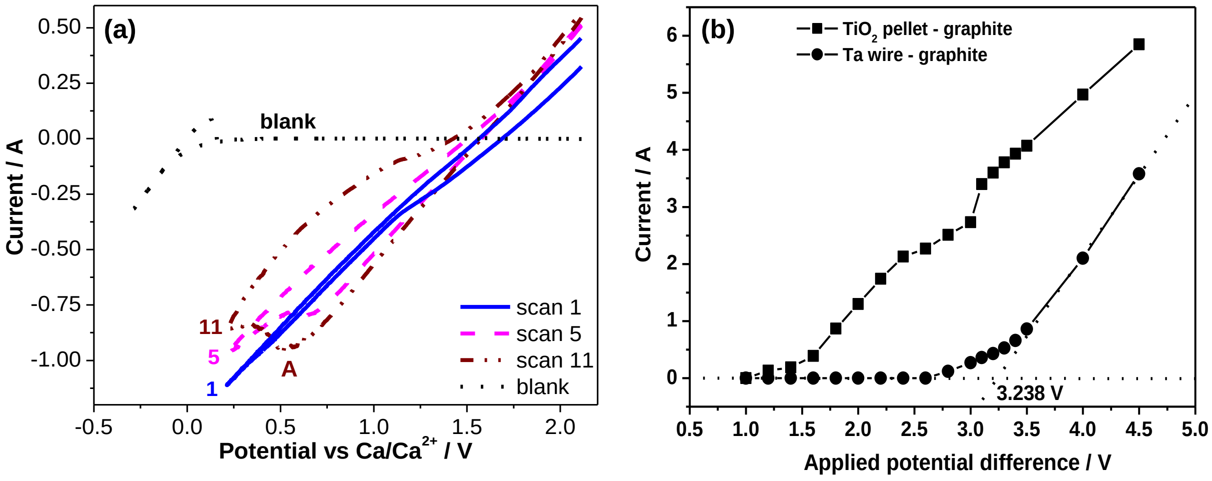

Fig. 4.3. CV and polarization studies on TiO_2 pellets in $CaCl_2$ melt at 1173 K (a) Successive scans during CV studies at 20 mV/s in tip dipped condition (scans 1, 5 and 11 are only shown) along with that carried out on tungsten shown as blank (b) Polarisation study of TiO_2 pellet-graphite and Ta wire-graphite.

Similar CV and polarisation experiments repeated with SiO_2 pellet electrodes (tip alone in contact with the melt) did not show any current and the cell behaved as if it was open. The behaviour indicated that SiO_2 electrode was not electrically conducting like TiO_2 in the cell. This aspect will be discussed in more detail towards the later part of this chapter.

4.3.2. Electrochemical reduction of TiO_2 powders in molten $CaCl_2$ medium

4.3.2.1. Effect of sintering temperature of TiO_2 powder on reduction in constant voltage mode of electrolysis

Two experiments, one each with TiO_2 powder (~1.5 g) sintered at 1423 K (T-1) and 1673 K (T-2), were carried out at 3.1 V for 22 h. Photographs of the configuration of the cathode and TiO_2 powder before electrolysis and cathode with occluded salt and the processed products after electrolysis are given in Fig. 4.4. The product of the T-1 experiment, after washing and vacuum drying, contained light grey coloured chunks and powder. The mass was found to be electrically conducting as per a continuity test with a multimeter and hence was probably reduced whereas the electrolysed sample of T-2 became grey coloured powdery mass and was not conducting as observed during the continuity test.

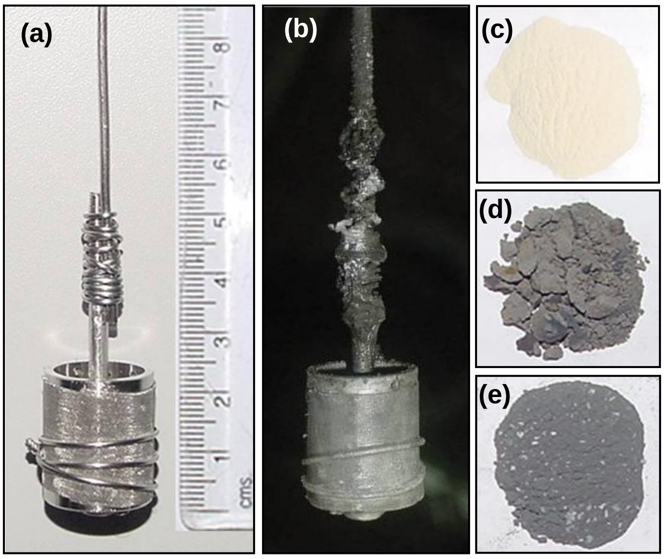

Fig. 4.4. Photographs showing (a) the cathode assembly (b) cathode with occluded salt after electrolysis (c) TiO_2 powder before electrolysis. (d) and (e) are the products of electrolysis from T-1 and T-2 experiments, respectively, carried out at 3.1 V for 22 h in $CaCl_2$ melt at 1173 K.

Fig. 4.5a shows the I-t curves obtained during electrolysis of TiO_2 powders in T-1 and T-2 experiments. X-ray diffractograms of the corresponding products of electrolysis are given in Figs. 4.5b and c, respectively. The total charges passed during electrolysis in T-1 and T-2 experiments were found to be 10.96 Ah and 9.11 Ah, respectively. X-ray diffraction analysis of the product from T-1 (Fig. 4.5b) confirmed that it had been completely converted to Ti metal. Its oxygen content was determined to be 1.4% by inert gas fusion technique. However, the product from T-2 contained Ti_3O as the major phase, along with trace levels of $CaTiO_3$ and $CaCO_3$ (Fig. 4.5c) and the oxygen content of the product was found to be 6.1%. Further, though all other experimental conditions, except the sintering temperature of the feed TiO_2 powder, were maintained identical it was noticed that the loss of weight of the graphite anode in the former case was more (0.60 g) when compared to that in the latter (0.37 g). Higher oxidative corrosion of graphite in the former case can be attributed to a higher rate of discharge of cathodically generated oxygen ions on the graphite to form CO/CO_2. The higher level of reduction occurred at the cathode in the former (T-1) is in line with the higher corrosion observed at the anode.

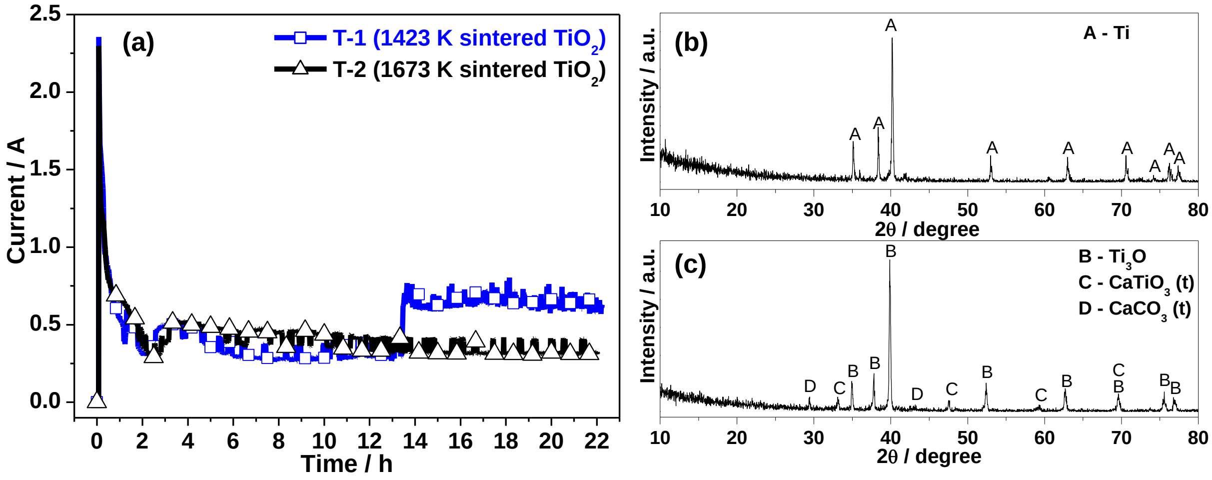

Fig. 4.5. (a) I-t curves obtained during the electrochemical reduction of 1.5 g of TiO_2 powder, sintered at 1423 K (T-1) and 1673 K (T-2) at 3.1 V for 22 h in $CaCl_2$ melt at 1173 K. XRD patterns of the products from T-1 and T-2 are given in (b) and (c), respectively.

Similar conclusions can be drawn from the results of SEM/EDX analysis of the reactants and products as given in Fig. 4.1 and Fig. 4.6, respectively. The product obtained from T-1 had many spherical particles of various sizes (not shown) of more or less similar morphology and had grains of size ~ 10 μm (Fig. 4.6a) when compared to the grains of 1-4 μm in the original rutile powder (Fig. 4.1b). EDX spectra at different regions of the product revealed that TiO_2 was completely-converted to Ti metal, which is also in line with the results of the XRD analysis of the sample.

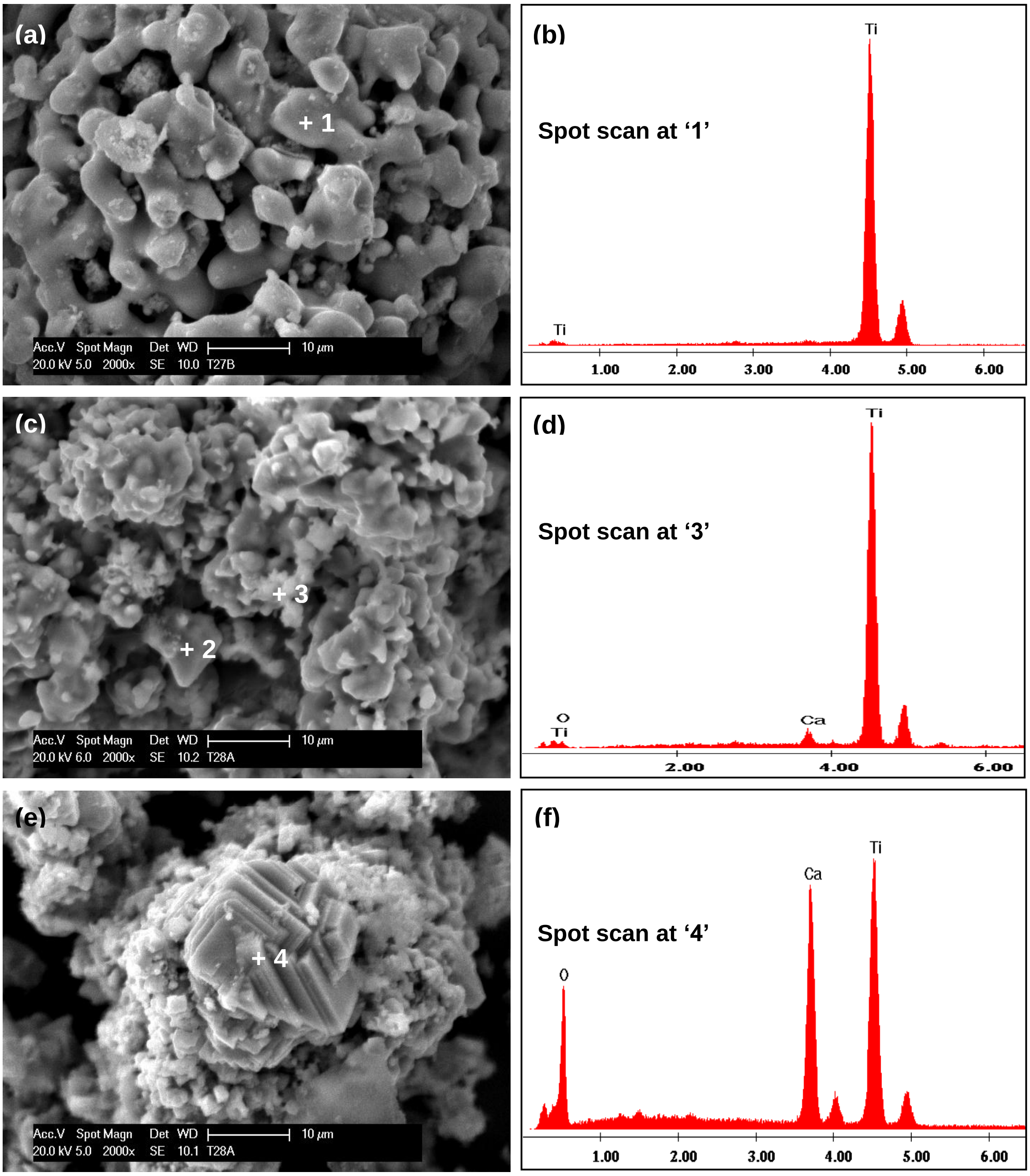

Fig. 4.6. Scanning electron micrographs of the electrolysis products from (a) T-1 and two regions from T-2 having different morphologies are given in (c) and (e). EDX spectrum of the spot scans (represented as '+') denoted by numbers 1, 3 and 4 are given in (b), (d) and (f), respectively.

A typical EDX spectrum of the sample taken at the spot '1' showed only the presence of Ti as given in Fig. 4.6b. However, a major part of the sample from T-2 showed a morphology (Fig.

4.6c) which is very different from that of the former. At some regions it presented particles having faceting kind of morphology as shown in Fig. 4.6e. EDX spot scans at various regions of the sample such as those at ‘3’ (Fig. 4.6d) showed the presence of Ti (73.4 atom %) and O (24.11 atom %) with lower levels of Ca (2.49 atom %) as against the presence of only Ti in grains at some other locations as indicated by ‘2’. The faceting kind of morphology of some of the particles and the presence of Ti and O with significant levels of Ca in the elemental profile of the EDX spectrum taken at ‘4’ (Fig. 4.6f) clearly indicated that some parts of the powder electrode (T-2) was not completely reduced and still remained as calcium titanates. This fact was also evident in the XRD analysis of the product (Fig. 4.5c).

The TSB-M and TIB of the melt (section 2.3.16, chapter 2) in T-1 were estimated to be 0.10% and 0.72% as against the respective values of 0.09% and 0.23% observed in the case of T-2. The values for TSB-C of T-1 and T-2 were found to be 0.24% and 13.41%, respectively. The higher TSB-M, TIB and lower TSB-C would suggest that the oxygen content of the sample is low and hence the sample underwent better reduction. This indeed was the case of T-1 as observed from results of XRD and residual oxygen analyses. In this case, the size of the TiO_2 spherical entities and the particles with which they are made of is small and more insertion reactions could have taken place. This could have released more number of O^{2-} ions later into the melt decreasing the TSB-C, increasing TSB-M and ultimately the TIB. However, the higher TSB-C, lower TSB-M and TIB values in the latter case indicate that oxide ions are being generated at the cathode at 22 h of electrolysis and hence reduction is still progressing. In the case of T-2, particles as well as the grains in the spherical entities are more densified (Fig. 4.1c) due to higher temperature sintering so that the open porosity of the entity is significantly reduced compared to the sample from T-1. As the particles on outside surface of the spherical entities are sintered, this would have limited the access of the electrolyte to its bulk and hence reduction of the interior parts of the ball-like structure. So in brief, the decrease of open porosity of the spherical entities could have made the reduction difficult towards the centre of the entities. From the results discussed above, it can be concluded that TiO_2 powder sintered at 1423 K is better than that sintered at 1673 K for electro-reduction. The experiments were repeated with CC mode of electrolysis as follows.

4.3.2.2. Effect of sintering temperature of TiO_2 powder on reduction in constant current mode of electrolysis

Fig. 4.7a shows the V-t curves obtained during the constant current (200 mA) electrolysis of TiO_2 powders sintered at 1423 K (T-3) and 1673 K (T-4) at 0.2 A for 22 h in $CaCl_2$ melt at 1173 K. The X-ray diffractograms of the products from T-3 and T-4 are given in Figs. 4.7b and c, respectively. The product from T-3 showed only the presence of Ti_3O whereas that from T-4 showed the presence of Ti_3O as the major phase along with trace levels of $CaTiO_3$, $CaTi_2O_4$ and $CaCO_3$ phases and the corresponding residual oxygen contents of the products were found to be 1.4% and 4.2%, respectively. With increase in time of electrolysis, the cathode polarized to more and more cathodic values whereas the anodic potential remained more or less constant; change in cell voltage was due to the change in the cathodic potential. The cathodic potential in both the cases showed steps indicating the formation of various intermediate phases during the reduction process. However, the cathodic potential from T-3 reached ~0.5 V and then ~0.3 V vs. Ca/Ca^{2+} rather promptly than that from T-4. Thereafter, the potentials of the cathodes from both the experiments remained at more or less similar values. The lower particle size and the high open porosity of T-3 essentially gave a high effective surface area, which facilitated electrochemical reactions to take place rapidly throughout the cathode enhancing its deoxidation as is evident from the cathodic potential behaviour.

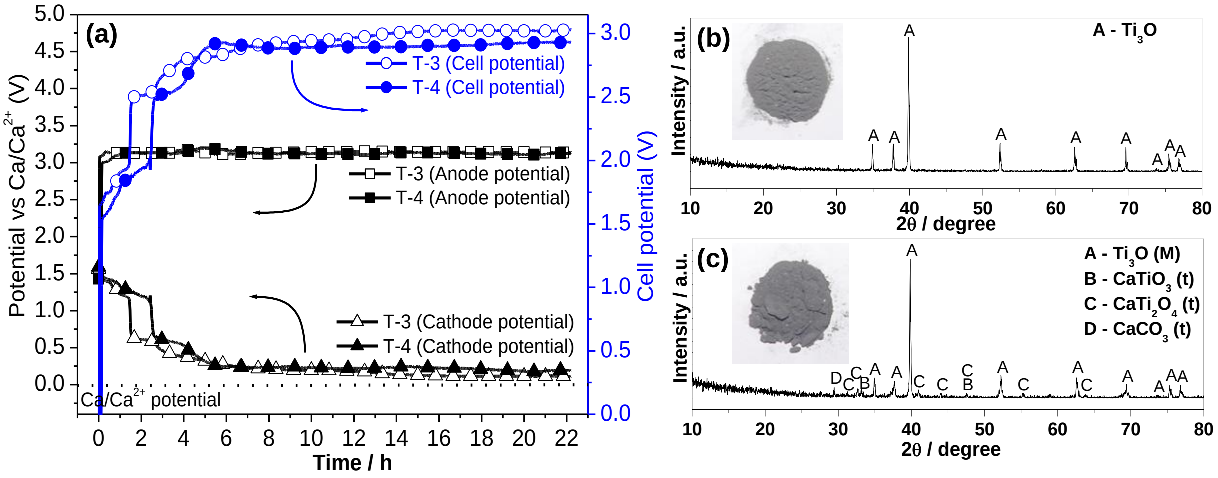

Fig. 4.7. (a) V-t curves during the electrochemical reduction of 1.5 g of TiO_2 powder sintered at 1423 K (T-3) and 1673 K (T-4) at 200 mA. (b) and (c) shows the XRD patterns of the products from T-3 and T-4, respectively. Photographs of the products are given in insets of the respective figures.

The microstructures of the products from T-3 and T-4 are given in Figs. 4.8a and b, respectively. An in depth analysis of the product from T-3 showed the presence of two kinds of morphological features in its microstructure - cubic structures represented by ‘1’ present smaller in number, which are scattered in a matrix containing irregular structures denoted by ‘2’ and ‘3’. EDX analysis of the cubic structures showed the presence of elements Ca, Ti, O and Cl indicating the possibility of entrapment of small quantities of $CaCl_2$ in Ca-Ti-O compounds whereas that of the irregular structures were found to be Ti with varying levels of O. However, the microstructure of the product from T-4 showed the presence of faceting crystallites represented by ‘4’ with higher levels of Ca, O and Ti suggesting that they are calcium titanates. Structures such as those represented by ‘5’ showed the elemental profile consisting of Ti with lower levels of Ca, O indicating that these could have been formed by unification of suboxides of titanium and small amount of calcium titanates. Regions ‘6’ and ‘7’ showed the presence of Ti with varying levels of oxygen. The SEM-EDX results showed that complete metallization has not taken place in both the cases of T-3 and T-4. However, like in the case of Con-V mode of electrolysis discussed previously, in CC mode of electrolysis also better reduction was observed with TiO_2 sintered at 1423 K than that sintered at 1673 K.

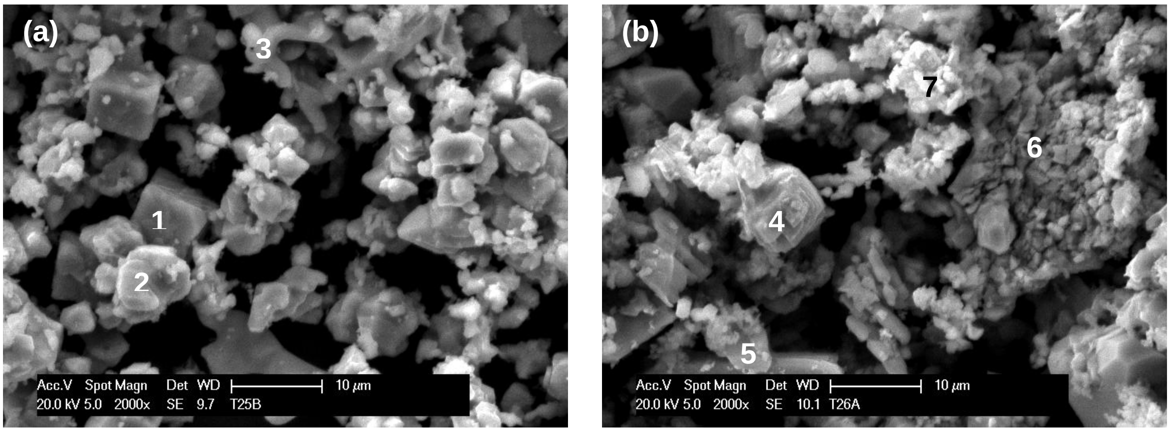

Fig. 4.8. Scanning electron micrographs of the products from (a) T-3 and (b) T-4. Various locations where EDX analysis was carried out were represented by legends '1' to '7'.

4.3.2.3. Effect of increase in mass of TiO_2 on reduction in Con-V mode of electrolysis

The results of the electro-reduction experiments with 1.5 g of TiO_2 powders discussed above showed that better reduction was observed in Con-V mode of electrolysis. Therefore two experiments were carried out at 3.1 V, namely, T-5 and T-6 with 10 g of TiO_2 powders sintered at the two temperatures i.e., 1423 K and 1673 K, respectively. The I-t curves obtained during the electrolysis and the XRD patterns of the products after electrolysis are given in Fig. 4.9.

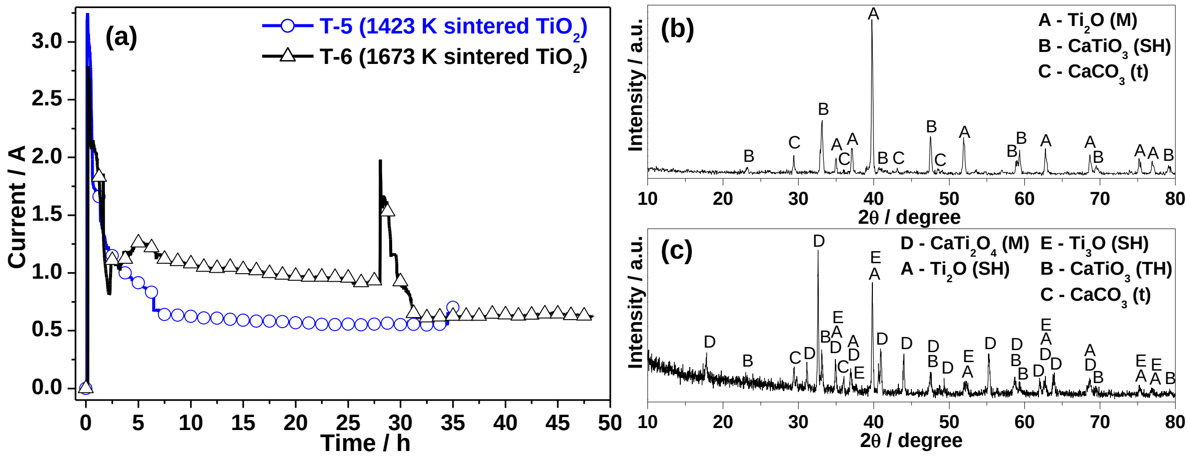

Fig. 4.9. (a) The I-t curves during the electrochemical reduction of 10 g of TiO_2 powder in T-5 and T-6 experiments at 3.1 V in $CaCl_2$ melt at 1173 K. The XRD patterns of the products from T-5 and T-6 are given in (b) and (c), respectively.

The current decreased with time in a usual manner. In case of T-6, after 28 h of electrolysis the cathode cup was rotated by 180º which caused a temporary surge in the current. This was done assuming that a better overall reduction of the cathode (despite the larger grain size of TiO_2) may be achieved by bringing the opposite face of the cathode nearer to the graphite anode, which was away from the anode till then. The total amount of charges passed in T-5 and T-6 were found to be 24.64 Ah and 44.69 Ah, respectively. The photographs of the electrodes before and after electrolysis are given in Fig. 4.10.

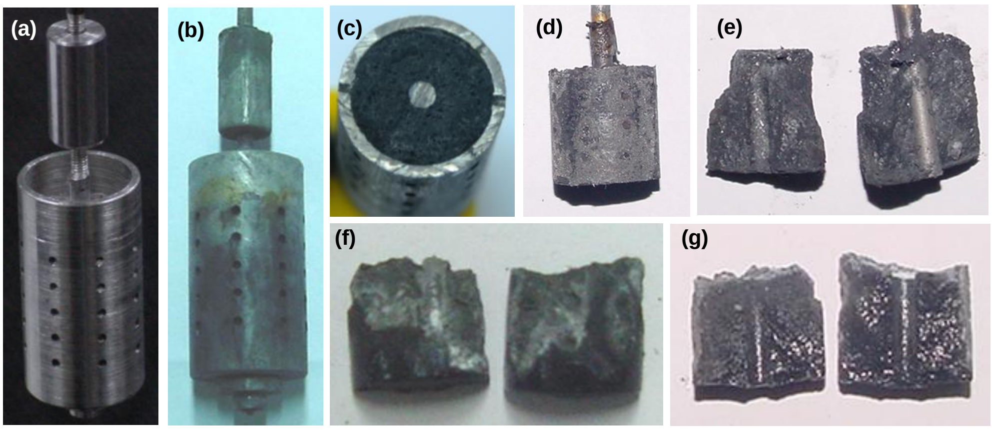

Fig. 4.10. Photographs: (a) The cathode assembly with 10 g of TiO_2 powder before electrolysis (b) after electrolysis (c) radial cross section of the cup from T-5 (d) the electrolysis product separated from the cup (e) longitudinal section of the product (f) surface of the product from T-6 and (g) longitudinal section of the product.

The cathode cup in T-5 was cut radially as well as longitudinally and an examination of the cross section of the rock like product (Fig. 4.10c) showed a uniformly blackish grey mass. Even though the charge equivalent to twice the theoretical charge required for complete reduction was passed, the product from T-5 was found to be Ti_2O with significant amounts of $CaTiO_3$ and traces of $CaCO_3$ as evident from Fig. 4.9b. The oxygen content of the sample was found to be 16.5 %. Higher currents were observed in the case of T-6 and the electrolysis was terminated after passing the charge equivalent to more than 3 times that was theoretically required for complete reduction. Nevertheless, complete reduction could not be achieved. Physically two distinct regions were observed across the cross section of the product; one along the inner surface of the cup and the other towards the bulk. The portion near the curved surface of the cup was carefully separated and XRD analysis (not shown) confirmed that it comprised of Ti_3O whereas the bulk had $CaTi_2O_4$ as the major phase (Fig. 4.9c) with significant levels of Ti_3O, Ti_2O, $CaTiO_3$ and trace levels of $CaCO_3$. Obviously better reduction was observed near the curved surface of the cup than that at the bulk and the oxygen content of the uniformly ground sample was found to be 22.1 %. The results showed again that the powder sintered at 1423 K undergoes better reduction compared to that sintered at 1673 K, even after passing excess amount of charge in the latter case. This apart the study proves that the reduction of the bulk of a TiO_2 electrode is difficult, even when the electrode is the powder (highly porous). A simple model of the propagation of reduction in TiO_2 powder electrode is proposed below.

The results indicated that the size of the spherical entities and the size of individual grains within them influence the electrochemical reduction of TiO_2 powders. Fig. 4.11 shows the schematic representation of the progress of electro-reduction of TiO_2 powder electrode in molten $CaCl_2$.

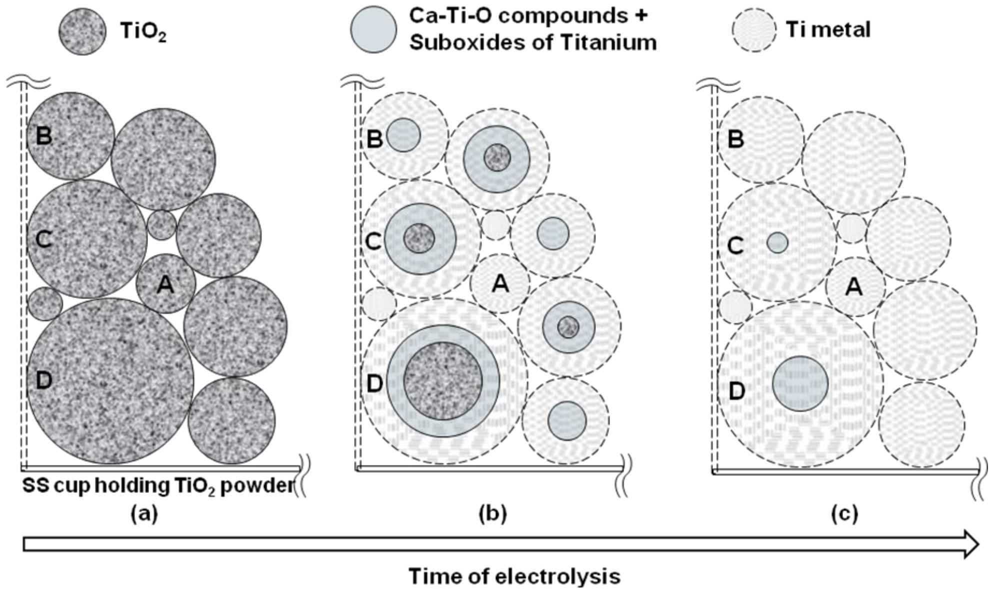

Fig. 4.11. A model of the progress of electro-reduction of a TiO_2 powder electrode in $CaCl_2$ melt.

Assuming a spherical shape for the TiO_2 particles, various sizes that are possible in an electrode are marked as A, B, C and D in the increasing order of size in an infinitesimally small region of the cathode cup as shown in Fig. 4.11a. After elapse of electrolysis, the electrode may get changed as shown in Fig. 4.11b. The application of potential could make electrochemical insertion of Ca^{2+} ions into the surface of the particles possible leading to the formation of Ca-Ti-O compounds and suboxides of Ti. The decomposition of these compounds and/or the removal of oxygen (by oxygen ionisation) under the cathodic polarization conditions could cause the reduction of surface of the particles to Ti and release of O^{2-} ions into the melt in its surroundings. As the particles are electrically conducting, this extends to particles which are away from the cup's surface. The particles start reducing everywhere in the preform with enhanced reduction in the smaller particles. If the particles are bigger in size, as the case of C and D, the deoxidation as well as the formation of a mixture of ternary compounds and suboxides of Ti might occur on the outer surface and in the region next to the outer surface of the particle, without practically effecting the reduction at the bulk of the particle. The bulk of the electrode contains some particles of intermediate size and they might be converted to ternary intermediates and suboxides of Ti as in the case of 'B'. On continuation of electrolysis, the extension of reduction to interior of the electrode would lead to complete reduction of the particle 'B', though the inner core of the bigger particles 'C' and 'D' could remain as a mixture of Ca-Ti-O compounds and suboxides of Ti as shown in Fig. 4.11c. In general, the scheme shown in Fig. 4.11 is applicable to TiO_2 powder sintered at any temperature. However in the case of the low temperature (1423 K) sintered powder both the particle as well as grain sizes are small and relatively higher porosity could be observed in the spherical entities. This could have lead to enhanced diffusion of the released O^{2-} ions and its removal from bulk of the spherical entities and hence a better reduction in case of the powder sintered at 1423 K than that sintered at 1673 K.

As TiO_2 is a good conductor, the TiO_2 particles in the cathode are amenable for insertion/deoxidation reactions throughout. In other words, the availability of large surface area of the powders enables a host of electrochemical reactions occurring due to which significant amounts of oxide ions are released within the cathode cup. Excess O^{2-} and Ca^{2+} ions chemically react with the matrix forming $CaTiO_3$/$CaTi_2O_4$. The rate of reduction may be slowed down due to the locally generated and accumulated excess oxide ions, as reported previously [18]. The reduction may be further slowed down with increase in the mass of the powder and diameter of the cup as diffusion of the electro-generated oxide ions from the bulk of the cathode to the melt becomes more and more difficult under such conditions. Also, in such cases, reduction of some particles may be taking place with the simultaneous conversion of other particles to $Ca_xTi_yO_z$. Since the rate of reduction towards the bulk retarded due to larger size of the spherical entities and those of the individual grains within them, the reduction was found to be less in case of the TiO_2 powder sintered at 1673 K. Another issue that would lead not only to a decrease in the rate of reduction but also to the contamination of the reduced product, i.e., titanium, is the entrapment of $CaCl_2$ or CaO within the solid matrix, as reported by Kartik Rao et al. [112].

4.3.3. Electro-reduction behaviour of TiO_2 and SiO_2 pellets

As discussed previously in chapter 1, the phase diagram of Ti-O system (Fig. 1.11c) showed the presence of different suboxides, including the Magnelli phases. TiO_2 was reported to be a semiconductor and its electrical properties changes with the oxygen partial pressures [179]. So TiO_2 can be expected to be a good electron-conductor at high temperatures both in ambient air and in inert atmosphere. It was reported that during electro-reduction of TiO_2 in molten $CaCl_2$ various ternary Ca-Ti-O compounds and Ti-O suboxides are formed [12]. The formation of electrically conducting Magnelli phases reportedly enhances the electrochemical reduction of the oxide in the FFC cell [38]. The ternary intermediate Ca-Ti-O compounds (e.g., $CaTiO_3$) which are formed during the reduction process were also reported to be good electrical conductors [180] leading to the enhanced electrochemical reduction of the TiO_2. Silicon is the second most abundant element on the earth's crust and available in the form of its oxide or minerals. SiO_2 exists in both amorphous as well as a number of crystalline forms such as cristobalite, quartz etc. In general, SiO_2 has a tetrahedral structure in which all the four corners are occupied by oxygen atoms, which are further shared by adjacent tetrahedrons. Different forms of SiO_2 have varying Si-O-Si bond angles and Si-O bond lengths and hence their bond strengths in view of removing oxygen from SiO_2 matrix. However, unlike the semiconducting TiO_2, SiO_2 is an insulator [5] even at high temperatures due to the lack of mobile electrons resulting from a larger band gap (>5 eV) between the valence and conduction bands. The electrochemical production of Si directly from SiO_2 has been thought to be difficult until recent past due to the insulating nature of SiO_2. However, the oxide too was electrochemically reduced to Si by the DOER process.

A novel study was taken up to understand the mechanism of electro-reduction in both these oxides particularly with an aim to understand the role of the conducting nature of the oxides on their electro-reduction behaviour. For this, both TiO_2 and SiO_2 pellets (sintered at 1573 K) were electrolysed in $CaCl_2$ (1173 K) and LiCl (923 K) melts in fully immersed and tip alone immersed conditions in separate experiments.

4.3.5. Electro-reduction of TiO_2 pellets in $CaCl_2$ and LiCl melts.

The current variation curves of the electrolysis of two pellets (weight ~1.5 g, ~1.5 mm thick, ~21 mm dia., OP~20%) in fully immersed (T-3) and tip immersed (T-4) conditions in $CaCl_2$ melt are shown in Fig. 4.12A and the photographs of the pellets before and after electrolysis are given in Fig. 4.12B. Current could be passed through the cell when the tip alone was touching the melt as is evidenced by the current vs. time graph. This confirmed that the TiO_2 was able to conduct electrons through its body to the reaction interface for effecting the reduction. The pellet employed for electrolysis in fully dipped condition was wound with Ta wire so as to give maximum number of contact points as shown in Fig. 4.12Ba. Therefore, due to more effective surface area the charge passed in fully immersed condition was more (8.98 Ah) when compared to that in tip immersed condition (1.84 Ah).

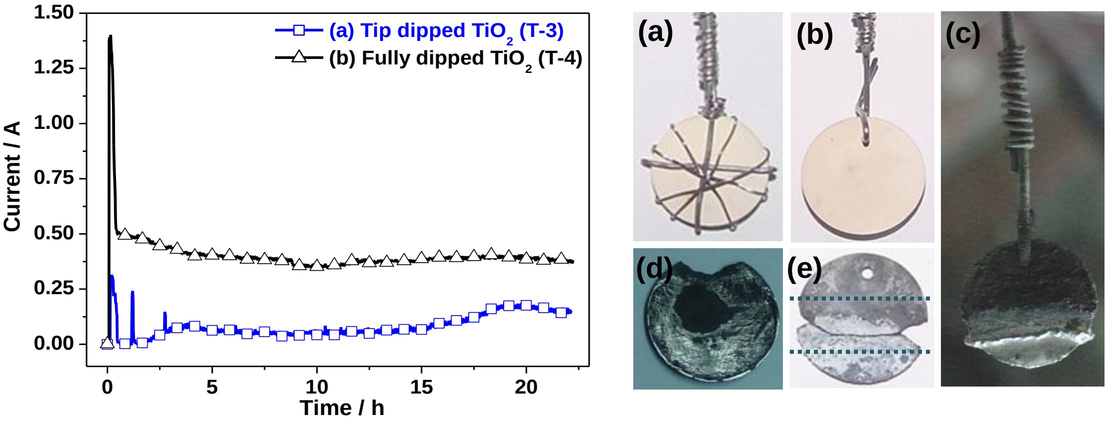

(A) (B)

Fig. 4.12. (A) I-t curves obtained during the electrolysis of TiO_2 pellets in (a) tip dipped (T-3) and (b) fully dipped (T-4) conditions in $CaCl_2$ melt at 1173 K (B) Photographs of the pellets: before electrolysis in (a) fully dipped and (b) tip dipped conditions; After electrolysis in (c) tip dipped condition with occluded salt; Washed and vacuum dried product after electrolysis in (d) fully dipped and (e) tip dipped conditions.

The pellet electrolysed in tip dipped condition was partitioned, as indicated by dotted lines in Fig. 4.12Be, into three regions – the top, intermediate and bottom regions and the X-ray diffractograms of the individual regions in addition to that of uniformly ground pellet electrolysed in fully dipped condition are given in Fig. 4.13. The pellet electrolysed in tip immersed condition showed different phases in the three regions. The top region contained $CaTiO_3$ as the major phase with significant levels of Ti_2O_3, TiO, $TiO_{0.997}$ and trace levels of $CaTi_2O_4$ whereas the intermediate region had $CaTiO_3$, $CaTi_2O_4$, Ti_2O and the bottom melt dipped region contained $CaTiO_3$, $CaTi_2O_4$, Ti_2O and TiO phases. The pellet electrolysed in fully dipped condition was, however, uniformly converted to Ti metal with slight amount of dissolved oxygen and the residual oxygen content of the Ti thus obtained was found to be 4.3%.

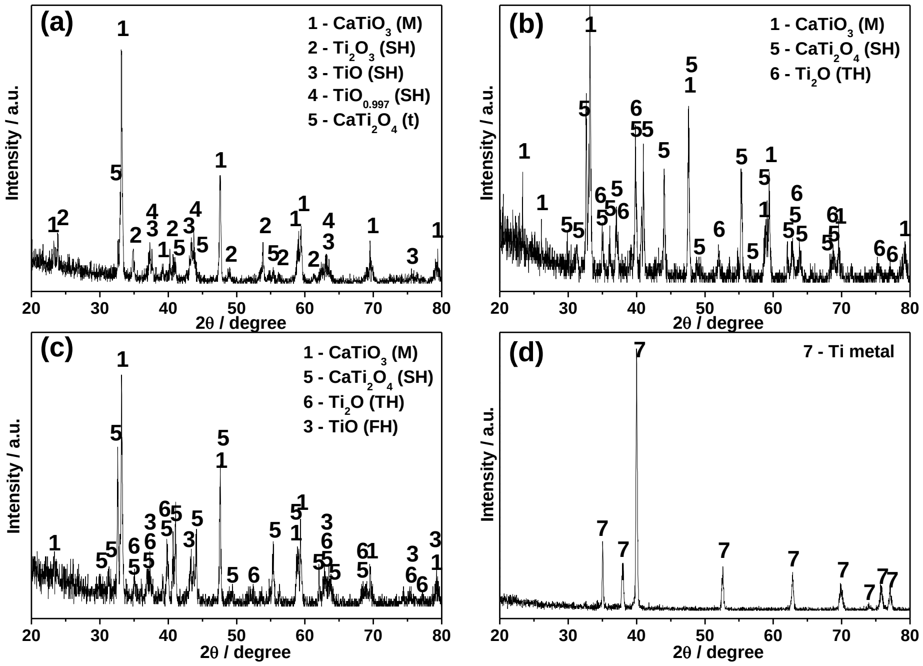

Fig. 4.13. X-ray diffractograms of the products from TiO_2 (T-3) pellet electrolysed in tip dipped condition (a) top (b) intermediate (c) bottom regions and (d) uniformly ground pellet electrolysed in full dipped condition (T-4).

The microstructural analysis of the cross sections of the samples, given in Fig. 4.14 revealed some more interesting aspects. The pellet sintered at 1573 K showed interconnected grains of TiO_2 (Fig. 4.14a). The tip of the pellet electrolysed in tip dipped condition (Fig. 4.14b) showed a rather packed structure due to the electro-insertion of Ca^{2+} ions into the pellet causing a significant change in the morphology of the matrix due to the formation of a mixture of Ca-Ti-O compounds and suboxides of titanium. The presence of elements Ca, Ti and O in the EDX spectrum and the X-ray diffractogram of this region confirm this.

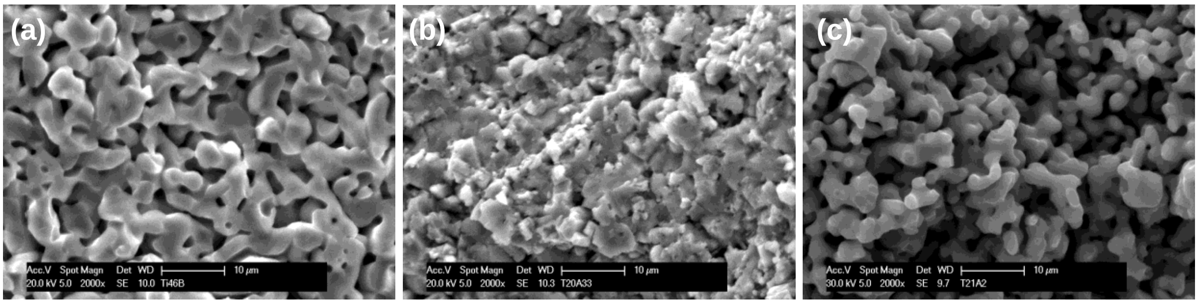

Fig. 4.14. SEM images of the cross sections of (a) TiO_2 pellet sintered at 1573 K for 3 h before electrolysis and (b) bottom region of the pellet electrolysed in tip dipped condition and (c) the pellet electrolysed in fully dipped condition.

The pellet electrolysed in fully dipped condition (Fig. 4.14c) showed nodular grains of Ti which was very much different from the other two. The results showed that though the pellet acted as a conductor, the rate of electrochemical reaction was significantly lowered probably due to a potential drop as the reaction site is away from the metallic conductor.

Similar experiments with TiO_2 pellets in fully dipped (T-5) and tip dipped (T-6) configurations, as discussed above, were carried out at 3.1 V in LiCl melt at 923 K. During electrolysis, an abrupt drop of the current was observed (not shown) after ~ 2 h and ~ 1 h of electrolysis, in the former and latter cases, respectively. The currents observed during the initial time periods of electrolysis were low in LiCl melt indicating that the electrochemical reactions at the cathode were taking place at relatively lower rates in LiCl melt (923 K) when compared to that in $CaCl_2$ melt at 1173 K. After electrolysis, the pellets were found to be broken in both the cases and the abrupt drop of currents was attributed to this effect. Few pieces of the pellet remained with the tantalum current collector/tie wire and the rest of the pieces had fallen into the melt in T-5 where as only the top region of the pellet remained with the current collector and the intermediate and tip regions collapsed and had fallen into the melt in case of T-6. The XRD analysis of the pieces of the pellet retrieved from the Ta tie wire in T-5 showed the presence of $LiTiO_2$ and Ti_3O whereas the pieces retrieved from the melt were identified as a mixture of TiO_2 and $Li_{0.3}Ti_{2.94}O_6$ phases. The top region from T-6, retrieved from the current collector, was found to contain various Li-Ti-O compounds along with traces of Ti_2O. The intermediate region, retrieved from the melt, was found to contain TiO_2, $Li_{0.3}Ti_{2.94}O_6$ along with traces of Li_2TiO_3 whereas the tip of the pellet contained only TiO_2 and $Li_{0.3}Ti_{2.94}O_6$ phases. Breaking of the pellets during electrolysis in LiCl melt in both the cases in the present study indicates that the intermediates formed during reduction in the melt are not mechanically stable and hence destabilised the integrity of the pellet which can be seen from the microstructural changes in the pellet during reduction as discussed below.

The SEM images of the cross section of the fully dipped pellet retrieved from the Ta tie wire was found to have coarse grains with rough surface which were loosely bound with each other in both fully dipped (Fig. 4.15b) and in the top region of the tip dipped pellets (Fig. 4.15c) when compared to the smooth surfaced and interconnected grains in the original pellet (Fig. 4.15a). The cross section of the tip of the pellet electrolysed in tip dipped condition retrieved from the melt showed the presence of a columnar bar like structures at the bulk (Fig. 4.15d) as against the coarse morphology of the grains at the surface which are similar to those given in Fig. 4.15c. The pellet piece (Fig. 4.15b) was brittle and its disintegration during washing (after electrolysis) also revealed its poor mechanical integrity.

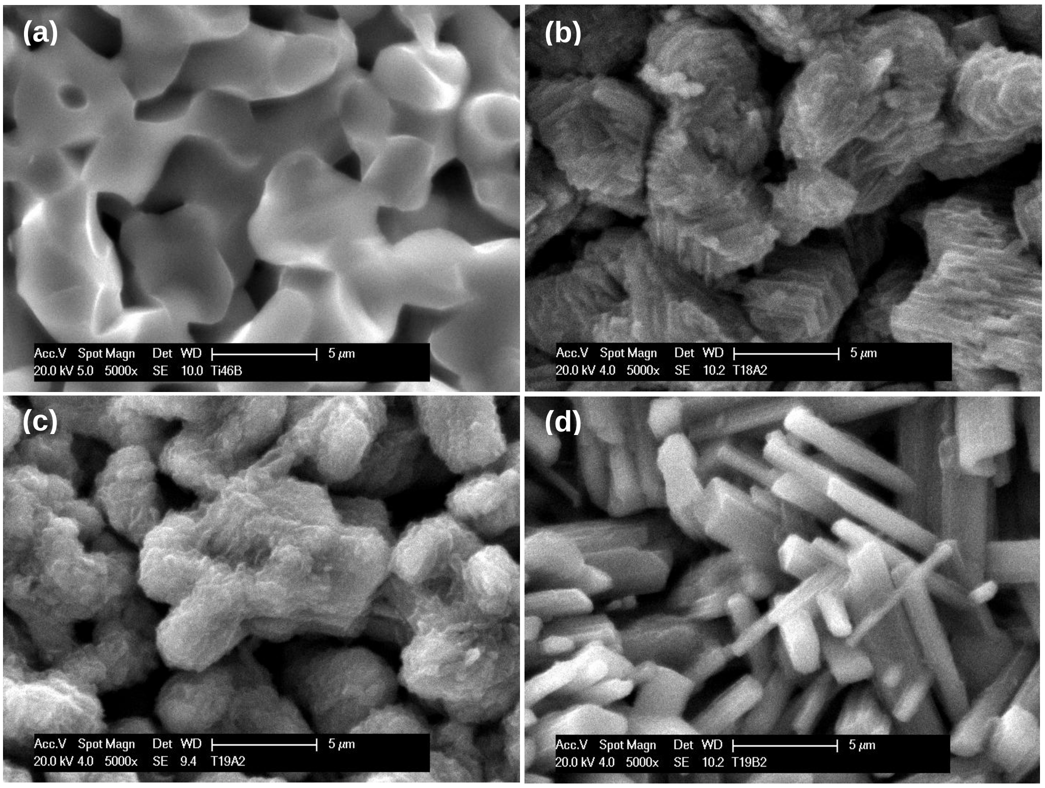

Fig. 4.15. SEM images of the cross sections of (a) TiO_2 pellet sintered at 1573 K for 3 h before electrolysis and the pellet after electrolysis in LiCl melt at 923 K in (b) fully dipped condition (c) tip dipped condition - top region (d) tip dipped condition – bottom region.

The results clearly indicated that the pellet was acting as a conductor during electro-reduction at 923 K in LiCl melt too. The results also show that the reduction progresses in LiCl melt via the formation and decomposition of Li-Ti-O compounds and titanium suboxides in the melt.

4.3.6. Electrochemical reduction studies on SiO_2 pellets in $CaCl_2$ and LiCl melts

SiO_2 belongs to the insulator class of oxide systems and similar investigations, as discussed above, were carried out with SiO_2 pellets (~1.5 g, ~25 mm dia., ~2 mm thick, OP ~ 40%) in $CaCl_2$ (1173 K) and LiCl (923 K) melts. In addition, the effect of applied voltage on the electro-reduction of SiO_2 pellets was also studied in $CaCl_2$ melt. The results are discussed below.

4.3.6.1. Electrolysis of SiO_2 pellets in fully dipped condition

The I-t curves during electrolysis of the pellets in fully dipped condition in $CaCl_2$ (S-1) and LiCl (S-2) melts are given in Figs. 4.16A. The XRD patterns of the samples before and after electrolysis are given in Figs. 4.16B. As seen from the I-t curves, the currents observed in LiCl melt (S-2) were relatively lower, when compared to those observed in $CaCl_2$ melt (S-1). The charges passed were found to be 4.77 Ah (S-2) and 16.34 Ah (S-1). The pellet reduced in LiCl melt (S-2) contained a mixture of white and grayish brown mass (inset ‘b’ in Fig. 4.16A). Both the masses were separately analysed by XRD. The grayish brown mass was identified as Si with trace levels of SiO_2 (Fig. 4.16Bc) and the white mass as SiO_2. Silicon and SiO_2 were the only phases identified in the product of electrolysis in fully dipped condition in LiCl melt. During post electrolytic washing of the product from S-1, severe reactivity of the pellet was observed with water. The XRD analysis of the washed and vacuum dried product (inset ‘a’ in Fig. 4.16A) showed the presence of CaSi (Fig. 4.16Bb) as against SiO_2 in the original pellet (Fig. 4.16Ba). Though, the same potential was applied in both the cases, only partial reduction took place in the former case whereas the reduction was complete and led to the formation of CaSi in the latter. It was reported that the rate of electrochemical reduction of SiO_2 was enhanced by an increase in the experimental temperature [71]. Therefore, the lower temperature would have led to a lower extent of reduction in LiCl melt, than in $CaCl_2$ melt.

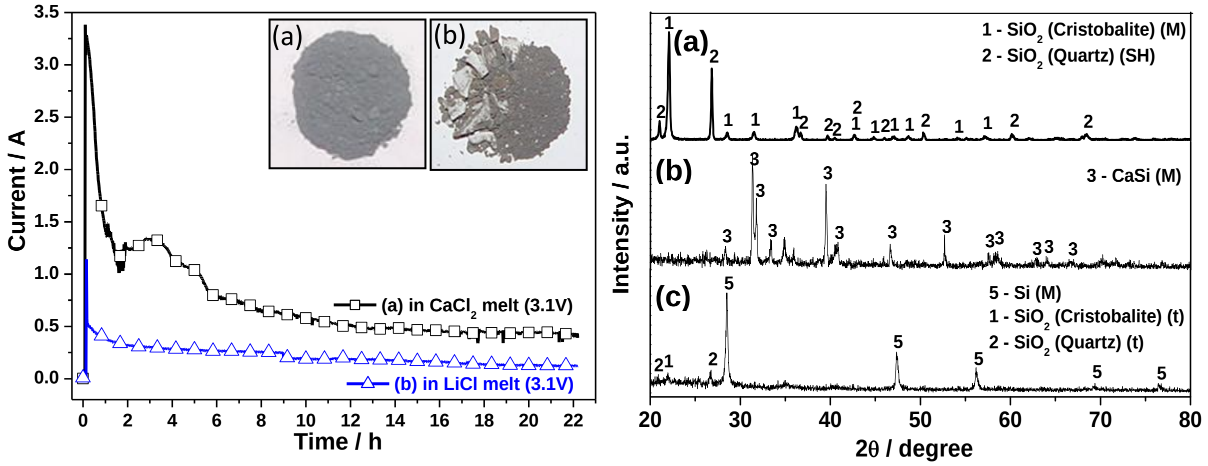

(A) (B)

Fig. 4.16. (A) The variation of current with time during electro-reduction of SiO_2 pellets in fully dipped condition in (a) $CaCl_2$ (b) LiCl melts. Insets show the photographs of the respective products. (B) XRD patterns of: (a) SiO_2 sintered at 1573 K before electrolysis and products after electrolysis at 3.1 V in (b) $CaCl_2$ melt at 1173 K and (c) LiCl melt at 923 K.

In addition to the temperature, various other factors could also have led to the lower extent of reduction of SiO_2 in LiCl melt. After electrolysis, it was observed that the LiCl melt was contaminated to a greater extent with carbon particles than that of $CaCl_2$ melt. The melt was covered with black layer of particles and the surface of the melt was irregular. Such contamination was previously observed during the electrochemical reduction of UO_2 in LiCl-Li_2O melt with graphite as the anode and the contamination was attributed to the carbon particles and Li_2CO_3 [181]. The combined effect of the release of carbon particles and the formation of Li_2CO_3 in the present case too would have led to the contamination of the melt. It can be seen from the photographs given in Fig. 4.17 that while the electrodes (cathode, anode etc.) were lifting out of the melt, held with them a sort of black stuff. The uneven surface of the melt shown in Fig. 4.17d indicated that the surface of the contaminated melt became too viscous. At the top, a floating layer of graphite might have restricted the free release of CO_2 from the melt generated at the anode, leading to the formation of higher quantities of Li_2CO_3. The carbonate cycling thus set and the carbon particles in the melt could have affected the reduction process in LiCl melt.

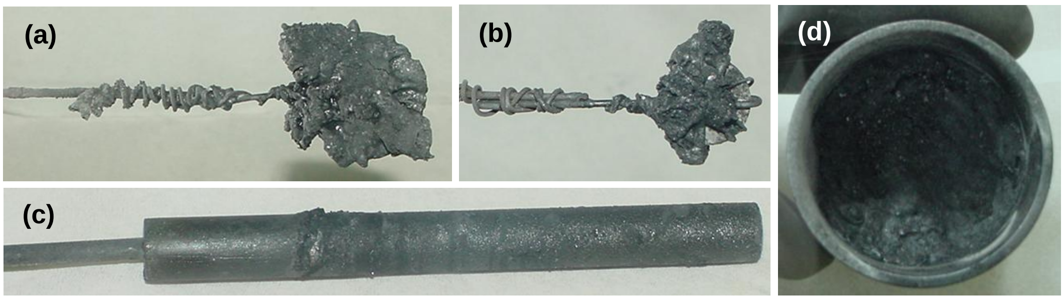

Fig. 4.17. Photographs showing contamination of (a) cathode (b) pellet kept for immersion test (c) graphite anode and (d) LiCl melt with a sort of black stuff after electrolysis of SiO_2 pellet at 3.1 V for 22 h at 923 K, in LiCl melt.

4.3.6.2. Electrolysis of SiO_2 pellets in tip immersed condition

About ~ 4 mm height at the bottom region of the pellet was dipped into the $CaCl_2$ and LiCl melts. A multimeter was used to check the continuity of the circuit of graphite-melt-SiO_2 pellet immediately after dipping. Unlike TiO_2 pellets, no continuity could be observed and this showed that the pellet was acting as an insulator. However, after ~ 10 minutes of dipping, signals of continuity with very high resistance were observed. This could be due to the melt reaching the current collector region of the pellet by capillary action. The electrolysis was carried out in tip immersed condition at 3.1 V in $CaCl_2$ (S-3) and LiCl (S-4) melts for 22 h and the photographs of the pellets before and after electrolysis in both the cases are given in Fig. 4.18.

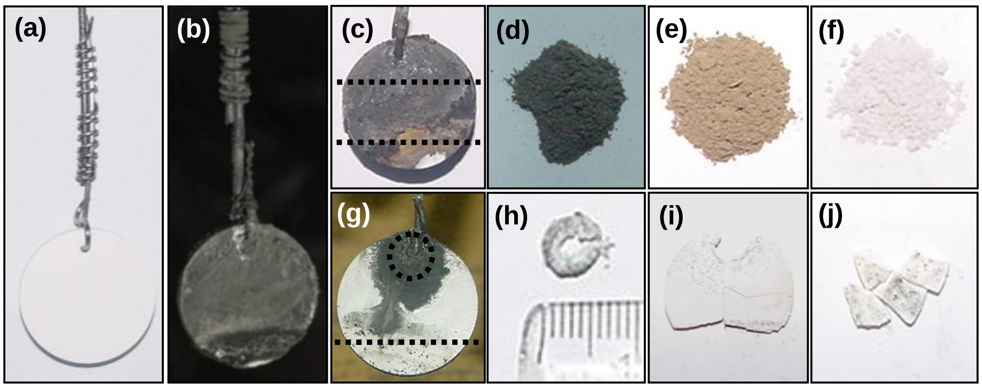

Fig. 4.18. Photographs showing a SiO_2 pellet (a) before and (b) with occluded salt after electrolysis in tip immersed condition in $CaCl_2$ melt. The pellet [in (b)] after washing is shown in (c). Three regions were separated, as indicated by dotted lines, from the pellet namely (d) top (e) intermediate (f) bottom regions. (g) Pellet electrolysed in LiCl melt and its three regions namely (h) ring like region at the current collector (i) intermediate and (j) bottom regions.

It can be seen from Fig. 4.18b that the bottom region of the pellet only was directly dipped into the melt and the melt has penetrated along the walls of the pellet and reached the region of current collector. The pellets showed different, visibly distinct regions as indicated by dotted lines in Figs. 4.18c and g. In both cases the pellets were partitioned into three regions – top (Figs. 4.18d and h), intermediate (Figs. 4.18e and i) and bottom (Figs. 4.18f and j) regions for characterisation.

The I-t curves obtained during electrolysis and X-ray diffractograms of the products after electrolysis are given in Fig. 4.19A and B, respectively. During electrolysis, the current gently increased with time in $CaCl_2$ melt, whereas an opposite behavior was observed in case of LiCl. The charges passed during electrolysis in each of the cases were found to be 1.14 Ah and 0.07 Ah, respectively, which are relatively less, compared to those in fully dipped condition (Fig. 4.16A) under similar experimental conditions. The top region of the pellet electrolysed in $CaCl_2$ melt showed the presence of $CaSiO_3$, $CaCO_3$, Si phases along with traces of SiO_2. The intermediate region contained $CaSiO_3$, SiO_2 and Si whereas the bottom region that had been dipped in the melt remained as SiO_2. The ring like region at the current collector of the pellet electrolysed in LiCl melt was found to be a mixture of Li_2SiO_3 and Si whereas the intermediate and the bottom regions remained as SiO_2. The presence of Si in the top regions in both the cases shows that some amount of SiO_2 would have got reduced by electro-reduction. However due to the limited availability of the melt, the immediate removal of O^{2-} ions from the reaction interface is difficult. The presence of excess O^{2-} ions and significant porosity of the pellet (OP ~ 40%) allowed its chemical reaction with SiO_2 available in the vicinity to form $CaSiO_3$ and Li_2SiO_3, respectively. Also in $CaCl_2$ melt the excess of O^{2-} ions at the surface region at the top of the pellet would have absorbed the CO_2 released from the anode leading to the formation of $CaCO_3$. Though electrolysed for sufficient time, due to the lack of sufficient amount of electrolyte melt, small amounts of

SiO_2 still remained in the top region of the pellet. The gentle increase of current in $CaCl_2$ melt (Fig. 4.19Aa) indicated that the effective surface area for electro-reduction reaction was increasing with time. This was also supported by the observation of formation of a sort of black and dark yellow layers at the surface of the pellet whose combined thickness decreased towards the tip, which roofed the white colored SiO_2 (Fig. 4.18c). As a result of this phenomenon more of the white coloured pellet got converted to various regions having different colors. Also, as the Si produced is semiconducting and its conductivity increases with temperature, more reduction would have taken place in $CaCl_2$ melt when compared to that in LiCl at 923 K. The decomposition potential of SiO_2 decreases with increasing temperature and more reduction is expected to take place at 3.1 V in $CaCl_2$, when compared to that in LiCl melt, which is also in line with the observation.

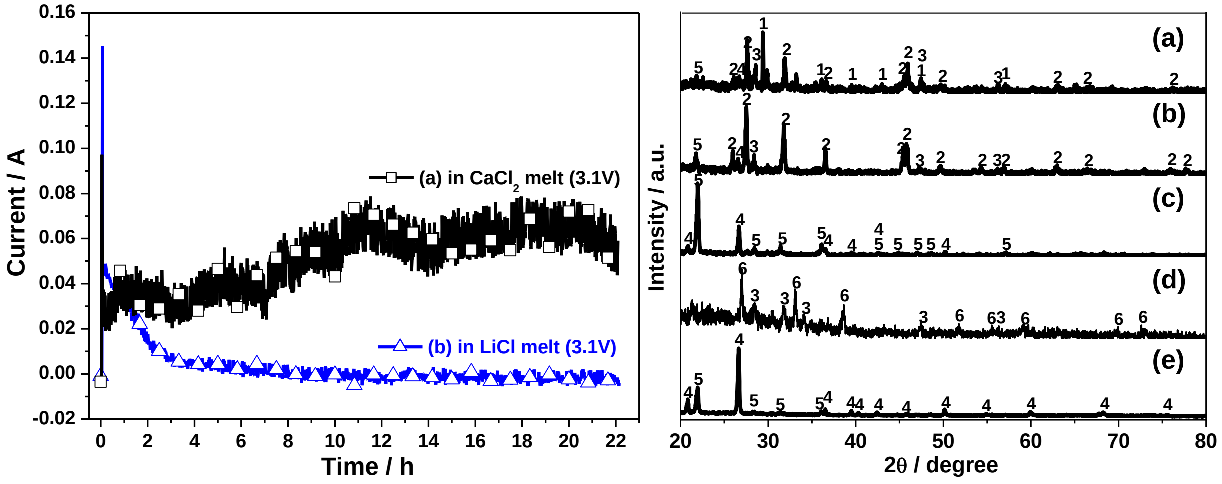

(A) (B)

Fig. 4.19. (A) The current variation with time during electrochemical reduction of SiO_2 in tip dipped condition at 3.1 V in (a) $CaCl_2$ at 1173 K and (b) LiCl melt at 923 K. (B) X-ray diffractograms of the products (a) top (b) intermediate and (c) bottom regions of the pellet electrolysed in $CaCl_2$ melt. (d) Ring like top region at the current collector and (e) bottom region of the pellet electrolysed in LiCl melt. The phases are represented by 1 - $CaCO_3$, 2 - $CaSiO_3$, 3 - Si, 4 - SiO_2 (quartz), 5 - SiO_2 (cristobalite) and 6 - Li_2SiO_3.

Significant microstructural changes have been observed in various regions of the pellets electrolysed in tip dipped condition in $CaCl_2$ and LiCl melts, as could be seen from the microstructures given in Fig. 4.20. The cross section of the ring like region at the current collector from the pellet electrolysed in LiCl melt, which was found to be rich in Li_2SiO_3, showed a typical morphology, similar to water hyacinths, with grains of relatively larger size (Fig. 4.20b) when compared to that of the pellet before electrolysis (Fig. 4.20a). The cross section of the dark yellow intermediate region of the pellet whose thickness was about ~ 1.5 mm, electrolysed in tip dipped condition in $CaCl_2$ melt was found to have columnar morphology with length of the grains being of the order of ~ 50 µm. EDX analysis of the cross section showed an elemental profile containing Ca, Si and O and the region contained $CaSiO_3$ as the major phase as analysed by XRD.

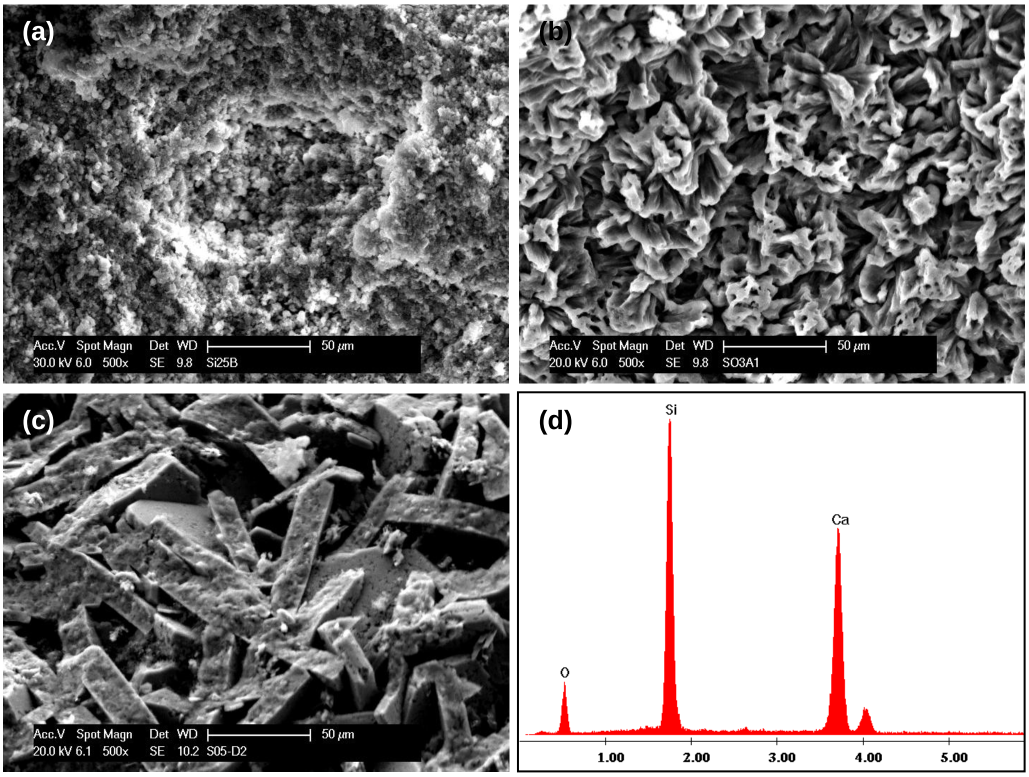

Fig. 4.20. The micrographs of the cross sections of (a) SiO_2 pellet sintered at 1573 K for 3 h before electrolysis (b) The ring like region near the current collector, rich in Li_2SiO_3 obtained from electrolysis in tip dipped condition in LiCl melt (c) The intermediate region of the pellet electrolysed $CaCl_2$ melt rich in $CaSiO_3$ and (d) the corresponding EDX spectrum.

It is observed that the melt immersed tips of SiO_2 pellets electrolysed in tip immersed condition in both the melts were not reduced and remained as SiO_2. However, in the case of TiO_2 pellets electrolysed in tip dipped condition, reduction was found to occur at the tip of the pellet indicating that the oxide acts as a conductor under the electro-reduction experimental conditions. The preferential reduction of SiO_2 pellets at the current collector-oxide-melt regions indicated that the electrochemical reduction of SiO_2 takes place only at the three phase interlines (3PIs) due to the insulating nature of the silicon oxide.

4.3.6.3. Effect of applied voltage on the electro-reduction of SiO_2 pellets in $CaCl_2$ melt

Electrolysis was carried out in $CaCl_2$ melt at 2.5 V for 6 h (S-6) and 2.8 V for 4 h (S-5). The I-t curves during electrolysis and the X-ray diffractograms of the products after electrolysis are given in Fig. 4.21 A and B, respectively.

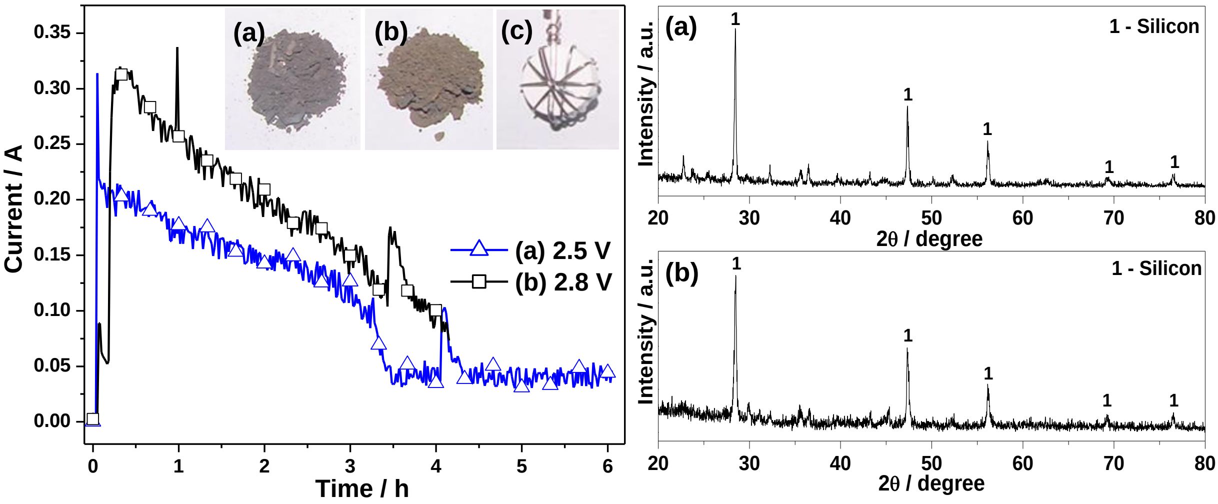

(A) (B)

Fig. 4.21. (A) Electrolysis of SiO_2 pellets in $CaCl_2$ at 1173 K carried out by the application of (a) 2.5 V and (b) 2.8 V. Photographs in insets in (a) and (b) show the products after electrolysis at 2.5 V and 2.8 V, respectively and (c) shows the SiO_2 pellet before electrolysis (B) XRD patterns of the products from experiments carried out at (a) 2.5 V and (b) 2.8 V.

The photos of products of electrolysis are given in insets of Fig. 4.21A. When the applied voltage was high, the corresponding current also was found to be high. Silicon was formed in both the cases, as seen from the X-ray diffractograms in Fig. 4.21B whereas the electrolysis at 3.1 V lead to the formation of CaSi, as discussed previously. Though the formation of Si was observed in LiCl melt during the electrolysis at 3.1 V, the extent of reduction was found to be less. It is a common knowledge that the rate of electrochemical reduction increases with increase in the applied potential. However, when the potential approaches Ca^{2+}/Ca potential, the formation of Ca-Si alloys was observed which was not observed in case of the electrochemical reduction of the oxides of Ti and Nb.

The SEM analysis of the product obtained after electrolyzing the pellets at 2.5 V and 2.8 V are given in Figs. 4.22a and b, respectively. The morphology of Si produced in both the cases was similar and contained particles of Si ranging from tens of nm to µm with the development of appreciable porosity within the silicon matrix.

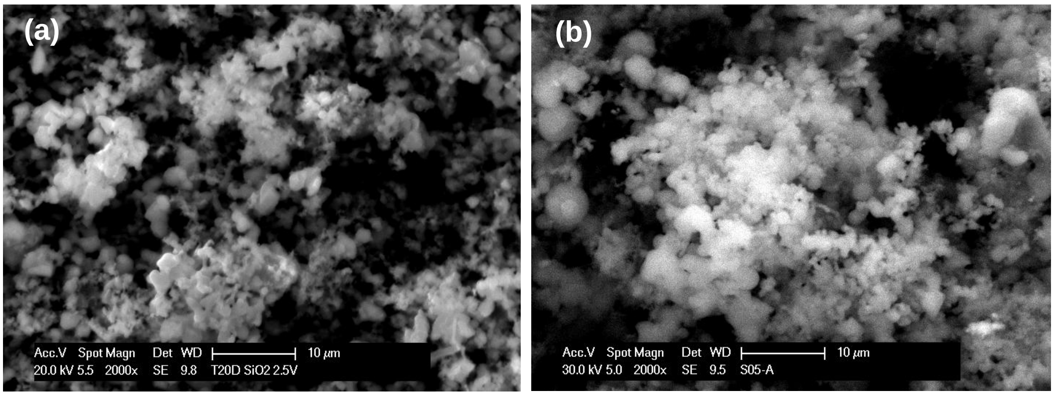

Fig. 4.22. Scanning electron micrographs of porous silicon produced during the electro-reduction of SiO_2 pellets at (a) 2.5 V and (b) 2.8 V in $CaCl_2$ melt at 1173 K.

4.3.6.4. Mechanism of the electrochemical reduction of SiO_2 pellets

The phase diagram of Si - O system [168] doesn't show the presence of suboxides of Si and such compounds were not observed during the electrochemical reduction of SiO_2 in the present case too. During electrolysis in tip dipped condition, SiO_2 showed deoxidation only at the region around the current collector, but not at the region dipped into the melt confirming the occurrence of reduction only at three phase (conductor - oxide - electrolyte) interlines. The electrolyte at the conductor region was provided by the capillary action of the melt. Based on the results, mechanism of direct electrochemical reduction of SiO_2 pellets is represented as

$$SiO_2 + 4e^- \rightarrow Si + 2\,O^{2-} \qquad (4.1)$$

This was in agreement with the mechanism reported in literature [64]. The Si produced was found to be extremely porous. If the reduction zone is not surrounded by excess electrolyte as observed in the case of electro-reduction in tip dipped condition, the released oxide ions react chemically with adjacent SiO_2 particles in the presence of Ca^{2+} or Li^{+} ions to form $CaSiO_3$ or Li_2SiO_3 as follows.

$$Ca^{2+} + SiO_2 + O^{2-} \rightarrow CaSiO_3 \qquad (4.2)$$

$$2Li^{+} + SiO_2 + O^{2-} \rightarrow Li_2SiO_3 \qquad (4.3)$$

In the case of fully dipped condition, the oxide ions might have instantaneously diffused away from the reaction interface due to the porous nature of the Si produced and the availability of plenty of electrolyte, making the chemical reaction less probable. An infinitesimally thin layer of $CaSiO_3$ and Li_2SiO_3, though it had formed, would have undergone electro-reduction instantaneously by the reactions (4.4) and (4.5), given below, producing silicon.

$$CaSiO_3 + 4e^{-} \rightarrow Ca^{2+} + Si + 3O^{2-} \qquad (4.4)$$

$$Li_2SiO_3 + 4e^{-} \rightarrow 2Li^{+} + Si + 3O^{2-} \qquad (4.5)$$

Though reaction (4.1) was considered to be the major one, depending on the experimental conditions and the rates of chemical reactions of (4.2) and (4.3), electrochemical reactions (4.4) and (4.5) would occur simultaneously. Since Si is highly porous and would aid easy removal of the generated oxide ions from the reaction site, ternary intermediates were not seen in the pellets electrolysed in fully dipped conditions in most of the studies [62-64,66-68,71,74].

4.4. Conclusions

The study gave good insight into the reduction behaviour of TiO_2 powder in $CaCl_2$ melt and the pellets of TiO_2 and SiO_2 in both $CaCl_2$ and LiCl melts. The results indicated that the size of the spherical entities of the powder and the size of the grains within them play an important role in the successful reduction of TiO_2 powder. The powder sintered at lower temperature (1423 K) was found to have smaller particle and grain sizes and underwent better reduction over that sintered at higher temperature (1673 K). This was attributed to the cage like spherical entities existing in the powder upon sintering and this geometry caused blocking the melt from its contact to the inside grains. Fusion of the grains at the surface of the entities, due to high temperature sintering makes the melt penetration to inside more difficult. Also as the mass of the powder and diameter of the cup was increased, the reduction of the bulk of the sample was found more difficult. The diffusion of oxide ions from the bulk of the cathode cup as well as from the interior parts of the spherical entity to its surface, it appears, contributed to this problem. The difference in the reduction behaviour of TiO_2 and SiO_2 was studied with respect to electrical contact points. The experiments further proved that TiO_2 pellet is electrically conducting whereas SiO_2 is not. As the electrical conductivities of the two electrodes are different, the mechanism of electro-reduction of the two oxides should also be different. In the case of SiO_2, it becomes essential that the electron conducting metal part should be in contact with the electrolyte and oxide to commence reduction at the three phase interlines (3PIs) i.e., at conductor-melt-oxide phase interlines, for establishing the condition of electro-reduction. As the SiO_2 is reduced at the 3PIs, the Si formed will act as a conductor for the adjoining particles so that the reduction can proceed as $SiO_2 + 4e^- \rightarrow Si + 2O^{2-}$. As electrons are conducted through the TiO_2 matrix, supply of electrons by a metal compartment is not required and hence the conducting oxide and the melt need only be present for reduction to occur. In this sense, the mechanism of reduction is reduced to two phase interface (2PIs) mechanism for conducting oxides so that the reduction occurs at two phase (oxide-melt) interfaces.

Chapter 5

Direct electrochemical reduction of solid UO_2 to U metal in $CaCl_2$-48mol.% NaCl melt

5.1. Introduction

As discussed in detail in section 1.3.3 of chapter 1, many studies have been reported on the electrochemical reduction of UO_2 in LiCl-Li_2O melt at 923 K with platinum as the anode [78,79,82,83,87,135,182]. Investigations carried out on the electrochemical reduction of UO_2 pellets in $CaCl_2$-48mol.% NaCl melt with graphite as the anode are discussed in detail in this chapter. The detailed study, the first of its kind for the DOER of UO_2 with the new electrolyte and graphite anode, is designed to probe the mechanism of electro-reduction of UO_2 pellets as well as the factors that are influencing the electrochemical process. The genesis of selecting such an alternate electrolyte and graphite anode for the electro-reduction studies also has been discussed in detail in chapter 1. In addition, results of preliminary studies of the electrochemical reduction of UO_2 to U in low melting LiCl-KCl-$CaCl_2$ (50.5:44.2:5.3 mol.%) were also briefly discussed towards the end of the chapter.

5.2. Experimental

Pre-dried $CaCl_2$ and NaCl salts were mixed in appropriate quantities to obtain ~260 g of the $CaCl_2$-48mol.% NaCl eutectic mixture, which was employed as the electrolyte in the study. LiCl-KCl-$CaCl_2$ (50.5:44.2:5.3 mol.%) eutectic was also prepared in a similar way by mixing individual salts. Cyclic voltammetry of inert tungsten (cathodic polarisation) and graphite (anodic polarisation) working electrodes were carried out to obtain the electrochemical window of the melt. Also polarisation measurements were carried out with inert SS wire and UO_2 pellet as the cathode and graphite as the anode, as discussed in chapter 2 and 3. The UO_2 pellets tied with SS wire were employed as cathode in the electro-reduction experiments. A Ni/NiO was employed as the reference electrode in the CV measurements and also during electrolysis experiments.

After the completion of the electro-reduction experiments, the surface and a uniformly ground piece (UGP) of the sample in each case were characterised by XRD. A portion of the remaining products of the electro-reduction experiments were washed either with water or with 1:1 ethanol-water mixture for sufficient time to remove the occluded salt, followed by vacuum drying at room temperature. Freshly broken cross sections of the samples were analysed by SEM-EDX. The residual oxygen contents of the samples were also determined.

5.3. Results and discussion

5.3.1. Theoretical considerations

The experiments were carried out at temperatures of 923 K or higher, which are well above the melting temperature of $CaCl_2$-48mol.% NaCl (m.p., 773±2 K). Table 5.1 shows a set of possible reactions and their theoretical decomposition potentials at 923 K ($E_{d,923K}$) from the available thermodynamic data [159].

Table 5.1. Possible reactions and their decomposition potentials calculated from thermodynamic data at 923 K [159].

S.No.	Possible reactions	ΔG^o_{923K} (kJ)	$E_{d,923K}$ (V)
1	$CaCl_2 \rightarrow Ca + Cl_2$ (g)	653.14	-3.385
2	NaCl(s)$\rightarrow$Na(l)+1/2Cl_2 (g)	325.79	-3.376
3	CaO(s)$\rightarrow$Ca(s)+1/2O_2 (g)	540.00	-2.798
4	UO_2(s)$\rightarrow$U(s)+O_2 (g)	925.90	-2.399
5	CaO(s)+C(s)$\rightarrow$Ca(s)+CO(g)	346.90	-1.798
6	CaO(s)+1/2C(s)$\rightarrow$Ca(s)+1/2CO_2(g)	342.29	-1.774
7	$CaCO_3$(s) $\rightarrow$Ca(s)+C(s)+3/2O_2(g)	969.69	-1.675
8	Na_2O(s)$\rightarrow$2Na(l)+1/2O_2 (g)	291.16	-1.509
9	UO_2(s)+2C(s)$\rightarrow$U(s)+2CO(g)	539.69	-1.398
10	UO_2(s)+C(s)$\rightarrow$U(s)+CO_2 (g)	530.48	-1.374
11	UO_2(s)+4Na(l)$\rightarrow$U(s)+2Na_2O(s)	343.58	-0.890
12	Na_2O(s)+C(s)$\rightarrow$2Na(l)+CO(g)	98.06	-0.508
13	Na_2O(s)+1/2C(s)$\rightarrow$2Na(l)+1/2CO_2(g)	93.45	-0.484
14	UO_2(s)+2Ca(s)$\rightarrow$U(s)+2CaO(s)	-154.10	+0.399

From the table, it can be seen that the reduction of UO_2 by Ca alone is thermodynamically feasible. The Gibbs energies of reactions involving UO_2 resulting in the evolution of CO_2 and CO are less compared to those involving evolution of O_2 gas. A potential of 3.3 V, which is above the $E_{d,923K}$ of UO_2 but below that of the individual salts, i.e, $CaCl_2$ (3.385 V) and NaCl (3.376 V), was selected for the constant voltage electro-reduction experiments.

5.3.2. Cyclic voltammetry (CV) and decomposition potential measurements

The results of the CV study with W and graphite WEs in the melt are given in Fig. 5.1a and 5.1b, respectively and those of the polarization measurements with SS and UO_2 pellet as cathodes and graphite as anode are shown in Fig. 5.1c.

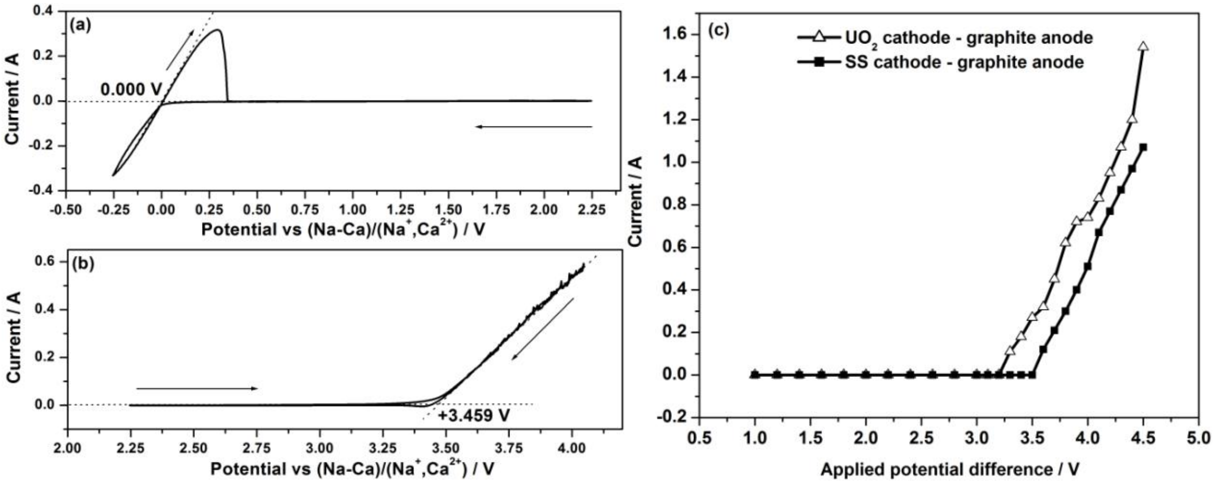

Fig. 5.1. Cyclic voltammograms obtained during cathodic polarisation of (a) W wire (area 0.04 cm^2) and anodic polarisation of (b) graphite rod (area 1.10 cm^2) electrodes in $CaCl_2$-48mol.% NaCl melt at 923 K. Scan rate 20 mV/s. Ni/NiO was used as the reference electrode and the potentials were represented vs. (Na-Ca)/(Na$^+$,Ca^{2+}) potential. (c) Polarization curves obtained with SS wire/UO_2 pellet as cathode and graphite as anode in the melt at 923 K.

The x-axes in Figs. 5.1a and b are represented by potential vs. (Na-Ca)/(Na$^+$,Ca^{2+}) potential. The theoretical deposition potentials for Ca^{2+} ions and Na$^+$ ions are very close to each other (Table 5.1). Therefore, a sharp increase in the current seen at the cathodic limit in the CV (Fig. 5.1a) was attributed to the co-deposition of Ca and Na on W wire, which gets oxidized during the reverse scan as shown by a current hump. A cross over observed between the currents in the forward and reverse scans at potentials cathodic to (Na-Ca)/(Na$^+$,Ca^{2+}) potential indicated that the deposition of Na-Ca alloy on W is associated with certain degree of nucleation over potential, as reported previously [183]. Though the measurements were carried out at 923 K, the characteristics of the CVs were similar to those reported at 823 K

[183] and 958 K [45]. The reversible (Na-Ca)/(Na^+,Ca^{2+}) potential was found out to be -2.246 V vs. Ni/NiO. Similarly, anodic polarization of graphite showed the Cl^-/Cl_2 potential as +1.213 V vs. Ni/NiO. Thus the potential window of the melt is deduced as 3.459 V. The current flow was observed to take place from 3.5 V with SS whereas it started from 3.3 V with the UO_2 pellet. This typical behavior may be attributed to the low energy electrochemical reactions taking place at the UO_2 cathode.

5.3.3. Feasibility studies on the electro-reduction of UO_2 in $CaCl_2$-48mol.% NaCl melt

The feasibility of electro-reduction of UO_2 in $CaCl_2$-48mol.% NaCl was explored by electrolysis at 3.3 V for 44 h by using graphite as the anode. The variation of cathode and anode potentials and the current behaviour of the cell during electrolysis are depicted in Fig. 5.2A. The X-ray diffractograms of a uniformly ground piece (UGP) of the pellet before and after electrolysis are given in Fig. 5.2B (a) and (b), respectively.

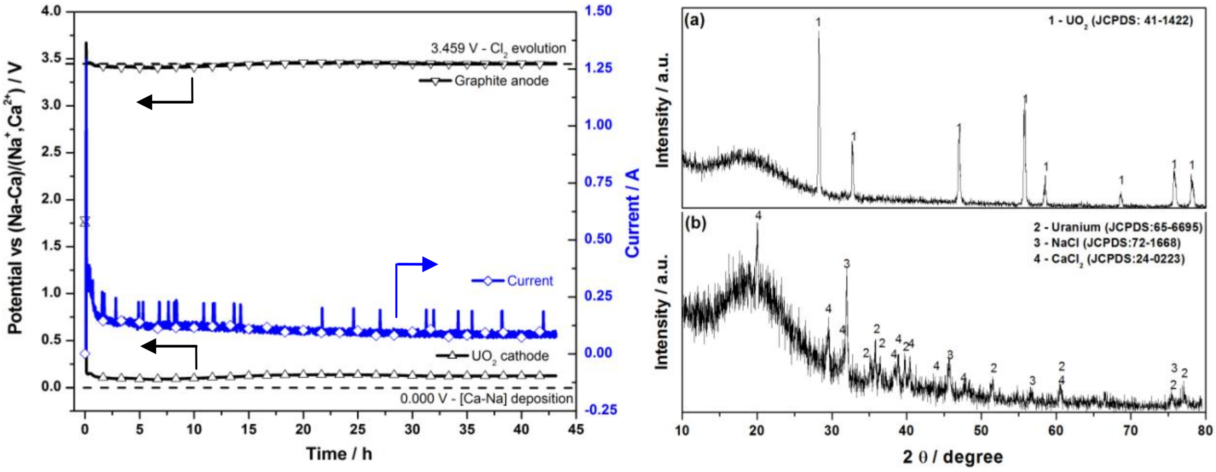

(A) (B)

Fig. 5.2. (A) The variation of potentials of UO_2 cathode and graphite anode vs. (Na-Ca)/(Na^+,Ca^{2+}) and corresponding variation in current during the electrolysis at 3.3 V for 44 h. (B) XRD patterns of the UGP of the pellet (a) before and (b) after electrolysis.

At the instant of impressing of 3.3 V to the cell, the potential of cathode sharply decreased from the open circuit potential of +1.760 V vs. (Na-Ca)/(Na^+,Ca^{2+}) to +0.170 V and within 1.6 h it reached ~+0.100 V and remained in the range +0.100 - +0.135 V during the remaining period of electrolysis. The anodic potential was below that of Cl_2 evolution potential at the beginning of the electrolysis. The current in the beginning showed a high value (1.3 A). It sharply decreased to ~0.140 A in 2 h and thereafter gently decreased during the remaining period of electrolysis. XRD analysis showed that UO_2 is the only phase present in the pellet before electrolysis whereas peaks corresponding to U along with those for NaCl and $CaCl_2$ were observed in the product after 44 h of electrolysis. From the experiment, it becomes evident that the electro-reduction of UO_2 in the melt is feasible.

5.3.4. Factors influencing the electro-reduction of UO_2 in $CaCl_2$-48 mol.% NaCl melt

5.3.4.1. Effect of duration of electrolysis

Table 5.2 shows the details of independent electro-reduction experiments carried out with UO_2 pellets of similar masses.

Table 5.2. Details of the UO_2 electrolysis experiments carried in $CaCl_2$-48mol.% NaCl melt.

Expt. ID	parameter studied	particulars	Pellet after electrolysis	
			regions	phases identified by XRD
U-1 – U-5	Time of electrolysis	~2.5 g, 5% OP, 3.3 V for 6,12,19,35 and 44h	2 or 1	U(surface) + UO_2(bulk). CaO after 19 h in UGP. Above 35h fully reduced
U-6	Temperature	2.64 g, 5% OP, 3.1 V for 25 h, 1173 K	2	Surface: U(M), UO_2(m), NaCl(t); UGP: UO_2(M), NaCl(t)
U-7	Temperature	2.72 g, 5% OP, 3.1 V for 25 h, 1023 K	2	Surface: U; UGP: NaCl(M), UO_2(SH),$CaCl_2$(TH),U(FH)
U-8	Temperature, Applied voltage	2.49 g, 5% OP, 3.1 V for 25 h, 923 K	2	Surface: U(M), NaCl(t); UGP: UO_2(M)
U-9	Applied voltage	2.50 g, 5% OP, 2.8 V for 25 h, 923 K	2	Surface: UO_2(M); UGP:UO_2(M)
U-10	Applied voltage, Time, OP on Con-V mode of electrolysis	2.46 g, 5% OP, 3.3 V for 25 h, 923 K	2	Surface: U(M), NaCl(SH) UGP: UO_2(M), U(SH), CaO(m) and NaCl(t)
U-11	OP on Con-V mode of electrolysis	2.58 g, 48% OP, 3.3 V for 25 h, 923 K	2	Surface: U(M), NaCl(SH), $CaCl_2$(TH);UGP:UO_2(M), NaCl(SH),$CaCl_2$(TH),U(FH)
U-12	OP on CC mode of electrolysis	1.70 g, 5% OP, 200 mA for 19 h, 923 K	2	UGP: U(M), UO_2(SH) and CaO(TH)
U-13	OP on CC mode of electrolysis	1.76 g, 48% OP, 200 mA for 19 h, 923 K	2	UGP: UO_2(M), NaCl(SH) and $CaCl_2$(TH), U(FH)

OP=open porosity, CC=constant current, Con-V=constant voltage, UGP=uniformly ground piece of pellet, M=major, SH=second highest, TH=third highest, FH=fourth highest, m=minor, t=trace

The current behaviour of these experiments is given in Fig. 5.3A (a-f) along with the photographs of the electrolysed pellets in insets of the respective I-t plots. The variation of charge passed with time for 35 and 44 h of electrolysis is shown in Fig. 5.3B. Physical examination as well as the electrical continuity measurements of the cross-section of the electrolysed pellets showed that the reduction started at the surface of the pellet.

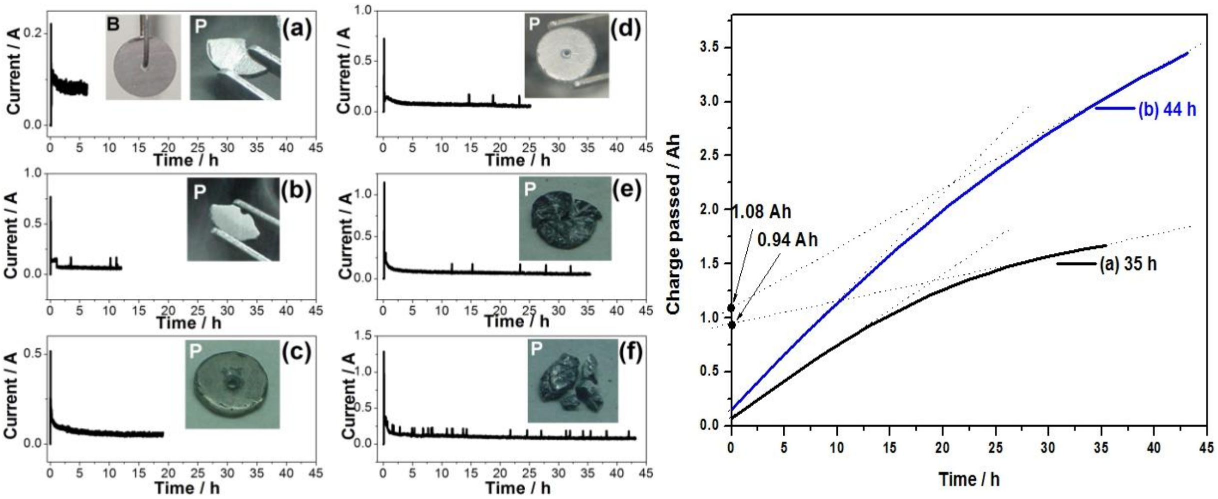

(A) (B)

Fig. 5.3. (A) Variation of current with time for different durations of electrolysis of UO_2 pellets at 3.3 V in $CaCl_2$-48mol.% NaCl melt at 923 K. Inset shows the photographs of the UO_2 pellet before electrolysis (B) and that of products (P) after electrolysis. (B) Plot of charge passed vs. time for (a) 35 h and (b) 44 h of electrolysis.

X-ray diffractograms of surface (after polishing) and the UGP of the electrolysed pellets (Fig. 5.4 a-i) showed decreasing amount of UO_2 and increasing amount of U with time. As the duration of electrolysis increased, the reduction extended inwardly to the bulk of the pellet and the pellet was uniformly reduced to U metal containing 1% and 1.9% of residual oxygen in 35 and 44 h of electrolysis, respectively. In all the other cases, the surfaces of the pellets were preferentially reduced and the depth to which the metallisation occurred depended on the duration of electrolysis. Only U metal, UO_2 and CaO were detected in the partially reduced samples and no ternary compounds like Ca_xUO_y or Na_xUO_y could be detected. This result showed that such intermediate compounds were not formed or the stability of the compounds, if formed, was so less that they were reduced to U metal under the electrolysis conditions. It is appropriate to mention here that such intermediate compounds were not detected during electro-deoxidation of UO_2 in LiCl melt too [85]. Holc and Kolar investigated the phase diagram of UO_2 and CaO under dry reducing atmosphere at temperatures in excess of 1273 K and reported that compounds of the type Ca_xUO_y with uranium in +4 oxidation state (e.g., $CaUO_3$) do not exist [184]. This makes it more or less clear that, though the temperature regime of the present experiments is far below than that of the above controlled experiments [184], Ca_xUO_y compounds are not formed in the present system.

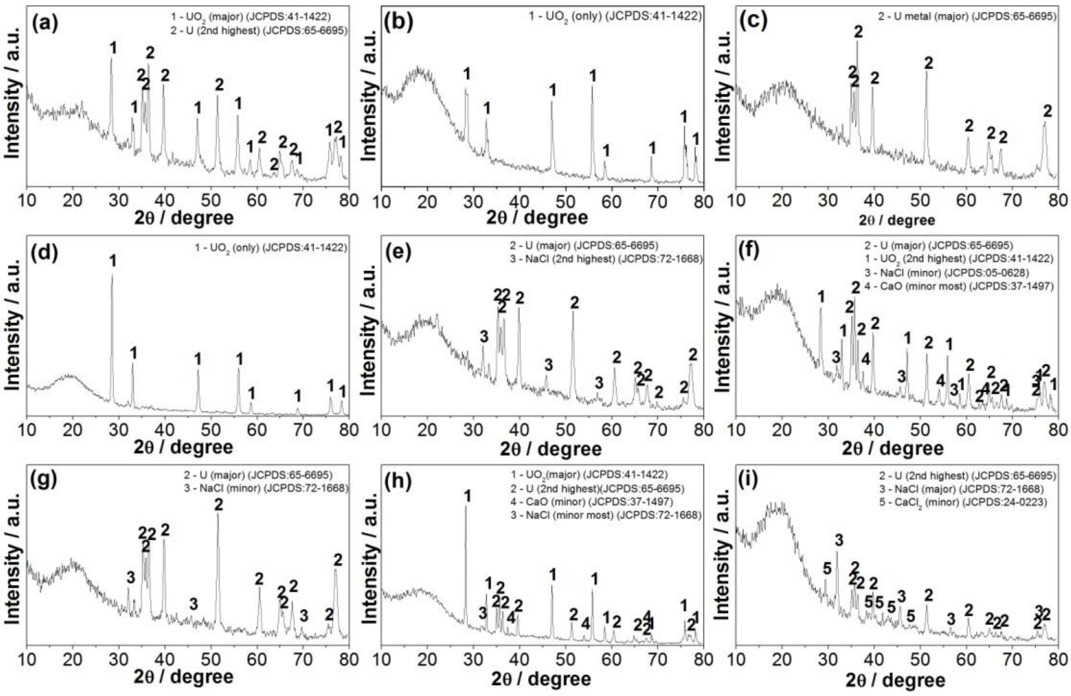

Fig. 5.4. XRD patterns of the UO_2 samples subjected to electrochemical reduction at 3.3 V for different durations of time. Polished surface of the pellet electrolysed for (a) 6 h, (c) 12 h (e) 19 h and (g) 25 h and a uniformly ground piece of pellet electrolysed for (b) 6 h (d) 12 h, (f) 19 h, (h) 25 h and (i) 35 h.

The charge passed for 6, 12, 19, 25, 35 and 44 h was found to be 0.518, 0.885, 1.265, 1.859, 2.621 and 4.544 Ah, respectively. Consider the cases of pellets electrolysed for 35 and 44 h which were fully converted to U metal. As shown in Fig. 5.3B, the charge passed increased with time and the curves ‘a’ (35 h) and ‘b’ (44 h) showed two linear regions, one in the beginning and the other at the end of electrolysis, with two different slopes. Wu et al. [42]

extrapolated the linear part of the later stage of electrolysis of such curves to y-axis to obtain the net charge passed for the electrochemical reduction of Nb_2O_5 to Nb. The method was employed in the present study and it was estimated that net charges of 0.94 Ah (35 h) and 1.08 Ah (44 h) were used up in the two instances. However, the actual amounts of charge that was passed through the cell during the respective periods of electrolysis were 2.621 Ah and 4.544 Ah. The net charges obtained in the two cases by the extrapolation method were close to the charge that was required theoretically for complete reduction of the pellets, i.e., 0.92 Ah and 1.02 Ah in the former and the latter cases, respectively. The above data make it clear that the actual charge passed was three to four times higher than that theoretically required for reducing the pellets. The current efficiency of the process in the present case after 35 h of electrolysis was found to be 34.9% as against 23.8% after 44 h. The poor current efficiency of the solid state electro-deoxidation is well known and reported by many [12,42,58]. Issues like the prevalence of secondary reactions, redox carbonate cycling and electronic conductivity of the melt were the reasons attributed to the poor current efficiency of the process [139]. Considering CO_2 as the anodic gas produced during the process, as discussed later in section 5.3.5, the energy efficiency for the two periods of electrolysis was found to be 14.53% and 9.91%, respectively. The current efficiency as well as the energy efficiency of the process decreased with increase in the duration of electrolysis. This suggests that a significant part of the charge is consumed by secondary reactions in a similar way as observed in the electro-deoxidation reactions carried out in $CaCl_2$ melt [12,139]. The electrolysis energy for the electrochemical production of U, based on data from 35 h of electrolysis, was worked out as 4.2 kWh/kg-U.

Microstructural changes resulting from electro-deoxidation

To show three important aspects during the DOER of UO_2 in the present case, SEM images of fractured surfaces of the pellets before and after 35 and 44 h of electrolysis are given in Fig. 5.5 in three different magnifications. Fig. 5.5(a), (d), (g) shows SEM images before electrolysis, 5.5(b), (e), (h) after electrolysis for 35 h and 5.5(c), (f) and (i) after 44 h of electrolysis.

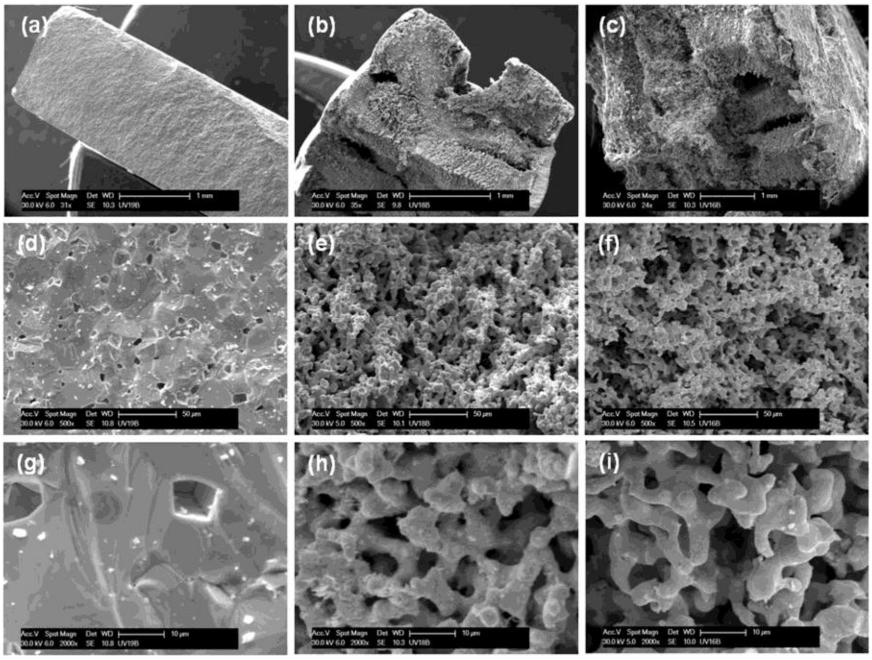

Fig. 5.5. SEM images of cross sections of UO_2 pellet before electrolysis [(a), (d) and (g)] and U metal after electrolysis for 35 h [(b), (e) and (h)] and 44 h [(c), (f) and (i)]. The images are given in three different magnifications to indicate various features.

The microstructures of the samples in the images given in Fig. 5.5(a), (b) and (c) are mostly similar in nature (homogeneity wise). However, in Fig. 5.5(b) and (c) in addition to homogeneity, cracks perpendicular to the thickness of the pellet were observed, which were not present in the pellet before electrolysis. Therefore cracks must have developed during electrolysis. It is possible that the phase changes of the oxide electrode during its transition from the oxide to metal phase caused the cracking. The cracks thus formed in the electrolysed pellet and the absence of sintering might have facilitated easy penetration of the melt to the bulk parts of the pellet and helped in the complete reduction of the pellet. Such a phenomenon was not observed in the DOER of UO_2 using either LiCl-Li_2O or $CaCl_2$ melt as electrolytes. Fig. 5.5(d) shows the uniform nature and distribution of pores within the high dense UO_2 pellet. Substantial increase in the porosity of the pellets with increase in the electrolysis time can be observed in Fig. 5.5(f), when compared to the image in Fig. 5.5(e). The porous matrix, it appears, trapped significant amounts of the electrolyte in its pores, as revealed by the XRD analysis of the unwashed samples (Fig. 5.4i and 5.2B b). The images given in Fig. 5.5(g), (h) and (i) clearly show that the densely packed UO_2 matrix of the original pellet was transformed to a porous nodular structure, typical of a metal produced by DOER, at the end of electrolysis. No sintering of the metal was noticed.

Fig. 5.6 shows the SEM images of the freshly broken cross section of the washed products electro-reduced for different durations of time. Insets given in Fig. 5.6b, c, d and e show the thicknesses of cross section of U metal layers after the respective time periods of electrolysis. The average thicknesses of the surface metal layer after 6, 12, 19 and 25 h of electrolysis are 220 µm, 370 µm, 470 µm and 630 µm, respectively. Obviously the thickness of the surface metal layer is increasing with time. The microstructure of the U metal layer is also seen to undergo change during the course of electrodeoxidation. It is interesting to note that size of the U particles formed is increasing with increase in duration of electrolysis. Thus the average size of the U particles grew to 2-4 µm (Fig. 5.6b), 3-6 µm (Fig. 5.6c), 4-8 µm (Fig. 5.6d) and 4-8 µm (Fig. 5.6e) after 6, 12, 19 and 25 h of electrolysis, respectively. The original high dense pellet contained large grains of UO_2 which were densely packed thus leaving behind a very low porosity in the solid matrix (~5%) as could be seen from Fig. 5.6a. With increase in time of electrolysis, freshly formed U grains coalesced together leading to the formation of larger grains. It was observed that the size of the grains in the regions closer to the surface was larger. This is on expected lines as the reduction commenced at the surface and hence the U metal grains in the surface layer became older and grew in size with time compared to the newer and smaller ones formed later, away from the surface during the course of electro-reduction. The microstructures of the completely reduced samples after 35 and 44 h of electrolysis were similar with distinct grains (Fig. 5.6f and 5.6g). The U metal front moved inwardly towards the bulk with time and the partially reduced samples contained only U and UO_2 phases. Generally the cross section of a partially electro-reduced TiO_2 pellet showed presence of many ternary intermediate compounds and suboxides in three or more distinct layers with two or more boundaries [11]. The fact that only two phases, i.e., U and UO_2 existed in the partially reduced UO_2 pellets and with a distinct boundary between the two different phases as seen in the SEM image in Fig. 5.6h can, therefore, be taken as an evidence to support the theory that the electro-reduction of UO_2 to U was taking place without formation of any ternary intermediate compounds. The metal layers from the samples could be easily separated and their residual oxygen contents in each case after 6, 12, 19 and 25 h were determined to be 3.56, 2.24, 2.82 and 1.82%, respectively. The unreduced bulk displayed large grains of UO_2 (Fig. 5.6i) similar to those observed in the original UO_2 pellet (Fig. 5.6a).

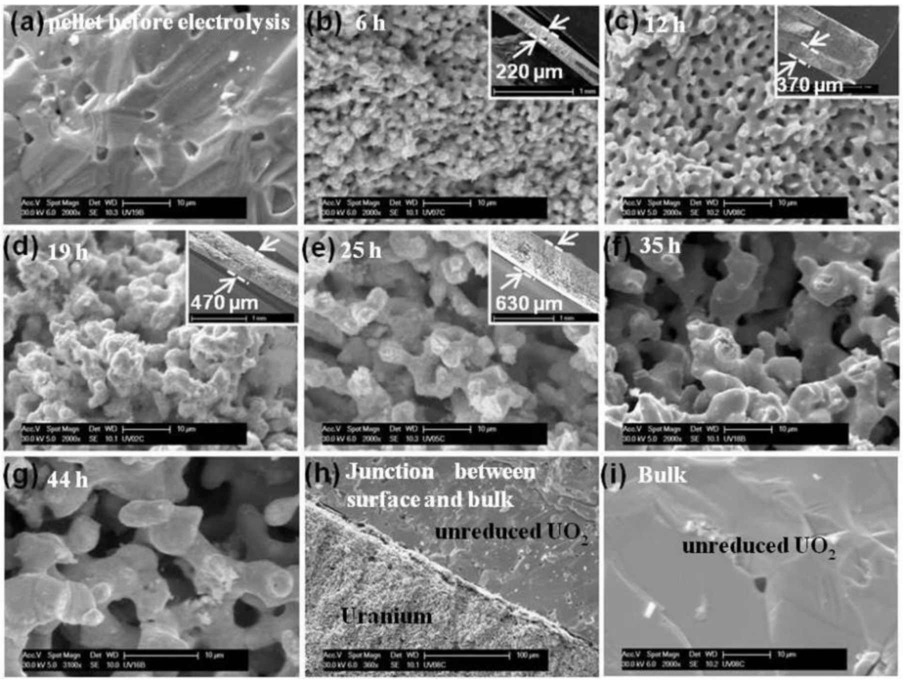

Fig. 5.6. SEM images of the cross section of (a) UO_2 pellet before electrolysis and the surface metal layer of the products after electrolysis at 3.3 V for (b) 6 h (c) 12 h (d) 19 h (e) 25 h (f) 35 h and (g) 44 h. The magnified images of a junction of the U metal layer and unreduced UO_2 and that of unreduced bulk of partially reduced samples are shown in (h) and (i) respectively. Insets are given in (b), (c), (d) and (e) to show the increasing thickness of the U metal layer after respective time periods of electrolysis.

5.3.4.2. Effect of temperature of electrolysis

In order to study the effect of temperature on the electrochemical reduction of UO_2 pellets, experiments were carried out at 923 K, 1023 K and 1173 K at 3.1 V for 25 h (U-6, U-7 and U-8 in Table 5.2). The current vs. time curves obtained during electrolysis are shown in Fig. 5.7A along with photographs of polished surface and cross section of the electrolysed pellets in the insets. The charge passed in each case was found to be 1.032 Ah (923 K), 1.837 Ah (1023 K) and 5.633 Ah (1173 K). Fig. 5.7B shows the X-ray diffractograms of the products after electrolysis.

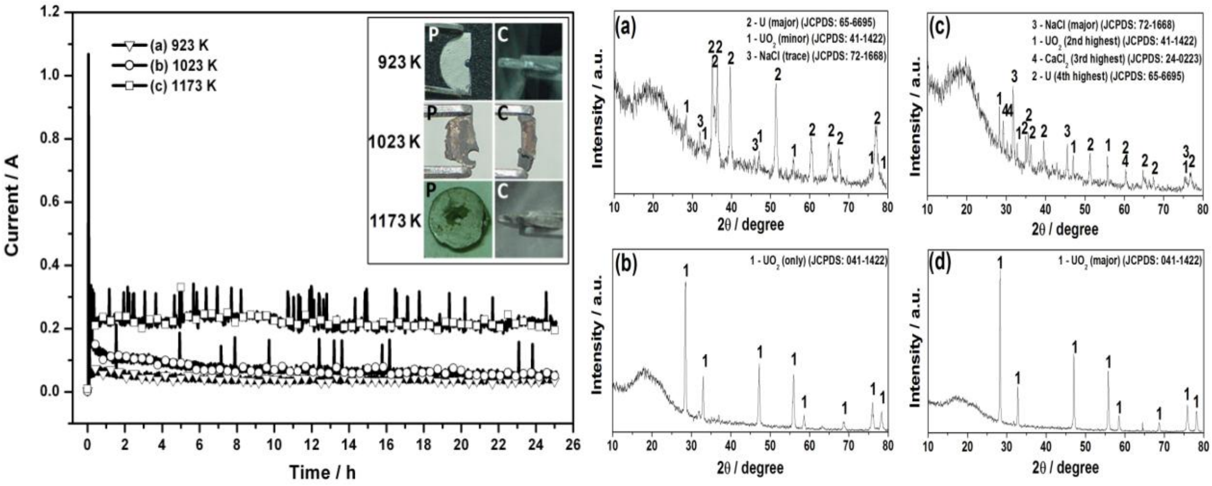

(A) (B)

Fig. 5.7. (A) Variation of current during the electrochemical reduction of dense UO_2 pellets at 3.1 V in $CaCl_2$-48mol.% NaCl melt for 25 h at (a) 923 K (b) 1023 K and (c) 1173 K. Photographs of polished surface and cross section of the products are given in the insets (P, the product after electrolysis and C, the cross section of the product). (B) XRD patterns of products after electrolysis (a) the polished surface of the UO_2 pellet electrolysed at 1173 K. Figures (b), (c) and (d) are XRD patterns of the UGP of the product electrolysed at 923 K, 1023 K and 1173 K, respectively.

The XRD patterns of the polished surfaces of the electrolysis products from the three experiments showed that the surfaces in all the cases were reduced to U metal. However, while only the peaks of U metal were shown in the XRD patterns of samples processed at 923 K and 1023 K (patterns not shown), some peaks corresponding to UO_2 were also shown in the XRD pattern of the sample processed at 1173 K (Fig. 5.7B a). It appears that some metal oxide particles were trapped in the surface metal layer of the sample from the experiment carried out at 1173 K.

The XRD patterns of the UGP of the electrolysis products, obtained from the three experiments are given in Fig. 5.7B (b), (c) and (d). The three patterns show the presence of either UO_2 only (923 K and 1173K) or a mixture of U and UO_2 (1023 K). This indicates that the bulk of the pellets electrolysed at 923 K and 1173 K were not reduced and that of the sample at 1023 K was partially reduced. At the lowest temperature (923 K), the kinetics must have been slow for electro-generation of oxygen ions and their subsequent diffusion from the bulk parts of the dense pellet. Based on this theory, the opposite should have happened for the pellet electrolysed at 1173 K, but here again the bulk of the pellet was not reduced. As mentioned previously, the sintering of U metal particles formed on the surface of the pellet to an impermeable layer would have prevented the penetration of the electrolyte melt to the bulk parts of the pellet and hence reduction of those parts of the pellet. This in essence means that the poor bulk reduction of the UO_2 pellets at 923 K and 1173 K are attributable to entirely different reasons. A relatively better reduction of the bulk of the pellet at 1023 K compared to that at the other two temperatures indicated better access of the electrolyte melt to the bulk parts of the pellet. This temperature can be considered as the most favourable for better kinetics of the electro-generation of oxide ion and diffusion and also for formation of a rather porous surface metal layer. An analysis of the microstructure of the electrolysed pellets, carried out in the following paragraph, makes this point clear.

The SEM images of cross sections of the pellets electrolysed at the three different temperatures are shown in Fig. 5.8. A magnified image of the cross section and the high resolution micrographs of the distinct surface layer and bulk parts of the cross section are given in the figures. In all the three cases, a surface metal layer up to a few hundred µm depth and an unreduced UO_2 bulk are clearly seen. The average thicknesses of the surface metal layers formed at 923 K, 1023 K and 1173 K are 340 µm (Figs. 5.8a), 600 µm (Fig. 5.8d) and 380 µm (Fig. 5.8g), respectively. The higher thickness of the U metal layer of the sample reduced at 1023 K suggests that the process temperature was better for reduction to occur on the oxide layers beneath the surface so that the thickness of the reduced layer could increase. The cross section of the metal layer in the sample processed at 923 K (Fig. 5.8b) shows nodular grains of ~5 µm size and grains of this kind are not observed in the other two cases. As expected the porosity of the metal layer in the high temperature sample (1173 K, Fig. 5.8h) is negligible due to the metal sintering, but that in the pellet reduced at the intermediate temperature (1023 K, Fig. 5.8e) is significant.

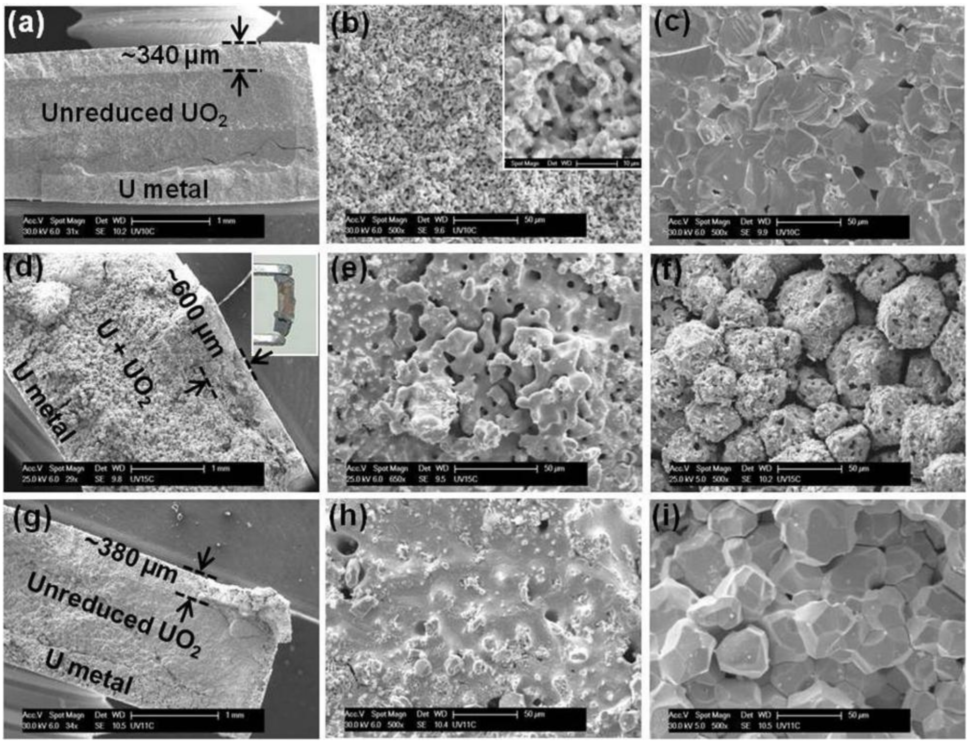

Fig. 5.8. SEM images of dense UO_2 pellets electrolysed at 3.1 V for 25 h at different temperatures. At 923 K: (a) pellet (b) surface and (c) bulk; at 1023 K: (d) pellet (e) surface and (f) bulk; at 1173 K: (g) pellet (h) surface and (i) bulk. Insets in (b) and (d) show the SEM image at higher magnification and photograph of the cross section of the pellet.

The metal grains have also grown in size to 15-20 µm in this case. Morphology of the individual grains seen at the bulk at all the three temperatures can be seen as different (Fig. 5.8c, f and i). Wetting of the grains could be seen in the latter two cases, but not in the former case. The lack of wetting of the sample processed at 923 K may be attributed to the high viscosity of the melt at the low operation temperature. Though, etching was observed at the grain boundaries of both the samples processed at 1023 K and 1173 K, the coarsening of the grains and formation of open spaces between the grains in the former sample (Fig. 5.8f) are noteworthy. The porous metal layer would have allowed penetration of the melt to the bulk parts of the pellet and hence the partial bulk reduction of the pellet. Another interesting aspect noticed is that the oxygen content of the U metal layer formed at 1023 K (1.8%) was less than that at 923 K (2%) and 1173 K (3.1%). This again may be pointing to the porous nature of the metal layer, which permits a larger area of the layer to be in contact with the electrolyte melt and hence a relatively faster and easier de-oxygenation of the metal layer.

As discussed previously, the reduction starts at the surface of UO_2 pellet and slowly progresses towards the bulk. Increase in the process temperature is helpful to the reduction process in different ways as (i) the decomposition potential of UO_2 decreases with increase in temperature (ii) the electrical conductivity of the semiconducting oxide pellet increases with temperature, which in turn increases the rate of electro-deoxidation (iii) the diffusion of O^{2-} ions across the grain in the solid oxide, its diffusion through the pores of the cathode and across the electrolyte between cathode and anode are improved with increase in the temperature, (iv) the viscosity of the melt decreases with increase in the temperature and this helps to improve the wetting of the oxide and also in the enhanced mobility of the electro-generated O^{2-} ions in the melt (iv) the enhanced solubility of O^{2-} ions in the melt at higher temperatures leads to the faster removal of O^{2-} ions from the reaction interface. The low O^{2-} ion activity at the reaction interface enhances the rate of diffusion of oxygen in the solid matrix and also in the electro-generation of fresh O^{2-} ions. However increase in the temperature also increases the rate of sintering of the U metal particles, which adversely affects the reduction process, as discussed above.

5.3.4.3. Effect of applied voltage

The details of electro-reduction experiments (U-9, U-10 and U-11) carried out at three different voltages, viz. 2.8 V, 3.1 V and 3.3 V for 25 h at 923 K are given in Table 5.2. The corresponding electrolysis (I-t) curves are given in Fig. 5.9. The variation of the cathodic potentials for the initial 4 h of electrolysis in all the three cases is given in the inset of Fig. 5.9. It is evident from the figure that the magnitude of current increased with increase in the magnitude of applied voltage. The charge passed in each case was found to be 0.237 Ah (2.8 V), 1.032 Ah (3.1 V) and 1.859 Ah (3.3 V). The XRD patterns of both the surface and uniformly ground pieces of pellets (UGP) showed that no reduction occurred to the pellet subjected to electrolysis at 2.8 V. Further, in case of the other pellets, the average thickness of U metal layer was increased from 340 µm to 630 µm with increase in the applied voltage from 3.1 V to 3.3 V as could be seen from the micrographs given in Fig. 5.8(a) and 5.6(e), respectively. The residual oxygen contents of the corresponding metal layers were found to be 2% and 1.8%.

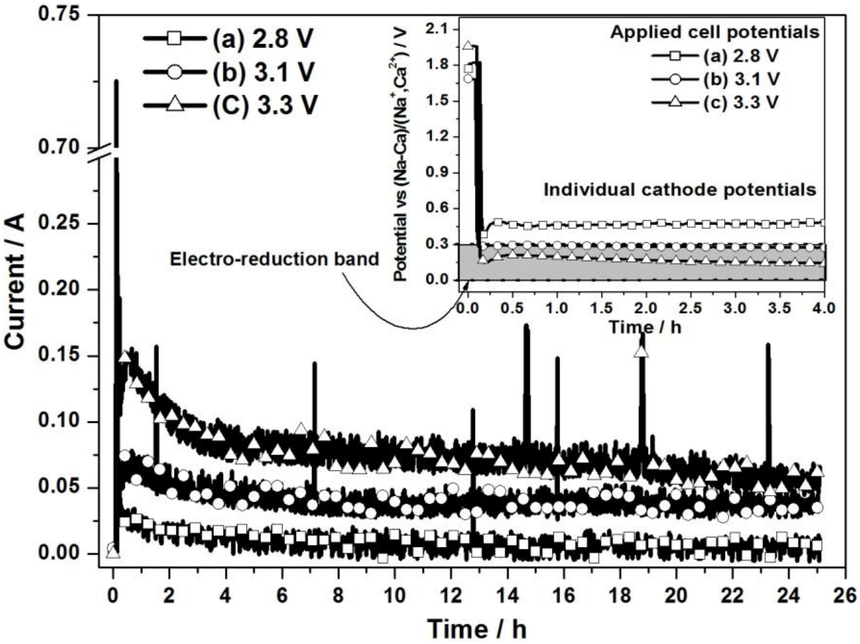

Fig. 5.9. I-t curves during the electro-reduction of dense UO_2 pellets at 923 K for 25 h in $CaCl_2$-48mol.% NaCl melt at (a) 2.8 V, (b) 3.1 V and (c) 3.3 V. Inset shows the individual potentials of the cathode for the initial 4 h of electrolysis at the different applied potentials.

From Table 5.1, the theoretical potential for the reaction under investigation i.e., $UO_2(s) + C(s) \rightarrow U(s) + CO_2\ (g)$ at 923 K is seen as -1.374 V [159]. But as mentioned previously, the reduction of UO_2 could not be effected even at 2.8 V. The minimum applied potential required for the reduction was found to be 3.1 V. Even after considering the fact that the products may not be in their standard states of unit activity during the electro-reduction process and hence the estimated theoretical potential could be more than that deduced under the standard conditions, the applied potential of 3.1 V is very high. This kind of a high overvoltage was observed in most of the reduction studies in the FFC Cambridge process and a significant part of it is considered to be due to the polarisation of the graphite anode for gaseous CO_2 evolution [15]. During electrolysis at different applied voltages, the cathode attained different potentials and remained at a more or less stable value as shown in Fig. 5.9 (inset). At the applied cell voltage of 3.1 V, the potential was around +0.300 V vs. (Na-Ca)/(Na^+,Ca^{2+}). When the applied voltage was increased to 3.3 V, the cathode potential too showed a corresponding increase. Based on the results, it is concluded that a cathodic potential of +0.300 V or higher is required for observable electro-deoxidation of UO_2 to U. Further it can be stated that a cathodic potential within the potential range of ~ +0.300 V to 0.000 V vs. (Na-Ca)/(Na^+,Ca^{2+}), herein termed as the ‘electro-reduction band’, is necessary to effect electrochemical reduction of UO_2 to U without taking recourse to metallothermic reduction by the electro-generated Ca-Na alloy on the electrode. It is obvious that the kinetics of electro-deoxidation of UO_2 will increase as the cathode potential becomes more and more close to the reversible (Na-Ca)/(Na^+,Ca^{2+}) potential of the melt.

5.3.4.4. Effect of porosity of UO_2 pellets

Fig. 5.10A shows the current behaviour of two UO_2 electrodes with open porosity 5% (P1) and 48% (P2) during cathodic polarisation at 3.3 V for 25 h at 923 K (U-10 and U-11 in Table 5.2). The XRD patterns of P2 after electrolysis are given in Fig. 5.10B. Inset given in

Fig. 5.10A shows the exploded view of the highlighted region of the I-t curves for the initial 4 h of electrolysis along with the photographs of pellets before and after electrolysis. The currents on both the electrodes were low initially up to 0.25 h, then showed a significant difference during the period 0.25 h - 1.00 h and subsequently decreased continuously to register more or less identical values in the next 3 h period of electrolysis. The current behaviour of both the electrodes was similar for the remaining period of electrolysis.

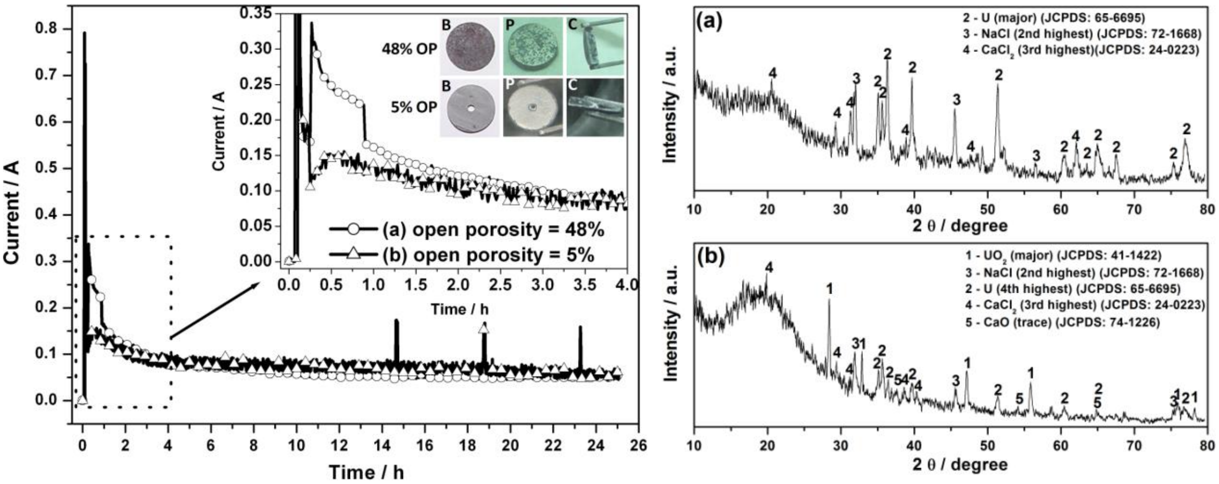

(A) (B)

Fig. 5.10. (A) Current variation during electrochemical reduction of UO_2 pellets with open porosity (a) 48% and (b) 5% at 3.3 V for 25 h at 923 K. Inset shows the exploded view of the highlighted portion of the electrolysis curve along with photographs of the pellets before and after electrochemical reduction (B = before electrolysis, P = product after electrolysis and C = cross section of P). (B) XRD patterns of the product of electrolysis of the 48% porous UO_2 pellet (a) the polished surface and (b) the UGP. Numbers 1 to 5 also show the relative abundance of phases present in the sample in decreasing order.

The two pellets P1 and P2 have different open porosities and hence different surface areas. The magnitude of current is related to the electro-active area of the electrode. The surface area of highly porous P2 being significantly higher than that of P1 must have resulted in higher current of the electrode. As the high current existed only for about an hour in the beginning of electrolysis, it is possibly arising from a surface-area dependent reaction, i.e., adsorption of positively charged ions present in the electrolyte on to the negatively charged surface of oxide electrode. As these surface active sites were saturated, the current decreased with time. The decrease of current thereafter for a long period of time on both the electrodes can be attributed to the electro-reduction reaction. While the charge passed during the initial 1 h of electrolysis with P1 and P2 electrodes was 0.140 Ah and 0.228 Ah, respectively, the total charge passed during the 25 h of electrolysis was estimated to be 1.859 Ah and 1.764 Ah, respectively. The low charge consumption on P2 during the electro-reduction phase, despite the higher open porosity and hence larger surface area, probably indicates a poorer reduction of the pellet though the opposite was expected. The results of analysis, discussed below, too support this observation.

The XRD patterns of the polished surface and UGP of the electrolysed pellet (P2) showed that the surface of the pellet was completely converted to U metal (Fig. 5.10B a) whereas the bulk contained UO_2 as the major phase along with significant amounts of U and trace levels of CaO (Fig. 5.10B b). The SEM images of the pellet before and after electrolysis are shown in Fig. 5.11a and b. The images reveal that a layer of ~1.1 mm on the surface of the pellet was converted to U metal and the bulk remained more or less similar to the original oxide. The microstructures of the reduced region and that of the unreduced bulk are given in Fig. 5.11c and d, respectively. Fig. 5.11c resembles the typical microstructure of a metal produced by the electro-reduction process. Some round-shaped and bright particles are visible in Fig. 5.11d. Energy dispersive X-ray analysis showed that the particles were composed of Ca and O whereas the background was composed of uranium and oxygen with insignificant amounts of Ca present. The results make it very clear that calcium oxide was precipitated in the bulk parts of the pellet during the course of electro-reduction process. Based on the application of in situ synchrotron diffraction technique during DOER of TiO_2, it was reported that the deoxidation occurred only after the removal of the locally generated CaO within the pellet [18]. Accumulation of CaO in the solid oxide matrix adversely affects the reduction process and this would have happened in the case of the porous UO_2 pellet (P2) in this study too. As the mass of the two pellets P1 and P2 were kept similar (~2.5 g), the thickness of the high-porous P2 became almost double than that of P1. An analysis of the thickness of the metal layer reduced in both the cases (Figs. 5.11b and 5.6e) indicated that if thicknesses of the porous (P2) and dense (P1) pellets were similar, the porous pellet would have got reduced completely. The combined effect of higher thickness of P2 and the nature of the melt in the present case, it appears, slowed down the dissolution of the electro-generated CaO in the bulk parts of the pellet into the melt and hence its dissipation from the reaction interface. Recently, Choi et al. [89] reported that the size of the UO_2 electrode is the most critical factor in the electro-reduction and showed that a more efficient reduction was possible with small-sized and porous UO_2 pellets. This study too supports this.

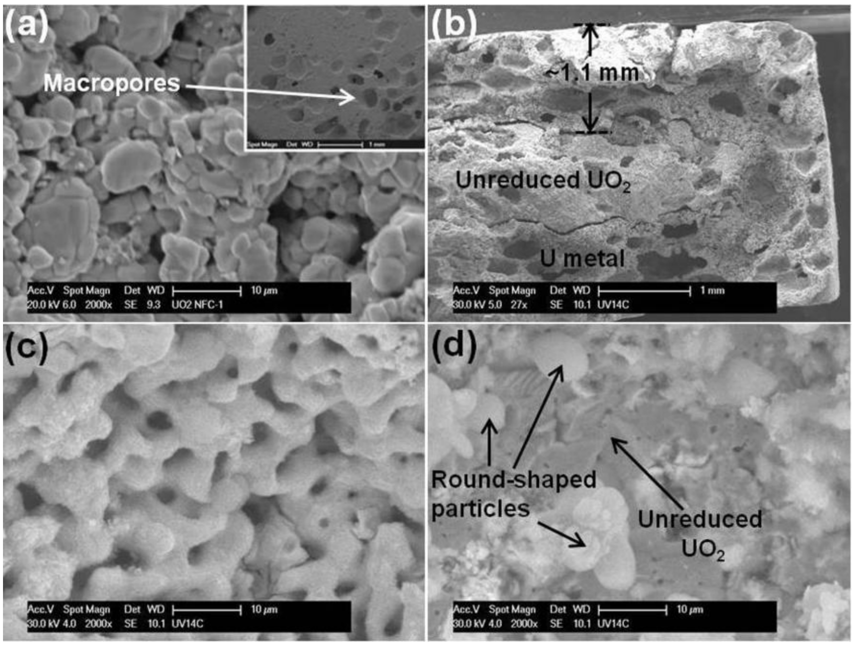

Fig. 5.11. SEM images of (a) porous UO_2 pellet (OP, 48%) before electrolysis (b) fractured surface of the pellet electrolysed at 3.3 V for 25 h showing U metal layer at the surface and unreduced UO_2 at the bulk, the magnified images of (c) the reduced U metal layer and (d) the unreduced UO_2 bulk. EDS analysis: the bright round-shaped particles in (d) were composed of Ca and O where as the background was composed of U and O with minor quantities of Ca.

5.3.4.5. Effect of mode of electrolysis

One dense UO_2 pellet (OP, 5%) each was cathodically polarised for 19 h in constant current (CC) and constant voltage (Con-V) modes in the melt at 200 mA and 3.3 V, respectively. Fig. 5.12A shows the variation of potentials of the UO_2 electrodes for the initial 10 h of electrolysis. The corresponding cell voltages are given in the inset. A detailed version of electrolysis curve for CC mode in case of dense UO_2 shown in Fig. 5.12A is given in Fig. 5.12B. A porous UO_2 pellet (OP, 48%) was also electrolysed in the CC (200 mA) mode for the purpose of comparison and potential-time curve of the cell is given in Fig. 5.12A.

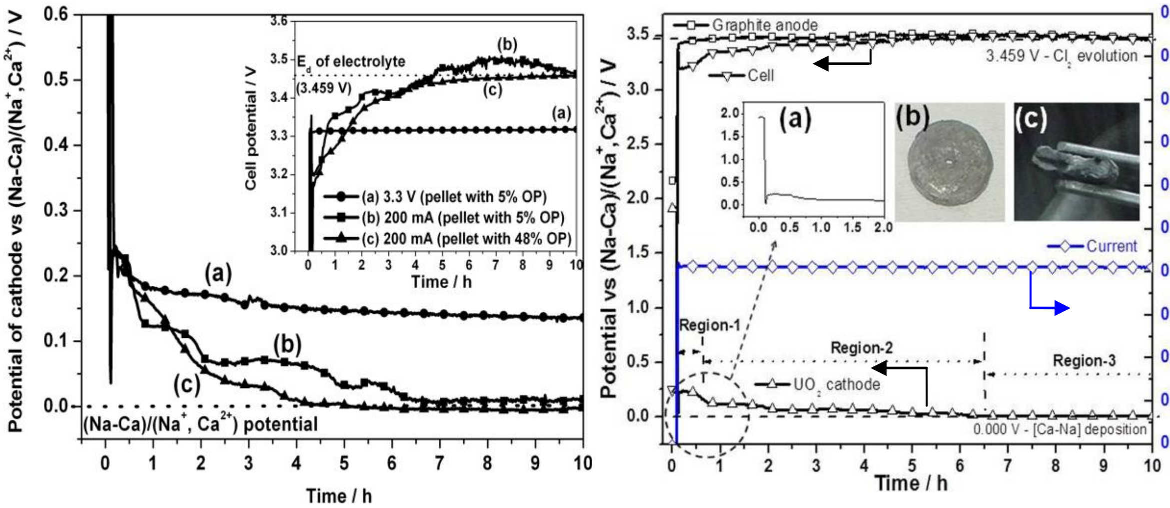

(A) (B)

Fig. 5.12 (A) Variation of cathode potential for the initial 10 h during the electrochemical reduction of dense UO_2 pellet (5% OP) in (a) Con-V mode at 3.3 V and (b) CC mode at 200 mA and a porous UO_2 pellet (48% OP) in (c) CC mode at 200 mA. Corresponding cell potentials are given in the inset. (B) A detailed version of CC mode of electrolysis of the dense UO_2 pellet from (A) given along with the potentials of UO_2 and graphite vs. (Na-Ca)/(Na$^+$,Ca^{2+}). Inset given as (a), (b) and (c) show the magnification of the encircled region of the cathodic potential, the photographs of pellet and its cross section after electrolysis, respectively. The different stages of the electrolysis curves are marked as Region-1, 2 and 3.

The variation of the cathodic potentials during electrolysis in the Con-V (curve 'a') and in the CC (curve 'b') modes shows a marked difference. An electrolytic cell working under the CC mode is free to attain the appropriate electrode potential to sustain the imposed current. However, in the Con-V mode, the electrode potentials are restricted by the magnitude of the applied voltage and the applied voltage will be distributed between the cathode and the anode. This becomes evident from the E-t curves of the three cells given in Fig. 5.12A. From CV studies, as discussed previously, Cl_2 evolution and Ca-Na alloy deposition potentials of the melt take place at +3.459 V and 0.00V vs. (Na-Ca)/(Na$^+$,Ca^{2+}) respectively. It can be seen from E-t curves in Fig. 5.12A (curves ‘b’ and ‘c’) that Ca-Na alloy was deposited on both the dense and porous UO_2 electrodes polarised in the CC mode, but not on the electrode polarised in the Con-V mode (curve ‘a’). However, the surfaces of all the three electrodes were reduced to U metal as revealed by XRD analysis. The Ca-Na deposited electrodes would have undergone metallothermic reduction by the alloy. To gain better insight, a detailed version of CC mode of electrolysis of the dense UO_2 pellet from Fig. 5.12A is separately given in Fig. 5.12B. Three distinct regions designated as ‘Region-1, 2 and 3’ are seen on the cathodic and cell potentials whereas only a plateau is seen in the potential of the anode. For a better visualisation, the variation of potential of UO_2 cathode for initial 2 h of electrolysis was given by (a) in the inset of Fig. 5.12B. It can be seen that the potential of cathode suddenly changed to ~+0.050 V upon the impression of current and thereafter it increased rapidly to less cathodic values (~+ 0.250 V). Further polarisation of the cathode towards more cathodic values up to 6.5 h indicated the occurrence of higher energy reactions to maintain the applied current. The potential of the cathode as well as that of the cell after 6.5 h of electrolysis, in region-3 clearly indicated the decomposition of the electrolyte. The deposition of (Na-Ca) alloys at the cathode then onwards might have led to the metallothermic reduction of the pellet. A detailed discussion on the cathodic potential behaviour will be given in section 5.3.6. The presence of U metal along with UO_2 and CaO in the product without any Ca_xUO_y or Na_xUO_y type of compounds again suggests that such compounds are not formed in the CC mode too. However, in this case, a sort of bulging of the bulk mass of the electrolysed pellet was observed (Fig. 5.12B b and c), the reasons for which are not clearly understood. Also it looked more porous and friable and could be easily ground to powder.

The SEM images of the reduced surface of the three electrodes are shown in Fig. 5.6d (curve a), Fig. 5.13a (curve b) and Fig. 5.13b (curve c). When compared to the microstructure of the metal layer of a sample subjected to electrolysis for 44 h (Fig. 5.6g), the microstructures of the metal layers of the three samples, electrolysed for 19 h, are not well defined and this may be attributed to the presence of oxygen in the metal layers. The oxygen content of the metal layers was determined as 2.82%, 2.99% and 2.6% corresponding to microstructures in Fig. 5.6d, Fig. 5.13a and Fig. 5.13b respectively. Between the dense and porous electrodes, electrolysed in CC mode, the oxygen content was less for the porous electrode. Also the grains are seen more refined in the sample (Fig. 5.13b).

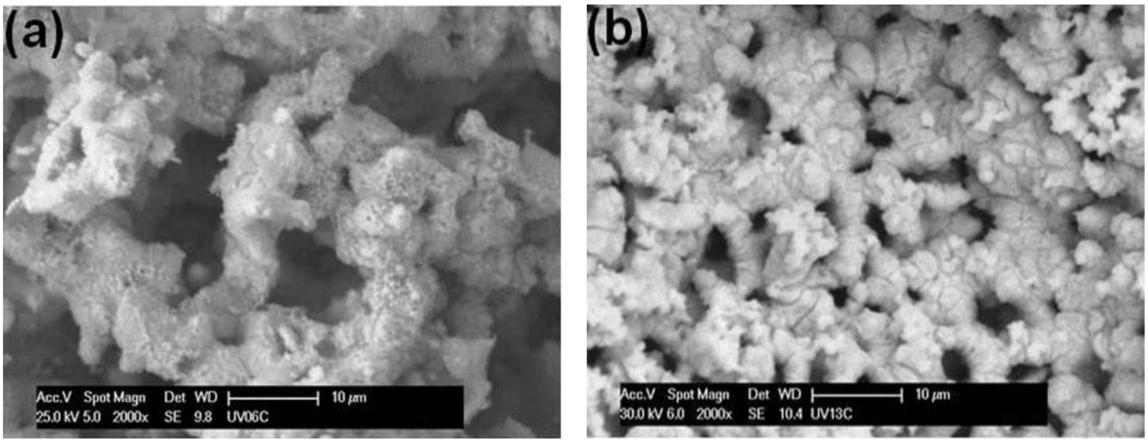

Fig. 5.13. SEM images of the cross section of the reduced surface layer of (a) dense (5% OP) and (b) porous (48% OP) UO_2 pellets after electrolysis at 200 mA for 19 h. Large interconnected grains with open pores of ~10 µm size are formed in (a) where as relatively smaller grains and pores (3-5 µm) are formed in (b).

The ease of oxygen removal from the porous matrix must have helped the sample to achieve a lower level of oxygen. Even as Ca-Na alloy was deposited on both the pellets and their surfaces were reduced to U, the bulk remained unreduced, showing the non-uniform nature of reduction of the solid oxide. Cathodic deposition of lithium on uranium oxide electrodes was reported to slow down the bulk reduction as the deposited metal layer inhibits the movement of oxygen ions from the surface of the pellet to the melt [88,130]. This could have also contributed to the poor reduction of the two Ca-Na alloy deposited UO_2 pellets in this study. Another interesting aspect noticed with both the pellets was that they were bulged suggesting thereby the volume expansion of the electrodes on electrolysis. The reason for this behaviour is not quite clear, though it appears that the metal layer formed on the surface owing to the deposition of Ca-Na layer inhibited free material transfer from inside the pellet to the melt and the strain resulted in the bulging of the electrodes.

5.3.5. Mechanism of electro-deoxidation of solid UO_2 to U in $CaCl_2$-48mol.% NaCl melt

The mechanism of electrochemical reduction of high dense UO_2 pellet to a porous U pellet in the present case is described as a combination of two aspects: (1) Electro-deoxidation at UO_2 entities and (2) The progression of reduction from surface to bulk.

(1) Electro-deoxidation at UO_2 entities

Based on the experimental results, the overall reaction occurring at the UO_2 cathode can be represented as

$$UO_2 + 4\,e^- \rightarrow U + 2\,O^{2-} \qquad (5.1)$$

Generally in $CaCl_2$ melt, the electro-deoxidation of an oxide electrode proceeds via the formation and decomposition of ternary compounds of the type Ca_xMO_y [12]. But as mentioned previously, no such compounds of the type Ca_xUO_y or Na_xUO_y were detected in the present case, which excludes the possibility of a calcium (or sodium) insertion reaction (eq. (5.2)) or a direct chemical reaction between UO_2 and CaO to form $CaUO_3$ (eq. (5.3))

$$2UO_2 + Ca^{2+} + 2e^- \rightarrow CaUO_3 + UO \qquad (5.2)$$

$$UO_2 + CaO \rightarrow CaUO_3 \qquad (5.3)$$

It is appropriate to mention here that Biju Joseph et al. [85] and Herrmann et al. [138] reported that the reduction of UO_2 in LiCl or LiCl-Li_2O melt also do not show formation of any intermediate compounds containing Li. The reduction was reported to occur mainly by chemical reaction of electro-generated lithium metal with the oxide electrode [138] as given by eqs. (5.4)-(5.6). It needs to be mentioned here that the decomposition potential of the Li_2O at 923 K is 2.45 V and that of LiCl is 3.45 V and hence electro-deoxidation of UO_2 in LiCl-Li_2O melt at 3.3 V makes lithium metal formation possible by decomposition of Li_2O in the melt.

$$Li_2O \rightarrow 2Li^+ + O^{2-} \qquad (5.4)$$

$$2Li^+ + 2e^- \rightarrow 2Li \qquad (5.5)$$

$$½\, UO_2 + 2Li \rightarrow ½\, U + Li_2O \qquad (5.6)$$

It was also reported that the reduction would occur directly [138] via ‘oxygen ionisation’ as per eq. (5.1), though its magnitude should be significanly less compared to that by the ‘lithium reduction’, when Li_2O was added to the melt. In the present case, chemical reduction by calcium metal of unit activity cannot be envisaged as the cathodic potential was 150 mV positive to the calcium deposition potential of the melt. As CaO is not added to the melt, generation of calcium metal from CaO at the applied potential is also not possible. $CaCl_2$ melt, when subjected to a potential difference close to its decomposition potential is known to possess strong reducing environment due to the generation of calcium species (calcium metal below unit activity or Ca^+ ions). The role of such underpotential calcium currents in the electro-deoxidation of Nb_2O_5 has been discussed in chapter 3. However, unlike in the case of pure $CaCl_2$ melt at 1173 K, the present $CaCl_2$-48mol.% NaCl melt at 923 K does not show any significant underpotential calcium currents (Fig. 5.1a). It may be that the lower temperature of the melt kinetically suppressed the generation of the calcium species. It is also possible that the solubility of the calcium metal in the melt was decreased due to the presence of NaCl in the melt and this in turn would have adversely affected the generation of the calcium species. Whatever be the reason, a significant contribution from the reducing environment of the melt cannot be considered in the present case for the observed reduction of UO_2 pellets. Under these circumstances, the reduction of the oxide can be considered to take place by a cathodic reaction involving Ca^{2+} ions as

$$UO_2 + 2Ca^{2+} + 4e^- \rightarrow U + 2CaO \qquad (5.7)$$

The fact that the presence of CaO was detected in many of the partially electro-deoxidised samples (Table 5.1) strongly supports this mechanism. The fact that intermediate compounds of measurable stability were not formed during the electro-reduction of UO_2 to U metal, in addition to the above observations, indicates that the reduction of UO_2 to U occurred in a single step. The oxygen ionisation as given by eq. (5.1) also may be contributing to the overall reduction process. Reduction of UO_2 by sodium is thermodynamically not feasible and hence a mechanism involving Na^+ ions is highly unlikely.

(2) The progression of reduction from surface to bulk

High density of the UO_2 pellet would not allow the melt to penetrate to the bulk part of the pellet and this prevents the electrochemical reduction taking place uniformly throughout the pellet. The above reaction is thus initiated at the surface of the pellet, which extends towards the bulk with time as shown by the model given in Fig. 5.14. The conversion of the surface layer of the oxide pellet to metal makes the surface very porous and this enables penetration of the melt to the interior parts of the pellet and hence reduction of those areas. As the electro-generated oxide ions diffuse out from the outer layer, more melt comes in contact with the freshly exposed UO_2 grains. As this process continues, the metal front moves inwardly to the bulk as shown by the increase in the expansion of the bright region towards the bulk of the pellet with time. As the thickness of metal layer increased towards the bulk, the core containing UO_2 shrank. This process continued until complete reduction of the pellet and in the present case, the pellet was completely reduced after 35 h of electrolysis. Some amount of CaO was found at the core of few samples and it appears that the compound was physically trapped in those areas during the reduction. $CaCl_2$ has a high solubility for oxide ions, but the addition of NaCl could have decreased its solubility. This would have retarded the otherwise faster dissolution and diffusion of the electro-generated O^{2-} in the melt resulting in its accumulation in the bulk of the pellet as shown by the XRD analysis. The observation of the changes in the microstructure of the products at different durations of electrolysis (Fig. 5.6) conclusively proved that the reduction of the oxide pellet commenced at the surface and the reduction extended towards the inner centre of the pellet with time and as the process continued the grains of the U metal produced grew in size.

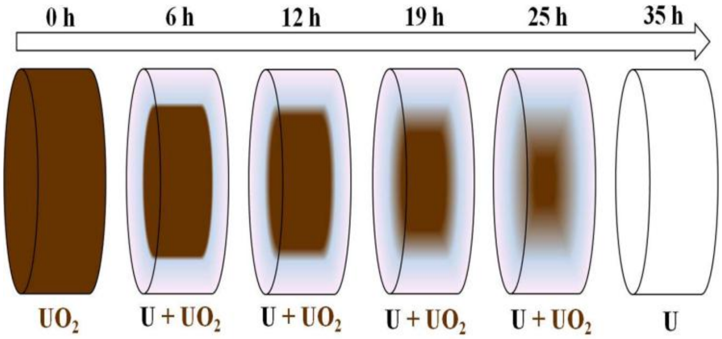

Fig. 5.14. A physical model showing the progression of reduction from surface to the bulk with increase in time of electrolysis (UO_2 is represented as dark region and uranium metal by the bright region).

Some information on the mechanism and progress of electrochemical reduction of UO_2 can also be obtained from the variation of the cathode potential of the cell during low current galvanostatic polarisation experiment, the results of which are given in Fig. 5.12B. A sudden change in the potential of the cathode to ~+0.050 V up on the impression of current, represented in region-1 indicates a high energy process, probably the activation of the reaction sites at the oxide pellet. This activation process would have triggered low energy reactions as indicated by a shift of the potential of the cathode to more anodic values (~+0.250 V). This may be attributed to the electrochemical adsorption of Ca^{2+} and Na^{+} ions on the active surface sites of UO_2 pellet. The electrode slowly gets polarised to ~+0.120 V in region-2, most probably due to the onset of the high energy demanding deoxidation reactions. With time, the location of active sites for deoxidation gradually move away from the surface towards the bulk and the cathode polarised to more cathodic potentials up to 6.5 h as shown in Fig. 5.12B. After 6.5 h, the potential of cathode reached 0.000 V vs. (Na-Ca)/ (Na^{+},Ca^{2+}) as represented by region-3, indicating the deposition of (Na-Ca) alloy on the surface of UO_2 pellet which could possibly cause calciothermic reduction, as sodiothermic reduction is thermodynamically not feasible (Table 5.1). The cell potential given in Fig. 5.12B indicates that electrochemical deoxidation reactions commenced at the surface from ~3.2 V onwards and increased to more than 3.3 V, which is also evidenced in polarisation study using UO_2 as the cathode (Fig. 5.1c). The increase in the cathodic potential with time could be related to the gradual decrease of the oxygen concentration of the pellet and the increasing difficulty in its ionisation and diffusion from the interior parts of the pellet. As the deoxidation of the inner mass of the cathode was kinetically hindered, the cell potential was raised to that of the decomposition potential of the electrolyte to sustain the applied current in the galvanostatic polarisation.

5.2.6. The graphite anode, its effect and corrosion during electro-deoxidation of UO_2

Different reactions can take place at a graphite anode of an electro-deoxidation cell and the nature of reaction will be reflected in the weight loss and/or corrosion of the electrode. Possible reactions at a graphite anode are:

$$2\ Cl^- \rightarrow Cl_2(g) + 2\ e^- \qquad (5.8)$$

$$C + 2\ O^{2-} \rightarrow CO_2(g) + 4\ e^- \qquad (5.9)$$

$$C + O^{2-} \rightarrow CO(g) + 2\ e^- \qquad (5.10)$$

$$O^{2-} \rightarrow 1/2\ O_2\ (g) + 2\ e^- \qquad (5.11)$$

The Cl_2 and O_2 evolution reactions (eq. (5.8) and (5.11)) are not expected to cause any weight loss of the anode whereas the formation of CO or CO_2 necessarily consume the anode material resulting in its loss of weight. This is made use of in gaining some information on the electro-deoxidation process as described below. The weight loss of high density (HD) graphite anodes used in the experimental runs is given in Fig. 5.15. The mass balance of carbon equivalent to weight loss of graphite indicated that a major part of the gases released at the anode is CO_2. Thermodynamically, the formation of CO_2 in the melt at 923 K is more favoured over CO formation and the results obtained agree with this. The loss of weight of the anodes in some cases was even less than that theoretically calculated for CO_2 evolution.

This would probably mean that the anodic reaction was not exclusively CO_2 evolution, but a fraction of the gases would have escaped at the anode as oxygen. Compared to $CaCl_2$ melt used under similar electrolysis conditions but at 1173 K, the contamination of the present melt by free carbon particles is relatively low. This difference may be related to the chemistry of the melts in the two cases. It is known that the anodically produced CO_2 gas dissolves in the $CaCl_2$ melt and it chemically reacts with the dissolved CaO to generate $CaCO_3$ in the melt. The $CaCO_3$ undergoes electrolysis to produce free carbon, which is one of the reasons for the generation of free carbon particles in the melt as given below [139].

$$O^{2-} + CO_2 \rightarrow CO_3^{2-} \qquad (5.12)$$

$$CO_3^{2-} + 4e^- \rightarrow C + 3O^{2-} \qquad (5.13)$$

The presence of 48 mol.% NaCl in the melt should have reduced the CaO concentration in the melt which in turn would have reduced the dissolution of CO_2 in the melt. This might have played a role in the significant reduction in the generation of carbon particles in the melt.

The weight loss of graphite anode under different experimental conditions such as the time, temperature and applied voltage of electrolysis is given in Fig. 5.15a-c. In all the cases, as the magnitude of the parameter under investigation was increased, the weight loss of the graphite too increased. Obviously the charge passed through the cell was increased in each case, which in turn was reflected in the weight loss of the graphite. However, due to the existence of many secondary processes in an electro-reduction cell with graphite anode [139], all the charge passed through the cell may not be accounted by CO_2 and hence to the removal of oxygen from the cathode. For instance for the data in Fig. 5.15a, the expected loss of weights of graphite, by theoretical estimation, are 0.0580 g (0.518 Ah), 0.2081 g (1.859 Ah) and 0.5086 g (4.544 Ah) respectively. But the losses actually observed are only 0.0169 g, 0.0710 g and 0.1093 g. This shows that significant amount of charge passed through such cells are used for reactions other than the electro-reduction reaction. At high temperatures, as discussed previously, formation of the impermeable U metal layer on the surface of the pellet prevents the bulk reduction so that a significant part of the pellet remains as unreduced UO_2 at 1173 K. This again shows that a significant part of the high current observed at the high operation temperature, is due to transport of species other than O^{2-} ions [139].

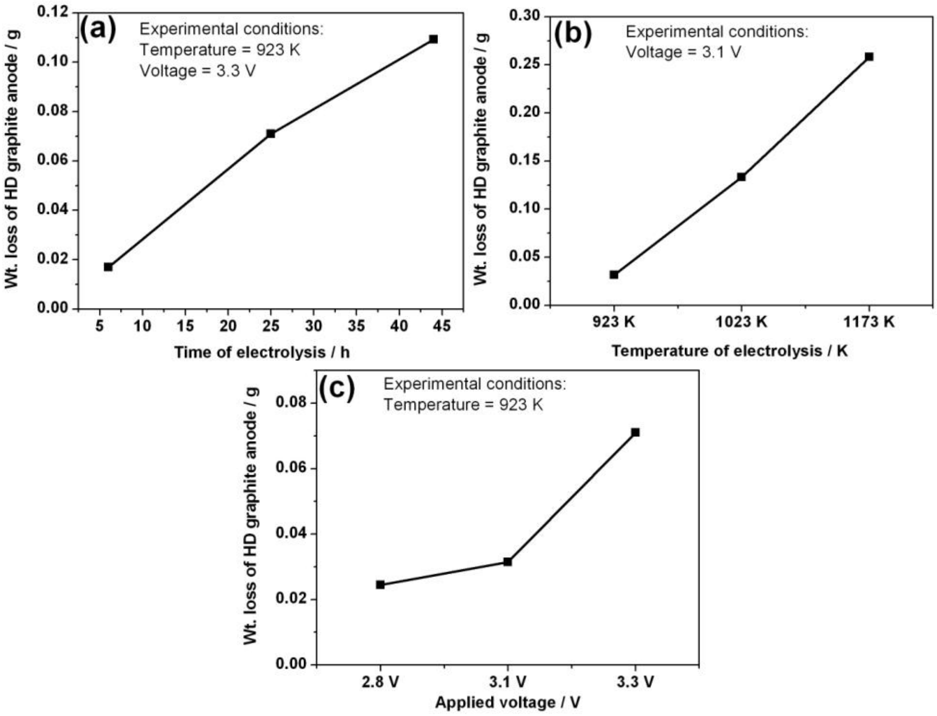

Fig. 5.15. Weight loss of graphite anode during electrochemical reduction of UO_2 pellets in $CaCl_2$-48mol.% NaCl melt as a function of (a) time (b) temperature and (c) applied voltage.

The loss of graphite was noticed to increase drastically as the cell temperature and voltage was increased. CO is more stable than CO_2 at temperatures above ~ 990 K and hence the CO content of the anodic gas was likely to increase with increase in the cell temperature. For a given amount of oxygen, formation of CO requires almost double the quantity of graphite (carbon) than that required for the formation of CO_2. The change in composition of the anodic gas may be reflecting in the increased loss of graphite at higher temperatures. However, the amount of carbon particulate matter in the melt was found to be significantly less than that observed in pure $CaCl_2$ melt at similar experimental conditions. Though the U-

C phase diagram [185] shows the existence of alpha-uranium + UC phase at temperatures below 923 K, the XRD analysis of the polished surface of the pellets in the present study didn't reveal the existence of any carbide phase in the sample. Probably, the uranium carbides were not formed under the present set of experimental conditions and/or the polishing might have removed negligible quantities of carbides present at the surface, if formed. More investigations, with sizeable quantity of the UO_2, are necessary to ascertain the findings of this study for their application to practical UO_2 reduction cells.

Reducing the temperature of operation of the process is an important issue particularly in the nuclear context. Therefore, preliminary study on the DOER of UO_2 was carried out in low melting LiCl-KCl-$CaCl_2$ (50.5:44.2:5.3 mol.%) eutectic at 673 K.

5.3.7. Feasibility study of the reduction of UO_2 in LiCl-KCl-$CaCl_2$ (50.5:44.2:5.3 mol.%).

CV studies carried out on the melt at 673 K, in a similar way discussed previously, showed that the anodic limit of electrochemical window of the melt was evolution of Cl_2 gas and the cathodic limit was deposition of Ca occurring at about -3.750 V (vs. Cl_2/Cl^- potential). Thus the potential window of the melt was found to be 3.750 V. Two reduction peaks, designated as '1' and '2', were observed at the cathodic limit of the melt as shown in Fig. 5.16(a). Peaks '1' and '2' were attributed to the deposition of Ca^{2+} ions (i.e., $Ca^{2+} + 2e^- \rightarrow Ca$) and Li^+ ions (i.e., $Li^+ + e^- \rightarrow Li$), respectively. During the reverse scan, the oxidation peaks for both the elements Li and Ca are not well resolved, probably due to the oxidation of Ca-Li alloys [73] that are formed. Recently, Shen et al. [186] reported similar observations in the context of electrochemical removal of $CaCl_2$ from LiCl-KCl melt. The results are in line with the $E_{d,673K}$ of KCl, LiCl and $CaCl_2$ calculated from the thermodynamic data [159].

Electrochemical reduction of UO_2 in the melt was carried out at 3.9 V for 25 h at 673 K. X-ray diffractograms of the UGP of the pellet after electrolysis showed the presence of

UO_2, U and CaO (trace) phases in addition to KCl. The result shows that the reduction of UO_2 in the melt is feasible though some amount of UO_2 still remained in the product. Fig. 5.16(b) shows the variation of the potentials of individual electrodes (with reference to Cl_2/Cl^- potential) and current during the electrolysis.

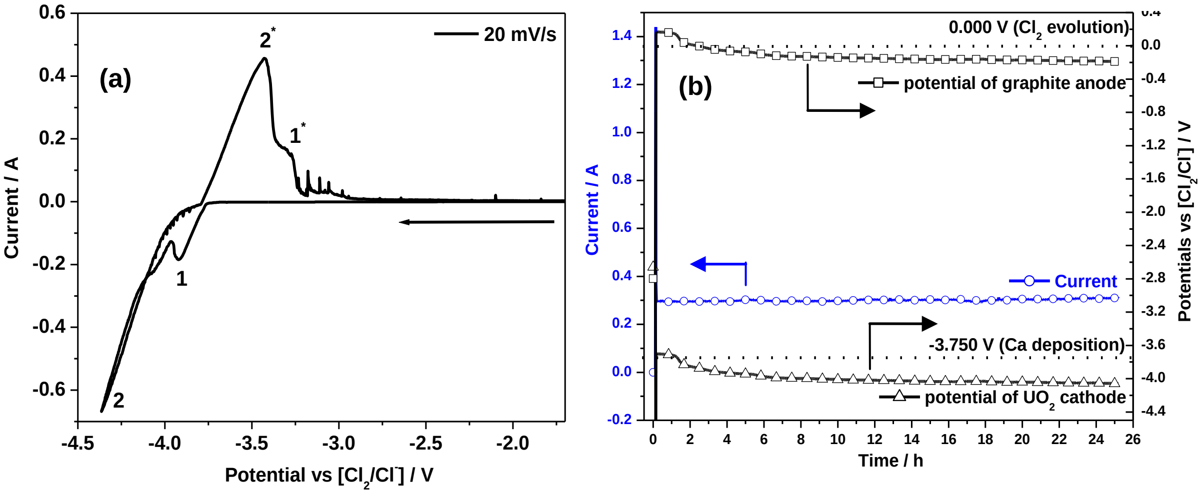

Fig. 5.16. (a) Cyclic voltammogram obtained on tungsten WE on cathodic polarisation in LiCl-KCl-$CaCl_2$ melt at 673 K, represented with respect to Cl_2/Cl^- potential. (b) The variation of current (left y-axis) and potentials (right y-axis) during the electrochemical reduction of UO_2 pellets at 3.9 V for 25 h in LiCl-KCl-$CaCl_2$ melt at 673 K. The potentials of individual electrodes are represented vs. Cl_2/Cl^- potential.

The potentials for Ca/Ca^{2+} and Cl_2/Cl^- are also indicated in the figure by dotted lines. The current remained more or less at ~300 mA for the entire period of electrolysis. It can be seen from the figure that the anodic potential was well above the Cl_2 evolution for about 2.4 h in the beginning of the electrolysis. During this period (up to 1.4 h), the potential of the cathode remained below the deposition of Ca from the melt. Later, the cathode slowly polarised beyond the potential of Ca/Ca^{2+}, leading to the electro-generated calcium induced reduction of UO_2 to U in addition to the electro-reduction that might be taking place when the cathode potential was below that of Ca/Ca^{2+}. Eventually, the potential of the anode slowly attained more or less stable values which are cathodic to Cl_2 evolution indicating the setting up of low energy reactions such as the evolution of $CO_2/O_2/CO$ gases at the anode. The potential of cathode was in the range –3.75V to –4.1V during the process, indicating that the reduction of

UO_2 is taking place mostly by electro-generated-calcium. A fraction of the $CaCl_2$ content of the melt would have converted to Ca^{2+} and O^{2-} ions in due course of electrolysis and enhanced further reduction of UO_2. In addition to the benefit of $CaCl_2$ in forming low melting eutectic with LiCl and KCl, calcium metal generated from $CaCl_2$ during electrolysis participated in the reduction of UO_2. The results of the preliminary studies of UO_2 reduction in the melt suggest that such melts containing low-levels of calcium chloride can be used to achieve electro-reduction at lower temperatures.

5.4. Conclusions

The results discussed above clearly show that $CaCl_2$-48mol.% NaCl at 923 K can be used as an electrolyte medium for electro-reduction of UO_2. With the added advantage of the strong reducing power of calcium, as discussed previously in the introduction, the $CaCl_2$-48 mol.% NaCl melt may prove to be a better electrolyte than LiCl melt for the UO_2 reduction. Unlike in the case of high melting $CaCl_2$ melt (m.p., 1045 K), the low-melting $CaCl_2$-48mol.% NaCl allows the electro-reduced U metal to remain porous and thus to extend the reduction to the bulk parts of the dense solid oxide preform. The results of this study suggest that the reduction may become better by enhancing the process temperature of the melt to1023 K. An important result of this study is that it conclusively proves that no stable intermediate compounds of the type Ca_xUO_y are formed during the reduction process. The study makes it amply clear that no calcium metal of unit activity was deposited on to the UO_2 electrode in the constant voltage mode of electrolysis at 3.3 V in the melt and hence the reduction was not effected by a chemical reaction with the electro-generated metal. Also as revealed by cyclic voltammetry, the $CaCl_2$-48mol.% NaCl binary melt at 923 K does not exhibit any significant underpotential calcium currents and hence it is not expected to play any significant role in the reduction of the UO_2 electrode under the present set of experimental conditions either. The electrochemical conversion of UO_2 to U is most probably occurring by the cathodic reaction, $UO_2 + 2Ca^{2+} + 4e^- \rightarrow U + 2CaO$, in which no intermediate compounds of measurable stability were formed and in that sense the reduction of UO_2 to U occurred in a single step. Apart from this, electro-deoxidation by oxygen ionisation also would have contributed to the overall reduction process of UO_2. The results obtained also indicated that the consumption/corrosion of graphite anodes was significantly less in the melt compared to that of $CaCl_2$ melt employed at 1173 K. The limited results of this study could be taken as an indication that graphite anodes can be used with less operational problems and with increased current efficiency in the binary melt. More studies are necessary to confirm this. Preliminary studies of the DOER of UO_2 in low melting LiCl-KCl-$CaCl_2$ eutectic indicated that the melt can be used as an electrolyte for the electrochemical reduction of UO_2 at lower temperatures.

Chapter 6

Hydrogen sensor based method for determination of extent of reduction of UO_2 cathodes from direct electrochemical reduction studies in molten salts

6.1. Introduction

Electro-chemical reduction experiments carried out with UO_2 pellets in molten $CaCl_2$ and LiCl yielded incompletely reduced products, as discussed previously in chapter 5. In order to develop a better understanding of the reduction process, it was necessary to study the extent of reduction of the oxide to U metal and the propagation of the metal phase in the solid UO_2 matrix. This required estimation of the amount of metallic uranium present in the incompletely reduced solid product. Few estimation methods have been reported in the literature, but an innovative method based on the measurement of hydrogen liberated from reaction between U and an acid was conceived, developed and applied as part of this work. The present chapter deals with various stages of the development of the methodology and validation of the ‘metal estimation by hydrogen sensor (MEHS)’. The method was applied to incompletely reduced UO_2 samples and a possible mechanism of propagation of the reduction in the solid UO_2 matrix was proposed based on the results obtained. Also, the results of the U estimation by the MEHS method have been compared with those obtained by the standard ICPOES method.

6.1.1. Existing methods for estimation of U metal in uranium-uranium oxide mixtures

Many methods have been reported for the estimation of U metal in the presence of its oxides by different investigators. The U metal in incompletely reduced UO_2 samples was estimated by the weight gain attained by the sample during oxidation using TGA/DTA [126,128,187]. Alternatively, uranium in the mixture was dissolved in an acid and the volume of H_2 released in the reaction of U metal with the acid was estimated by a gas-burette [152,153]. U metal was also estimated by Inductively Coupled Plasma Mass Spectrometry (ICPMS) after selectively dissolving the metal in the reduced product in solvents such as Br_2/ethyl acetate [123,154]. Though not directly related, residual oxygen content determined by inert gas fusion technique was also used to arrive at the U metal content in the electrolysed product [31,57].

6.1.2. Metal estimation by hydrogen sensor (MEHS)

The principle of hydrogen estimation in the MEHS method, the experimental set up, its calibration and demonstration of the method for hydrogen released from reaction of Zn and U metals with hydrobromic acid (HBr) have been discussed in detail in chapter 2. It needs to be mentioned here that the MEHS is an extension of a proton exchange membrane based hydrogen sensor (PEMHS), developed earlier at Indira Gandhi Centre for Atomic Research (IGCAR), India and which was effectively put to use for monitoring the corrosion rate of carbon steel in acid medium [158,188]. The unique feature of measurement of hydrogen in ppm levels in hydrogen-argon mixture by the sensor has been exploited in the estimation of U metal by reaction of U with an acid in the present study. Hydrobromic acid (HBr), which readily dissolves metals forming bromides and H_2 gas, was selected as the candidate acid for the MEHS method.

6.1.3. Extent of reduction in the context of electrodeoxidation of UO_2

In the present study, the extent of reduction after electrolysis is defined as the weight percentage of the initially taken UO_2 (in a part of the separated and weighed electrolysed product or whole of it) that got converted to U metal. An expression, as follows, has been derived (see appendix-I) to calculate the extent of reduction (E_R) in the partially electro-deoxidised samples:

$$E_R = \{1 / [\alpha + \beta\ (W_p / W_U)]\} \text{ x } 100\% \qquad (6.1)$$

Where, E_R is the extent of reduction of UO_2 sample after electrolysis; ‘α’ and ‘β’, constants whose values are 0.1185 and 0.8815 respectively; W_U, the estimated weight of uranium metal in the electrolysed product and W_p, the weight of the electrolysed product taken. Although, the MEHS method developed in this study can be used for determining both the extent of reduction in different parts of the pellet or the bulk, only the extent of reduction at various electrochemically significant areas of the electrolysed UO_2 pellet or chunks has been determined in this work.

6.2. Experimental

As mentioned previously in chapter 2, the hydrogen measurement system was calibrated with argon-hydrogen gas mixtures containing different concentrations of hydrogen. The calibrated sensor was used to measure the hydrogen released from the Zn-HBr and U-HBr reactions and thus to estimate the two metals present in the acid solutions. The sensor was calibrated for hydrogen concentrations up to 5,000 ppm in the former case and 3,000 ppm in the latter case. The MEHS was subsequently used to estimate the U metal present in the U-UO_2 mixtures and finally to estimate the U metal present in the electro-reduced UO_2 samples. The results of these studies are briefly discussed below.

6.3. Results and discussion

6.3.1. Calibration of the sensor

The calibration plot of PEMHS obtained by plotting varying concentrations of H_2 in argon against the sensor response is shown in Fig. 6.1a. The calibration plot shows linear relationship between the concentration of hydrogen and the sensor response. In order to ascertain the accuracy of H_2 estimation, known concentration (1,485 ppm) of H_2 in argon gas was passed through the sensor for 15 minutes at a constant flow rate of 200 sccm and the response of the sensor is shown in Fig. 6.1b. The current increased instantly when H_2 was introduced to the sensor and slowly stabilised at the plateau region indicating the limiting current condition. The limiting current was always used as the signal corresponding to the hydrogen concentration in the argon-hydrogen gas mixture. The experiments were repeated and the results are shown in Table 6.1. The results indicate that the actual values and the estimated values are in agreement within ±5% and the relative standard deviation is ± 1.8 %.

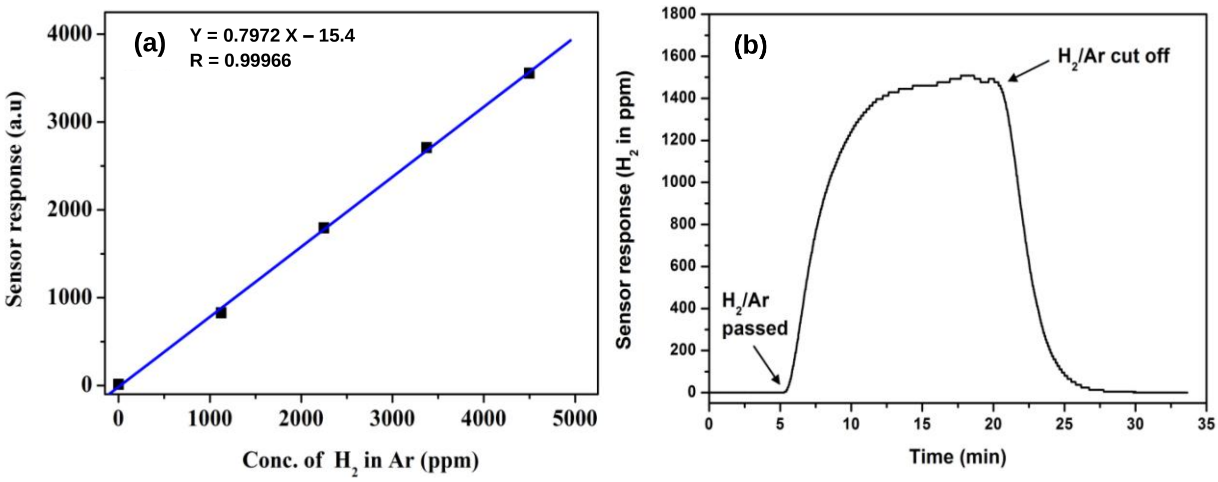

Fig. 6.1. (a) Calibration plot of the sensor with argon + hydrogen gas mixtures (b) Typical response of the sensor for 1485 *ppm* of hydrogen in argon.

Table 6.1. Variation of volume of H_2 estimated for known volume of H_2.

Sl.No.	H_2 passed (SCC)	H_2 estimated (SCC)	% Error	Mean (RSD)
1	4.455	4.582	2.86	4.46 (± 1.8%)
2	4.455	4.488	0.74	
3	4.455	4.662	4.65	
4	4.455	4.515	1.35	
5	4.455	4.562	2.40	
6	4.455	4.498	0.97	
7	4.455	4.338	-2.63	
8	4.455	4.273	-4.08	
9	4.455	4.229	-5.07	

6.3.2. Estimation of Zn by MEHS method

Estimation of Zn was attempted by the MEHS method in order to test and validate the method. Fig. 6.2a shows the hydrogen release pattern obtained during the estimation of zinc using the sensor. From the area under this curve, total amount of hydrogen liberated can be calculated using eq. (2.24). Fig. 6.2b is the plot of number of moles of H_2 evolved vs. number of moles of Zn metal. The slope for the plot is close to 1. The value of the slope clearly confirms that the reaction between Zn and HBr occurs with stoichiometry of 1:2 as evident in eq. (6.2)

$$Zn(s) + 2\,HBr(aq) \rightarrow ZnBr_2(aq) + H_2\uparrow(g) \qquad (6.2)$$

Thus, the stochiometry of reaction between Zn metal and HBr can be arrived from the slope of the plot of number of moles of H_2 evolved vs. number of moles of Zn metal.

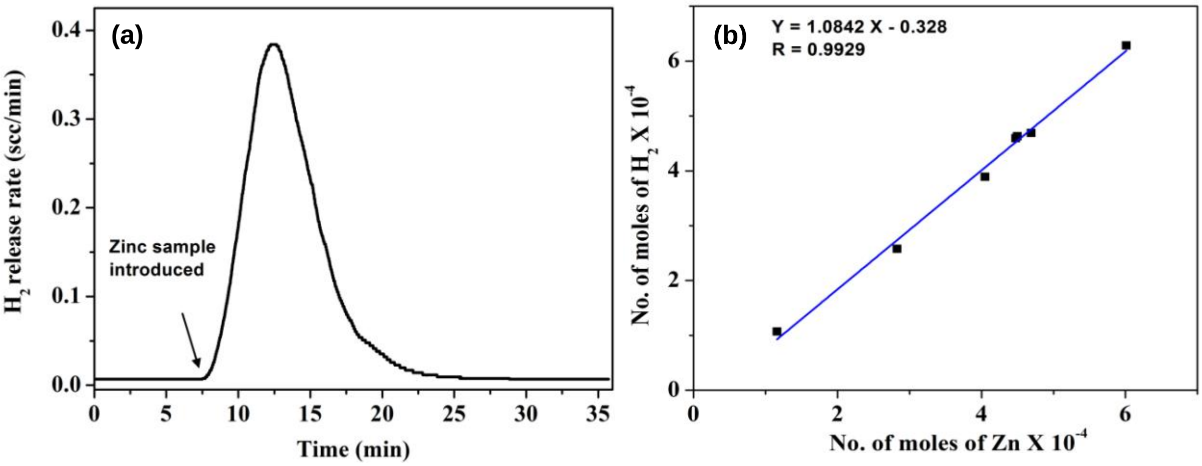

Fig. 6.2. (a) Typical H_2 release pattern obtained from the sensor response for zinc dissolution (b) Plot of number of moles of hydrogen liberated vs. number of moles of zinc metal taken.

The weight of Zn metal taken for dissolution can be estimated by using the equation obtained from the calibration plot as given below.

$$W_{Zn} = N_{Zn} \times 65.38 \text{ g mol}^{-1} \quad (6.3)$$

$$N_{Zn} = [N_{H2} + 0.328 \times 10^{-4}] / 1.0842 \quad (6.4)$$

where, N_{Zn} is the number of moles of Zn metal taken for dissolution and N_{H2} the number of moles of H_2 obtained from the sensor’s output. Eq. (6.4) gave good results when tested for estimation of samples of known weight of Zn metal by the MEHS method by their dissolution in HBr.

6.3.3. Estimation of uranium by MEHS method

A typical current response curve (converted to rate of hydrogen release) of the sensor for reaction of HBr with small pieces uranium metal (weighing 25-80 mg) is shown in Fig. 6.3b. The photograph of the double walled reaction chamber showing the dissolution of U metal in HBr is given in Fig. 6.3a. It was visually observed that the H_2 evolution and hence the dissolution rate of U was lower than that of Zn metal.

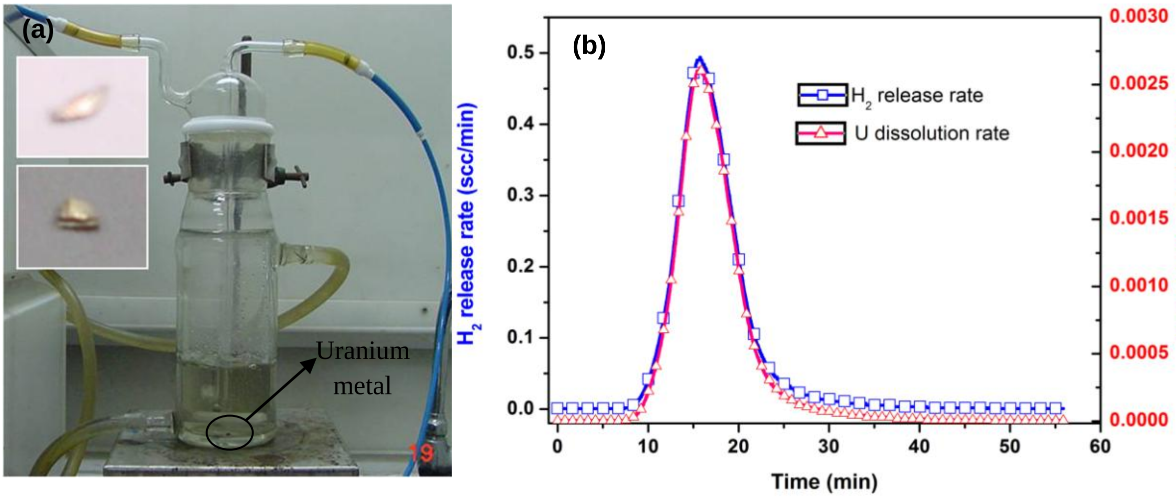

Fig. 6.3. (a) Photograph of the double walled reaction chamber showing the dissolution of uranium metal in HBr. (Insets: pictures of uranium metal pieces before dissolution) (b) Typical hydrogen evolution pattern of the reaction of uranium samples in HBr.

Derivative and integral plots of Fig. 6.3b are given in Fig. 6.4a and Fig. 6.4b, respectively. The derivative plot shows the rate of change of hydrogen release rate. The integral plot gives useful information about the progress of dissolution of U metal in HBr. Even though the total reaction time was about 35 minutes, 90% of the reaction was completed within about 15 minutes after immersion of sample in HBr. A series of increasing weights of metallic U samples were dissolved in a similar way and the liberated H_2 was measured using the sensor.

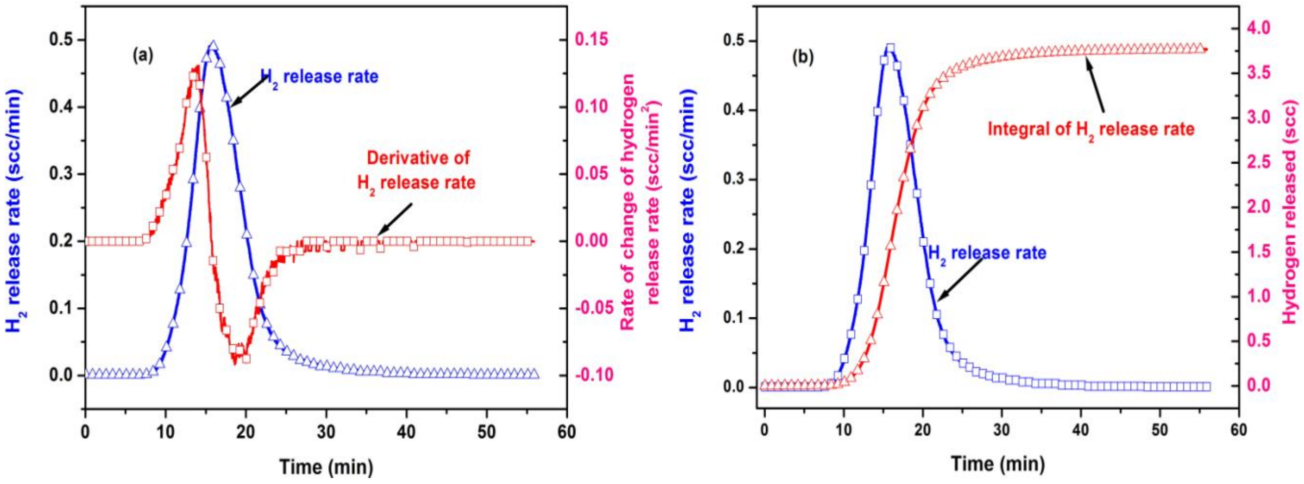

Fig. 6.4. Response curves of the dissolution of uranium in hydrobromic acid, (a) Hydrogen release behaviour and the rate of change of hydrogen release, (b) Hydrogen release behaviour and the amount of hydrogen released with time.

Fig. 6.5a shows the H_2 release behaviour of various U samples, weighing in the range 25.5 to 80 mg. The H_2 release rate was observed to change randomly with respect to mass, which was attributed to the non-linearly varying surface area of the uranium samples. The samples were not having definite shape as they were prepared by chiselling out from a uranium rod. Fig. 6.5b shows the normalized plot of progress of U dissolution. Normalization was carried out by considering the percentage of dissolved uranium with respect to total uranium taken.

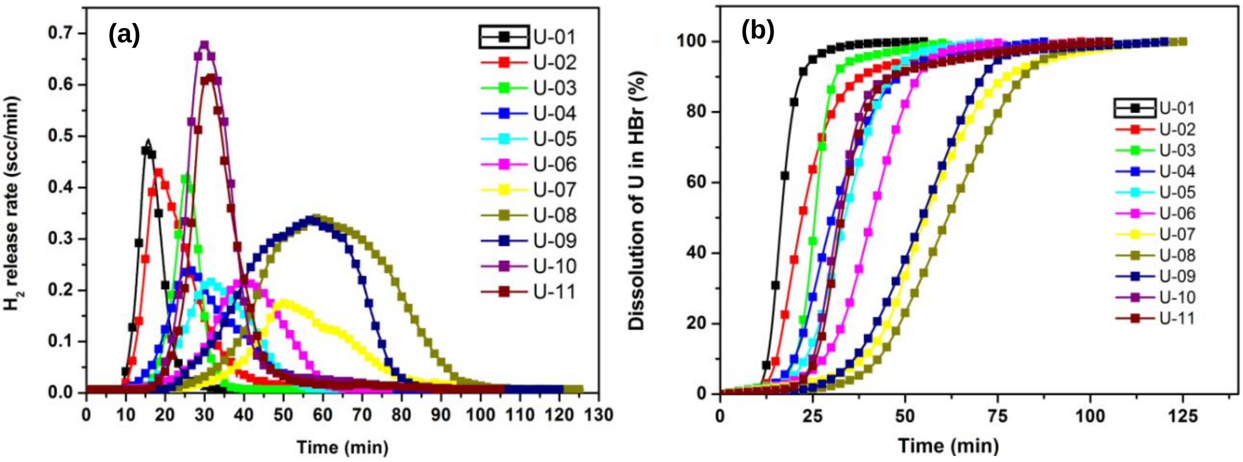

Fig. 6.5. (a) Plot of dissolution behaviour of U samples of various amounts in HBr solution (b) Plot of normalised dissolution behaviour of U samples of various amounts in HBr solution.

A plot of number of moles of H_2 evolved against number of moles of U metal taken is given in Fig. 6.6 which shows the linear dependence of the amount of H_2 evolved on the amount of U metal taken. The slope of the plot gives a value of 1.9357 (close to 2). Hence the possible reaction taking place during the dissolution of U metal must be $U_{(s)} + 4\ HBr_{(aq)} \rightarrow UBr_{4(aq)} + 2H_2\uparrow_{(g)}$, and therefore, the stoichiometry of reaction of U with HBr is ascertained as 1:4. The number of moles of U could be calculated from eq. (6.5) obtained from the calibration plot given in Fig. 6.6, from which the mass of the U metal can be estimated.

$$N_U = [N_{H2} + 0.3823 \times 10^{-4}] / 1.9357 \qquad (6.5)$$

$$W_U = N_U \times 238\ \text{g mol}^{-1} \qquad (6.6)$$

where, N_U is the number of moles of U metal and the N_{H2} the number of moles of liberated H_2.

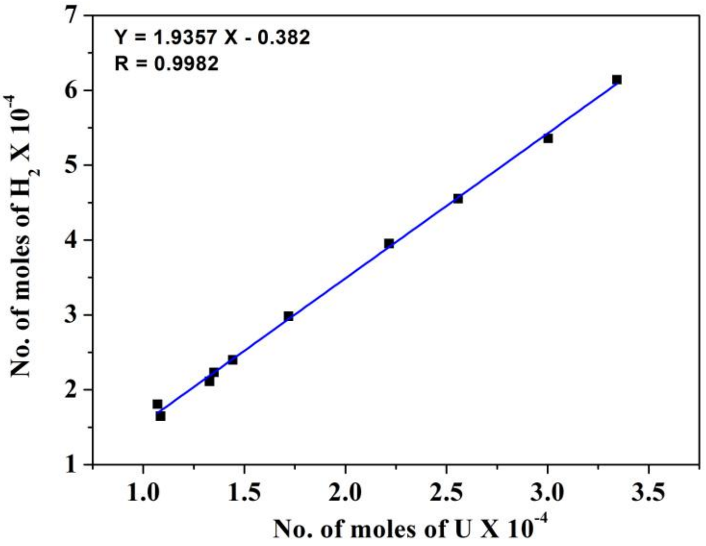

Fig. 6.6. Plot of number of moles of H_2 liberated vs. number of moles of uranium metal dissolved in HBr.

Samples collected from the uranium dissolved hydrobromic acid solutions were analysed for uranium content by inductively coupled plasma optical emission spectroscopy (ICPOES). The mass of U taken and the mass of U estimated by MEHS and ICPOES methods are given in Table 6.2.

Table 6.2. Comparison of results of estimation of uranium by MEHS and ICPOES methods.

Sl. No.	Weight of U sample (W_s) (*mg*)	Estimation by MEHS method			Estimation by ICPOES method		
		Estimated weight (W_m) (*mg*)	W_{nm} (=W_m/W_s)	Deviation of W_{nm} from 1	Estimated weight (W_i) (*mg*)	W_{ni} (=W_i/W_s)	Deviation of W_{ni} from 1
1	25.50	26.93	1.06	***1.00 ±0.06***	25.8	1.01	***1.00 ±0.07***
2	40.92	41.36	1.01		38.3	0.94	
3	25.85	24.95	0.97		24.5	0.95	
4	32.14	32.14	1.00		30.0	0.93	
5	34.34	34.20	1.00		33.4	0.97	
6	79.56	80.20	1.01		81.4	1.02	
7	71.47	70.56	0.99		73.9	1.03	
8	60.88	60.67	1.00		65.0	1.07	
9	52.74	53.29	1.01		55.6	1.05	

The precision in the estimation of U metal by MEHS is comparable to that for the estimation by ICPOES. MEHS is based on the estimation of H_2 released during the reaction of metal with acid and hence any oxide dissolution will not interfere with the estimation. Hence the method can be comfortably used for metal estimation in a mixture of metal-metal oxide, if the oxide dissolution is not accompanied with hydrogen release. Thus the present method is well suited for estimation of uranium metal in incompletely reduced uranium oxides obtained from direct electrochemical reduction studies.

6.3.4. Standardisation of uranium estimation in a mixture of U-UO_2 by MEHS

The hydrogen response of the sensor for reaction of UO_2 powder in HBr is given by curve (1) in Fig. 6.7a.

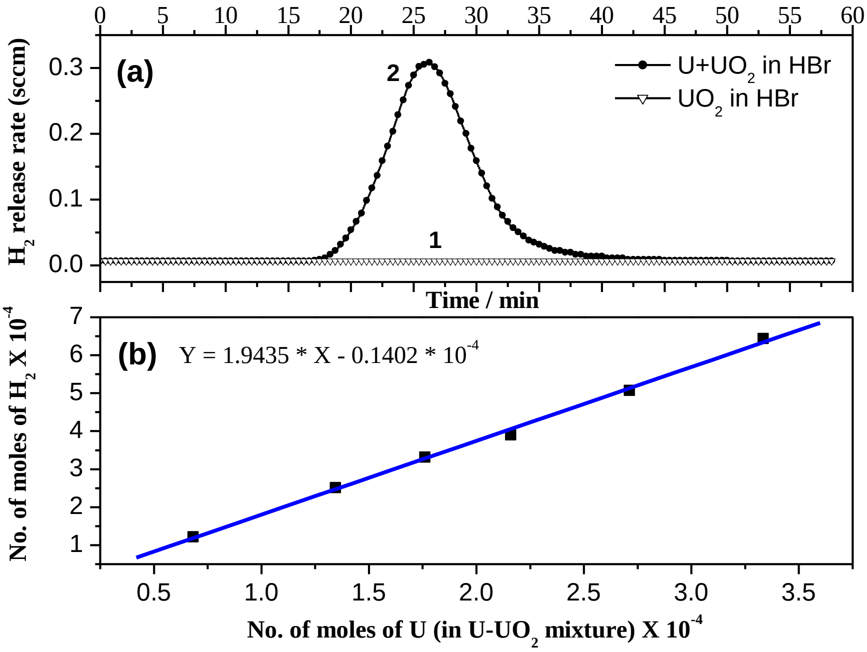

Fig. 6.7. (a) H_2 response curves for the interaction of (1) UO_2 with HBr and (2) U+UO_2 mixture with HBr. (b) Plot of number of moles of H_2 liberated vs. number of moles of uranium metal present in a mixture of U-UO_2 dissolved in HBr.

The signal indicates that there is no reaction between UO_2 and HBr, which produces H_2. Curve (2) in Fig. 6.7a shows the evolution of H_2 liberated as per the reaction, $U_{(s)} + 4HBr_{(aq)} \rightarrow UBr_{4(aq)} + 2H_2\uparrow_{(g)}$, when a mixture of U-$UO_2$ was introduced into the reaction chamber. Although both U and UO_2 are present in the mixture, U metal only liberates H_2 as per the above reaction and hence the amount of H_2 released can be directly related to the amount of U metal present in the sample. However, UO_2 can also undergo slow dissolution in HBr without evolution of hydrogen [189] as per the following equation:

$$UO_{2(s)} + 4HBr_{(aq)} \rightarrow UBr_{4(aq)} + 2H_2O_{(aq)} \qquad (6.7)$$

But, ICPOES analysis of the resulting HBr solution (Table 6.3) for the sample containing UO_2 alone showed that the uranium concentration was below the detection limit of the instrument which strongly suggested that UO_2 dissolution in HBr was negligible in the time frame of the experiment. The quantities of metallic U estimated in the mixture by both MEHS and ICPOES methods are compared in Table 6.3 and the two sets of values are in agreement.

Table 6.3. Results of U metal estimation in U-UO_2 mixture by MEHS method and ICPOES.

S. No.	Wt. of U-UO_2 mixture (mg)	Wt. of U metal taken (mg)	Wt. of U estimated by MEHS method (mg)	% error with MEHS method	Wt. of U estimated by ICPOES (mg)	% error with ICPOES
1	0.00	0.0	0.0	0.0	<DL	-
2*	100.1	0.0	0.0	0.0	<DL	-
3	100.2	16.3	16.6	+2.2	16.4	+0.9
4	100.0	32.0	32.5	+1.7	33.4	+4.3
5	100.5	41.9	42.3	+1.0	43.6	+4.1
6	100.2	51.4	49.5	-3.6	49.9	-2.9
7	100.1	64.6	63.9	-1.1	61.3	-5.0
8	100.4	79.4	80.6	+1.6	81.6	+2.8

DL=Detection Limit; * blank

The plot of number of moles of H_2 liberated against the amount of U in the standard mixtures of U-UO_2 is linear with slope 1.9435, as shown in Fig. 6.7b. This slope is close to the value 1.9357 (Fig. 6.6), observed for the dissolution of uranium metal in HBr, confirming absence of interference of UO_2 in the estimation. Hence, it is inferred that the dissolution behaviour of pure U and U in UO_2 are similar. The calibration plot can be used to calculate the weight of U in samples by using the following equations:

$$N_U = [N_{H2} + 0.1402 \text{ X } 10^{-4}] / 1.9435 \qquad (6.8)$$

$$W_U = N_U \; X \; 238 \; g \; mol^{-1} \tag{6.9}$$

Where, N_U is the number of moles of U metal and N_{H2} the number of moles of liberated H_2.

6.3.5. Standardisation of uranium estimation in a mixture of U-U_3O_8 by MEHS

During the electrochemical reduction of U_3O_8, it gets converted to UO_2 first and then to uranium metal [128,132]. Electrolysed samples of U_3O_8 could result in a mixture of U metal and uranium oxides (U+UO_2 or U+U_3O_8 or U+UO_2+U_3O_8), if reduction is incomplete. As UO_2 could not liberate H_2 as discussed, its presence need not be considered in the estimation of the U metal in the mixture by dissolution in HBr. The H_2 responses for U_3O_8 and U-U_3O_8 mixtures in HBr are given in Fig. 6.8a, which are similar to that of UO_2 and U-UO_2 mixtures in HBr discussed above. No H_2 is liberated from the interaction of U_3O_8 with HBr. Fig. 6.8b shows the plot of number of moles of H_2 liberated against the amount of U in standard mixtures of U-U_3O_8.

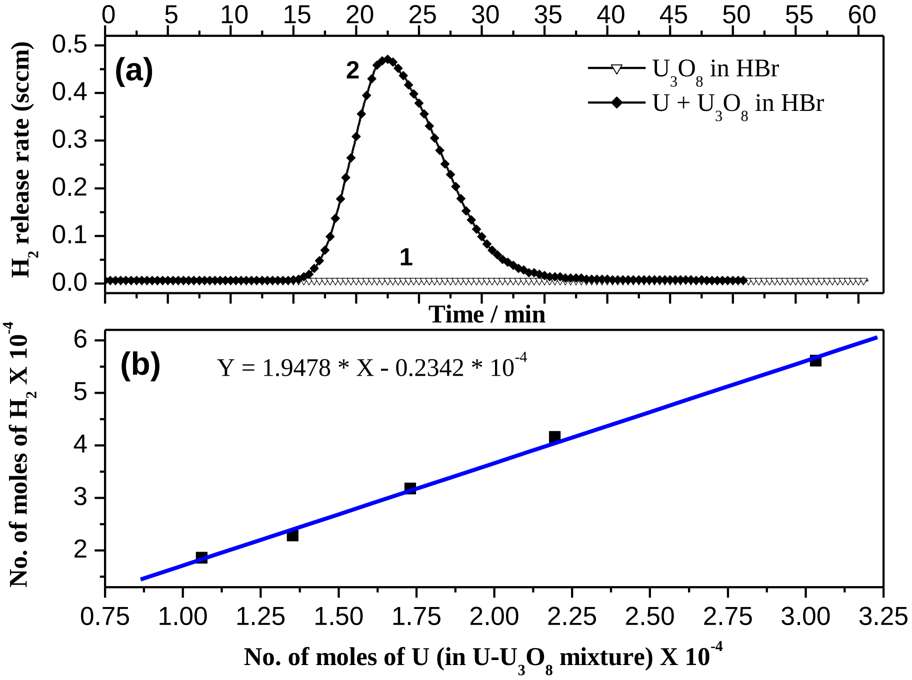

Fig. 6.8. (a) H_2 response curves for the interaction of (1) U_3O_8 with HBr and (2) U+U_3O_8 mixture with HBr. (b) Plot of number of moles of H_2 liberated vs. number of moles of uranium metal present in a mixture of U-U_3O_8 dissolved in HBr.

The slope of the plot in this case too indicates the insignificant effect of U_3O_8 matrix on the dissolution of U in HBr. The equation, as given below, has been derived from the plot for the estimation of uranium:

$$N_U = [N_{H2} + 0.2342 X 10^{-4}] / 1.9478 \tag{6.10}$$

$$W_U = N_U X 238 g mol^{-1} \tag{6.11}$$

where, N_U is the number of moles of U metal and N_{H2} the number of moles of liberated H_2.

The results of the estimation of U in U-U_3O_8 mixture after dissolution of the samples in HBr by MEHS and ICPOES are given in Table 6.4. To the best of the author's knowledge, the data on the dissolution behavior of U_3O_8 in HBr is not available in the open literature. ICPOES results showed that the dissolution of U_3O_8 in HBr is relatively more than that of UO_2 under identical conditions, the reasons for which are not clearly understood. However, it was observed that the error in the estimation of U by MEHS is relatively less compared to that from the ICPOES analysis. The error in the latter technique gradually increased with the increase in weight of U_3O_8 in U-U_3O_8 mixture and this may be attributed to the inherent dissolution behaviour of U_3O_8 in con. HBr. Though U_3O_8 dissolves in HBr, it does not contribute to the H_2 liberated as noticed with the UO_2 dissolution in HBr, discussed in the previous section. So, estimation of U in both UO_2 and U_3O_8 matrices by MEHS method can be expected to be similar.

Table 6.4. Results of U metal estimation in U-U_3O_8 mixture by MEHS method and ICPOES.

S. No.	Wt. of U-U_3O_8 mixture (mg)	Wt. of U metal taken (mg)	Wt. of U estimated by MEHS method (mg)	% error with MEHS method	Wt. of U estimated by ICPOES (mg)	% error with ICPOES
1*	100.7	0.0	0.0	0.0	17.9	-
2	100.3	25.2	25.6	+1.2	33.3	+31.9
3	100.1	32.2	30.8	-4.5	34.8	+8.1
4	100.7	41.2	41.7	+1.2	45.0	+9.2
5	100.5	52.2	53.6	+2.7	52.8	+1.1
6	100.8	64.4	60.2	-6.5	62.8	-2.4
7	100.7	72.2	71.4	-1.0	72.2	0.0

* blank

6.3.6. Studies on the extent of reduction of electro-reduced samples

Samples of electrolysed products from five UO_2 electro-reduction experiments, whose details are given in Table 6.5, were used in the determination of the extent of reduction by MEHS method. The experiments have been carried out with UO_2 pellets (OP, ~5% and ~13% and chunks (OP, ~5%) in $CaCl_2$ melt at 1173 K or LiCl melt at 923 K, as discussed previously in section 2.3.12 of chapter 2.

Table 6.5. Particulars of the electro-reduction experiments.

DOER Expt. ID	Details of cathode	Details of anode, electrolyte and mode of electrolysis
U-1 (P-1)	Two UO_2 pellets (each ~3.3 g, ~4 mm thick & 10 mm dia., OP 13%) taken in a Ta cup	Pt coil, $CaCl_2$- 2wt.% CaO at 1173 K. Current in steps from 0.5 to 1.0 A for 9 h.
U-2 (P-2)	UO_2 annular pellet (12.3651 g, 7.56 mm thick, 14.28 mm dia., OP 5%) hung by a SS wire through the central hole	Graphite, LiCl at 923 K. Voltage in steps from 4.0 V to 3.5 V for 24 h.
U-3 (P-3)	UO_2 annular pellet (12.3439 g, 8.70 mm thick, 14.30 mm dia., OP 5%)	Graphite, $CaCl_2$ at 1173 K. 3.0 V for 16 h.
U-4 (P_C-4)	SS mesh containing UO_2 chunks (~10 g, OP 5%) made from a pellet	Graphite, $CaCl_2$ at 1173 K. 3.0 V for 25 h.
U-5 (P_C-5 & P_C-6)	SS cup containing SS mesh having 5 chunks of UO_2 (~11 g, OP 5%)	Graphite, $CaCl_2$ at 1173 K. Voltage in steps from 3.0 to 3.5 V for 42 h.

OP – Open Porosity

As mentioned previously, incompletely reduced samples were obtained from electro-reduction experiments carried out in $CaCl_2$-CaO and LiCl-Li_2O melts with the anode being platinum or graphite. The use of graphite or platinum anode does not make any difference in the analysis of electro-reduced samples by MEHS method.

6.3.6.1. UO_2 pellet reduced in $CaCl_2$ -2 wt.% CaO using Pt anode

The photograph of the pellet designated as P-1 used in the present study before DOER experiment and the model of the same pellet after electrolysis are shown in Fig. 6.9(a) and (b), respectively. After electrolysis, the washed pellet was found to have a sheet like surface, which when polished, became shiny and lustrous. However, the bulk portion was found to contain a brownish mass, which was loosely bound and could be easily separated. Samples were collected from the outer surface ‘A’ and inner bulk ‘B’ as shown in Fig. 6.9(b).

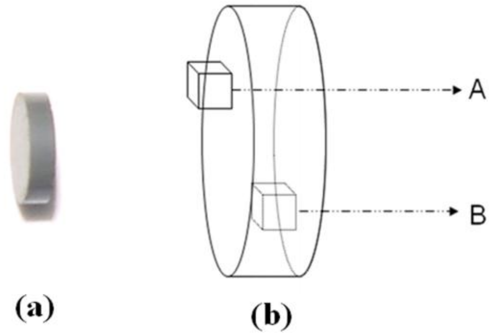

Fig. 6.9. UO_2 pellet P-1 (a) Photograph before DOER experiment (b) A model showing the different regions of the pellet after subjecting it to electro-reduction in $CaCl_2$-2wt.% CaO. Samples were collected from the regions A and B.

Analysis of samples from regions ‘A’ and ‘B’

Summary of weights of samples taken along with their details and the extent of reduction determined are given in Table 6.6.

Table 6.6. Results of the U metal estimation (by MEHS and ICPOES methods) and the extent of reduction of the electrochemically reduced samples (by MEHS method).

DOER Expt. ID	Sample ID	Region	Wt. of sample (mg)	Wt. of U estimated by ICPOES (mg)	Wt. of U estimated by MEHS (mg)	Extent of reduction (E_R) from MEHS (%)	Region from which sample is taken
U-1	P-1	A	12.6	13.8	10.9	88.3	Surface, thin sheet like
		B	300.8	19.9	9.9	3.7	Bulk, powder + fine lumps
U-2	P-2	C	11.8	13.8	12.6	100	Surface, single lump
		D	14.3	12.2	10.8	77.7	At current collector, lump
		E	271.5	<DL	0.0	0.0	Bulk, powder
		F	30.7	27.7	31.7	100	Surface away from current collector, single lump
U-3	P-3	-	100.9	<DL	0.0	0.0	Powdered sample
U-4	P_C-4	-	100.6	<DL	0.0	0.0	Powdered sample
U-5	P_C-5	-	127.5	97.7	73.5	60.7	Small lump
	P_C-6	-	100.1	73.1	37.8	40.8	Small lump

The H_2 release rate was converted to U dissolution rate by eq. (6.8) and (6.9). From the area under the curve of the dissolution rate as a function of time, the total quantity of metallic U in the unknown sample was estimated. The extent of reduction of the sheet like surface from region 'A' and the brownish powdery mass (having discrete fine lumps) from the region B were found to be 88.3% and 3.7%, respectively (Table 6.6). While the sample from region 'B' was in contact with the HBr, H_2 bubble formation was observed from small discrete lumps only. It appeared that the powdery mass did not react with HBr and hence liberate H_2 gas.

Fig. 6.10(a) shows the comparison of dissolution behaviour of samples collected from region A and B. A comparison of the extent of dissolution of these two samples with time is depicted in Fig. 6.10(b).

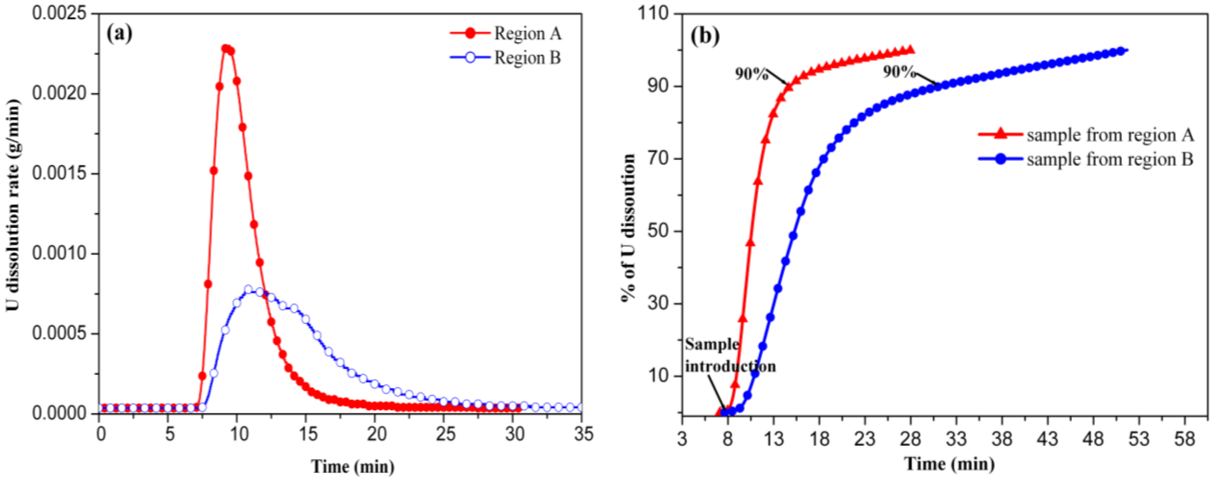

Fig. 6.10. (a) Uranium dissolution patterns in HBr and (b) the percentage of dissolution of samples collected from regions A and B of the electro-reduced pellet P-1 (Fig. 6.9b).

The time taken for 90% of U dissolution of the total U content for the sample from region 'A' is 7 minutes, where as it is 23.2 minutes for the sample taken from region 'B'. The U content of both the samples measured by MEHS method is comparable (Table 6.6) and hence it was logical to expect a complete reaction of U in both the samples in comparable duration. The longer duration of dissolution of U in the sample from region 'B' may be attributed to the physical hindrance by the solid UO_2 matrix, in which the U metal is dispersed, to reaction with HBr. Unlike the present method, the existing methods discussed in section 6.1.1 cannot be used as online monitors for assessment of the progress of the dissolution reaction. The XRD patterns of the sheet like surface from region A and sample from region B are given in Fig. 6.11(a) and 6.11(b), respectively. The patterns indicate the presence of metallic U as the major phase along with UO_2 (minor phase) in the sample from region A and only UO_2 phase in the sample from region B. The extent of reduction determined by MEHS for the sample from region 'A' shows that only 88.3% of the initial UO_2 got converted to U metal and the remaining UO_2 is present as such in the sample, which is in general agreement with the phases identified from the XRD pattern. However, MEHS method has indicated that only 3.7% UO_2 of the sample taken from region B got converted to U metal, which shows the ability of the method for determining the presence of even such lower quantities of U metal in incompletely reduced DOER samples.

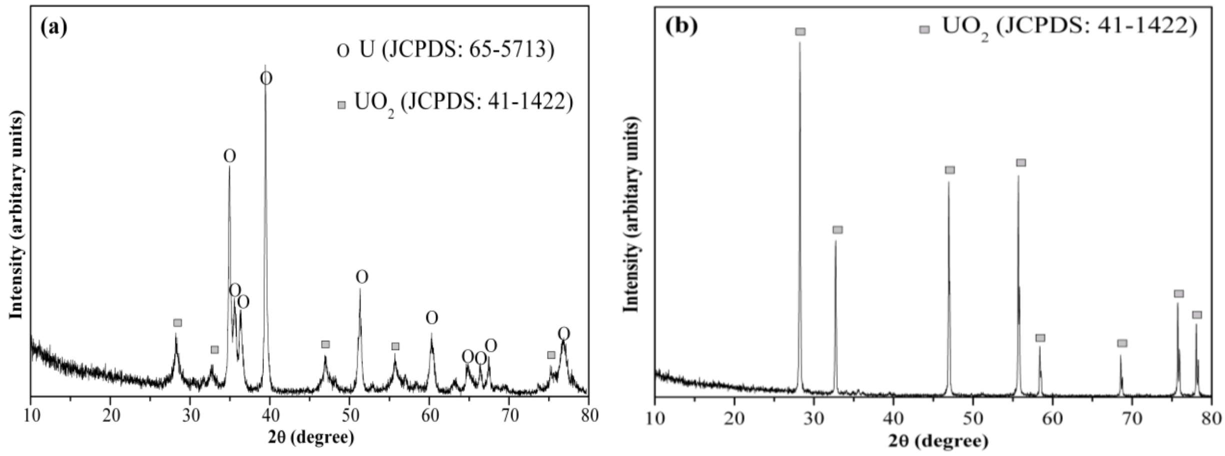

Fig. 6.11. XRD patterns of (a) the sheet like surface region A and (b) the brownish bulk region B of the electro-reduced pellet P-1 (Fig. 6.9b). The XRD patterns show the presence of both U (major) and UO_2 (minor) phases in region A and only UO_2 phase in region B.

The extent of reduction obtained in the above two regions clearly indicates that the reduction of the solid UO_2 cathode during electro-deoxidation is non-uniform across its thickness. It is known that, in addition to the other parameters like applied potential, nature of the electrolyte, cathode configuration, open porosity of the solid cathode, time of electrolysis etc., the thickness of the pellet and temperature of electrolysis has significant influence on the electro-reduction of solid oxide preforms. In the case of a thin pellet, oxide ions from the bulk of the pellet are expected to easily diffuse out to the electrolyte. Hence the extent of reduction in such pellets in $CaCl_2$-2wt.% CaO is expected to be more uniform and complete. The experience gained from electro-reduction of very thin (1 mm) pellets support this hypothesis. However, in a relatively thick pellet like that used in the present case (~4 mm), maximum reduction (~90%) was limited only to the surface and did not extend to the bulk. As reduction in $CaCl_2$ was carried out at 1173 K, the U metal particles formed on the surface of the pellet could have got sintered together and the impermeable metal layer thus formed would have prevented further entry of the electrolyte into the bulk of the pellet and hence the bulk reduction. The scanning electron micrograph of the flat surface of the sample from region A of pellet P-1 is given in Fig. 6.12 and it clearly shows that the surface metal layer is non-porous.

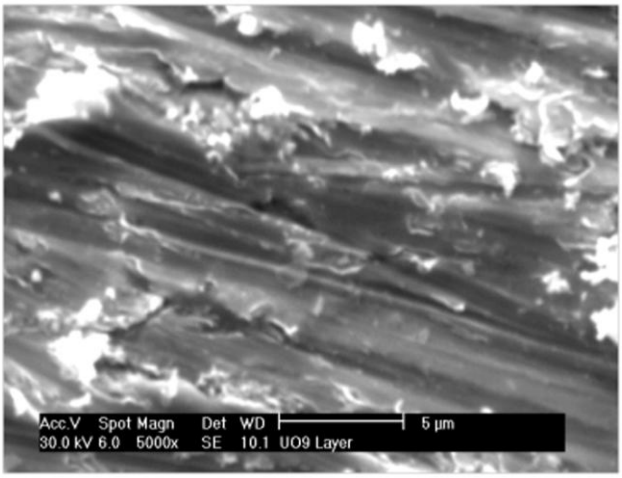

Fig. 6.12. SEM image of the flat surface of region A (Fig. 6.9b). The image shows that the reduced uranium metal layer is non-porous.

A similar observation was also reported by Sakamura et al. [79] during electro-deoxidation of a thin UO_2 disc in $CaCl_2$ melt at 1093 K. Generally sintering takes place significantly when the process temperature is higher than 2/3 rd of the m.p. of the metal. Solid metal oxides whose metals are high-melting (Ti, Zr, Nb, Ta, Cr, melting point ~ 2700 K) are generally electro-reduced at or below 1173 K in the DOER method and hence the electro-reduced metal layer is not sintered and remains as very porous. However, reduction of UO_2 in $CaCl_2$ melt at 1173 K produces U metal whose melting point is 1407 K. The proximity of the melting temperature of U metal to the process temperature makes the sintering of the metal particles possible and hence the formation of the impermeable surface metal layer [79]. The reduction experiments presented in this study often lasted 9-42 h and the long duration of the experiment enhanced the chances of higher levels of sintering, so that the layer became more and more non-porous. The sintered layer, it appears, had trapped in it the unreduced mass of UO_2 thus limiting the extent of reduction to 88.3%. The 3.7% reduction observed in the bulk could be due to the reduction that would have occurred in the bulk prior to the formation of the sintered surface metal layer.

6.3.6.2. UO_2 pellet reduced in LiCl using graphite anode

The samples were obtained from a DOER experiment (U-2 in Table 6.5), carried out at potentials above LiCl decomposition potential. In this case, the reduction was achieved by direct chemical reaction between the UO_2 and the lithium metal deposited on it.

The photograph of the annular UO_2 pellet (P-2, 95% TD) used in the study before electrochemical reduction is given in Fig. 6.13(a). The pellet was electrolysed for 24 h at 923 K and the electrolysed pellet was subjected to visual observation to check for any morphological change along its cross section. A surface layer having thickness of ~1 mm showed a morphology which is different from that of the bulk. The electrolysed pellet was modelled as shown in Fig. 6.13(b), with various regions from C to F. The regions were marked considering the morphology, which may be linked to the different degrees of reduction of the pellet. Totally four samples were collected from the pellet P-2, one each from regions C, D, E and F for the study by MEHS method.

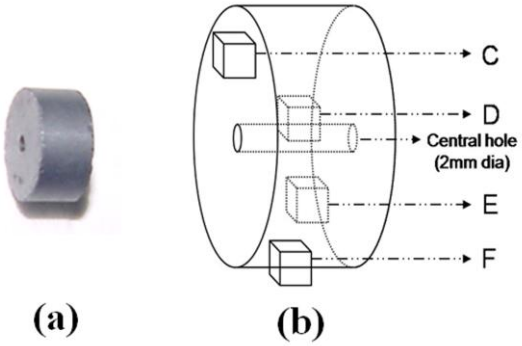

Fig. 6.13. Annular UO_2 pellet P-2. (a) Photograph before electro-reduction and (b) a model of the pellet after subjecting it to electrochemical reduction in LiCl medium. C, D, E and F represents the regions from which samples were collected.

Dissolution behavior of samples from regions 'C, D, E and F' of pellet P-2

The dissolution behavior of samples from regions C, D, E and F is given in Fig. 6.14(a) and their estimated extents of reduction are given in Table 6.6.

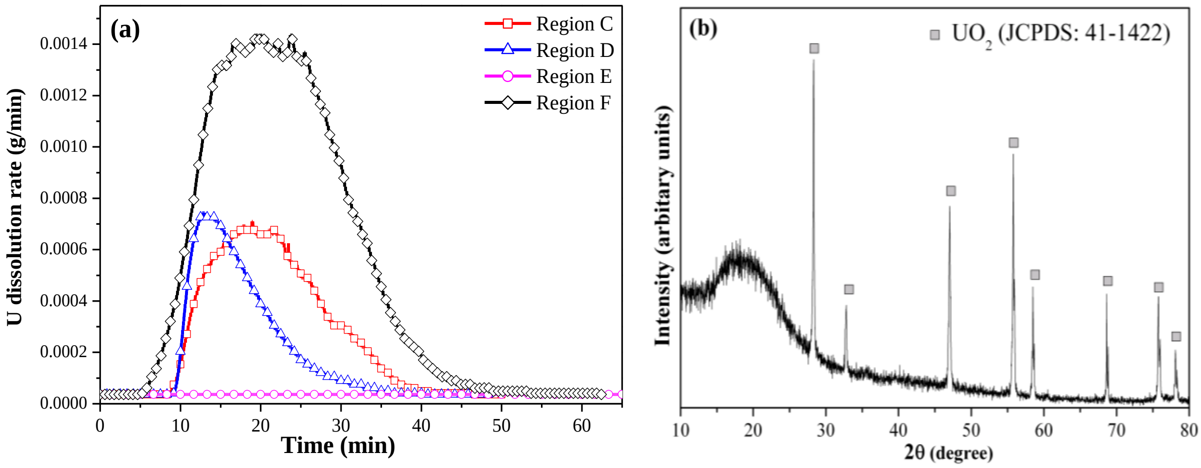

Fig. 6.14. (a) Uranium dissolution patterns of samples taken from regions C, D, E and F of pellet P-2 (Fig. 6.13b) and (b) XRD pattern of a sample from the bulk (at region 'E') shows that the phase present is UO_2.

The metallic U content estimated from a sample in the form of a small piece from the flat surface, collected from region 'C', indicated 100% reduction. The sample completely dissolved in the acid and the reaction was found to be vigorous. This indicated that the surface was completely reduced to U metal. Sample from region 'F', which is slightly away from the SS current collector wire (attached at the central hole) and the curved surface along the thickness of the pellet, also showed complete metallisation. As the pellet was electrolysed at a potential above LiCl decomposition, it is possible that the Li metal produced reacted at the surface and resulted in the surface reduction of the pellet to U metal.

For the electro-reduction to occur, three phases, viz. the current collector, the metal oxide and the molten salt need to coexist [151]. In the case of oxide electrodes with poor electrical conduction, the electro-deoxidation starts at the point of contact of the current collector with the oxide pellet. The specs of metal produced at the interface act as the conducting bridges to the adjacent oxide particles so that the reduction becomes possible on the adjacent sites. This process continues along the surface of the pellet exposed to the melt and eventually a metallic surface layer forms on the pellet. The surface metal conducts electrons to metal particles beneath it so that the reduction extends to the interior regions. Regions ‘C’ and ‘F’ are at the surface of the pellet and are preferentially reduced to U as could be seen from the estimated extents of reduction in these regions. The reduction in these regions could be due to the electro-generated Li metal which might have chemically reduced the oxide at the surface. A sample (having brownish colour) from region ‘E’, which is at the middle portion of the pellet (deep inside from all surfaces), on dissolution did not liberate any hydrogen, which indicated that this portion is not at all reduced. Further, samples from this region could easily be ground to a fine powder and its XRD pattern (Fig. 6.14b) confirmed the presence of only UO_2 phase. A sample collected from the current collector region ‘D’, showed the extent of reduction as 77.7%. This region, during the electro-reduction, must have got fully reduced, however, since it is very close to the unreduced bulk (region ‘E’), the sample might have contained some entrapped UO_2 which probably made the extent of reduction appear low. The probable causes for the variation in the extent of reduction in different regions of the electrolysed pellet may be explained as follows. The density of the UO_2 pellet in the present experiment is about 95% of its theoretical density (TD) and its thickness is 7.56 mm. Due to the high density and thickness, the contact of the electrolyte with bulk must have been rendered difficult so that the reduction of interior areas of the pellet became difficult. Also, the lower limit of solubility of the by-product, O^{2-}, in LiCl [151] might have led to the precipitation of Li_2O in the pores of the pellet's bulk and this could have adversely affected the bulk reduction. The combined effect of these factors might have hindered the reduction process at the bulk.

Microstructures of the four regions (given in Fig. 6.15) showed significant variation in the morphology across the UO_2 pellet. As shown in Fig. 6.15 (c), the region at 'E' has morphology with large sintered grains, typical of unreduced UO_2. The results of hydrogen measurement of this region too support the lack of reduction of this area. The microstructures of regions 'C' and 'F' are almost alike and resembled that of the typical morphology of metals produced by electro-deoxidation. The samples tested were found to be completely reduced too. The microstructure at the current collector region 'D' shows morphology which is different from that of other two regions and showed lower extent of reduction as shown by hydrogen estimation. The observations confirm that the electro-reduction of different parts of the pellet across the thickness was proceeding differently.

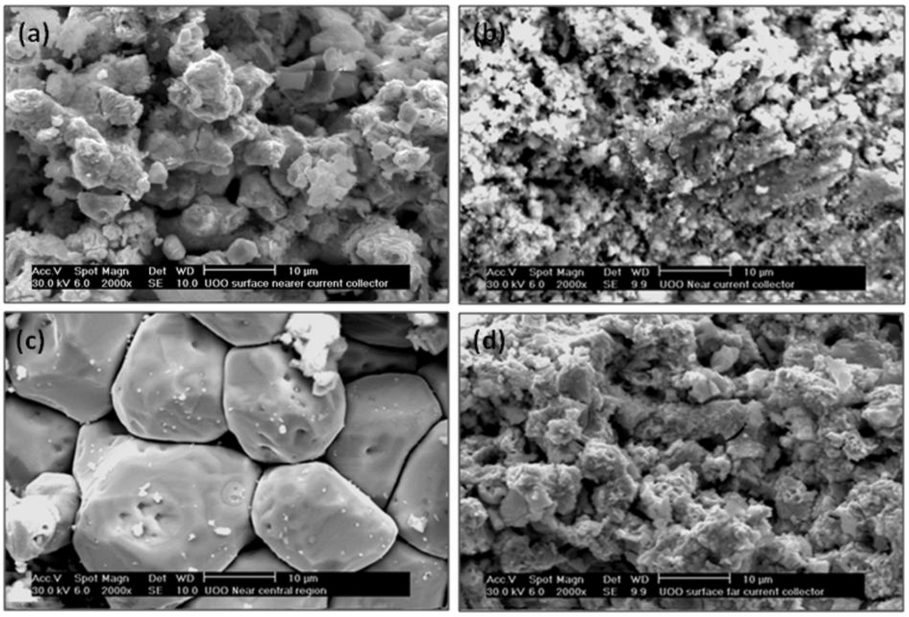

Fig. 6.15. SEM images of the different marked regions of pellet P-2 shown in Fig. 6.13 (a) region-C, (b) region-D, (c) region-E and (d) region-F.

It is interesting to compare the SEM images of the U metal formed in LiCl at 923 K (Figs. 6.15a and 6.15d) with that formed in $CaCl_2$ melt at 1173 K (Fig. 6.12). The microstructure of the former shows significant porosity as against the mostly non-porous nature of the latter. Similar observations have been reported previously also [79]. It is explained that the wider gap between the process temperature in LiCl melt (923 K) and the melting point of U (1405 K) did not allow sintering of U to take place, and therefore a relatively porous metal layer became possible in the LiCl melt [79].

6.3.6.3. UO_2 pellet and its chunks (irregular) reduced in $CaCl_2$ using graphite anode

Samples collected from P-3 and P_C-4 were powdered and analysed by XRD and MEHS. These samples showed no hydrogen evolution (Fig. 6.16a and 6.16b, respectively) and their corresponding XRD patterns (Fig. 6.16d and 6.16e, respectively) showed UO_2 as the only phase present. In both the cases, due to the high surface area of the sample (as it was powdered), the reduced metal would have got re-oxidized to uranium oxide and hence no hydrogen evolution was observed. The uranium dissolution patterns of samples collected from two different electrochemically reduced chunks P_C-5 and P_C-6 from U-5 experiment are shown in Fig. 6.16c and their extents of reduction are found to be 60.7% and 40.8%, respectively. This revealed that although these lumps were electro-reduced in the same experiment, their extents of reduction are different and also the reduction is incomplete. This is similar to the case explained in section 6.3.6.1 in which the impermeable layer in the sintered metal surface restricted the reduction of the bulk. The difficulty experienced in powdering the irregularly shaped electro-reduced sample for XRD analysis and the good electrical conductivity of its surface, as measured by using a multimeter, indicated the presence of a sintered metallic skin. The powder sample from its bulk was confirmed as UO_2 by XRD analysis (Fig. 6.16f). Also, the presence of undissolved mass of the electrolysis product left after the completion of hydrogen evolution reaction in HBr was attributed to the presence of unreduced UO_2. Therefore, even with the chunks of UO_2, only partial reduction was observed and the reduction is restricted to the surface of the chunks only. The results indicate that out of thickness, density and temperature, the effect of temperature is more significant in restricting the reduction to the surface of the UO_2 preform.

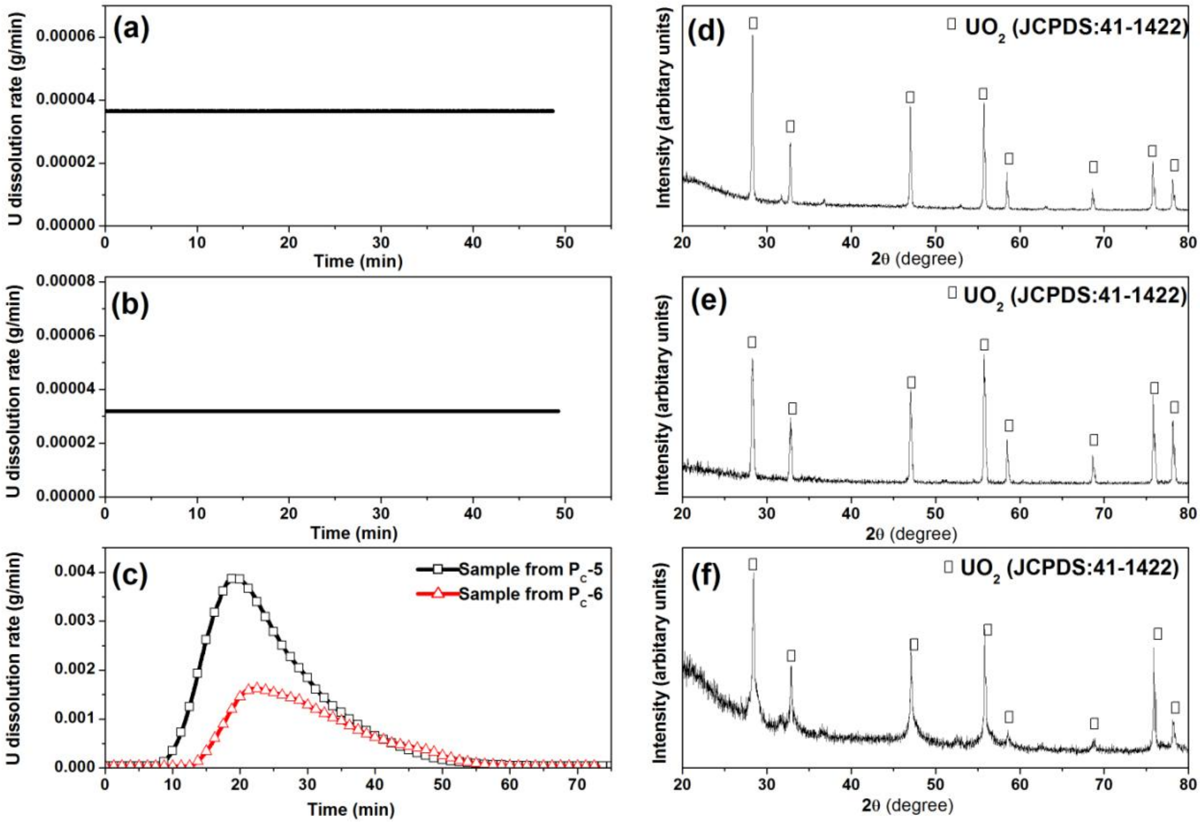

Fig. 6.16. Uranium dissolution behaviour of different electro-reduced uranium oxide samples referred to in Table 1. (a) P-3 of U-3 (b) P_C-4 of U-4 (c) P_C-5 and P_C-6 of U-5. The respective XRD patterns of the samples are shown in (d), (e) and (f).

Most often, it was difficult to completely powder this kind of samples (which are in the form of irregular lumps) as it contained both the metal oxide as well as highly dense metallic portions. Hence the XRD analysis of such samples is difficult. It has been observed that the effect of cohesive contraction and densification in the case of electrochemically obtained uranium (m.p., 1405 K) is very high compared to that of other metals like chromium (m.p., 2130 K) obtained under similar conditions [57], in which case it was reported that the fully reduced pellet could be easily crushed to powder manually. In the present case, since the temperature of the experiment (1173 K) is close to the melting point of uranium, it is highly likely that metallic particles might have coalesced to form dense lumps entrapping unreduced UO_2 in it so that the hard mass could not be powdered. In such cases the metallic portion can be analysed using the MEHS method. The coalescence of metal particles of the pellet chunks in the U-5 experiment also supported the theory of cohesion of the U metal particles in the DOER of UO_2 in $CaCl_2$ medium.

6.3.7. Comparison of results of MEHS and ICPOES for samples after incomplete electro-reduction

The results of U estimation of the electrochemically reduced samples by MEHS and ICPOES methods are shown in Table 6.6. The good agreement between the results of the controlled study with U-UO_2 standard mixtures (from Table 6.3) made it clear that the low-cost and simple MEHS method can be used as an alternative to ICPOES technique for analyzing the reduced samples. The results given by MEHS method are more reliable for the electro-reduced samples, as they depend only on the measurement of stoichiometric amount of H_2 equivalent to the U metal present in the mixture and is unaffected by the dissolution behavior of the oxide. However, the results obtained from the ICPOES often deviated from that of the results obtained with MEHS. This indicated that the dissolution behaviour of incompletely electro-reduced UO_2 (which may contain UO_2 alone or U+UO_2) in con. HBr is different from that of standard U-UO_2 mixture. This behaviour probably affects the reliability of the results of uranium estimated by ICPOES analysis of the incompletely electro-reduced UO_2.

6.4. Conclusion

A novel method called ‘metal estimation by hydrogen sensor (MEHS)’, for estimating the hydrogen released by the reaction of a metal with HBr, which in turn could help in the determination of the amount of the metal was developed in-house and the method was used in the estimation of Zn and U metals. The stoichiometry of the reaction of Zn-HBr and U-HBr could be accurately determined and the dissolution kinetics of Zn and U in HBr was studied by this method. The weights of the metals estimated using this method were compared with those from conventional analytical method, ICPOES and the results obtained are in very good agreement.

Application of the hydrogen sensor for measuring the liberated H_2 during the dissolution of U metal from an electro-reduced sample in HBr has been proved to be a relatively easier, simple and accurate method for the estimation of metallic U in a mixture of U and its oxides. The method is capable of estimating low quantities of U metal quantitatively, in samples of relatively smaller masses. It is also helpful in the analysis of uranium in irregularly shaped, incompletely reduced dense uranium lumps which are difficult either to powder or flatten for XRD analysis. The results indicated that the method is more reliable in analysing the extent of reduction in comparison to that of the ICPOES method, which is affected by the anomalous dissolution behavior of electro-reduced oxide. The rate of dissolution of uranium combined with the extent of reduction of the UO_2 pellet may give good insight to the nature of the metal layer formed and its propagation during DOER. Analysis of the samples collected from different regions of electro-reduced pellets by MEHS method proved that the surface of the pellet was metallised preferentially. MEHS method, with some modifications can be employed for the determination of the extent of reduction in other metal oxides like ZrO_2, NiO etc. after subjecting them to DOER. The technique can also be used in the estimation of low as well as high concentrations of metal present in a solid matrix, unreactive to HBr. MEHS method gave good results with a single metal, like uranium, in the reduced product. However, the method can’t be employed to determine the extent of reduction when a mixture of metals is present in the sample.

Chapter 7

Summary, conclusions and scope of future work

Production of metals is an important activity from time immemorial as metals play a significant role in the development of mankind. Barring silver, gold and platinum, all metals exist in nature as metal compounds. Several metals were produced by chemical reduction methods in which the metal compound was reduced to metal by reaction with electropositive metals like Na, Mg or Li (metallothermic reduction) or by reaction with carbon (carbothermic reduction). With the discovery of electricity in the nineteenth century, electrochemical methods of metal production became possible and a host of metals like Al, Mg, Na, K, Li etc. were produced on large scale by molten salt electrolysis. Metal production from their oxides was generally difficult due to contamination of the metal with oxygen and hence needed an intermediate step of conversion of the oxide to halide and its subsequent chemical reduction to metal. A metallurgical process for production of metals directly from their oxides was of great interest and the FFC Cambridge process, discovered at the University of Cambridge in 1997, was a breakthrough in this context. Needless to say, the process was investigated in different laboratories across the world for production of a host of metals from oxides. A large number of publications on various aspects of the process with different metal oxides are now available in the open literature.

Nb, Ti and U are strategically and technologically important metals and many studies have been reported on the direct oxide electrochemical reduction (DOER) of their oxides too. However, a critical assessment of the information available on the DOER of these oxides showed that the available data can be augmented by further research, so as to develop a more comprehensive understanding of the reduction process of these oxides. Hence these three metal oxides have been selected for study as part of the thesis work. The electrical characteristics of the metal oxides have a strong influence on their electro-reduction properties and to demonstrate this important aspect, SiO_2 which possesses very different electrical properties compared to the other three oxides, was also selected for study. The major findings of the research work carried out on the four oxides and some novel methods developed and employed in these studies, which are described in detail in chapters 3-6 of the thesis, are summarised below.

7.1. Electrochemical reactivity of the oxide materials

Cyclic voltammetry of the oxide electrodes (Nb_2O_5, TiO_2, SiO_2 and UO_2) showed that Nb_2O_5 and TiO_2 behave as good electrical conductors at the FFC cell conditions and both the oxides were electrochemically active in the electrolyte melts used in the study. Ternary intermediate compounds of the kind $A_xM_yO_z$ were formed by electrochemical insertion of the cation 'A' of the melt into the cathodically polarised Nb_2O_5 and TiO_2 electrodes. Though UO_2 also acted as an electrical conductor at the FFC cell conditions, no electrochemical insertion reactions were observed in the melt. Unlike the above three oxide electrodes, SiO_2 pellet electrode remained as an insulator in the cell and it required an electron-conducting metal (cathode current collector) to be in physical contact with it so that the reduction could commence at the oxide-conductor-melt three phase interlines. Being good electrical conductors, Nb_2O_5 and TiO_2 could be reduced without the cathode current collector in direct contact with the melt soaked areas of the pellet. This essentially meant that for electro-reduction of good conducting oxide electrodes, two physically distinct phases, i.e., the oxide and melt need only be coexisting. This further suggested the possibility that the whole area of such electrodes, which is in contact with the melt, can be electrochemically active and hence the possibility of a faster and efficient reduction of such oxide electrodes.

7.2. Application of the novel methods to the study of DOER

Novel methods such as indicator pellet technique (IPT) and counter electrode potential monitoring (CEPM) methods were conceived and employed in the present study for understanding the fundamental issues of electrochemical reduction and the reactions occurring at the cathode, anode and in the melt.

In IPT, a pellet (indicator pellet) was kept immersed in the melt, in which the electro-deoxidation of another pellet of the same oxide was simultaneously taking place. The potential of the indicator pellet, which was not connected to current circuit, is monitored using a reference electrode. The chemical changes taking place on the indicator pellet will be manifested in the emf of the pellet-reference cell, which in turn can be correlated to the change in the melt chemistry on account of electrolysis. If the indicator pellet gets reduced to the respective metal, without it being electrolysed, it would mean that a reductant metal was generated in the melt and it reacted with the pellet. During the electrolysis of Nb_2O_5 pellet, an indicator pellet placed in the melt was converted to Nb metal and this showed that calcium metal was generated in the melt. This experiment shows that the calcium metal could be generated in an electro-reduction cell, even when the applied potential is below than that necessary for the decomposition of the calcium chloride electrolyte, and the electro-generated metal could react chemically with the oxide pellet and thus aid in the reduction process.

In the CEPM technique, the counter electrode potential of a cyclic voltammetry cell is monitored against a reference electrode. The measured potential of the counter electrode for a corresponding electrochemical reaction at the working electrode gives a comprehensive knowledge of the electrode reactions taking place in the cell. This kind of measurement is very useful when there are more than one kind of anions and cations present in the molten electrolyte. This technique was effectively employed to gain information on the reactions taking place on a graphite counter electrode of a cell with Nb_2O_5 as the working electrode (chapter 3). It was confirmed through CEPM measurements that Nb_2O_5 is cathodically reactive to Ca^{2+} ions of the melt and the Cl^- ions thus released to the melt are discharged at the graphite anode as Cl_2 gas. The results confirmed that the decomposition of calcium chloride could take place at potentials below than that of the theoretical decomposition potential of the salt, when the cathode is reactive to Ca^{2+} ions and anodic chlorine evolution does take place under such conditions.

Properties of the melt such as total solubilised basicity (TSB) and total insolubilised basicity (TIB), as discussed in detail in section 2.3.16 (chapter 2), were measured and innovatively used for interpretation of the reactions occurring in the electro-deoxidation cell. TSB of the melt, which is given in terms of the wt.% CaO in the melt determined by acid-base titration method, showed that some amount of $CaCl_2$ decomposed during DOER of reactive metal oxides which is also in line with the results obtained with CEPM measurements. TIB of the melt, given in terms of the wt.% $CaCO_3$ in the melt and determined by a back titration method, gave insight into the quantitative information on $CaCO_3$ formed by the dissolution of CO_2 in the $CaCl_2$ melt, which is considered to be one of the reasons for the low efficiency of the DOER process. It was observed that the TIB of the melt, during the electrolysis in constant voltage mode, increased with duration of electrolysis. The information on the TSB and TIB measured during electro-reduction of Nb_2O_5 gave significant information on the chemistry of the melt and it could be put to effective use in elucidating the mechanism of reduction of the oxide as discussed in detail in section 3.3.3 (chapter 3).

7.3. Formation of ternary intermediate compounds and mechanism of electro-reduction of various metal oxides

The fundamental issues and the mechanism of the electrochemical reduction of Nb_2O_5, TiO_2, SiO_2 and UO_2 have been studied. Various ternary intermediates and suboxides were observed in partially reduced pellets of the Nb_2O_5 and TiO_2. This was the case when the reduction was carried out even in NaCl and LiCl melts. Only ternary Ca-Si-O (in $CaCl_2$ melt) or Li-Si-O (in LiCl melt) intermediates, but not the suboxides, were seen in the case of SiO_2 whereas neither the ternary intermediates nor the suboxides of uranium were observed in the case of UO_2. Various calcium niobates like $CaNbO_3$, $CaNb_2O_6$, $Ca_3Nb_2O_8$ and $Ca_4Nb_2O_9$ have been observed during the electro-reduction of Nb_2O_5 in $CaCl_2$ melt. Two ternary intermediates, namely, $CaTiO_3$ and $CaTi_2O_4$ were observed in the case of TiO_2 whereas $CaSiO_3$ was the only ternary intermediate observed during the DOER of SiO_2. The less porous and more reactive product of electrolysis of Nb_2O_5 and TiO_2 probably trapped the calcium oxide in their bulk, which lead to the formation of various ternary intermediates whereas the highly porous product of electrolysis of SiO_2 reduced the probability of retention of CaO inside the bulk parts and hence its reaction with SiO_2 to form $CaSiO_3$. The highly porous structure of the reduced Si layers would have allowed the removal of the released oxide ions from the reaction interface to the melt rather quickly. However, depending on the experimental conditions, as in the case of electrolysis of SiO_2 pellet in the tip alone immersed in the melt configuration, the released oxide ions were found to accumulate within the cathode matrix and react chemically with SiO_2 to form $CaSiO_3$.

The electrochemical reduction behaviours of various metal oxides with different chemical properties are different. The mechanism of electrodeoxidation of solid metal oxides, such as Nb_2O_5 and TiO_2 in $CaCl_2$ melt was found to occur by a collective contribution from any one or all of the three schemes of reactions, occurring in different proportions simultaneously or successively. They are (1) Scheme-I: Reduction by deoxidation (oxygen ionisation mechanism) (2) Scheme-II: Reduction via the formation of ternary intermediates and suboxides and (3) Scheme-III: Electro-induced-metallothermic reduction of the metal oxide taken. It was found that the reduction behaviour of Nb_2O_5 and TiO_2 in $CaCl_2$ melt was similar and the reduction proceeds through all the three schemes of reactions. The formation and decomposition of ternary intermediate compounds and various lower oxides of the system Nb-O or Ti-O were observed in the electrolysed products. SiO_2 is an insulator and its reduction occurred through direct removal of oxygen from the matrix leaving behind the semiconducting Si. The formation of ternary intermediates, such as Li_2SiO_3 in LiCl or $CaSiO_3$ in $CaCl_2$, was observed only by chemical reactions and the results indicated that these can be electrochemically reduced to Si upon further electrolysis. The case of UO_2 is entirely different and the presence of any ternary intermediate compounds and suboxides of uranium could not be noticed in partially electrolysed samples. It can be concluded that the UO_2 electrode does not react electrochemically or chemically with the melt and hence the reactions indicated by scheme II were absent. It was further proved that the reduction of UO_2 was occurring by scheme I and scheme III, the latter being significantly predominant at higher current densities and high applied voltages.

The reduction of the tip of Nb_2O_5 and TiO_2 pellets, showed that the conducting nature of the pellets enabled reduction in the melt dipped area. However, in the case of SiO_2 pellets, the reduction was not observed on the tip of the pellet that was soaked in the melt, but it happened on an area around the upper point where the current collector tantalum wire was in contact with the pellet. It seems that the electrolyte melt rose to the upper part of the pellet by capillary action so that the current collector-melt-oxide three phase interlines could be established around the metal wire and hence the reduction of the oxide. The study showed that the electro-reduction behaviours of Nb_2O_5 and TiO_2 are quite similar. The reduction of both the oxides occurred at all points where the oxide electrode was in physical contact with the melt ie., at oxide-melt interfaces, in sharp contrast to that of a SiO_2 electrode where the reduction occurred only at the oxide-conductor-melt three phase (3PI) interlines. The difference between the initiation and propagation of electro-reduction in electrically conducting oxides like Nb_2O_5 and TiO_2 and electrically insulating oxides like SiO_2 has been clearly brought out in this study. The study also shows that the conducting nature of the oxide and the stability of intermediate compounds formed during electro-reduction are key factors for the successful reduction of the metal oxides.

Though the electrochemical reduction behaviour of UO_2 was found to be similar to that of Nb_2O_5 and TiO_2 in view of its conducting nature, the mechanism of electro-reduction was found to be very different. It has been proved in this study that, unlike Nb_2O_5 and TiO_2, the reduction of UO_2 to U does not involve formation of intermediate compounds and hence is a one step reduction process. It is proved in this study that electro-generation of calcium in $CaCl_2$ based melts (or lithium in LiCl melt) and its chemical reaction with UO_2 is not technically necessary for effecting reduction, as has been reported before. The electro-reduction of UO_2 to U is confirmed at cathodic potentials positive to the Ca deposition. However, the reduction is very slow and hence for achieving higher rates of reduction it may be required to operate cells above the metal deposition potential. The study showed that $CaCl_2$-48 mol.% NaCl could be a better electrolytic medium than $CaCl_2$ and LiCl-Li_2O melts for electro-reduction of UO_2, using graphite as the anode.

7.4. Influence of various parameters on solid state electro-reduction of different oxides

Increase in the time of electrolysis increased the extent of reduction of the oxides. However, once the reduction is complete, further electrolysis leads to a fall in the efficiency of the process. An increase in the temperature of electrolysis to 1173 K in case of Nb_2O_5, TiO_2 and SiO_2 led to enhancement of the extent of reduction whereas an opposite behaviour was observed in the case of UO_2 as the sintering of the uranium metal particles on the surface led to the formation of an impermeable metal layer around the pellet. As the porosity of the pellets or the applied voltage was increased, the extent of reduction also increased. In the case of SiO_2, the electro-reduced Si reacted with Ca to form Ca-Si alloy at the cathodic limit. But this kind of calcium alloy formation was not observed with Nb, Ti or U due to the lack of affinity of these metals for Ca. The use of a pyrolytic graphite (PyG) plate in place of high density graphite (HDG) rod as the anode in the electro-reduction of Nb_2O_5 in $CaCl_2$ melt at 1173 K resulted in a melt with relatively lower carbon contamination. Experimental results also suggested that lower temperature of operation could further reduce the carbon contamination of the melt. During the electrolysis of Nb_2O_5 and TiO_2 electrodes in the constant current mode at lower currents, the potentials of the cathode and anode always remained at lower values than that required for Ca deposition and Cl_2 evolution, respectively. The cell behaviour indicated that secondary reactions were taking place even as the cathode was undergoing electro-deoxidation. The efficiency of reduction was higher, when the pellets were wrapped around with conducting tie wires and electrolysed in fully dipped (into the melt) condition than those placed in a cup. The cup configuration, it appeared, hindered the diffusion of electro-generated oxide ions from the cathode to the bulk electrolyte outside. Use of alumina crucibles as containers for $CaCl_2$ melt was found to give less background cell currents compared to SS crucibles. It is possible that the electro-generated calcium metal was consumed in reaction with the inner surface of Al_2O_3 crucibles and thus reduced the background current due to dissolved calcium. In the case of electrochemical reduction of TiO_2 powder in molten $CaCl_2$, the powder sintered at a lower temperature of 1423 K exhibited enhanced reduction than that sintered at higher temperature (1673 K), possibly due to the smaller size of the TiO_2 grains in the former case. The electrochemical reduction of Nb_2O_5 to Nb could be carried out in alternate melts such as NaCl and KCl, though the reduction of the oxide by Na or K was thermodynamically not feasible under such conditions. In the case of UO_2, the electro-reduction of UO_2 to U took place directly without the formation of the cation (of the melt) based intermediate compounds. The observations probably indicated that a reaction involving the cathodically polarised oxide electrode and the cation of the melt and/or a metallothermic reduction with the electro-generated alkali/alkaline-earth metals from the melt are not necessary for the electrochemical reduction of metal oxides, though the reduction by electro-generated alkali/alkaline-earth metal is desirable to obtain lower levels of oxygen in the reduced metal. The studies also showed that the reduction mechanism and the final product obtained are strongly dependent on the physico-chemical characteristics of the metal oxides and also of the melt in addition to the experimental parameters such as temperature, composition of the melt etc. Nb metal obtained from electro-reduction experiments carried out in $CaCl_2$ melt with high density pellets of Nb_2O_5 was hard whereas that obtained from NaCl melt was spongy in nature. Nb metal obtained from electrolysis of Nb_2O_5 in KCl and KCl-25mol.% $CaCl_2$ melts crumbled to powder during post electro-reduction treatment processes.

7.5. Metal estimation by hydrogen sensor (MEHS) method and its application to the characterisation of partially electro-reduced samples

Another important component of the thesis work is the measurement of hydrogen gas released from the partially electro-reduced samples using an in-house developed hydrogen sensor. The method, called ‘the MEHS method’, measured the hydrogen gas released when the partially deoxidised sample containing uranium metal was allowed to react with HBr. The method was found to be very useful in determining the extent of metallisation of the oxide electrode. In the present study with partially reduced UO_2 pellets, the hydrogen measured from different areas of the solid electrode was different, which suggested the non-uniform reduction of the pellet. Based on the results from MEHS measurements and other additional input data, the progress of reduction of the UO_2 pellet as well as its reduction mechanism could be elucidated.

7.6. Scope for future studies

Solid state electrochemical conversion of metal oxides to metals is a new research area and the scope of further research in this area is enormous. R&D in the field has seen a phenomenal increase since the discovery of FFC Cambridge process in 1997; but what has been achieved so far is relatively small in magnitude compared to the potential and scope of the work that lies ahead for future. Unlike many other metal production processes which are suitable for production of few metals at the best, the solid-state electro-reduction process has proven to have the ability to be used for production of several metals and semi-metals of the periodic table from their respective oxides, sulphides etc. The research carried on the process so far, by and large, is of fundamental in nature and practical cells need to be designed and operated for producing each metal. Several challenging issues like the design of oxide electrodes and electro-reduction cells for efficient reduction, collection of freshly produced metal without contaminating it with oxygen and carbon are major issues that will require serious attention in the large scale production of metals by this process.

Some of the work, which will be of use in the production of strategic metals by this process in future, are listed below

1. Production of zirconium, cerium, plutonium and boron from their oxides by the electro-deoxidation method is an area of considerable interest, especially for nuclear industry. Production of cerium and other lanthanide metals is also of interest to other applications such as production of magnets etc. Though not discussed in the thesis, a few attempts were made on the electro-reduction of CeO_2. It was observed that the electrochemical reduction of CeO_2 could not be achieved as the electrode was converted to stable CeOCl. Due to similar chemical characteristics, cerium is considered as a surrogate for plutonium and hence reduction of PuO_2 is also likely to end up as PuOCl. This is an important area of work and the reduction may become possible by selection of an appropriate electrolyte medium and electrolysis conditions, which do not support formation of the oxychloride. Electro-reduction of B_2O_3 in calcium chloride melt at 1173 K was difficult as the metal compound evaporated at the high operation temperature. It may be worth carrying out the studies with a low-melting electrolyte system like LiCl-KCl eutectic (m.p., 623 K), LiCl-KCl-$CaCl_2$ eutectic (m.p., 605 K) or LiCl-KCl-CsCl eutectic (m.p., 538 K).

2. The fundamental issues of reduction of UO_2 have been reported by many researchers and also studied as part of this thesis work. At present LiCl-(1-3) wt.% Li_2O electrolyte with platinum anode is used in the electrochemical conversion of UO_2 to U. The results of the detailed study carried out with UO_2 pellets in $CaCl_2$-48mol.% NaCl melt showed that the electrolyte may be more suitable for the work. Electro-reduction cells of different sizes and with different cathode assemblies need to be operated with $CaCl_2$-48mol.% NaCl at 923 K to ascertain the suitability of the melt for efficient production of U metal.

3. As discussed in detail in chapter 1, the DOER method is a very important process to convert spent nuclear oxide fuel to metal fuel so that it can be further processed by the molten salt electrorefining process. Significant R&D work is now underway in different laboratories in this context. Study of the electro-reduction behaviour of un-irradiated metal oxide samples simulating the nuclear fuel (SIMFUEL) and also the actual irradiated oxide fuel are areas which will be of great significance in nuclear industry. As a first step towards this, the electrochemical reduction of un-irradiated MOX (mixed plutonium and uranium oxides) fuel can be taken up.

4. The choice of a proper anode is an important area craving attention for economical operation of electro-reduction cells. The use of costly platinum will make the process expensive and uneconomical. At the same time, use of graphite anode in oxide ion containing melts may make cells dirty with carbon and dissolved carbon dioxide. Also the environmental problem of release of CO and CO_2 from such cells is a discouraging factor. Hence there is a big interest to develop an inert anode on which oxygen gas will evolve. Development of inert oxygen evolving anode is therefore a major area of research in the electrodeoxidation by molten salt electrolysis in chloride melts.

REFERENCES

[1] C.K. Gupta, Chemical metallurgy: principles and practices, Weinheim, Wiley-VCG Verlag GmbH & Co. KgaA, (2003) 359-399.

[2] D.J. Fray, G.Z. Chen, *Mater. Sci. Technol.,* 20 (2004) 295.

[3] D.J. Fray, T.W. Farthing, G.Z. Chen, 1999, International patent no. WO 9964638.

[4] G.Z. Chen, D.J. Fray, T.W. Farthing, *Nature*, 407 (2000) 361.

[5] J.K. Srivastava, M. Prasad, J.B. Wagner (Jr.), *J. Electrochem. Soc.*, 132 (4) (1985) 955.

[6] A.M. Abdelkader, K.T. Kilby, A. Cox, D.J. Fray, *Chem. Rev.*, 113 (2013) 2863.

[7] G.Z. Chen, The FFC Cambridge process for metal production: Principle, practice and prospect, 3rd Int.ernational Slag Valorisation Symposium, Leuven, 19-20, March, 2012, p. 217-233.

[8] D. Wang, X. Jin and G.Z. Chen, *Annu. Rep. Prog. Chem. Sect. C*, 104 (2008) 189.

[9] Ch. R.V.S. Nagesh, C.S. Ramachandran, R.B. Subramanyam, *Trans. Indian Inst. Met.,* 61 (2008) 341.

[10] D.T.L. Alexander, C. Schwandt, D.J. Fray, *Electrochim. Acta,* 56 (2011) 3286.

[11] K.S. Mohandas, D.J. Fray, Influence of the physico-chemical characteristics of powder compacted metal oxide cathodes on the direct electro-deoxidation in molten $CaCl_2$ medium, in: Florian Kongoli (Ed.), *Molten salts and Ionic liquids,* Vol.3, 2011, p. 219.

[12] C. Schwandt, D.J. Fray, *Electrochim. Acta,* 51 (2005) 66.

[13] H.S. Shin, J.M. Hur, S.M. Jeong, K.Y. Jung, *J. Industrial Eng. Chem.*, 18 (2012) 438.

[14] M. Gibilaro, J. Pivato, L. Cassayre, L. Massot, P. Chamelot, P. Taxil, *Electrochim. Acta,* 56 (2011) 5410.

[15] K.S. Mohandas, D.J. Fray, *J. Appl. Electrochem.*, 41 (2011) 321.

[16] C. Schwandt, D.T.L. Alexander, D.J. Fray, *Electrochim. Acta*, 54 (2009) 3819.

[17] R.V.S. Nagesh, C.S. Ramachandran, *Trans. Nonferrous Met. Soc. China,* 17 (2007) 429.

[18] R. Bhagat, D. Dye, S.L. Raghunathan, R.J. Talling, D. Inman, B.K. Jackson, K.K. Rao, R.J. Dashwood, *Acta Mater.*, 58 (2010) 5057.

[19] K. Dring, R. Dashwood, D. Inman, *J. Electrochem. Soc.*, 152 (2005) E104.

[20] G.Z. Chen, D.J. Fray, *J. Electrochem. Soc.*, 149 (2002) E455.

[21] K. Dring, R. Dashwood, D. Inman, *J. Electrochem. Soc.*, 152 (2005) D184.

[22] C. Schwandt, G.R. Doughty, D.J. Fray, *Key Eng. Mater.*, 436 (2010) 13.

[23] S. Liu, *Procedia Earth Planet. Sci.*, 2 (2011) 1.

[24] M. Bertolini, L. Shaw, L. England, K. Rao, J. Deane, J. Collins, *Key Eng. Mater.*, 436 (2010) 75.

[25] K. Dring, *Key Eng. Mater.*, 436 (2010) 27.

[26] W. Bixia, Z. Lian, L. Xinzhe, Z. Xicheng, C. Jingtao, *Rare Metal Mat. Eng.*, 39 (2010) 1513.

[27] J. Mohanty, P.C. Rath, T. Subbaiah, K.G. Mishra, R.K. Paramguru, *Trans. Indian Inst. Met.*, 62 (2009) 249.

[28] R. Lilia Centeno-Sanchez, D.J. Fray, G.Z. Chen, *J. Mater. Sci.*, 42 (2007) 7494.

[29] V.A. Lebedev, V.I. Salnikov, I.A. Sizikov, D.A. Rymkevich, *Russ. J. Appl. Chem+.*, 80 (2007) 1503.

[30] V.A. Lebedev, V.I. Salnikov, M.V. Tarabaev, I.A. Sizikov, D.A. Rymkevich, *Russ. J. Appl. Chem+.*, 80 (2007) 1491.

[31] P.K. Tripathy, M. Gauthier, D.J. Fray, *Metall. Mater. Trans. B*, 38B (2007) 893.

[32] M. Ma, D. Wang, W. Wang, X. Hu, X. Jin, G.Z. Chen, *J. Alloy. Compd.*, 420 (2006) 37.

[33] N.X. Miao, D.L. Yan, B.C. Guang, C.D. Fu, Q.G. Bao, *Trans. Nonferrous Met. Soc. China*, 16 (2006) s723.

[34] K.S. Mohandas, D.J. Fray, *Trans. Indian Inst. Met.*, 57 (2004) 579.

[35] D.T.L. Alexander, C. Schwandt, D.J. Fray, *Acta Mater.*, 54 (2006) 2933.

[36] K. Yasuda, A. Ghicov, T. Nohira, N. Kani, R. Hagiwara, P. Schmuki, *Electrochem. Solid St.*, 11 (9) (2008) C51.

[37] K. Jiang, X. Hu, H. Sun, D. Wang, X. Jin, Y. Ren, G.Z. Chen, *Chem. Mater.*, 16 (2004) 4324.

[38] J.M. Hur, S.C. Lee, S.M. Jeong, C.S. Seo, *Chem. Lett.*, 36 (2007) 1028.

[39] G. Qiu, M. Ma, D. Wang, X. Jin, X. Hu, G.Z. Chen, *J. Electrochem. Soc.*, 152 (10) (2005) E328.

[40] G.Z. Chen, D.J. Fray, T.W. Farthing, *Metall. Mater. Trans. B*, 32 (2001) 1041.

[41] X.Y. Yan, D.J. Fray, *Metall. Mater. Trans.*, B 33B (2002) 685.

[42] T. Wu, W. Xiao, X. Jin, C. Liu, D. Wang, G.Z. Chen, *Phys. Chem. Chem. Phys.*, 10 (2008) 1809.

[43] X.Y. Yan, D.J. Fray, *J. Mater. Res.*, 18 (2003) 346.

[44] X.Y. Yan, D.J. Fray, *J. Electrochem. Soc.*, 152 (1) (2005) D12.

[45] X.Y. Yan, D.J. Fray, *J. Electrochem. Soc.*, 152 (10) (2005) E308.

[46] Q. Xu, L. Deng, Y. Wu, T. Ma, *J. Alloy. Compd.*, 396 (2005) 288.

[47] S.L. Wang, Y. Xue, H. Sun, *J. Electroanal. Chem.*, 595 (2006) 109.

[48] S.M. Jeong, H.Y. Yoo, J.M. Hur, C.S. Seo, *J. Alloy. Compd.*, 452 (2008) 27.

[49] G. Qiu, X. Feng, M. Liu, W. Tan, F. Liu, *Electrochim. Acta*, 53 (2008) 4074.

[50] Q.S. Song, Q. Xu, R. Tao, X. Kang, *Int. J. Electrochem. Sci.*, 7 (2012) 272.

[51] S.M. Jeong, J.Y. Jung, C.S. Seo, S.W. Park, *J. Alloy. Compd.*, 440 (2007) 210.

[52] Q.S. Song, Q. Xu, X. Kang, J.H. Du, Z.P. Xi, *J. Alloy. Compd.*, 490 (2010) 241.

[53] R. Barnett, K.T. Kilby, D.J. Fray, *Metall. Mater. Trans. B*, 40B (2009) 150.

[54] K.S. Mohandas, D.J. Fray, *Metall. Mater. Trans. B*, 40B (2009) 685.

[55] J. Peng, G. Li, H. Chen, D. Wang, X. Jin, G.Z. Chen, *J. Electrochem. Soc.*, 157 (1) (2010) F1.

[56] A.M. Abdelkader, A. Daher, R. Abdelkareem, *Metall. Mater. Trans. B,* 38B (2007) 35.

[57] G.Z. Chen, E. Gordo, D.J. Fray, *Metall. Mater. Trans. B,* 35B (2004) 223.

[58] E. Gordo, G.Z. Chen, D.J. Fray, *Electrochim. Acta*, 49 (2004) 2195.

[59] C. Schwandt, D.J. Fray, *Z. Naturforsch.*, 62a (2007) 655.

[60] G. Li, D. Wang, Z. Chen, *J. Mater. Sci. Technol.*, 25 (6) (2009) 767.

[61] M. Erdogan, I. Karakaya, *Metall. Mater. Trans. B,* 41B (2010) 798.

[62] T. Nohira, K. Yasuda, Y. Ito, *Nat. Mater.*, 2 (2003) 397.

[63] K. Yasuda, T. Nohira, R. Hagiwara, Y.H. Ogata, *Electrochim. Acta*, 53 (2007) 106.

[64] K. Yasuda, T. Nohira, K. Amezawa, Y.H. Ogata, Y. Ito, *J. Electrochem. Soc.*, 152 (4) (2005) D69.

[65] K. Yasuda, T. Nohira, R. Hagiwara, Y.H. Ogata, *J. Electrochem. Soc.*, 154 (7) (2007) E95.

[66] K. Yasuda, T. Nohira, K. Takahashi, R. Hagiwara, Y.H. Ogata, *J. Electrochem. Soc.*, 152 (12) (2005) D232.

[67] Y. Nishimura, T. Nohira, K. Kobayashi, R. Hagiwara, *J. Electrochem. Soc.*, 158 (6) (2011) E55.

[68] S.K. Cho, F.R.F. Fan, A.J. Bard, *Electrochim. Acta*, 65 (2012) 57.

[69] W. Xiao, X. Jin, Y. Deng, D. Wang, G.Z. Chen, *J. Electroanal. Chem.*, 639 (2010) 130.

[70] P.C. Pistorius, D.J. Fray, *J. S. Afr. Inst. Min. Metall.*, 106 (2006) 31.

[71] E. Ergul, I. Karakaya, M. Erdogan, *J. Alloy. Compd.*, 509 (2011) 899.

[72] S.C. Lee, J.M. Hur, C.S. Seo, *J. Ind. Eng. Chem.*, 14 (2008) 651.

[73] K. Yasuda, T. Nohira, Y.H. Ogata, Y. Ito, *J. Electrochem. Soc.*, 152 (11) (2005) D208.

[74] K. Yasuda, T. Nohira, Y. Ito, *J. Phys. Chem. Solids*, 66 (2005) 443.

[75] X. Jin, P. Gao, D. Wang, X. Hu, G.Z. Chen, *Angew. Chem.*, 116 (2004) 751.

[76] X.Y. Yan, D.J. Fray, *J. Appl. Electrochem.*, 39 (2009) 1349.

[77] H. Xie, H. Zhang, Y. Zhai, J. Wang, C. Li, *J. Mater. Sci. Technol.*, 25 (4) (2009) 459.

[78] K. Gourishankar, L. Redey, M. Williamson, *Light metals, TMS,* (2002) 1075.

[79] Y. Sakamura, M. Kurata, T. Inoue, *J. Electrochem. Soc.*, 153 (3) (2006) D31.

[80] S.D. Herrmann, S.X. Li, M.F. Simpson, S. Phongikaroon, *Sep. Sci. Technol.,* 41 (2006) 1965.

[81] S.M. Jeong, S.B. Park, S.S. Hong, C.S. Seo, S.W. Park, *J. Radioanal. Nucl. Chem.,* 268 (2006) 349.

[82] Biju Joseph, N. Sanil, K.S. Mohandas and K. Nagarajan, 'Studies on the direct electrochemical reduction of solid uranium oxide in molten lithium chloride medium', Proceedings of Nuclear and Radiochemistry symposium (NUCAR-2009), Jan.07-10, Mumbai, India (2009) p. 269.

[83] E.Y. Choi, J.M. Hur, I.K. Choi, S.G. Kwon, D.S. Kang, S.S. Hong, H.S. Shin, M.A. Yoo, S.M. Jeong, *J. Nucl. Mater.,* 418 (2011) 87.

[84] K. Nagarajan, B.P. Reddy, S. Ghosh, G. Ravishankar, K.S. Mohandas, U.K. Mudali, K.V.G. Kutty, K.V. Kasiviswanathan, C.A. Babu, P.K. Sundaram, P.R.V. Rao, B. Raj, *Energy Procedia,* 7 (2011) 431.

[85] Biju Joseph, N. Sanil, K.S. Mohandas, K. Nagarajan, Proceedings of Conference on Molten Salts in Nuclear Technology, January 9-11, 2013, held at BARC, Mumbai, India, p.226-229.

[86] M. Gibilaro, L. Cassayre, O. Lemoine, L. Massot, O. Dugne, R. Malmbeck, P. Chamelot, *J. Nucl. Mater.,* 414 (2011) 169.

[87] Y. Sakamura, *J. Nucl. Mater.,* 412 (2011) 177.

[88] Y. Sakamura, T. Omori, *Nucl. Technol.,* 171 (2010) 266.

[89] E.Y. Choi, J.K. Kim, H.S. Im, I.K. Choi, S.H. Na, J.W. Lee, S.M. Jeong, J.M. Hur, *J. Nucl. Mater.*, 437 (2013) 178.

[90] E.Y. Choi, C.Y. Won, J.S. Cha, W.S. Park, H.S. Im, S.S. Hong, J.M. Hur. *J. Nucl. Mater.*, 444 (2014) 261.

[91] D. Hu, W. Xiao, G.Z. Chen, *Metall. Mater. Trans.*, B 44B (2013) 272.

[92] J.J. Peng, K. Jiang, W. Xiao, D.H. Wang, X.B. Jin, G.Z. Chen, *Chem. Mater.*, 20 (2008) 7274.

[93] G. Qiu, D. Wang, M. Ma, X. Jin, G.Z. Chen, *J. Electroanal. Chem.*, 589 (2006) 139.

[94] B. Zhao, L. Wang, L. Dai, G. Cui, H. Zhou, R.V. Kumar, *J. Alloy. Compd.*, 468 (2009) 379.

[95] F. Meng, H. Lu, *Adv. Eng. Mater.*, 11 (3) (2009) 198.

[96] A.J.M. Wood, R.C. Copcutt, G.Z. Chen, D.J. Fray, *Adv. Eng. Mater.*, 5 (9) (2003) 650.

[97] D.J.S. Hyslop, A.M. Abdelkader, A. Cox, D.J. Fray, *J. Electrochem. Soc.*, 157 (7) (2010) E111.

[98] B.A. Glowacki, D.J. Fray, X.Y. Yan, G.Z. Chen, *Physica C,* 387 (2003) 242.

[99] G. Qiu, D. Wang, X. Jin, G.Z. Chen, *Electrochim. Acta,* 51 (2006) 5785.

[100] Y. Zhu, M. Ma, D. Wang, K. Jiang, X. Hu, X. Jin, G.Z. Chen, *Chinese Sci. Bull.*, 51 (20) (2006) 2535.

[101] B. Jackson, M. Jackson, D. Dye, D. Inman, R. Dashwood, *J. Electrochem. Soc.*, 155 (12) (2008) E171.

[102] K. Dring, R. Bhagat, M. Jackson, R. Dashwood, D. Inman, *J. Alloy. Compd.*, 419 (2006) 103.

[103] R. Bhagat, M. Jackson, D. Inman, R. Dashwood, *J. Electrochem. Soc.*, 156 (1) (2009) E1.

[104] R. Bhagat, M. Jackson, D. Inman, R. Dashwood, *J. Electrochem. Soc.*, 155 (6) (2008) E63.

[105] X.Y. Yan, D.J. Fray, *J. Alloy. Compd.*, 486 (2009) 154.

[106] X. Kang, Q. Xu, X. Yang, Q. Song, *Mater. Lett.*, 64 (2010) 2258.

[107] G. Li, D. Wang, X. Jin, G.Z. Chen, *Electrochem. Commun.*, 9 (2007) 1951.

[108] X. Ge, X. Wang, S. Seetharaman, *Electrochim. Acta,* 54 (2009) 4397.

[109] B. Claux, J. Serp, J. Fouletier, *Electrochim. Acta,* 56 (2011) 2771.

[110] R.V.S. Nagesh, *DRDO Technology Spectrum,* May 2012, pp.139-145.

[111] Pritish Kar, James W. Evans, *Electrochim. Acta,* 54 (2008) 835.

[112] Kartik Rao, James Deane, Lucy Grainger, John Clifford, Electrolytic reduction of powder, International Patent No. WO 2013/050772 A2.

[113] M. Ojaghi-Ilkhchi, H. Assadi, *Comp. Mater. Sci.*, 53 (1) (2012) 1.

[114] W.J. Kroll, *J. Franklin Inst.*, 260 (1955) 169.

[115] M. Kurata, N. Yahagi, S. Kitawaki, A. Nakayoshi, M. Fukushima, *Nucl. Technol.*, 164 (2008) 433.

[116] S.J. Oosthuizen, *J. S. Afr. Inst. Min. Metall.*, 111 (2011) 199.

[117] J.F. Ahearne, *Energ. Econ.*, 33 (2011) 572.

[118] S.K. Jain, *Energy Procedia,* 7 (2011) 5-20.

[119] R.B. Grover, *Curr. Sci.*, 78 (2000) 1191.

[120] http://barc.gov.in/reactor/tfc_3sinpp.html, accessed on 22-11-2013.

[121] T. Koyama, Y. Skamura, M. Iizuka, *ECS Trans.*, 33 (7) (2010) 339.

[122] J.J. Laidler, J.E. Battles, W.E. Miller, J.P. Ackerman, E.L. Carls, *Prog. Nucl. Energy,* 31 (1-2) (1997) 131.

[123] S. Herrmann, S. Li, M. Simpson, *J. Nucl. Sci. Technol.*, 44 (3) (2007) 361.

[124] Y. Sakamura, M. Akagi, *Nucl. Technol.*, 179 (2012) 220.

[125] H. Lee, J.M. Hur, J.G. Kim, D.H. Ahn, Y.Z. Cho, S.W. Park, *Energy Procedia,* 7 (2011) 391.

[126] J.M. Hur, C.S. Seo, I.S. Kim, S.S. Hong, D.S. Kang, S.W. Park, Development of electrochemical reduction technology for spent oxide fuels, *WM'03 Conference*, Feb. 23-27, Tucson, AZ (2003).

[127] B.H. Park, I.W. Lee, C.S. Seo, *Chem. Eng. Sci.*, 63 (2008) 3485.

[128] J.M. Hur, I.K. Choi, S.H. Cho, S.M. Jeong, C.S. Seo, *J. Alloy. Compd.*, 452 (2008) 23.

[129] S.M. Jeong, B.H. Park, J.M. Hur, C.S. Seo, H. Lee, K.C. Song, *Nucl. Engg. Tech.*, 42 (2) (2010) 183.

[130] S.M. Jeong, H.S. Shin, S.S. Hong, J.M. Hur, J. B.Do, H.S. Lee, *Electrochim. Acta,* 55 (2010) 1749.

[131] S.M. Jeong, J.M. Hur, S.S. Hong, D.S. Kang, M.S. Choung, C.S. Seo, J.S. Yoon, *Nucl. Technol.,* 162 (2008) 184.

[132] J.M. Hur, S.M. Jeong, H.S. Lee, *Electrochem. Commun.*, 12 (2010) 706.

[133] M. Kurata, T. Inoue, J. Serp, M. Ougier, J.P. Glatz, *J. Nucl. Mater.,* 328 (2004) 97.

[134] M. Iizuka, Y. Sakamura, T. Inoue, *J. Nucl. Mater.*, 359 (2006) 102.

[135] E.Y. Choi, J.W. Lee, J.J. Park, J.M. Hur, J.K. Kim, K.Y. Jung, S.M. Jeong, *Chem. Eng. J.,* 207-208 (2012) 514.

[136] B.H. Park, H.H. Lee, W.M. Choung, J.M. Hur, C.S. Seo, *Nucl. Technol.*, 171 (2010) 232.

[137] H. Ohta, T. Inoue, Y. Sakamura, *Nucl. Technol.*, 150 (2005) 153.

[138] S.D. Herrmann, S.X. Li, *Nucl. Technol.*, 171 (2010) 247.

[139] K.S. Mohandas, Direct electrochemical conversion of metal oxides to metal by molten salt electrolysis-An overview, in: Florian Kongoli (Ed.), *Molten salts and Ionic liquids,* Vol.3, 2011, p. 195.

[140] H.J. Rack, J.I. Qazi, *Mater. Sci. Eng. C,* 26 (2006) 1269.

[141] R.R. Boyer, *Mater. Sci. Eng. A*, 213 (1996) 103.

[142] Y. Katayama, B. Friedrich, in: D. Costa, H.C. De Long, R. Hagiwara, R.A. Mantz, G.R. Stafford, P.C. Trulove (Eds.), Molten Salts XIV, The Electrochemical Society Proceedings Series, Honolulu, Hawaii.

[143] R.O. Suzuki, M. Aizawa, K. Ono, *J. Alloy. Compd.,* 288 (1999) 173.

[144] I. Machlin, R.T. Begley, E.D. Weisert, Refractory metal alloys – Metallurgy and Technology, Plenum press, Newyork, 1968, p. 327.

[145] M.E. McCoy, Status of materials development for molten salt reactors, Report from Oak Ridge National Laboratory, published in January, 1978: ORNL/TM-5920. http://web.ornl.gov/info/reports/1978/3445603596348.pdf

[146] X.Y. Yan, D.J. Fray, *Adv. Funct. Mater.,* 15 (2005) 1757.

[147] H.A. Wilhelm, F.A. Schmidt, T.G. Ellis, *J. Metals.*, 12 (1966) 1303.

[148] G.R. Kamat, C.K. Gupta, *Metal. Trans.,* 2 (1971) 2817.

[149] J. Kruger, Relative extents of reduction by carbothermy and silicothermy of niobium, in: O. Winkler, R. Bakish (Eds.), vacuum metallurgy, Elsevier, Amsterdam, London, 1971, p.161.

[150] G.L. Miller, Tantalum and Niobium, Butterworths scientific publications, Great Britain, 1959, p.181, 205.

[151] Y. Deng, D. Wang, W. Xio, X. Jin, X. Hu, G.Z. Chen, *J. Phys. Chem. B,* 109 (29) (2005) 14043.

[152] T. Usami, M. Kurata, T. Inoue, H.E. Sims, S.A. Beetham, J.A. Jenkins, *J. Nucl. Mater*., 300 (2002) 15.

[153] M. Iizuka, T. Inoue, M. Ougier, J.P. Glatz, *J. Nucl. Sci. Technol.,* 44 (2007) 801.

[154] G.F. Brunzie, T.R. Johnson, R.K. Steunenberg, *Anal. Chem.,* 33 (8) (1961) 1005.

[155] C. Ramesh, G. Velayutham, N. Murugesan, V. Ganesan, K.S. Dhathathreyan, G. Periaswami, *J. Solid State Electrochem.*, 7 (2003) 511.

[156] G. Velayutham, C. Ramesh, N. Murugesan, V. Manivannan, G. Periaswami, *Ionics*, 10 (2004) 50.

[157] C. Ramesh, N. Murugesan, M.V. Krishnaiah, V. Ganesan, G. Periaswami, *J. Solid State Electrochem.*, 12 (2008) 1109.

[158] C. Ramesh, N. Murugesan, S. Velmurugan, A.A.M. Prince, V. Ganesan, S.V. Narasimhan, A measuring system for on-line measurement of corrosion rate of metals in an aqueous medium, Indian Patent No. 204092 (2006).

[159] FactSage (TM) 6.2, Thermfact and GTT-Technologies, (1976-2010).

[160] H.A. Johansen, J.G. Cleary, J. Electrochem. Soc., 109 (11) (1962) 1076.

[161] J. Nowotny, C.C. Sorrell, eds., Electrical properties of oxide materials, Trans tech publications, Switzerland (1997).

[162] A. Pura, K. Rubenis, D. Stepanovs, L.B. Cimdina, J. Ozolins, *Processing and Applications of Ceramics*, 6 (2) (2012) 91.

[163] S.H. Song, X. Wang, P. Xiao, *Mat. Sci. Eng.*, B94 (2002) 40.

[164] M. Radecka, M. Rekas, *J. Eur. Cer. Soc.*, 22 (2002) 2001.

[165] D. Eder, R. Kramer, *Phys. Chem. Chem. Phys.*, 5 (2003) 1314.

[166] D. Regonini, V. Adamaki, C.R. Bowen, S.R. Pennock, J. Taylor, A.C.E. Dent, *Solid State Ionics*, 229 (2012) 38.

[167] J. Yahia, *J. Phys. Chem. Solids*, 25 (1964) 881-887.

[168] H. Okamoto, *J. Phase Equilib. Diff.*, 28 (3) (2007) 309.

[169] H. Okamoto, *J. Phase Equilib. Diff.*, 28 (5) (2007) 497.

[170] J.L. Murray, H.A. Wriedt, *Bull. Alloy Phase Diagr.*, 8 (1987) 148.

[171] T.B. Massalski, ed., Binary alloy phase diagrams, 2nd ed., Materials Park, ASM International (1990).

[172] A.R. West, Solid state chemistry and its applications, Wiley India (P.) Ltd., New Delhi, Wiley-India Edition (2007).

[173] W.D. Callister Jr., Materials science and engineering, Wiley India (P.) Ltd, New Delhi, Sixth Edition (2009).

[174] A.J. Bard, L.R. Faulkner, Electrochemical methods: Fundamentals and applications, Second edition, John Wiley & Sons, Inc., (2000).

[175] H. Wendt, A. Khalil, C.E. Padberg, *J Appl. Electrochem.,* 21 (1991) 929.

[176] H. Wendt, S. Dermeik, A. Ziogas, *Werkstoffe und Korrosion,* 41 (1990) 457.

[177] R.J. Cava, B. Batlogg, J.J. Krajewski, H.F. Poulsen, P. Gammel, W.F. Peck (Jr.), L.W. Rupp (Jr.), *Phys. Rev. B,* 44 (1991) 6973.

[178] D.J. Fray, *JOM-J Min. Met. Mat. S.,* 53 (10) (2001) 27.

[179] H.S. Song, X. Wang, P. Xiao, *Mat. Sci. Eng.,* B94 (2004) 40.

[180] T. Bak, J. Nowotny, C.C. Sorrell, M.F. Zhou, *Ionics,* 10 (2004) 334.

[181] J.M. Hur, C.S. Seo, S.S. Hong, D.S. Kang, S.W. Park, ‘Electrochemical reduction of uranium oxides in Li_2O-LiCl molten salt’, *7th information exchange meeting on actinide and fission product partition and transmutation, Session-II: Progress in partitioning and waste forms,* Jeju, Republic of Korea, 14-16, Oct. 2002, p. 355-361.

[182] J.M. Hur, S.S. Hong, H.S. Lee, *J. Radioanal. Nucl. Chem.,* 295 (2013) 851.

[183] Y. Castrillejo, A. M. Martinez, R. Pardo, and G. M. Haarberg, *Electrochim. Acta*, 42 (1997) 1869.

[184] J. Holc, D. Kolar, *J. Solid State Chem.,* 61 (1986) 260.

[185] M.W. Mallett, A.F. Gerds, H.R. Nelson, *J. Electrochem. Soc.,* 99 (1952) 197.

[186] M. Shen, B. Li, J. Yu, *Electrochim. Acta,* 62 (2012) 153.

[187] T. Koyama, T. Hijikata, T. Usami, T. Inoue, S. Kitawaki, T. Shinozaki, M. Fukushima, M. Myochin, *J. Nucl. Sci. Technol.,* 44 (3) (2007) 382.

[188] C. Ramesh, N. Murugesan, A.A.M. Prince, S. Velmurugan, S.V. Narasimhan, V. Ganesan, *Corros. Sci.*, 43 (2001) 1865.

[189] C.A. Laue, D.G. Anderson, T.E. Fitch, *J Radioanal. Nucl. Chem.*, 261 (2004) 709.

APPENDIX-I

Derivation of equation for extent of reduction of the partially reduced product in the direct oxide electrochemical reduction of UO_2

The term 'extent of reduction (E_R)' should essentially imply the percentage of original UO_2 that is reduced to metallic U after subjecting it to electro-reduction. It means the extent of reduction will be expressed in terms of UO_2 only.

$E_R = (W_R / W_T) \text{ X } 100\%$

W_R = Wt. of UO_2 corresponding to wt. of electro-generated U metal (W_U g) and W_T = Wt. of the reduced product taken (Wp) expressed in terms of wt. of UO_2 = wt. of unreduced UO_2 in the electro-reduced product + wt. of UO_2 corresponding to W_U g of U metal. The above equation shows the percentage of the total UO_2 of the sample that was converted to U metal.

Wt. of UO_2 in the electrolysed product = $W_p – W_U$

Where, W_p is the weight of the electrolysed product taken and W_U, the wt. of U metal estimated in the electrolysed product by MEHS method.

Now, 270 g of UO_2 contains 238 g of U metal

W_R = Wt. of UO_2 corresponding to W_U g of U metal = $W_U \text{ X } (270/238) = 1.1344\, W_U$

$E_R = (W_R / W_T) \text{ X } 100\%$

= {wt. of UO_2 corresponding to W_U g of U metal / (wt. of unreduced UO_2 in the electro-reduced product + wt. of UO_2 corresponding to W_U g of U metal)} X 100%

$$= \{1.1344W_U / [\,(W_p\text{-}W_U) + 1.1344W_U\,]\} \text{ X } 100\%$$

$$= \{1.1344W_U / [W_p + 0.1344W_U]\} \text{ X } 100\%$$

Dividing the numerator and denominator by W_U, we get

$$E_R = \{1.1344 / [0.1344 + (W_p / W_U)]\} \text{ X } 100\%$$

Dividing the numerator and denominator by 1.1344, we get

$$E_R = \{1 / [0.1185 + 0.8815\,(W_p / W_U)]\} \text{ X } 100\%$$

Therefore, the extent of reduction of UO_2 after electrolysis (E_R) is given as

$$E_R = \{1 / [\alpha + \beta (W_p / W_U)]\} \times 100\%$$

Where α and β are constants with values as 0.1185 and 0.8815 respectively.